Synthesis, Structure, and Reactivity of N-O and N-N Donor-based Complexes of Boron

Ph.D. Thesis

by

Rahul Kumar Yadav

Under the supervision of

Dr. DIPAK KUMAR ROY

DEPARTMENT OF CHEMISTRY

INDIAN INSTITUTE OF TECHNOLOGY INDORE

November 2025

Synthesis, Structure, and Reactivity of N-O and N-N Donor-based Complexes of Boron

Ph.D. Thesis

by

Rahul Kumar Yadav

Under the supervision of

Dr. DIPAK KUMAR ROY

DEPARTMENT OF CHEMISTRY

INDIAN INSTITUTE OF TECHNOLOGY INDORE

November 2025

INDIAN INSTITUTE OF TECHNOLOGY
INDORE

I hereby certify that the work which is being presented in the thesis entitled "**Synthesis, Structure, and Reactivity of N-O and N-N Donor-based Complexes of Boron**" in the partial fulfillment of the requirements for the award of the degree of **Doctor of Philosophy** and submitted in the **Department of Chemistry, Indian Institute of Technology Indore**, is an authentic record of my own work carried out during the time period from **January 2020 to Novmber 2025** under the supervision of **Dr. Dipak Kumar Roy**, Associate Professor, Department of Chemistry, Indian Institute of Technology Indore.

The matter presented in this thesis has not been submitted by me for the award of any other degree of this or any other institute.

Signature of the student with date

(RAHUL KUMAR YADAV)

This is to certify that the above statement made by the candidate is correct to the best of my/our knowledge.

Signature of Thesis Supervisor with date

(Dr. DIPAK KUMAR ROY)

Rahul Kumar Yadav has successfully given his/her Ph.D. Oral Examination held on 21/11/2025

Signature of Thesis Supervisor with date

(Dr. DIPAK KUMAR ROY)

ACKNOWLEDGEMENT

Their constant presence, support, and motivation have been invaluable throughout this journey, and I am truly blessed to have them by my side. I am deeply grateful to everyone who directly or indirectly supported and guided me throughout my Ph.D. journey. Your contributions have made this experience truly meaningful and memorable.

“Dedicated to my Guru and Family”

x

LIST OF PUBLICATIONS

First author publications

[1] **Rahul Kumar Yadav**, Darakshan Parveen, Bijan Mondal* and Dipak Kumar Roy* (2024). The Role of Spacers as a Probe in Variation of Photoluminescence Properties of Mono-and Binuclear Boron Compounds. ***Chem. Asian J., 20, e202401113. DOI: 10.1002/asia.202401113***

[2] **Rahul Kumar Yadav,** Darakshan Parveen, Parmod Jangra, Bijan Mondal*, and Dipak Kumar Roy* (2025). Synthesis, Characterization, and Reactivity of Aminotroponiminate-Based Difluoroboranes: A Pathway Towards Bore(boro)nium Cation. ***Inorg. Chem. 64, 10780-10791. DOI: 10.1021/acs.inorgchem.5c00451***

[3] **Rahul Kumar Yadav,** Darakshan Parveen, Ritesh Shahu, Bijan Mondal, and Dipak Kumar Roy* Unveiling Borane Complexes with N, O Chelation: Synthesis, Reactivity, and Theoretical Perspectives. (*manuscript submitted*)

[4] **Rahul Kumar Yadav,** Darakshan Parveen, Parmod Jangra, and Dipak Kumar Roy* Synthesis of N-heterocyclic olefin borane adducts, and their reactivity with triflates and diacids. (*manuscript under preparation*)

Co-author publications

[1] Darakshan Parveen, Sougata Saha, **Rahul Kumar Yadav**, Swapan K. Pati* and Dipak Kumar Roy* (2025). Tri-Coordinated Magnesium-Mediated Cyanosilylation and Hydroboration of Aromatic and N-heterocyclic Aldehydes: An Experimental and Theoretical Study. ***Chem. Asian J.*** **e202401853. DOI: 10.1002/asia.202401853**

[2] Darakshan Parveen, **Rahul Kumar Yadav**, Felipe Fantuzzi* and Dipak Kumar Roy* (2025). Bis(diiminate)-Supported Bimetallic Complexes: Tri-Coordinated Zinc for Nitrile and

Carbodiimide Hydroboration. *ACS Omega*, **10, 2033–2043. DOI: 10.1021/acsomega.4c08068**

[3] Darakshan Parveen, **Rahul Kumar Yadav**, Bijan Modal, Marrie Dallon, Yann Sarazin and Dipak Kumar Roy* (2024). Bis(diiminate)-based Boron Difluoro Complexes: Effective Synthon For Bis (Borenium) Cations. *Dalton Trans.***, 53, 14139-14143. DOI: 10.1039/D4DT02050B**

[4] **Darakshan Parveen**, Rahul Kumar Yadav and Dipak Kumar Roy* (2024). Recent Progress In Beryllium Organometallic Chemistry. *Chem. Commun.***, 60, 1663-1673. DOI: 10.1039/D3CC04844F**

LIST OF CONFERENCES

1. *In-House Symposium, Department of Chemistry-2024, Department of Chemistry, IIT Indore*

   Poster: N, O, and N, N stabilized boranes: Synthesis and their reactivity.

2. *International INDO-GERMAN conference on Sustainable Chemistry,-2023, IIT Indore, M.P., India*

   Poster: β-diiminate ligands and their corresponding Boron complexes

3. *International Conference on Modern Trends in Inorganic Chemistry (MTIC-XIX)-2022, BHU, U.P., India*

   Poster: Towards the Synthesis of low-valent group 14 complexes supported by guadinate ligands.

4. *In-House Symposium, Department of Chemistry-2021, Department of Chemistry, IIT Indore, M.P., India*

   Poster: Synthesis and Reactivity of low-valent complexes of Si and Ge.

TABLE OF CONTENTS

Contents

LIST OF SCHEMES

LIST OF TABLES

ABBREVIATIONS

Å	Angstrom – unit of length, 1×10^{-10} m
e^-	An electron
Cat.	A catalytic amount
X	A halide
ATIs	Aminotroponiminates
br	Broad (NMR)
br	Broad (NMR)
CAAC	Cyclic (alkyl)(amino) carbene
Cal	Calorie (1 kcal = 4.184 J)
δ	Chemical shift
J	Coupling constant between nuclei
COT	1,3,5,7-Cyclooctatetraene
Cp	$(C_5H_5)^-$
Cy	Cyclohexyl group $(C_6H_{11})^-$
CV	Cyclic Voltammetry
d	Doublet (NMR)
DCM	Dichloromethane
DFT	Density functional theory
Dipp	2,6-Diisopentylphenyl
DHBTA	Dehydrogenative borylation of terminal alkyne
Priso	$[\{(DippN)_2\}C(NiPr_2)]^-$
e.g.	Exempli gratia/for example
ESI	Electrospray ionisation
g	Gram
L	Generic ligand
M	Generic metal
R	General organic substituent
Hz	Hertz, s^{-1}
HOMO	Highest occupied molecular orbital
i.e.	id est/it is, in other words
in vacuo	In a vacuum/under vacuum

*i*Pr	Isopropyl group ((CH$_3$)$_2$CH$^-$)
IR	Infrared
J	Joule
τ	Lifetime
LUMO	Lowest unoccupied molecular orbital
LUMO	Lowest unoccupied molecular orbital
τ	Lifetime
M	Molar
m	Multiplet (NMR)
Me	Methyl group (CH$_3$$^-$)
Mes	2,4,6-trimethylphenyl
MHz	Megahertz
mL	Millilitre/1x10^{-3}L
mol	Moles
ε	Molar Extinction Coefficient
*n*Bu	Normal butyl (CH$_3$(CH$_2$)$_2$CH$_2$$^-$)
NHC	N-heterocylic carbene
NHO	N-heterocylic olefin
Nu	Nuclear charge
NMR	Nuclear Magnetic Resonance
nm	Nanometer - unit of length, 1 x10^{-9}m
OTf	[OSO$_2$CF$_3$]$^-$
Ph	Phenyl group (C$_6$H$_5$$^-$)
ppm	Parts per million
Priso	[{(DippN)$_2$}C(N*i*Pr$_2$)]$^-$
Φ	Quantum Yield
s	Singlet (NMR)
Δv	Stoke Shift
K	Temperature
T	Temperature
t	Triplet (NMR)
THF	Tetrahydrofuran
UV	Ultra violet

V	Volts
vs	Versus
λ	Wavelength
v /cm^{-1}	Wavenumber
v̄	Wavelength

ABSTRACT

Synthesis, Structure, and Reactivity of N-O and N-N Donor-based Complexes of Boron

by

Rahul Kumar Yadav

Main Group and Organometallics (MGOM) Laboratory

Department of Chemistry

Indian Institute of Technology Indore, India.

Thesis supervisor: **Dr. Dipak Kumar Roy**

This thesis explores the diverse applications of bidentate ligands like N-O (salicylaldimine)and N-N (aminotroponiminates, ATIs) donors, along with the N-heterocyclic olefines. These ligands play a vital role in stabilizing boron complexes in both neutral and cationic states. This thesis delves into the versatile chemistry of N, N′-based mono ATIs, bis(ATIs), along with NHOs and N, O donor ligands, focusing on their role in the synthesis of fluorescent boron complexes and their subsequent use in the isolation of reactive borenium cations. ATIs ligands, with their strong electron-donating properties and steric tunability, serve as ideal scaffolds for stabilizing reactive species, enabling the isolation of both low valent as well as cationic complexes of semi(metals) across the periodic table. The synthesis of these complexes, however, presents significant challenges, including the precise control of reaction conditions to prevent unwanted side reactions such as disproportionation. Overcoming these challenges has enabled the successful synthesis of boron complexes and their corresponding boron cationic species.

Furthermore, we treated the NHO-Borane adduct with the various diacids like (manolinic, glutaric, pthalic, etc), leading to the formation of boroxilates through the condensation reactions. Parrally NHO-boranes on treatment with N-basesd triflates to facilitate the substituted NHO-boranes, signifying the nucleophilic reactivity of NHO-boranes, along with their potential in structural diversification of the boron center

NHO scaffold. Overall, this report demonstrates a wide range of functional group compatibility and modularity of the NHO-borane system in the construction of complex boron-based structures.

Looking ahead, the development of N-N and N-O-based boron complexes holds promise for applications in materials science and provides alternatives to metal-free catalytic systems.

Objectives and Scope of the Thesis

Boron ($Z = 5$), with its unique electronic properties, forms diverse and functional complexes with broad applications in catalysis, pharmaceuticals, biological imaging, and sensors. Organic dyes offer unique optical properties and numerous applications; however, current research aims to improve availability, colorfastness, and in-cast efficiency. The incorporation of the BF_2 moiety into π-conjugated systems significantly enhances the photostability and lifetime of the resulting dyes compared to their parent π-conjugated counterparts. Due to their high photostability, boron-based organic dyes have diverse applications in medical science, especially in diagnostics and therapeutics. Dipyrromethene BF_2 complexes (BODIPY) dyes are very famous boron complexes utilized in various fields such as fluorescent sensors, photodynamic therapy, artificial light harvesting materials, molecular photonic wires, and sensitizers for solar cells. BODIPY dyes, despite their favorable photophysical properties, exhibit certain limitations arising from strong π–π stacking interactions. These interactions often lead to small Stokes shifts and diminished fluorescence emission in both solid and solution phases. To overcome these problems, other alternatives have been tested. Among them, N, N, and N, O bidentate ligands play a crucial role in enhancing the spectroscopic properties can be tuned easily. N, N and N, O chelated boron complexes bearing halides serve as excellent precursors for the synthesis of boron cations and stabilize them with their tailored electronic and steric properties. ATI ligands have enabled them to function as competent catalysts of transition metal-based catalysts for various organic transformations involving the activation of strong

covalent bonds, such as H–H, Si–H, B–H, C–H, and C–C bonds. Boron (Z=5) is an easily available element with the naturally abundant element (about 0.001wt%) on Earth's crust, is inexpensive, and exhibits low toxicity, making it highly accessible and environmentally friendly. Their chemical versatility and ability to participate in a wide range of reactions further enhance their suitability for catalytic applications. These attributes place the main group elements as ideal candidates for advancing green and sustainable chemistry, offering an eco-friendly approach to modern chemical transformations.

ATIs ligand-based complexes of main group elements have emerged as versatile systems in both fundamental and applied chemistry. The N-N ligand framework, with its strong electron-donating ability and steric tunability, stabilizes reactive main group species in unusual oxidation states, allowing for the exploration of novel bonding and reactivity patterns. These ligands provide precise control over the electronic environment of the central element, mitigating the tendency for oxidation, disproportionation, or aggregation, and enabling the isolation of otherwise elusive species. Collectively, ATI-based main group cations represent a significant step forward in leveraging main group elements for the innovation of next-generation photoactive materials and catalysts.

The key findings and a summary of the thesis chapters are outlined as follows:

Chapter 1 This chapter gives an overview of the foundation principles underlying main group cations and low oxidation state chemistry, with an extensive focus on the pivotal role of N-O and N, N-based ligands, along with the role of NHC and NHO for the stabilization of unusual oxidation states of main group (non) metals. Aminotroponiminate (ATIs) are a class of N, N donor, monoanionic chelating ligands. Over the years, ligand chemistry has evolved and plays a significant role in the formation of multiple bond complexes rather than carbon. N-heterocyclic carbene and N-heterocyclic olefins play vital roles in

multiple-bonded chemistry of the main group elements because they have strong sigma-donating and π-accepting ability. Interestingly, the π-acceptor ability further boosts the stability of these complexes and is used in various chemical processes.

Chapter 2 The development of low molecular (small organic fluorophores) weight dyes has attracted great attention due to their remarkable optical properties, mainly in terms of photostability, thermostability, and penetration into biological objects. Interestingly, small organic fluorophores have been found in various applications in materials and medical science, including non-invasive bioimaging, molecular sensing, photovoltaics, photothermal therapy, optoelectronics, and laser optical recording. Dyes having BF_2 units have attracted attention due to their fluorescent properties, and stability can be directed by changing the structure of the ligand directly attached to the BF_2 unit, the chemical nature of the donor atom involved in the coordination, and the size of the chelate cycle formed. In this chapter, we discuss the photophysical and theoretical study of the mono- and bi-nuclear boron complexes. Furthermore, we studied the stimulus-responsive behaviour of the synthesized boranes, but among them, only the S-S-spacer-based boranes showed the ACQ behaviour in a mixture of Water/THF. As the percentage of water increased, the fluorescent intensity of the synthesized boranes gradually decreased.

Chapter 3 In the previous chapter, we discussed the synthesis of N-O chelated six-membered borane complexes and their photophysical and stimuli-responsive behavior. N-N chelated organoborane fluorophores have been extensively studied in comparison to their congeners. N-O chelated organoborane fluorophores have been limited. N-N bidentate organoborane complexes in a six-membered scaffold serve as the precursor to the synthesis of tri-coordinated boron cations. Our focus in this work is to study the reactivity of N-O bidentate-based boranes. To achieve our goal, we synthesized the 2-aminotropone ligands, which provide C_2NO core-stabilized boranes. All boranes are highly emissive in solution; their UV-visible and emission spectra were studied in DCM,

and their fluorescence lifetime was also recorded in DCM. Substituents present on the N atom play a decisive role in fluorescence decay time. Furthermore, we treated the synthesized boranes with TMS-OTf for the isolation of tri-coordinated boron cations. 2-aminotropone ligand (N-O, donor) based boranes facilitate the tetracoordinated boronium cation, stabilized by two units of 2-aminotropone ligand. This might happen due to the lack of steric hindrance and electronic stabilization. Moreover, N-N chelated boranes facilitate the boron cations because they provide favorable steric and electronic stabilization through strong electron donation from the chelated nitrogen atoms. In the next chapter, we will discuss the effect of N-N donor ligands

Chapter 4 In the previous chapter, we discussed the attempted synthesis of a boron cation using an N–O based ligand. However, this approach was unsuccessful, leading us to design and synthesize N–N based ligands in an effort to isolate the boron cation. Boron cations are strong Lewis acids because of the presence of a positive charge on boron. Due to the high reactivity of boron cations especially borenium cations their use in organic synthesis is limited. However, over the recent decades, the development of suitable supporting ligands, such as N-heterocyclic carbene (NHC), BDI, BODYPI, and formazanate, transformed them into efficient catalysts for the various transformation reactions including small molecule activations and strong covalent bonds such as B-H, C-H, and C-C bonds. The outline of this chapter includes the synthesis of symmetrical, unsymmetrical, and bis aminotroponiminate ligands and subsequently, they are treated with the $BF_3.OEt_2$ in the presence of triethyl amine as a base to facilitate the aminotroponiminate-based Difluoroboranes. All the ATI borane complexes are highly blue luminescent in the solution, and their fluorescence decay time was recorded in DCM. The observed decay time range was found to exist between 1.7 and 2.8 ns. Furthermore, boranes were treated with (TMS-OTf) trimethylsilyl triflate producing the tri-coordinated borenium cation. However, bis aminotroponiminate borane reacts with TMS-OTf

to facilitate the first water-stabilized bore(boro) nium cations in a unified molecular frame.

Chapter 5 In previous chapters, we discussed the synthesis and reactivity of the N, N, supported boranes, we moved to explore the N-heterocyclic olefin (NHO) supported borane chemistry. Initially, the borane adducts with traditional Lewis bases viz, amine and phosphine ligands, are exploited in hydroboration reactions in alkene and alkynes at room temperature. In contrast, they are used as hydride donor sources for H_2 production at low temperatures. In this present work, we took NHO, a counterpart of NHC, treated with $BH_3 \cdot SMe_2$ to form N-heterocyclic olefin borane adducts. Further, we tested the NHO-borane adduct reactivity with (malonic, oxalic, and phthalic acid) to facilitate the respective NHO-boryl oxalates at room temperature while NHC-boranes form NHC-boryl-oxalates at elevated temperature. NHO-boryl oxalates are well characterized by various spectroscopy techniques along with high-resolution mass spectrometry. Furthermore, we tested the reactivity of NHO-borane adduct with nitrogen-based triflates to facilitate the simple substituted boranes at ambient temperature.

Conclusions: Summarize the key findings of this work, which explores the rapidly evolving field of boron-based dyes, emphasizing their synthesis, photophysical study, and reactivity. Efficient methodologies were developed for the synthesis of dinucleating aminotroponiminate and Schiff base ligands, which serve as robust scaffolds for stabilizing the boron complexes. Several mono and binuclear boron complexes were successfully synthesized, thoroughly characterized, and their reactivity was tested with fluoride-loving reagents. We successfully synthesized a series of novel boron cations demonstrating the versatility of these ligand frameworks in main-group chemistry. Additionally, we synthesized a series of NHO-boryloxates by treating diacids with NHO-borane adduct.

This study underscores the significance of ligands ' role in boron chemistry and helps in isolating the discrete boron cations. Moving

forward, research will focus on refining ligand frameworks to enhance the stability of boron cations by providing sufficient steric and electronic neutrality to the electron-deficient center. The development of mono and bis(boronium) dications offers exciting possibilities for small-molecule activation, paving the way for sustainable and transition-metal-free catalytic methodologies.

Chapter 1

Introduction
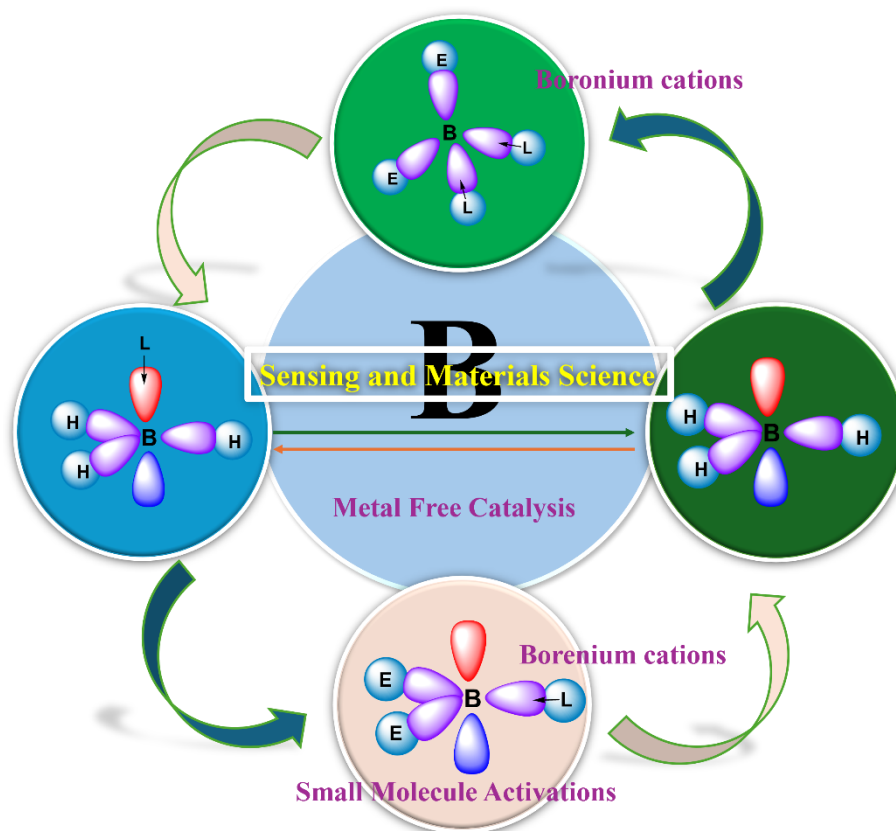
Background

Due to the presence of one vacant p-orbital, group 13 elements possess an inherent Lewis acidic character. Boron, aluminum, gallium, indium, and thallium, in their trivalent state with one vacant orbital, provide a unique electronic and reactivity profile. In recent years, the chemistry of group 13 elements has seen significant advancement from the classical domain of inorganic and organometallic compounds towards the reactive cationic species and advanced catalytic systems, along with the development of a new generation of functional materials. These prolongations are driven by the high demand for non-toxic, earth-abundant, and cost-effective alternatives replacement of transition metals in modern chemical transformations. In this context, boron-based complexes have played a pioneering role in growing the landscape of group 13 chemistry. The discovery of some boron compounds, such as boron hydrides, boronic acids, and carboranes, has been extensively listed, from organic transformation and molecular electronics to drug design and biological sensing materials.

Additionally, advances in the chemistry of higher congeners of boron, such as gallium and aluminum, open new horizons for the synthesis of cationic or low-valent species with excellent reactivity. Group 13 elements, one of the most abundant on Earth's crust, represent themselves as the best candidate for the sustainable main group chemistry. Moreover, in the stabilization of cationic complexes of group 13 elements, highly bulky, judicious, and trailered ligand design is required. To fulfill all these requirements, strong chelating ligands are needed. Ligands such as N-N and N-O donors (Schiff bases, Salen, and Bi-diketiminates, aminotroponiminate) play a crucial role in the isolation of discrete reactive complexes of group 13 elements. These complexes are promising candidates for the electrophilic activation of small molecules (H_2, CO, CO_2, N_2), ring opening, polymerization reactions, and participation in various organic transformation reactions. The progress of the main group chemistry from neutral material to well-defined cationic species has the potential to replace transition metal-

based catalysts up to a remarkable extent. In this context, the main group cations serve as important tools for investigating new reaction paradigms, particularly reserved for transition metals, exploring cooperative catalysis, frustrated Lewis pair (FLP) chemistry, and metal-free activation processes.

In summary, the advancement of the group 13 element-based materials and their cationic complexes represents a dynamic frontier domain in contemporary chemistry. Group 13 chemistry, bridging between materials science and catalysis through well-tailored ligand design, and with advanced molecular engineering, their chemistry continues to contribute to sustainable synthetic methodologies and transition metal-free catalytic systems.

1.1 General Introduction

Development of boron-based functional materials has gained significant attention in the field of materials and medical sciences. Due to their high photostability, they are utilized in bio-imaging and therapeutic applications.*[1-2]* Notably, the electron-deficient species of boron derived from parent borane complexes (boron halides and boron hydride $L(BX)_2$, or L (BX) where X stands for H, halides, and L stands for ligands exhibit transition metal-like reactivity, especially in unconventional or low oxidation states that were once considered unstable. *[3]* The introduction of bulky ligands has played a crucial role in kinetically stabilizing these reactive species, enabling their isolation and storage under ambient conditions. *[4]* These breakthroughs have greatly expanded the reactivity of p-block metals, redefining traditional concepts in main-group chemistry.

1.1.1 Role of boron in dye chemistry

Highly emissive organic π-conjugate dyes have drawn tremendous attention due to their potential application in sensors, bioimages, organic light-emitting diodes, organic solid-state lasers, and many more. [] Recent research has witnessed that the incorporation of BF_2 units into

the conjugate organic motif provides reasonable success in the synthesis of new functional materials with excellent photophysical and electronic properties. *[5-9]* Generally, based on the coordination number, boron-based fluorescent compounds have been divided into two classes: i) tri-coordinated boron dyes, ii) tetra-coordinated boron compounds.
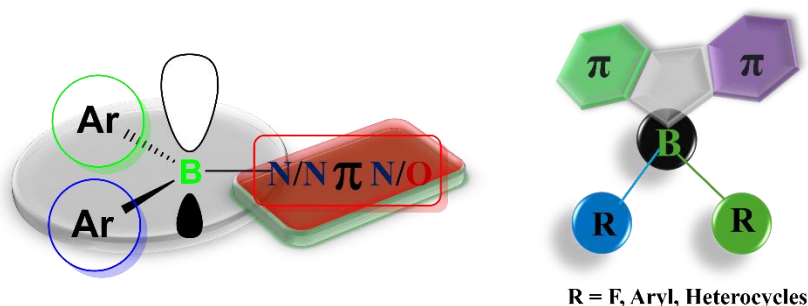
Figure 1.1 Schematic representation of tri-coordinated boron (left), tetra-coordinated boron compounds (right).

1.1.2 Tricoordinated boranes

Tricoordinate boron compounds are sp^2 hybridized and adopt a trigonal planar structure with a vacant pz orbital aligned perpendicular to the trigonal plane. The pz orbital on the central boron atom makes these compounds strong π acceptors, which helps in the delocalization of electrons when conjugated to an adjacent organic π system. Vacant orbitals on boron atoms in tricoordinate boranes are easily attacked by nucleophiles like water, which disturb the delocalization (conjugation) with the adjacent organic π moieties. To prevent the attack of nucleophiles on boron bulky ortho-substituted aryl groups such as duryl (2,3,5,6-tetramethylphenyl), mesityl (2,4,6-trimethylphenyl), fluoromesityl (2,4,6-tris(trifluoromethyl)phenyl), or tripyl (2,4,6-triisopropylphenyl), bulky ortho-substituted aryl groups are introduced. The bulky groups not only prevent the boron from moisture *[10,11]* but also prevent the intermolecular stacking and interaction in solid states, which results in strong fluorescence in the solution state and solid state as well. Cyanide and fluoride are smaller in size and can easily attack triaryl boranes, making this class of compounds selective sensors for F and CN. Moreover, from sensing, triaryl boranes have been used as

prominent candidates for fluorescent indicators *[11,12]* in bioimaging, nonlinear optical materials, efficient fluorescent emitters, and charge transport materials in OLEDs.

1.1.3 Tetra-coordinate boranes

Tetra-coordinate boron complexes exhibit higher stability than their tri-coordinated counterparts. Due to the coordination saturation in tetracoordinated boron compounds, which confers high chemical stability and rigidity, leading to higher fluorescence quantum yields and photostability. Therefore, considerable attention has been given to the tetracoordinated molecular design, which has been widely used in photo-responsive materials, bioimaging, sensors, and optoelectronics, including OLEDs. *[13-18]* In four coordinated boron complexes, the chelate ligands are mostly monoanionic and produce charge-neutral boron complexes. Lewis' acidic nature of the boron atom plays a vital role in stabilizing the anionic chelate ligand by making covalent bonds with the chelate and dissipating the negative charge on the ligand. As a result, chelation with boron imparts complete delocalization of electrons with π systems. Mostly, the lowest unoccupied molecular orbitals (LUMO) in four-coordinate boron complexes are generally occupied on the pi conjugate chelating moieties, while other frontier molecular orbitals, which are the highest occupied molecular orbital (HOMO) are occupied either on the chelating moieties or on the R group (Figure 1.1). Transitions such as π-π of the chelate moieties or charge transfer from the R group to the chelate ligands are responsible for the luminescent properties of this class of compounds. The variation of the R group brings a significant change in the photophysical properties. Four-coordinate luminescent boron compounds are categorized based on the donor atoms associated with the chelate ligands, namely, i) O-O, chelate boron complexes, ii) N-O, chelate boron complexes, iii) N-N, chelate boron complexes, and iv) O-S chelated boron complexes, and some other coordination types are known, such as N-C and O-C.
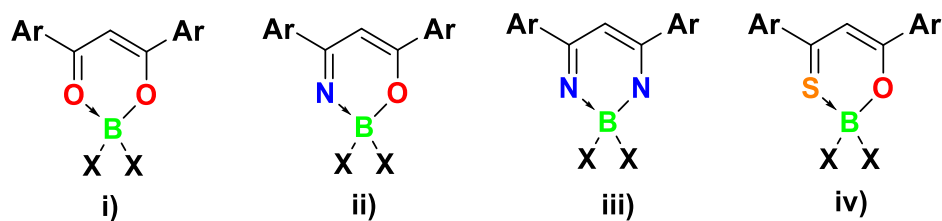
Figure 1.2 Tetra-coordinated boranes with variable donor atoms.

1.2.1 N, N donor ligands

In modern-day chemistry, ligands play a crucial role in the synthesis and isolation of long-sought intermediates and highly reactive species. N, N donor ligands are among the most studied ligands in the new age organometallic and coordination chemistry, because of their unique association with easy synthetic reach, following a facile but highly modular condensation protocol. The steric and electronic effects of such kinds of ligands can easily be tuned by changing the substituents on hetero atoms and their molecular framework. They have the potential to stabilize a wide range of metal ions, including s, p, d, and f blocks across the periodic table. In the variable oxidation states, metal ions have been shown to have better catalytic activity, selectivity, and stability in various processes, including hydrogenation, olefin polymerization, and cross-coupling reactions. Focusing on N donor ligand chemistry with the early transition metals provides breakthroughs, including the isolation of a plethora of highly reactive metal-ligand multiple bonds. For example, BDI is a class of NN donor ligands, with the help of this main group, chemists have isolated the metal-metal bonds in which the main group elements are present in different oxidation states, like transition metals. Nonetheless, they can stabilize multiple-bonded main-group complexes in low oxidation states. *[19-21]*

N donor ligands are sub-characterized into different classes as BDI, anilido, aminotroponimine, and priso (amidinates and guadinates) ligands. These ligands play a vital role in replacing the most expensive transition metal-based catalysts with cheap, earth-abundant, non-toxic main group elements. Over the recent decades, the main group elements

have been adept at catalyzing a host of various transformations like inter- and intra-hydro functionalization of unsaturated carbon-carbon bonds and dehydrogenative coupling. Main group elements also have the potential to activate small molecules like transition metal complexes, and this might be greatly influenced by the ligands. *[22-24]*

○ = possible site for tuning
Ar = aryl or alkyl froup
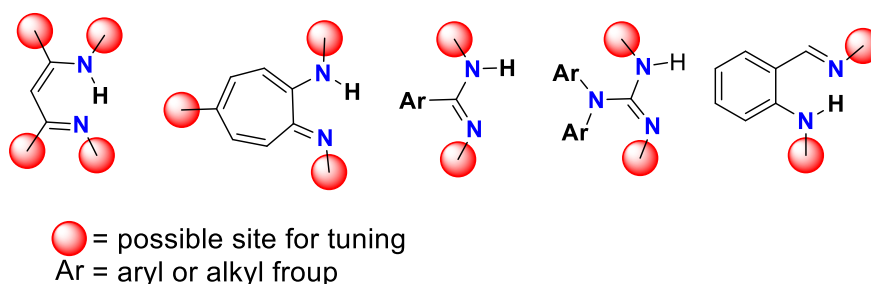
Figure 1.3 Schematic representation of N, N mono-anionic bidentate ligand.

Since the β ketoiminate, anilido, and priso (amidinates and gudadinate) ligands allow limited electronic and steric tunability, and their structural motif are (for example, in β-ketoiminate synthesis, the acetyl acetone motif amines) also pre-decided, so we cannot change substituents on carbon atoms after complexation according to our requirements/ application demands. Aminotroponimines (ATIs) allow the electronic and steric tunability of the nitrogen atoms *[25]* along with the C_7 backbone of carbon atoms. Interestingly, their electronic properties can be tuned after complex formations on the C_7 backbone. **Figure 1.4** shows the possible variable sites in aminotroponimine and β-ketoimine ligands. The versatile adaptability provides better stability to the highly reactive main group and transition metal complexes providing the valuable plaforms in organometallic chemistry, small molecule activations and catalysis.
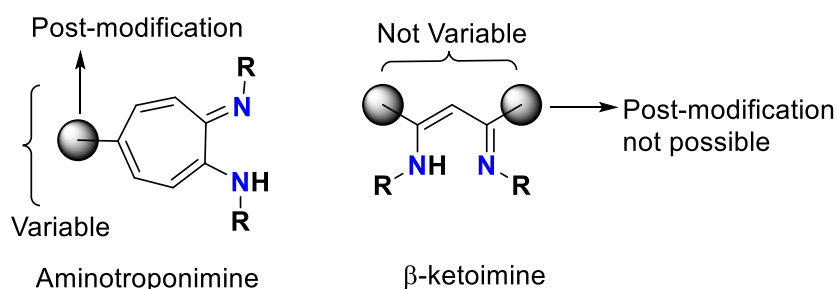
Figure 1.4 Possible electronic tunability in ATI and BDI ligand.

1.2.2 Aminotroponiminates (ATIs) ligands

Aminotroponiminates (ATIs) are bidentate monoanionic ligands with N, N-binding sites and a rigid, planar, unsaturated, C_7-ring as ligand backbone. Recent discoveries show that the ATI ligand backbone can play a vital role in ligand-centered reactivity, redox reaction, and coordination chemistry. Having one imino and one amino functionality acts as a bridge between the well-established phenylenediamine and diazadiene ligand scaffolds. **Figure 1.5** ATIs and β-diketiminates are structurally related to each other only they can be distinguished from these ligands by the presence of C_7 rigid backbone, which is a special structural feature of the ATIs ligand. ATIs have found a broad range of applications in stabilizing cationic group 13 complexes, *[26,27]* the synthesis of hypo- and hypervalent group 14 compounds, and in an investigation of spin delocalization of first-row-transition metal complexes.
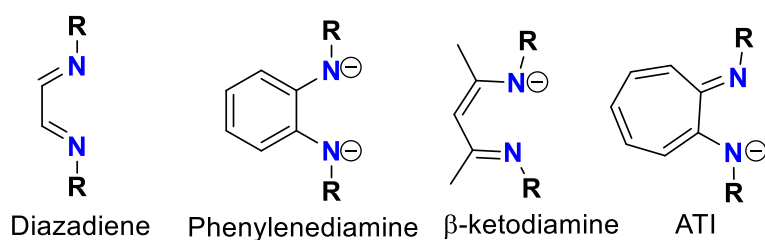
Figure 1.5 Bi-dentate N, N type neutral, monoanionic, and dianionic ligands.

In the beginning, ATIs have been exploited as molecules: i) monoanionic, ii) N, N-bidentate, iii)redox innocent under reducing environment, iv) chemically inert in C_7 backbone and spectator ligands (exception: chiral induction). Moreover, this traditional perception of the ATI ligands has recently been challenged. This is due to the chemistry of the C_7 backbone involving insights. Modern chemistry has revealed the potential of the ATI ligand to play an effective role in coordination chemistry, ligand cooperativity, and redox reactions.

1.2.3 Synthesis of (ATIs) ligand

The first introduction of the NR group on tropolone depends on the nucleophilicity of amines, bulky amines (Dipp and Mes) are less nucleophilic, for introduction need a Pd-based catalyst *[28]* while more nucleophilic amines tertbutyl and isopropyl amine, are introduced without any catalyst. *[29]* Further, the resulting aminotropones are commonly transformed into desired ATI ligands by the addition of Meerwein salt and the desired amine in a one-pot reaction.
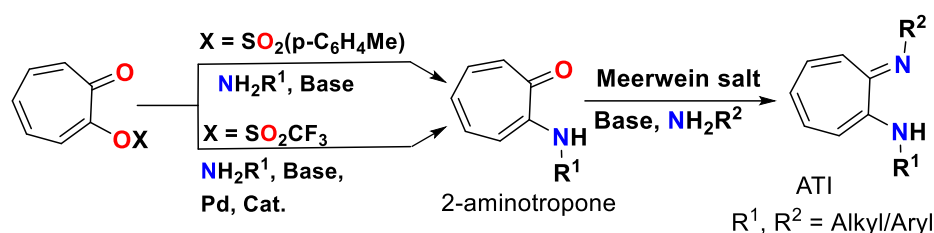
Scheme 1.1 Synthetic protocol of ATI ligands

1.2.4 Coordination modes of ATI ligands
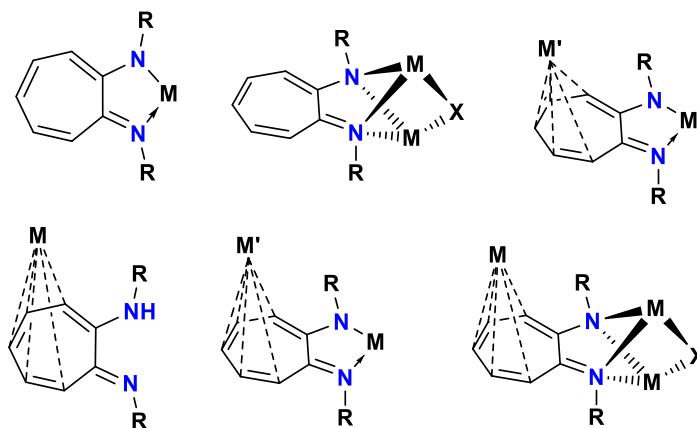
Figure 1.6 General representation of coordination modes of ATI ligands.

The coordination chemistry of ATI ligands is distinguished by their unique coordination modes, which vary in neutral and anionic conditions. This flexibility of the ATI ligands makes them unique from the other known monoanionic bidentate ligands; it provides N-M, M-C, and π-π (C-C) types of interactions across the periodic table (semi) metal complexes.*[30]*

1.2.5 Role of N, N donor ligands in boron-based dye

Dipyrromethene BF$_2$ complexes (BODIPY) dyes are very famous boron complex *[31,32]* supported by N-N donor ligands **Figure 1.7** This dye has two nitrogen donor atoms; one can form a covalent bond by sharing one electron, while the other nitrogen atom engages with the boron atom through a coordinate bond by donating one lone pair of electrons in the empty pz orbital present on the boron atom. Dyes belonging to the BODIPY family have excellent photostability, better spectroscopic properties such as narrow absorption and emission bands, high fluorescence quantum yields, high molar extinction coefficients, strong chemical and photochemical stability in solution and solid state.
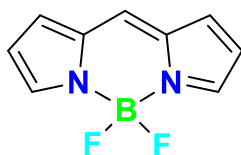
Figure 1.7 General representation of BODIPY dye.

Despite these excellent characteristics, BODIPY dyes have been used to study up to a significant extent in fluorescent sensors, photodynamic therapy, artificial light harvesting materials, as well as molecular photonic wires and sensitizer for solar cells. Moreover, in general, BODIPY dyes are weakly emissive in solid states, which restricts their optoelectronic applications. Due to the presence of strong π-π interactions in solid states, in BODYPI dyes leads *[33,34]* to luminescence quenching, formation of excimers and exciplexes, small Stokes shifts, and an increase in self-absorption of its fluorescence. Many research group have made their efforts to synthesize modified BODYPI fluorophore with excellent Stockes shift and better electroluminescent behaviours. For reference, highly emissive BODYPIs in solid state have been achieved by introducing aryl groups on classical BODYPI cores. *[35,36]*

Wang and co-workers reported the N-N chelated tetra-coordinated boron compounds **1-3 Figure 1.8** The emission spectra of complexes **1-3** have emission maxima at 475 nm for 7-azaindoyl (**1**), 516 nm for indolyl (**2**), and 445 nm for benzoimidazolyl (**3**) derivatives, revel that emission maxima can be tuned in these complexes by changing the location of the N-heteroatom in the chelating ring scaffolds. *[37,38]* To study the substituent effect on the luminescence properties, the electron-donating and methoxy and the electron-withdrawing chloro/fluoro atom were introduced on the 5-position of indole in complex **2**.
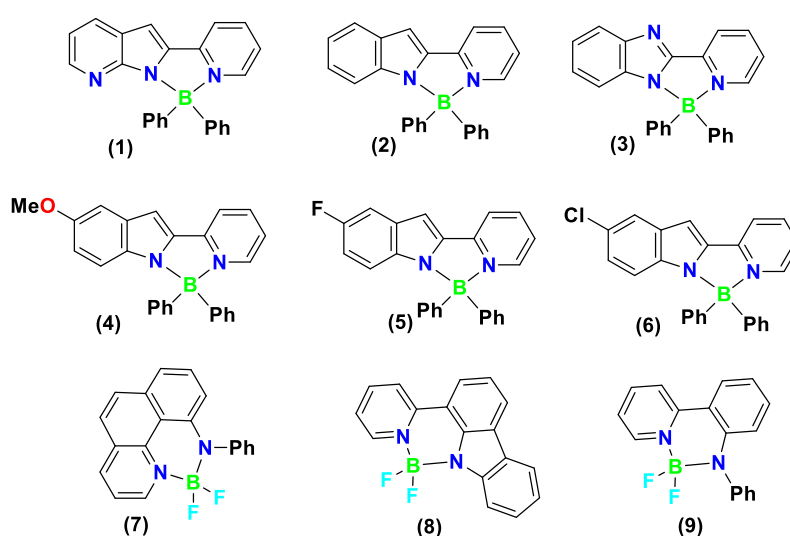
Figure 1.8 N-N coordinated boron complexes **1-9**.

The isolated compounds **4**, **5**, and **6** exhibit emission spectra at 532, 490, and 487 nm, respectively *[39]*. These results indicate that electron-donating groups shift the emission maxima to the red region while electron-withdrawing groups shift the emission maxima towards the blue region. Piers and his colleagues reported the six-membered N-N chelated boron difluoride complex **7-9** in anilido-pyridine *[40]* ligand scaffolds, which exhibit high photochemical stability and large Stokes shifts. Notably, these complexes have high fluorescence quantum yields in both solution and the solid state. This is due to the rigid and planar structure of the iminopyrrolidine Schiff base with the BF_2 unit; as a result, the molecular vibrations and rotations were restricted and contributed more to the radiative transitions.
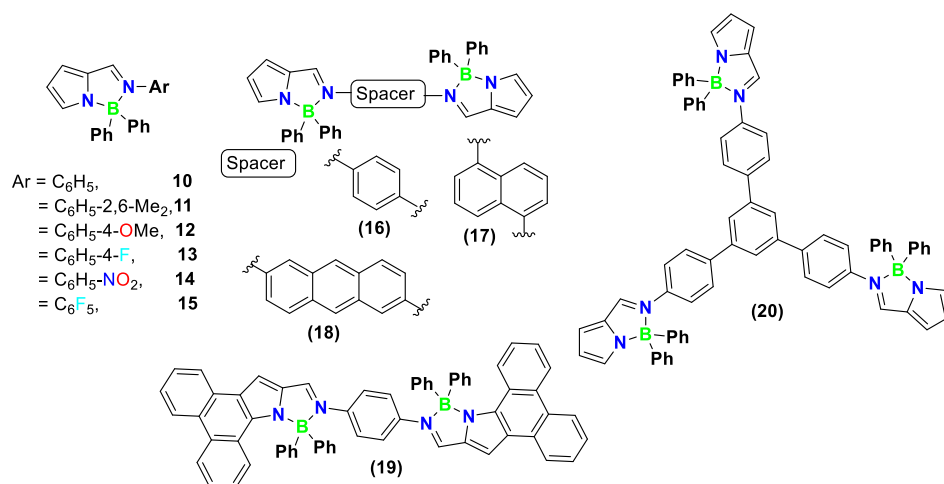
Figure 1.9 N, N chelated four-coordinate boron dyes.

Gomes and his colleagues synthesized a series of novel fluorescent boron complexes *[41,42]* containing 2-(N-aryl) formiminopyrrolyl ligands. Mononuclear boron compounds **10-15** exhibit emission **Figure 1.9** wavelengths ranging from blue to green by varying the steric and electronic environment of the N-aryl group. Moreover, they extended their study to the synthesis and characterization of bi- and tri-nuclear boron complexes **16-20** by introducing various pi conjugate spacers, and their application in fluorophore chemistry. The resulting bi-and tri-nuclear boron complexes were found to be excellently fluorescent, and their emission wavelength could be easily tuned from short wavelength to longer wavelength depending *[43]* on the length of π conjugation units. Bi-nuclear borane complexes were used in light-emitting diodes (OLEDs) without any external dopant. Recently, the same group reported the 2-(*N*-aryl) formiminophenanthro[9,10-c] pyrrolyl supported boron compound **19** with extended pi-conjugation over the pyrrole molecules and exhibited orange luminescence in solution as well as the solid state.

Gilroy and Otten had synthesized a series of boron complexes in the formazanate scaffolds **21-29**, which exhibited *[44,45]*pleasing luminescent and electrochemical properties **Figure 1.10**. A study of formazanate boron complexes revealed that the introduction of an electron-withdrawing group on the ligand core unit leads to an increase

in reduction potential and red-shifted absorption maxima along with emission maxima. Gilroy and his colleagues further studied the effect of extended π-conjugations in the formazanate boron complexes, and their study revealed that as the length of conjugation increases, the absorption and emission maxima shift towards the red region. Notably, complexes with extended π-conjugation fluorescence quantum yield 10-fold greater than complexes lacking the extended conjugations **24-26**.

R = H, CN, OMe (**21-23**) R^1 = Ph, CN, NO$_2$ (**24-26**) R^2 = Ph, Np, NO$_2$ (**27-29**)
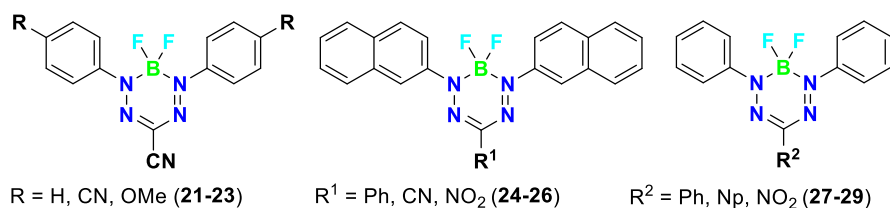
Figure 1.10 Formazanate stabilized boron complexes.

Very recent work of the Gilroy group synthesized BF$_2$-formazanate dyes **27-29** that exhibited electroluminescent (ECL) properties along with the AIEE phenomenon and were used as fluorescent cell-imaging agents; further, these complexes were used as monomers for the synthesis of formazanate-based polymeric boron dyes.*[46-48]*

1.2.6 N, O chelated boron complexes

Although BODYPI and BOPHY Dyes have tremendous applications in medicinal and materials science. But they have certain limitations, like being small, Stockes shift leading to low photostability, along with the low fluorescence quantum yields. To overcome these problems, scientists try to move to other alternative candidates. In this context, salicylaldimine-based boron dyes prove themselves as a next-generation photo-functional material. Mainly, N-O ligands are derived from salicylaldimine, oxime, or hydroxamic acid derivatives. *[49-51]* These ligands coordinated with the Lewis acidic boron center to facilitate the chelated boron complexes with unique electronic architectures. These ligands not only provide easy synthetic modularity and flexibility but also facilitate the alternative root for the formation of the donor-acceptor architectures that help in the intramolecular charge transfer (ICT), resulting in red-shifted absorption and emission maxima and enhanced

solvatochromic properties. Interestingly, the incorporation of an oxygen atom brings additional stability to the boron center and enhances stimulus-responsive luminescence via dynamic B-O interactions. *[52-55]*
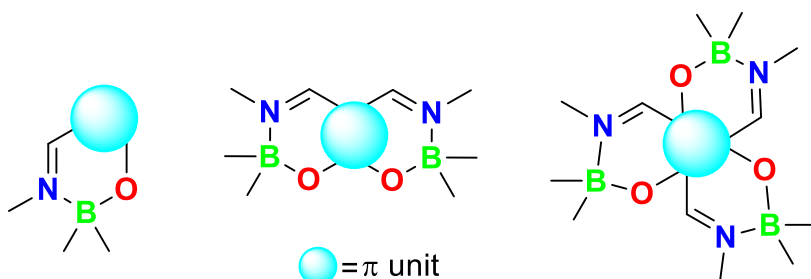
Figure 1.11 General representation of N-O chelated boron complexes.

Wang and his team isolated a series of 8-hydroxyquinolinate boron complexes with the general formula (QBR$_2$) Q stands for the 8-hydroxyquinolinate moiety. These boron complexes show greenish-blue emission with an emission wavelength of 495-500 nm, and their utility was also investigated in OLED as emitters and electron transporters membrane. *[56-58]* Additionally, they reported a series of linear and star-shaped multinuclear boron complexes in hydroxyquinolinate scaffolds to investigate the effect of π-conjugation along with the mutual effect of multiple boron centers. All the synthesized complexes exhibited emission maxima lying between 528-542 nm with high thermal stability.
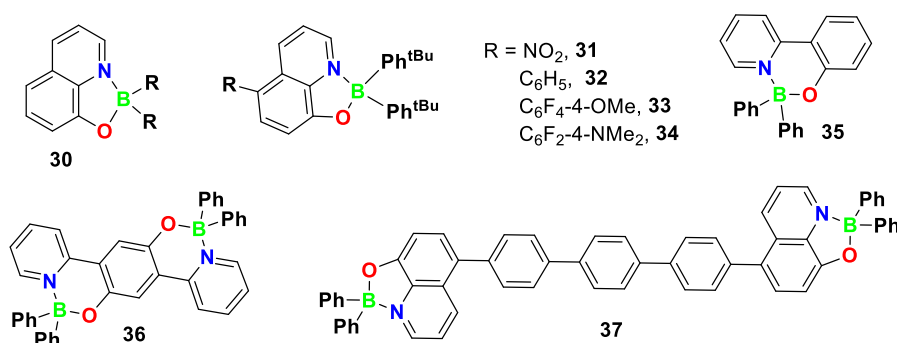
Figure 1.12 N-O chelated boron complexes.

Later, Jäkle and his coworkers reported the quinolate ligand-based boron dyes. They investigated the subtle effect of substituents present on the 5th position. Interestingly, they observed that the electron-withdrawing group shifted the emission maxima, then its non-substituted quinolate counterpart. *[59-65]* On the other hand, electron electron-releasing group at the 5th position shifted the emission and absorption maxima to the red region. Wang and his team *[66-68]* were able to isolate the binuclear ladder-type π-conjugated boron dyes. Emission maxima of these dyes were observed in the range from 584-604 nm, which was about 100 nm red-shifted from their mononuclear counterparts. Binuclear ladder dyes *[70]* exhibited high thermal stability and gave better performance in OLEDs in comparison to their mononuclear boron dyes.

Ziessel, Ulrich, and their coworkers *[71]* have developed a new class of N-O chelate boron complexes **38-41** known as boranils by the complexation of anils (aniline-imine) with boron trifluoride or BPh3. They observed that the spectroscopic properties of these were strongly dictated by the substituents present on the para positions of the amine and phenolic side of the aromatic ring. Later, they found that these boronil dyes can be utilized as a better candidate for bioconjugations to proteins like bovine serum albumin (BSA) in biological *[72-76]* systems. Recently, the Krishnan group reported salicylaldimine-based binuclear boron complexes **44**. These complexes were highly thermally stable and exhibited the emission maxima that ranged from 460 to 494 nm. A very similar class of boronil dyes, **42-43,** was reported by Muthusubramanian, and they explored their application in the detection of hydrogen peroxide. *[77]*
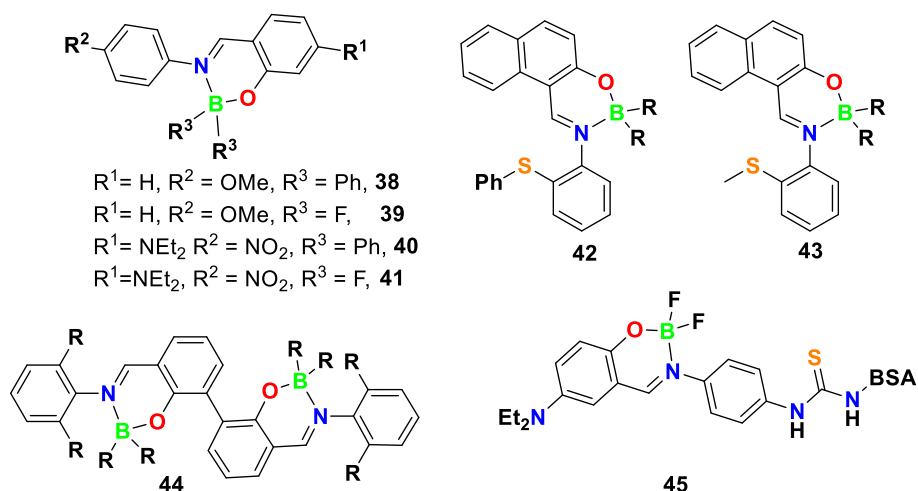
Figure 1.13 N-O chelated boronil dyes **38-45**.

Yaushiro, Kubota, M. Matsui, and their colleagues *[78]* reported the pyrazine and thiazole boron dyes, including a β-ketoiminate ligand that exhibited a large Stokes shift, aggregation-induced emission behavior, along with solid-state luminescence enhancements. Furthermore, they successfully reported the solid-state emissive dyes, AIEE-responsive pyrimidine mono and binuclear boron complexes bearing the BDI ligand. They found that pyrimidine boron dyes bearing the phenyl groups show more intense luminescence than their BF$_2$ counterparts. Pyrimidine-based binuclear boron complexes make a system such as D-π-A that leads to their emission in the NIR region in the solid state.*[79-81]*
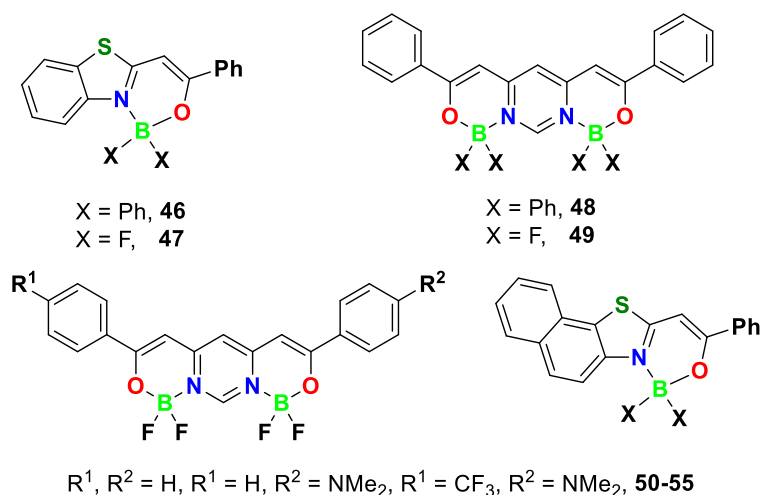
Figure 1.14 Ketoiminate-based boron dyes

A recent study of boron dihalides and their heavier congeners, dihalide complexes, chelated with N-N and N-O donor ligands, serves as a better precursor for the synthesis of cationic species of group 13 elements, along with excellent spectroscopic properties like high photochemical stability, high fluorescence quantum yields. These intrinsic properties of dyes make them versatile candidates for broad application in the field of medicinal and materials science.

1.3 Boron cations

Boron cations are mainly classified into three categories on the basis of coordination number. The coordination number of boron cations is two; then it is known as borinium, three, then it is known as borenium, and the coordination number of mono-boron cation is four, then it is known as boronium cation. The hybridization of the boron atom in the borinium cation is sp-hybridized and forms a linear geometry with 2e-donor electrons; in borenium, it forms a trigonal planar geometry. The electronic demands in borenium cations are compensated by the pi-donation of ligands into the vacant p-orbital. Boronium cations are more stable than the borinium and borenium cations because their octets are complete. The chemistry of the borenium cation has been explored more because its reactivity lies between highly reactive borinium and electronically saturated boronium cations. Hence, it is used in various metal-free catalysis processes. *[82-87]*
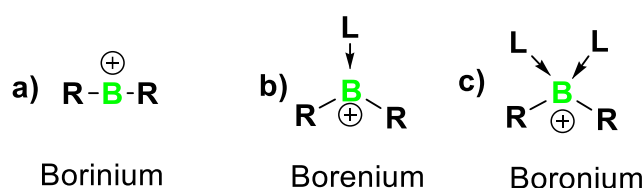
Figure 1.15 General representation of boron cations

1.3.1 Borinium cations (CN: 2)

Dicoordinated boron cations are highly reactive due to the high positive charge. lack of sufficient steric hindrance, low coordination, and prone to form neutral tricoordinate boron compounds with anionic ligands. The first stable, condensed phase borenium cation was not reported until

1982, isolation of borinium cation stabilized by bis(diisopropylamido) ligand marking a considerable *[88-90]* milestone in the low-coordinate boron chemistry. The first evidence of a structurally characterized moiety was an [AlBr4]⁻ salt, which holds the electrophilic boron center. This low-coordinate boron compound was stabilized by a tetramethylpiperidino ligand. These reports motivated the generations of a variety of bis(amido) borenium cations with various amido-substituted ligands or counter ions. Unfortunately, only the highly bulky benzyl-tert-butyl-amido ligand supported dicoordinated borinium cation has been characterized by X-ray crystallography. *[91-94]*
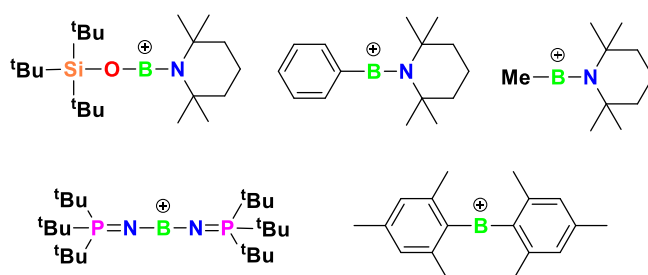
Figure 1.16 Previously reported di-coordinated boron cations

Despite several reports on borenium cations in the mid-1980s, research around condensed phase dicoordinated boron cations had been somehow neglected until the recent report by Stephan and his colleagues, who reported the extended borinium cation. *[93]* They isolated the extended borenium cation by treating two equivalents of phosphinimide ligand with $BH_3 \cdot SMe_2$, and this leads to the formation of disubstituted borane. Further, this borane was treated with trityl salt and facilitated the borinium ion. This borenium cation has two bulky tri-tert-butylphosphinimide ligands, which dictate the geometry and electronic properties of the borinium ion. The bulky phosphinimide ligand sterically protects the Lewis acidic boron atom and allows the delocalization of the positive charge on the adjacent nitrogen and phosphorus atoms. *[95,96]*

1.3.1.1 Borenium cations (CN: 3)

Reports on well-defined tricoordinate borenium cations have emerged like those of their dicoordinated counterparts, dicoordinated borenium

cations. *[97-100]* Only three examples of borenium cations had structural evidence before 1985. In each case, bulky bases are capable of electronic stabilization, but the five-membered ring system containing boron as a heteroatom was incapable of achieving the linear geometry which are essential for boron cations for the electronic stabilizations. Since then, very limited examples of tricoordinate borenium have been listed in **Figure 1.17**.
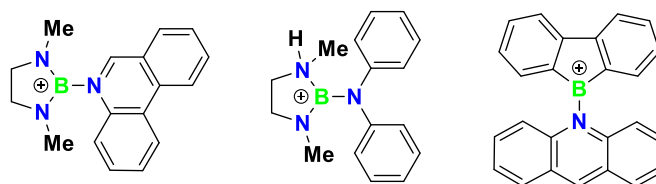
Figure 1.17 Borenium cations.

Jutzi and his colleagues isolated *[100,101]*the two novel tricoordinate borenium **Figure 1.18** cations from the reaction with dichloro(η^1-pentamethylcyclopentadienyl) borane with bulky bases such as acridine and phenanthridine, respectively. Formation of these salts was confirmed by the ^{11}BNMR, the signal appeared for the acridine ligated borenium cation was 32.8 ppm, while the phenanthridine ligated borenium [11]B signal appeared at 30.9 ppm.
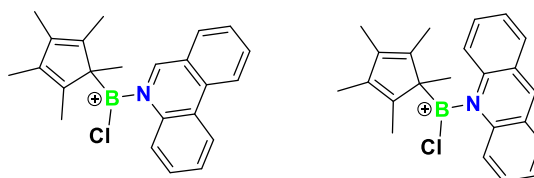
Figure 1.18 Cp* supported borenium cations.

BDI ligands are proving themselves to be a very effective tool for the support of a wide range of elements across the periodic table in diverse coordination modes and oxidation states. A. H. Cowley and co-workers reported the first X-ray crystal structure for a β-diketiminate-supported boron cation in 2004. *[102]*They isolated the borenium cation from the neutral tetracoordinated [(HC(CMe)$_2$(NAr)$_2$]BPhCl complexes. **Figure 1.19** They treated the boron complex with AlCl$_3$ leads to the formation of tricoordinate borenium cation supported by [Al$_2$Cl$_7$]⁻. Later, a similar

51

tricoordinate borenium cation was also reported by Cowley and co-workers in modified BDI ligand scaffolds. *[103]* In the same years, Piers and co-workers isolated the tricoordinate borenium cations supported by BODIPY dye. *[104]* Recently, our group reported the bis-borenium cation stabilized by the bis-BDI ligand scaffolds. Gilroy and his colleagues reported that the formazanate ligand stabilized a highly fluorescent borenium cation. *[105, 106]*
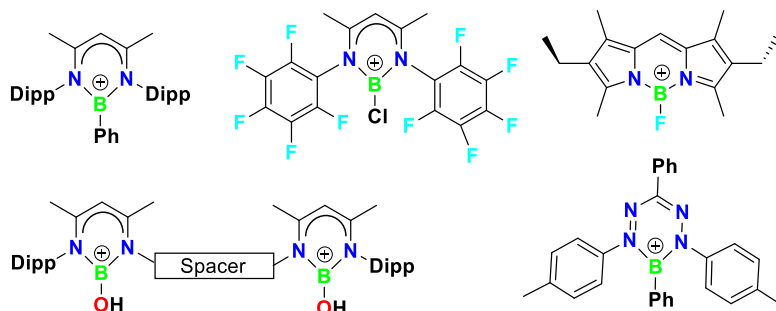
Figure 1.19 N, N-coordinated borenium cations in a six-membered ring scaffold.

1.3.1.2 N, O chelated borenium cations

N, O chelated boron cation chemistry is not much explored because N, O ligands are unable to fulfill the electronic and steric demands of cationic species. Consequently, the isolation and characterization of such complexes are more challenging under standard conditions. A recent study reveals that N, O ligands can stabilize the highly reactive boron cations through extended π-conjugation and incorporation of bulky bases such as NHC and bulky non-coordination anions.
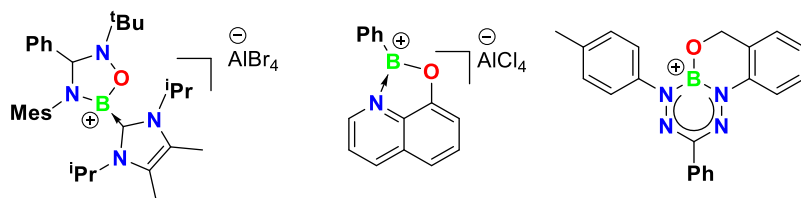
Figure 1.20 N, O coordinated borenium cations.

Ingelson and coworkers reported the first N-O chelated tricoordinate boron cations *[107]* in 2014 **Figure 1.20** They treated the 8-hydroxyaminoquinoline with the BPhCl$_2$ in the presence of a mild base,

and subsequently, this complex was treated with Lewis acid AlCl$_3$, leading to the formation of a tricoordinate boron cation stabilized by the 8-hydroxyaminoquinoline ligand scaffold. Synthesized borenium cation is highly chlorophilic in nature because significant interactions were observed between cationic species with its counter anion [AlCl$_4$⁻]. Additionally, L. Kong and colleagues also reported the N-O stabilized borenium cation in 2022. *[108]* They isolate the boron cation from terminal iminoborane [MesN=B·IPr$_2$Me$_2$][AlBr$_4$] via 3+2 addition reaction with one equiv. of N-tert-butyl-alpha-phenylnitrone with excellent 90% yields. Recently, Gilroy and co-workers reported formazanate-based tricoordinate borenium cations. *[109]* Notably, its counter neutral formazanate BF boranes were non-emissive in the solution state, but derived borenium ions were highly fluorescent in the solution state, and absorption maxima shifted from 530 nm to 650 nm in borenium cations. They also tested the sensing behaviour, and the borenium cation treated with the [nBu$_4$N][SiPh$_3$F$_2$], and it abstracts the F⁻ and exhibits the near-linear turn-off response. The absorption maxima, which appeared at 650 nm, disappeared due to the formation of a neutral tetracoordinate boron complex **Figure 1.20**.

1.3.1.3 Boronium cations (CN: 4)

Boronium cations are tetracoordinate species and have undoubtedly gained the most attention due to their relative stability, which arises due to the filled octet and complete coordination sphere. In general, boronium cations have two covalently bound ligands and two other sigma-donating ligands that serve to partially occupy the vacant orbital on the boron atoms. The isosteric correlation between the boronium ions and the secondary ammonium ion was conceptualized by Davis and his coworkers *[110]* to prepare the boronium analogue of the conjugate acid of the biologically active bicyclic tropane ring 8-azabicyclo [3.2.1] octane (structural elements of several neuroactive compounds; atropine). **Figure 1.21**. They prepared the borenium cation in one-step, one-pot synthesis from the bromoborane dimethylsufoxide adduct and homopiperazine at room temperature.
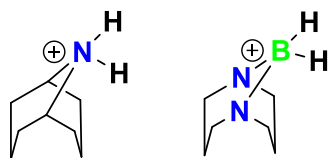
Figure 1.21 Conjugate acid of neuroactive amine and boronium cation.

Wagner and his co-workers have reported several borenium cations **Figure 1.22**, ferrocene-based 2,2'-bipyridylboronium salts) and investigated their utility as novel charge acceptors in various charge transfer complexes. The first boronium cation of ferrocene supported was prepared by treating the ferrocene core functionalized boranes with various bulky N-donor bases. *[111]* Further, they extended their study and functionalized the ferrocene for the synthesis of binuclear boronium cations by following the same standard reaction protocol. All boron cations were from the reaction mixtures as solid precipitates. ^{11}BNMR broad signals appeared for each salt, ranging from (δ = 6 to 11 ppm). The electrochemical study of these boronium cations suggested that they are suitable compounds for making nonlinear optical materials and amperometric biosensors.
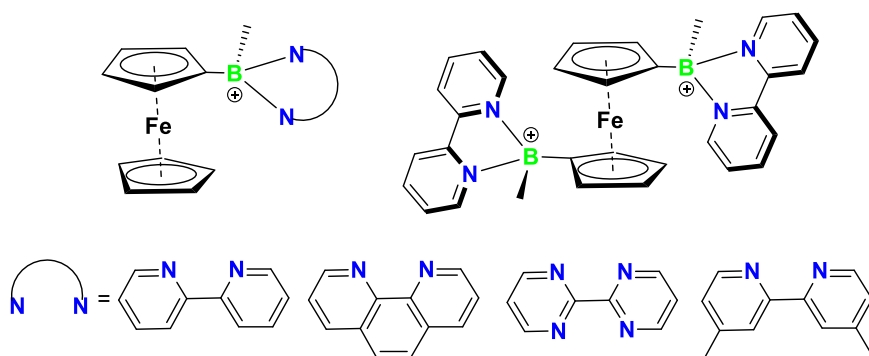
Figure 1.22 Ferrocene-stabilized boronium cations.

Recently, Clyburne and co-workers isolated a series of boronium cations **Figure 1.23** through the chloroboration reaction analogous to the hydroboration reactions, and the isolated cations can undergo facile addition across a C=O or C=N bond. *[112-115]* The reason behind using the bulky ligand was expected to provide steric bulk and π stabilization. Jutzi and co-workers isolated the pentamethylcyclopentadienyl-

coordinated boronium cations **Figure 1.23**. They treated the $C_{p*}BCl_2$ with a bidentate nitrogen donor ligand, bipyridine, and phenanthrene led to the formation of boronium cations.
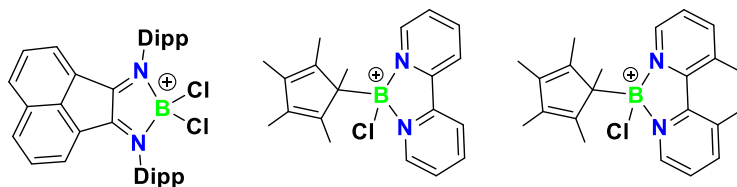
Figure 1.23 N, N-coordinated boronium cations.

K. Suenaga and his co-workers reported a series of luminescent boronium cations *[116]* supported by the ketoiminate ligands. They studied the effect of counteranions on the photophysical properties of synthesized boronium cations. they found that boronium cations with $[PF_6]^-$ counter anions exhibited fluorescence properties in both solid and solution phases, along with the stimulus-responsive behaviour. In 2025, Gilroy and his co-workers reported highly fluorescent boronium cations supported *[117]*by the tridentate acyl pyridylhydrazone ligands. non-emissive boron heterocycles based on π-conjugated *N*-acyl pyridylhydrazones with N,N′,N″ coordinated boranes were treated with Bronsted acid, leading to the formation of fluorescent boronium cations.

R = Me, Ph   X = Cl, PF_6^- , OTF
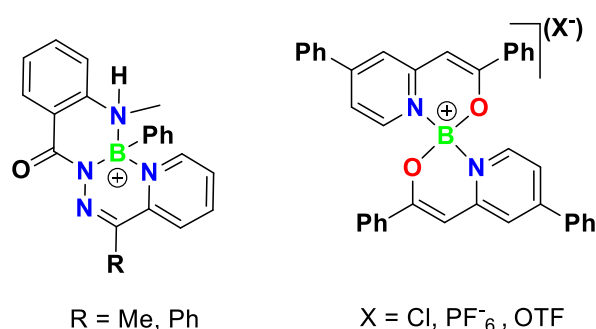
Figure 1.24 Fluorescent boronium cations.

1.4 N-heterocyclic carbenes (NHCs)

The first stable carbene (NHC) was discovered in 1991 by Arduengo and his coworkers *[118]* through the deprotonation of an imidazolium cation. NHCs are divalent carbon atoms, a singlet carbene attached directly to at least one nitrogen atom within a heterocyclic ring. Their

role as lone pair donor ligands, remarkably in transition metal chemistry and catalysis, is very challenging to overestimate. In recent years, there has been tremendous growth seen in the field of low-valent main group complexes. Considerable progress has been achieved in the synthesis and characterization of such species as Lewis acid/base adducts with strongly tunable NHC ligands. These discoveries have allowed for investigations of various novel compounds with unique electronic properties and opened new opportunities in the rational design of novel materials and organic catalysts. In low-valent main group chemistry, NHCs prove to be an important key for the stabilization of highly reactive low-coordinate main group complexes in different oxidation states, which is very difficult with traditional ligands. This was provided to the researcher, a wide playground, not only characterized, and get insights into the bonding in these reactive complexes and explore their unique reactivity and potential in catalysis and synthesis. *[119-122]*

The structural variety of NHC carbenes encompasses nitrogen atoms adjacent to the carbene carbon, as well as ring size, ring constitution, and functionalization. Electronic and structural properties of singlet carbenes have been discussed. *[123-127]* The π-electron-donating and the sigma electron-withdrawing nature of nitrogen atom(s), **Figure 1.25** in a cyclic scaffold of NHCs decreases the energy of HOMO (Sp^2-hybridized lone pair orbital, sigma-orbital) and increases the LUMO energy (unoccupied $p\pi$ orbital), resulting in increased energy separation gap between these orbitals and along with the singlet and triplet ground states. All acting factors are responsible for the high nucleophilic (basic) character, and making them strong sigma donors, sharply different from other classes of traditional ligands and carbenes. *[128-131]*

π-electron donation in NHC and CAAC

NHCs   CAACs   NHO
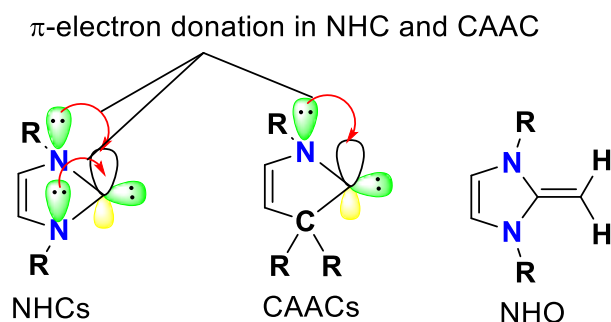
Figure 1.25 General electronic effects in NHC, CAAC, and NHO.

1.4.1 NHCs in boron cation chemistry

Boron-centred cationic complexes, owing to their inherent electrophilicity and electron deficiency, make boron cation complexes a magic tool in modern-day chemistry, especially in catalysis chemistry. The stabilization of boron cations via N-heterocyclic carbenes (NHCs) has gained significant attention due to their unique steric and electronic properties. NHCs are strong σ-donors and poor π-acceptors, which makes the NHCs able to donate adequate electron density to the electron-deficient species. Such interactions not only increased the stability of boron cations but also allowed the fine-tuning of their electronic environment, which helps in a broad range of applications in catalytic processes. Moreover, NHC-stabilized boron cations exhibited notable reactivity in hydrosilylations, hydrodefluorination, and hydroborations reactions. The electronic properties of NHC ligands can be tuned via changing the backbone substituents, along with the N-substituents, which provide a versatile platform for the rational design of boron-based catalysts tailored for the selective transformations. This opened a new pathway in main group catalysis, providing sustainable alternatives to traditional transition metal catalysts.

Several borenium cations stabilized by N-heterocyclic carbenes have been published over the past decades. Here we discussed the synthesis and isolation of borenium cations stabilized by classical carbene, mesoionic carbene, and chiral carbene, respectively. **Figure 1.26** Stephen and his co-workers reported that the classical carbene-stabilized borenium cation 9-BBN and NHC adduct with trityl salt facilitates the

formation of a tricoordinate borenium cation. Besides, classical carbenes, other carbenes such as cyclic alkyl amino carbenes (CAACs), meso-ionic carbenes (MICs) were also explored as stabilizing borenium cations.
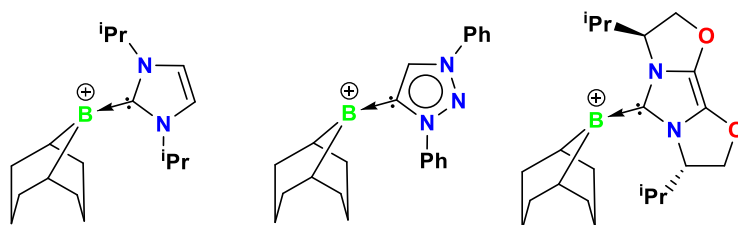
Figure 1.26 Classical, meso, and chiral carbene supported borenium cation.

Crudden and co-workers isolated the tricoordinate borenium cation stabilized by the MIC carbene, *[141]* which can serve as an alternative catalyst for FLP hydrogenations. MICs are stronger σ donors than their cousin NHC, which increases σ donation to the borenium ion centre because of weaker heteroatom stabilizations. This provided the enhanced stability to the borenium cation and increased the hydricity of the B-H bond, allowing facile hydride delivery in the catalytic cycle. Melen, Crudden, Stephan, and their co-workers synthesized several chiral NHC- or MIC borane adducts and studied their reactivity as pre-catalysts for enantioselective hydrogenation of imine. *[142-146]*

1.4.2 Cyclic alkyl amino carbenes (CAACs)

Cyclic(alkyl)(amino) carbenes are singlet carbene ligands having one amino and one sp^3 alkyl group near the carbene carbon atom. CAACs are a modified subset of N-heterocyclic carbenes (NHCs) in which an amino group is replaced by a saturated carbon atom, **Figure 1.27** resulting in a new carbene donor which have better σ-donating ability and π-accepting tendency than the classical NHCs. *[132-140]* The lone pair is present on both nitrogen atoms in NHCs and is involved in π-backdonation, while in the case of CAACs, one nitrogen is replaced by a carbon atom, resulting in weak π-donation because only one nitrogen

is taking part in back donations, making the CAACs strong π-acceptors and more electrophilic than the classical carbenes.
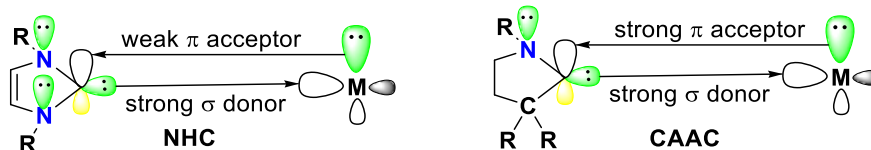
Figure 1.27 Electronic representation of NHC and CAAC.

1.4.3 NHCs stabilized borylenes

Borylene is the analogue of divalent carbon (carbenes) with the general formula R-B: a boron atom bearing an organic moiety with two unshared electrons, like their carbene counterparts. These are highly reactive species because borylenes are Lewis acidic and have a propensity to form strong bonds with other molecules. For this reason, borylene is much more uncommon than the stable carbenes; they can only be inferred by chemical trapping. H. Braunscheig and his co-workers reported the first stable terminal borylene coordinated with the transition metal [(CO)$_5$WBN(SiMe$_3$)$_2$]. *[147]* Lewis bases such as NHCs and cyclic alkyl amino carbenes (CAACs) stabilized the borylenes either in a discrete form or as bis-adducts.

The first example of a borylene stabilized by a single Lewis base was reported in 2007 and exists as a dimer diborene. An (NHC)BBr$_3$ adduct was reduced to generate a probable (NHC)B-H intermediate that subsequently dimerized to form the diborene. Several similar compounds have been generated and isolated, and several studies involving putative mono-Lewis base-stabilized borylene intermediates have been reported. *[148]* However, an isolable example remained elusive until 2014. Betrand et al. reported the (CAAC)borylene from the NHC-borane adduct. They treated the NHC-borane adduct with 2 equiv. of Cp*$_2$Co leads to the formation of (CAAC)borylene. Another group followed a similar synthetic strategy using DAC (diamidocarbene); the reduction of a DAC borane*[149, 50, 151]* derivative afforded an analogous (DAC)borylene. **Figure 1.28** The first example of dinitrogen fixation at a p-block element was published in 2018 by Holger

Braunschweig et al., whereby one molecule of dinitrogen is bound by two transient mono-Lewis base-stabilized borylene species.[151]
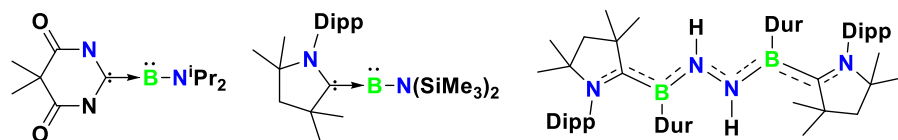
Figure 1.28 CAACs stabilized borylenes and their reactivity with N_2.

1.4.4 Role of CAACs in small molecule activations

CAACs are ambiphilic in nature. Due to this, they can donate and accept electrons. They have a small singlet-triplet gap, and this allows them to activate small molecules and enthalpically strong covalent bonds of CO, H2, B-H, Si-H, N-H, and C-H. As a result, cyclic alkyl amino carbenes are utilized as a metal-free catalyst in numerous transformation reactions that can require traditionally transition metal-based catalysts for similar types of transformation reactions. [153-155]
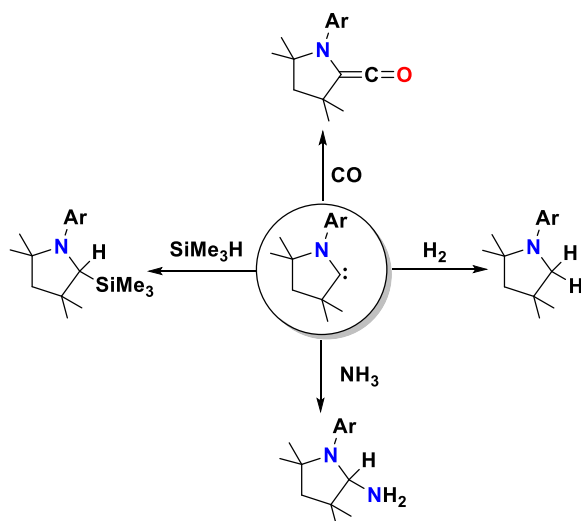
Scheme 1.2 Small molecule activation by CAAC

1.4.5 NHCs stabilize main group cations

N-Heterocyclic carbenes (NHCs) have emerged as powerful neutral ligands for the stabilization of highly reactive main group cationic species. Their exceptional σ-donor strength, combined with tunable steric bulk, allows for effective coordination to electron-deficient

centers, thereby imparting both kinetic and thermodynamic stability to the resulting cationic complexes. In particular, NHCs have been instrumental in isolating and characterizing main group cations such as borenium (R_2B^+), aluminyl (R_2Al^+), and silylium (R_3Si^+) species, which are otherwise prone to oligomerization or decomposition due to their high electrophilicity. The carbene ligand donates electron density into the vacant p-orbitals of the main group center, mitigating the charge density and stabilizing the cationic framework. Moreover, the bulky substituents on NHCs provide steric shielding that prevents unwanted side reactions or dimerization. This unique stabilization has enabled the exploration of main group cations in areas such as Lewis acid catalysis, anion sensing, hydride abstraction, and small molecule activation. As a result, NHC-stabilized main group cations represent a rapidly expanding field, opening new avenues for designing reactive intermediates and functional main group-based materials. *[160-165]*
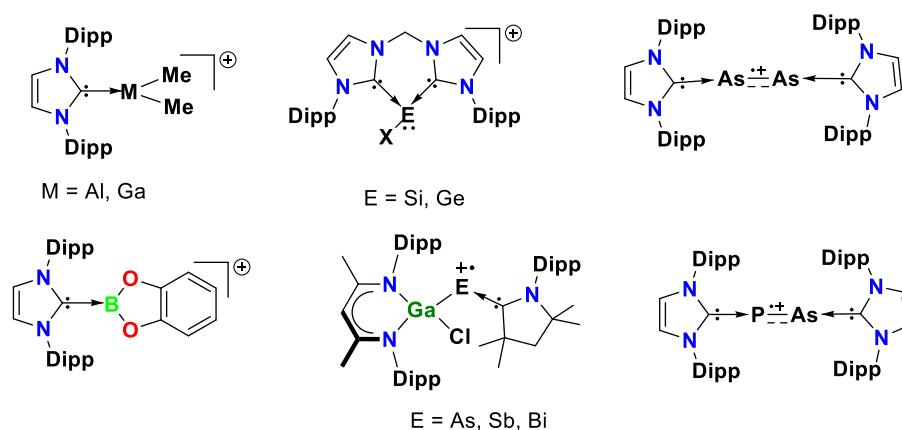
Figure 1.31 NHCs stabilized main group cations and radical cations.

1.5 N-heterocyclic olefins (NHOs)

NHOs (N-heterocyclic olefin) have highly polarised carbon-carbon bond (C=C) double bond as well as highly electron-rich moieties, due to the presence of heteroatoms in the ring. As a result, olefins are more nucleophilic. NHOs are also known as the deoxy-Breslow intermediate in terms of Michael acceptors. Efficacious progress has been made in organic chemistry in the domain of NHOs within the last few decades, including C-F bond functionalization, amination, *[166-170]*

hydrosilylations, and hydroboration, along with CO_2 sequestration, ring-opening reaction of aziridine, epoxide, and asymmetric catalysis reported by several groups.
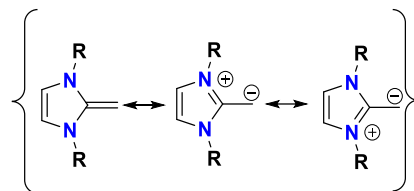
Figure 1.31 Resonating structures of NHO.

1.5.1 Role of NHO in low-valent main group chemistry and its applications

N-heterocyclic olefines are a relatively young class of strong sigma donor ligands in coordination chemistry. Sigma donor ability of NHOs is higher than the classical N-heterocyclic carbene. Due to its strong sigma donor ability and electronic and steric tunability, it can stabilize the highly reactive main group cations and low valent main group species. Main group cations, especially group 13 and 14 elements, are inherently electron-deficient species because of low coordination and the presence of vacant sites. These species are highly sensitive, highly reactive, and transient unless suitably stabilized. Well-known traditional ligands fail to provide the required steric protection and electronic donations necessary for the isolation of low-valent and cationic species of main group compounds in discrete forms.

Numerous reports have highlighted the successful stabilization of main group cations using NHO ligands. The coordination of NHOs to electron-deficient boron centers not only mitigates the Lewis acidity but also allows the isolation of boron cations with unique structural and electronic properties. *[170-174]* NHO–borane compounds have been exploited to generate borinium and borenium species, with significant implications in small molecule activation, catalysis, and material design. The strong donor character of NHOs also enhances the thermal and oxidative stability of these complexes, making them suitable for further functional elaboration. In the context of low-valent main group

compounds, particularly those involving heavier p-block elements (e.g., Ga(I), In(I), or Sn(II)), NHOs have demonstrated the ability to stabilize unusual oxidation states. These species often display reactivity profiles reminiscent of transition metals, with potential applications in bond activation, catalysis, and electronic materials. The strong σ-donating and weak π-accepting properties of NHOs help prevent disproportionation or dimerization, which are common decomposition pathways for low-valent complexes. *[175,176]*
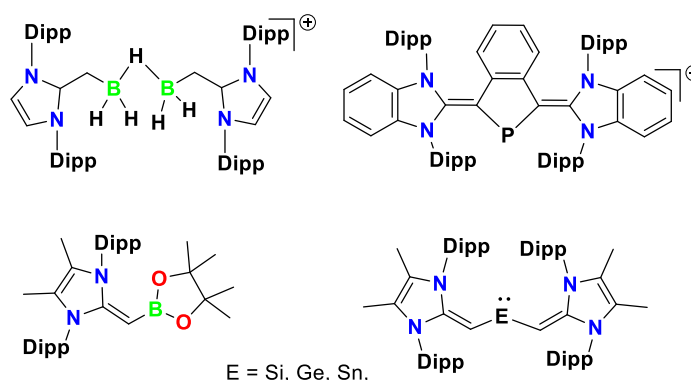
Figure 1.32 NHO stabilized main group complexes.

NHO-stabilized main group complexes have demonstrated remarkable activity across a variety of transformations, including hydroelementation, small-molecule activation, and polymerization catalysis. The ability of NHOs to modulate both the electronic and steric environment of the central atom facilitates fine-tuning of reactivity and selectivity, a critical advantage in catalytic design. Moreover, their robust σ-donation helps prevent rapid decomposition or undesired side reactions, thereby enhancing catalyst *[177-180]* stability and turnover numbers. As such, NHO ligands are increasingly recognized as indispensable tools in the development of sustainable and efficient main group catalysis, offering new opportunities for replacing transition metal-based systems with earth-abundant main group alternatives.

References

[1] Colling, M., Braunschweig, H. (2003) The Chemistry of Borylene Complexes. Eur. J. Inorg. Chem., 393-403. (DOI: 10.1002/ejic.200390054)

[2] Englert, U., Kollann, C., Braunschweig, H. (1998) Synthesis and Structure of the First Terminal Borylene Complexes. Angew. Chem. Int. Ed., 37, 3179-3180. (DOI: 10.1002/(SICI)1521-3773)

[3] Power, P. P. (2010) Main-group elements as transition metals. Nature., 463, 171-177. (DOI: 10.1038/nature08634)

[4] Kays, D. L. (2015) Extremely bulky amide ligands in main group chemistry. Chem. Soc. Rev., 45, 1004-1018. (DOI: 10.1039/C5CS00513B)

[5] Anthony, J. E., Facchetti, A., Heeney, M., Marder, S. R., Zhan, X. (2010) n-Type Organic Semiconductors in Organic Electronics. Adv. Mater., 22, 3876-3892 (DOI: 10.1002/adma.200903628)

[6] D'Andrade, B. W., Forrest, S. R. (2004) White Organic Light-Emitting Devices for Solid-State Lighting .Adv. Mater., 16, 1585 .(DOI: 10.1002/adma.200400684)

[7] Ashton, T. D., Jolliffe, K. A., Pfeffer, F. M. (2015) Luminescent probes for the bioimaging of small anionic species in vitro and in vivo. Chem. Soc. Rev., 44,4547., (DOI: 10.1039/C4CS00372A)

[8] Figueira-Duarte, T. M., Müllen, K. (2011) Pyrene-Based Materials for Organic Electronics. Chem. Rev., 111, 7260.(DOI: 10.1021/cr100428a)

[9] Mishra, A., Bäuerle, P. (2012) Small Molecule Organic Semiconductors on the Move: Promises for Future Solar Energy Technology. Chem. Int. Ed., 51, 2020. (DOI: 10.1002/anie.201102326)

[10] Wade, C. R., Broomsgrove, A. E. J., Aldridge, S., Gabbaï, (2010) F. P. Fluoride ion complexation and sensing using organoboron compounds. Chem. Rev., 110, 3985.(DOI: 10.1021/cr900401a)

[11] Hudson, Z. M. Wang, S. (2009) Impact of Donor−Acceptor Geometry and Metal Chelation on Photophysical Properties and Applications of Triarylboranes. Acc. Chem. Res., 42, 1584. (DOI: 10.1021/ar900072u)

[12] Entwistle, C. D., Marder, T. B. (2004) Applications of Three-Coordinate Organoboron Compounds and Polymers in Optoelectronics. Chem. Mater., 16, 4574.(DOI: 10.1021/cm0495717)

[13] Ji, L., Griesbeck, S., Marder, T. B. (2017) Recent developments in and perspectives on three-coordinate boron materials: a bright future. Chem. Sci., 8, 846.(DOI: 10.1039/C6SC04245G)

[14] Wang, S. (2001) Luminescence and electroluminescence of Al(III), B(III), Be(II) and Zn(II) complexes with nitrogen donors. Coord. Chem. Rev., 215,79. (DOI: 10.1016/S0010-8545(00)00403-3)

[15] Li, D., Zhang, H., Wang, Y. (2013) Four-coordinate organoboron compounds for organic light-emitting diodes (OLEDs). Chem. Soc. Rev., 42, 8416.(DOI: 10.1039/C3CS60170F)

[16] Tanaka, K., Chujo, Y. (2015) Recent progress of optical functional nanomaterials based on organoboron complexes with β-diketonate, ketoiminate and diiminate. Asia Mater., 7, e223.(DOI: 10.1038/am.2015.118)

[17] Rao, Y.-L., Wang, S. (2011) Four-Coordinate Organoboron Compounds with a π-Conjugated Chelate Ligand for Optoelectronic Applications. Inorg. Chem., 50, 12263. (DOI: 10.1021/ic200658v)

[18] Frath, D., Massue, J., Ulrich, G., Ziessel, R. (2014) Luminescent Materials: Locking π-Conjugated and Heterocyclic Ligands with Boron(III). Angew. Chem. Int. Ed. Engl., 53, 2290. (DOI: 10.1002/anie.201305554)

[19] Dias, H. V. R., Wang Z., Jin, W. (1998) Aminotroponiminato complexes of silicon, germanium, tin and lead. Coord. Chem. Rev.,176, 67-86. (10.1016/S0010-8545(98)00112-X)

[20] Dagorne, S., Atwood, D. A. (2008) Synthesis, Characterization, and Applications of Group 13 Cationic Compounds. Chem. Rev., 108, 4037-4071. (10.1021/cr078351k)

[21] Kühl, O. (2004) N-heterocyclic germylenes and related compounds. Coord. Chem. Rev., 248, 411-427. (10.1016/j.ccr.2003.12.004)

[22] Holm, R. H., O'Connor, M. J. (1971) The Stereochemistry of Bis-Chelate Metal (II) Complexes. Prog. Inorg. Chem., 14, 241-401. (10.1002/9780470166154.ch5)

[23] Jenter, J., Lühl, A., Roesky, P. W. (2011) Aminotroponiminate zinc complexes as catalysts for the intramolecular hydroamination. J. Organomet. Chem., 696, 406-418. (10.1016/j.jorganchem.2010.10.017)

[24] Hicks, F. A., Brookhart, M. (2000) Synthesis of 2-Anilinotropones via Palladium-Catalyzed Amination of 2-Triflatotropone. Org. Lett., 2, 219–221. (10.1021/ol991310t)

[25] Hicks, F. A., Brookhart, M. (2000) Synthesis of 2-Anilinotropones via Palladium-Catalyzed Amination of 2-Triflatotropone. Org. Lett., 2, 219–221. (10.1021/ol991310t)

[26] Claramunt, R. M., Sanz, D., Torralba, M. P., Pinilla, E., Torres, M. R., Elguero, J. (2004) Solid-State Structure and Tautomerism of 2-Aminotroponimines Studied by X-ray Crystallography and Multinuclear NMR Spectroscopy. Eur. J. Org. Chem., 4452‑4466. (10.1002/ejoc.200400389)

[27] Korolev, A. V., Ihara, E., Guzei, I., A., Young, V. G., Jordan, R. (2001) Cationic Aluminum Alkyl Complexes Incorporating Aminotroponiminate. Ligands. J. Am. Chem. Soc., 123, 8291–8309. (doi.org/10.1021/ja010242e)

[28] Roesky, P. W. (2000) The co-ordination chemistry of aminotroponiminates. Chem. Soc. Rev., 29, 335-345. (10.1039/A906763I)

[29]] Nozoe, T., Shindo, K., Ishikawa, S. (1988) Novel Intermolecular Heterocycle Exchange Reaction of Cyclohepta[b][1,4]benzoxazines and Their S-Analogs with 1,2-Bifunctional Reagents. Chem. Lett., 17, 1593-1596. (10.1246/cl.1988.1593)

[30]Nozoe, T., Okai, H., Someya, T., (1978) Reactive Troponoids and o-Aminophenol. I. Synthesis of Cyclohepta[b][1,4] benzoxazine. Bull. Chem. Soc. Jpn., 51, 2185-2186. (10.1246/bcsj.51.2185)

[31] Rao, Y.-L., Amarne, H., Wang, S. (2012) Photochromic four-coordinate N, C-chelate boron compounds Coord. Chem. Rev., 256, 759. (DOI: 10.1016/j.ccr.2011.11.009)

[32] Loudet, A., Burgess, K. (2007) BODIPY Dyes and Their Derivatives: Syntheses and Spectroscopic Properties. Chem. Rev., 107, 4891.(DOI: 10.1021/cr078381n)

[33] Ulrich, G., Ziessel, R., Harriman, A. (2008) The chemistry of fluorescent bodipy dyes: versatility unsurpassed. Angew. Chem. Int. Ed. 47, 1184., (DOI: 10.1002/anie.200702070)

[34] Ziessel, R., Ulrich, G., Harriman, A. (2007) The chemistry of Bodipy: A new El Dorado for fluorescence tools. New J. Chem., 31, 496 (DOI: 10.1039/B617972J)

[35] Lakshmi, V., Ravikanth, M. (2011) Synthesis of Sterically Crowded Polyarylated Boron-Dipyrromethenes. J. Org. Chem., 76, 8466.(DOI: 10.1021/jo2010022)

[36] Burghart, A., Thoresen, L. H., Chen, J., Burgess, K., Bergstrom, F., Johansson, L. B. A. (2000) Energy transfer cassettes based on BODIPY Chem. Commun., 2203. (DOI: 10.1039/B006769P)

[37] Ge, Y., O'Shea, D. F. (2016) Azadipyrromethenes: from traditional dye chemistry to leading edge applications. Chem. Soc. Rev., 45, 3846. (DOI: 10.1039/C6CS00200E)

[38] Zhang, D., Wen, Y., Xiao, Y., Yu, G., Liu, Y., Qian, X. (2008) Bulky 4-tritylphenylethynyl substituted boradiazaindacene: pure red emission, relatively large Stokes shift and inhibition of self-quenching. Chem. Commun., 4777. (DOI: 10.1039/b808681h)

[39] Liu, S.-F., Wu, Q., Schmider, H. L., Aziz, H., Hu, N.-X., Popovi, Z., Wang, S. (2000) Syntheses, Structures, and Electroluminescence of New Blue/Green Luminescent Chelate Compounds: Zn(2-py-in)2(THF), BPh2(2-py-in), Be(2-py-in)2, and BPh2(2-py-aza) [2-py-in) 2-(2-pyridyl)indole; 2-py-aza) 2-(2-pyridyl)-7-azaindole] J. Am. Chem. Soc., 122, 3671-3678. (DOI: 10.1021/ja9944249)

[40] Liang, F. S. Cheng, Y. X., Su, G. P., Ma, D. G., Wang, L. X.; Jing, X. B., Wang, F. S. White organic electroluminescence based on a new boron complex. Synth. Met., 137, 1109. (DOI: 10.1016/j.mssp.2023.107382)

[41] Liu, Q., Mudadu, M. S., Schmider, H., Thummel, R., Tao, Y., Wang, S. (2002) Tuning the Luminescence and Electroluminescence of Diphenylboron Complexes of 5-Substituted 2-(2'Pyridyl)indoles. Organometallics. 21, 4743 (DOI: 10.1021/om020446j)

[42] Liddle, B. J., Silva, R. M., Morin, T. J., Macedo, F. P., Shukla, R., Lindeman, S. V., Gardinier, J. R. (2007) BORAZANs: Tunable Fluorophores Based on 2-(Pyrazolyl)aniline Chelates of Diphenylboron. J. Org. Chem., 72, 5637. (DOI: 10.1021/jo0705420)

[43] Araneda, J. F., Piers, W. E., Heyne, B., Parvez, M., McDonald, R. (2011) High Stokes Shift Anilido-Pyridine Boron Difluoride Dyes. Angew. Chem. Int., Ed., 50, 12214. (DOI: 10.1002/anie.201105228)

[44] Calhorda, M. J., Suresh, D., Gomes, P. T., Di Paolo, R. E., Macanita, A. L. (2012) Photophysical properties of iminopyrrolyl boron

complexes: A DFT interpretation. Dalton Trans., 41, 13210. (DOI: 10.1039/C2DT31104F)

[45] Suresh, D., Lopes, P. S., Ferreira, B., Figueira, C. A., Gomes, C. S. B., Gomes, P. T., Di Paolo, R. E., MaçAnita, A. L., Duarte, M. T., Charas, A., Morgado, J., Calhorda, M. (2014) Tunable Fluorophores Based on 2-(N-Arylimino)pyrrolyl Chelates of Diphenylboron: Synthesis, Structure, Photophysical Characterization, and Application in OLEDs. Chem. Eur. J., 20, 4126.(DOI: 10.1002/chem.201303607)

[46] Suresh, D., Gomes, C. S. B., Lopes, P. S., Figueira, C. A., Ferreira, B., Gomes, P. T., Di Paolo, R. E., Macanita, A. L., Duarte, M. T., Charas, A., Morgado, J., Vila-Vicosa, D., Calhorda, M. (2015) Luminescent Di- and Trinuclear Boron Complexes Based on Aromatic Iminopyrrolyl Spacer Ligands: Synthesis, Characterization, and Application in OLEDs. Chem.- Eur. J., 21, 9133.(DOI: 10.1002/chem.201500109)

[47] Suresh, D., Ferreira, B., Lopes, P. S., Gomes, C. S. B., Krishnamoorthy, P., Charas, A., Vila-Vicosa, D., Morgado, J., Calhorda, M. J., Macanita, A. L.,Gomes, P. T. (2016) Boron complexes of aromatic ring fused iminopyrrolyl ligands: synthesis, structure, and luminescence properties Dalton Trans., 45, 15603. (DOI:).

[48] Barbon, S. M., Reinkeluers, P. A., Price, J. T., Staroverov, V. N., Gilroy, J. B. (2014) Structurally Tunable 3-Cyanoformazanate Boron Difluoride Dyes. Chem. Eur. J., 20, 11340.(DOI: 10.1002/chem.201404297)

[49] Moiola, M., Crespi, S., Memeo, M., Collina, S., Overkleeft, Florea, B., Quadrelli, P. (2019) Scope and Limitations of Boron Fluorescent Complexes from Stable Nitrile Oxides in ABPP Assays. ACS Omega, 4, 7766-7774. (DOI: 10.1021/acsomega.9b00672)

[50] Nakamura, M., Kanetani, Gon, M., Tanaka, K. (2024) NIR-II Absorption/Fluorescence of D–A π-Conjugated Polymers Composed of Strong Electron Acceptors Based on Boron-Fused Azobenzene

Complexes. Angew. Chem. Int. Ed., 63, e20240417. (DOI:10.1002/anie.202404178)

[51] Zhou, Y., Xiao, Y., Chi, S., Qian, X. (2008) Isomeric Boron−Fluorine Complexes with Donor−Acceptor Architecture: Strong Solid/Liquid Fluorescence and Large Stokes Shift. Org. Lett., 10, 633-636. (DOI:10.1021/ol702963w)

[52] Chen, C.-T. (2004) Evolution of Red Organic Light-Emitting Diodes: Materials and Devices. Chem. Mater., 16, 4389-4400. (DOI:10.1021/cm049679m)

[53] Ikeshita, M., Watanabe, S., Suzuki, S., Kitahara, M., Imai, Y., Tsuno, T. (2023) Circularly Polarized Luminescence from Schiff-base [4]Helicene Boron Complexes. Chem Asian J., 19, e202301024. (DOI: 10.1002/asia.202301024)

[54] Corona-López, M.-M., Muñoz-Flores, B.-M., Chaari, M., Nuñez, R., Jiménez-Pérez, V. M. (2021) Far-Red and Near-Infrared Boron Schiff Bases (BOSCHIBAs) Dyes Bearing Anionic Boron Clusters. Eur. J. Inorg. Chem., 2047-2054. (DOI: 10.1002/ejic.202100144)

[55] Chang, M. C., Chantzis, A., Jacquemin, D., Otten, E.(2016) Boron difluorides with formazanate ligands: redox-switchable fluorescent dyes with large Stokes shifts. Dalton Trans.,45,9477.(DOI: 10.1039/C6DT01226D)

[56] Wu, Q., Esteghamatian, M., Hu, N.-X., Popovic, Z., Enright, G., Tao, Y., D'Iorio, M., Wang, S.(1999) Synthesis, Structure, and Electroluminescence of BR2Q (R = Et, Ph, 2-Naphthyl and Q = 8 Hydroxyquinolato) Chem. Mater., 12, 79. (DOI: 10.1021/cm990372a).

[57] Cui, Y., Wang, S. (2006) Diboron and Triboron Compounds Based on Linear and Star-Shaped Conjugated Ligands with 8-Hydroxyquinolate Functionality: Impact of Intermolecular Interaction and Boron Coordination on Luminescence. J. Org. Chem., 71, 6485.(DOI: 10.1021/jo060841).

[58] Qin, Y., Kiburu, I., Shah, S., Jaekle, F.(2006) Luminescence Tuning of Organoboron Quinolates through Substituent Variation at the 5-Position of the Quinolato Moiety. Org. Lett., 8, 5227.(DOI: 10.1021/ol0619664).

[59] Qin, Y., Kiburu, I., Shah, S., Jaekle, F.(2006) Luminescence Tuning of Organoboron Quinolates through Substituent Variation at the 5-Position of the Quinolato Moiety. Org. Lett., 8, 5227.(DOI: 10.1021/ol0619664).

[60] Barbon, S. M., Price, J. T., Reinkeluers, P. A., Gilroy, J. B.(2014) Substituent-Dependent Optical and Electrochemical Properties of Triarylformazanate Boron Difluoride Complexes. Inorg. Chem., 53, 10585.(DOI: 10.1021/ic5016912)

[61] Chang, M. C., Otten, E. (2014) Synthesis and ligand-based reduction chemistry of boron difluoride complexes with redox-active formazanate ligands. Chem.Commun., 50, 7431.(DOI: 10.1039/C4CC03244F)

[62] Barbon, S. M., Staroverov, V. N., Gilroy, J. B. (2015) Effect of Extended π Conjugation on the Spectroscopic and Electrochemical Properties of Boron Difluoride Formazanate Complexes. J. Org. Chem.,80, 5226.(DOI: 10.1021/acs.joc.5b00620)

[63] Hesari, M., Barbon, S. M., Staroverov, V. N., Ding, Z., Gilroy, J. B. (2015) Efficient electrochemiluminescence of a readily accessible boron difluoride formazanate dye. Chem. Commun., 51, 3766.(DOI: 10.1039/C4CC10038G)

[64] Maar, R. R., Gilroy, J. B. J. Mater.(2016) Aggregation-induced emission enhancement in boron difluoride complexes of 3-cyanoformazanates Chem. Mater. 4, 6478.(DOI: 10.1039/C6TC01782G)

[65] Maar, R. R., Barbon, S. M., Sharma, N., Groom, H., Luyt, L. G., Gilroy, J. B.(2015) Evaluation of Anisole-Substituted Boron Difluoride

Formazanate Complexes for Fluorescence Cell Imaging. Chem. Eur. J., 21, 15589. (DOI: 10.1002/chem.201502821)

[66] Novoa, S., Paquette, J. A., Barbon, S. M., Maar, R. R., Gilroy, J. B. (2016) Side-chain boron difluoride formazanate polymers via ring-opening metathesis polymerization. J. Mater. Chem. C., 4, 3987.(DOI:)

[67] Wang, X., Wu, Y., Liu, Q., Li, Z., Yan, H., Ji, C., Duan, J., Liu, Z. (2015) Side-chain boron difluoride formazanate polymers via ring-opening metathesis polymerization. Chem. Commun. 51, 784. (DOI: 10.1039/C5TC03287C)

[68] Qiu, F., Zhang, F., Tang, R., Fu, Y., Wang, X., Han, S., Zhuang, X., Feng, X. (2016) Triple Boron-Cored Chromophores Bearing Discotic 5,11,17-Triazatrinaphthylene-Based Ligands. Org. Lett., 18, 1398. (DOI:10.1021/acs.orglett.6b00335)

[69] Wu, Q., Esteghamatian, M., Hu, N.-X., Popovic, Z., Enright, G., Tao, Y., D'Iorio, M., Wang, S.(1999) Synthesis, Structure, and Electroluminescence of BR2q (R = Et, Ph, 2-Naphthyl and q = 8 Hydroxyquinolato) Chem. Mater., 12, 79.(DOI: 10.1021/cm990372a)

[70] Cui, Y., Wang, S. (2006) Diboron and Triboron Compounds Based on Linear and Star-Shaped Conjugated Ligands with 8-Hydroxyquinolate Functionality: Impact of Intermolecular Interaction and Boron Coordination on Luminescence. J. Org. Chem., 71, 6485.(DOI: 10.1021/jo060841)

[71] Qin, Y., Kiburu, I., Shah, S., Jaekle, F.(2006) Luminescence Tuning of Organoboron Quinolates through Substituent Variation at the 5-Position of the Quinolato Moiety. Org. Lett., 8, 5227.(DOI: 10.1021/ol0619664)

[72] Zhang, Z., Bi, H., Zhang, Y., Yao, D., Gao, H., Fan, Y., Zhang, H., Wang, Y., Wang, Y., Chen, Z., Ma, D. (2009) Luminescent Boron-Contained Ladder-Type π-Conjugated Compounds. Inorg. Chem. 48, 7230.(DOI: 10.1021/ic900673s)

[73] Frath, D., Azizi, S., Ulrich, G., Retailleau, P., Ziessel, R.(2011) Facile Synthesis of Highly Fluorescent Boranil Complexes. Org. Lett., 13, 3414.(DOI: 10.1021/ol2011665)

[74] Frath, D., Azizi, S., Ulrich, G., Ziessel, R.(2012) Chemistry on Boranils: An Entry to Functionalized Fluorescent Dyes Org. Lett., 14, 4774.(DOI: 10.1021/ol3020573)

[75] Dhanunjayarao, K., Mukundam, V., Ramesh, M., Venkatasubbaiah, K. (2014) Eur. J. Inorg. Chem., 539.(DOI:)

[76] Moiola, M., Crespi, S., Memeo, M., Collina, S., Overkleeft, Florea, B., Quadrelli, P. (2019) Scope and Limitations of Boron Fluorescent Complexes from Stable Nitrile Oxides in ABPP Assays. ACS Omega, 4, 7766-7774. (DOI: 10.1021/acsomega.9b00672)

[77] Shanmugapriya, S., Rajaguru, K, Sivaraman, S., Muthusubramanian, S., Bhuvanesh, N. (2016) Boranil dye based "turn-on" fluorescent probes for detection of hydrogen peroxide and their cell imaging application. RSC Adv., 6, 85838-85843. (DOI: 10.1039/C6RA17863D)

[78] Kubota, Y., Hara, H., Tanaka, S., Funabiki, K., Matsui, M. (2011) Synthesis and Fluorescence Properties of Novel Pyrazine–Boron Complexes Bearing a β-Iminoketone Ligand. Org. Lett., 13, 6544-6547. (DOI:10.1021/ol202819w)

[79] Kubota, Y., Tanaka, S., Funabiki, K., Matsui, M. (2012) Synthesis and Fluorescence Properties of Thiazole–Boron Complexes Bearing a β-Ketoiminate Ligand. Org. Lett., 14, 4682-4685. (DOI:10.1021/ol302179r)

[80] Kubota, Y., Ozaki, Y., Funabiki, K., Matsui, M. (2013) Synthesis and Fluorescence Properties of Pyrimidine Mono- and Bisboron Complexes. J. Org. Chem., 78, 7058–7067. (DOI: 10.1021/jo400879g)

[81] Kubota, Y., Kasatani, K., Niwa, T., Sato, H., Funabiki, K., Matsui, M. (2015) Synthesis and Fluorescence Properties of Pyrimidine-Based

Diboron Complexes with Donor–π–Acceptor Structures. Chem. Eur. J., 22, 1816-1824. (DOI: 10.1002/chem.201503625)

[82] Katzman, B. D., Maar, R. R., Cappello, D., Sattler, M. O., Boyle, Staroverov, V. N., Gilroy, J. B. (2021) A strongly Lewis-acidic and fluorescent borenium cation supported by a tridentate formazanate ligand. Chem. Commun., 57, 9530-9533. (10.1039/D1CC03873G).

[83] Kim, H. Gilliard, R. J. Jr. (2025) Coordination Chemistry Meets Boron Helices: Cationic Double-Stranded diborahelicates and Bora[7]helicenes with Multicolor Emission. J. Am. Chem. Soc., 147, 23213-23225. (10.1021/jacs.5c07436)

[84] Piers, W. E., Bourke, S. C., Conroy, K. D. (2005) Borinium, borenium, and boronium ions: synthesis, reactivity, and applications. Angew. Chem. Int. Ed., 44, 5016-5036. (DOI: 10.1002/anie.200500402)

[85] Tan, X., Wang, H. (2022) Recent advances in borenium catalysis. Chem. Soc. Rev., 51, 2583-2600. (DOI: 10.1039/D2CS00044J)

[86] Franz, D., Inoue, S. (2019) cationic complexes of boron and aluminum: An early 21st century viewpoint. Chem. Eur. J., 25, 2898-2926. (DOI: 10.1002/chem.201803370)

[87] Chen, C., Li, J., Daniliuc, C. G., Mück-Lichtenfeld, C., Kehr, G., Erker, G. (2020) The $[(NHC)B(H)C_6F_5]^+$ cations and their $[B](H)-CO$ borane carbonyls. Angew. Chem. Int. Ed., 59, 21460-21464 (DOI: 10.1002/anie.202009353)

[88] Noeth, H., Staudigl, R., Wagner, H. U. (1982) Contributions to the chemistry of boron. 121. Dicoordinate amidoboron cations. Inorg. Chem., 21, 706-716. (DOI: 10.1021/ic00132a048)

[89] Kölle, P., Nöth, H. (1986) Beiträge zur Chemie des Bors, 164. Über (Benzyl-tert-butylamino)borane und Bis(benzyl-tert-butylamino)bor(1+)-Salze. Chem. Ber., 119, 313-324. (DOI: 10.1002/cber.19861190127]

[90] Higashi, J., Eastman, A. D., Paryy, R. W. (1982) Synthesis and characterization of salts of the bis(diisopropylamido)boron(III) cation and attempted reactions to make the corresponding

bis(dimethylamido)boron(III) cation. Inorg. Chem., 21, 716-720. (DOI: 10.1021/ic00132a049).

[91] Lenz, T., Hebenbrock, M. (2025) Crystal structure of bis-(diiso-propyl-amino)-fluoro-borane. Crystallogr Commun., 17, 401-404. (DOI: 10.1107/S2056989025003160)

[92] Major, C. J., Qu, Z. W., Grimme, S., Stephane, D. (2022) The Non-Ancillary Nature of Trimethylsilylamide Substituents in Boranes and Borinium Cations. Chem. Eur. J., 28, e202200698 (DOI: 10.1002/chem.202200698)

[93] Kölle, P., Nöth, H., (1986) Beiträge zur Chemie des Bors, 180. Zur Kenntnis von [(Trimethylsilyl)amino]borinium-Kationen. Chem. Ber., 119, 3849-3855, (DOI: 10.1002/cber.19861191227)

[94] Nöth, H., Weber, S. (1985) Beiträge zur Chemie des Bors, 154. Addition von Trimethylsily-Verbindungen und von anderen Elektrophilen an (tert-Butylimino) (tetramethylpiperidino)boran. Chem. Ber., 118, 2144-2146. (DOI: 10.1002/cber.19851180536)

[95] Nöth, H., Kölle, P. (1986) Beiträge zur Chemie des Bors, 180. Zur Kenntnis von [(Trimethylsilyl)amino]borinium-Kationen. Chem. Ber., 119, 3849-3855. (DOI: 10.1002/cber.19861191227)

[96] Dipl.-Chem., J. R., Hartmann, M., Frenking, G. (2001) π-Donation and Stabilizing Effects of Pnicogens in Carbenium and Silicenium Ions: A Theoretical Study of [C(XH2)3]+ and [Si(XH2)3]+ (X=N, P, As, Sb, Bi) Chem. Eur. J., 7, 2834 – 2841.(DOI:10.1002/1521-3765)

[97] Narula, C. K., Noeth, H. (1984) Preparation and characterization of salts containing cations of tricoordinate boron. Inorg. Chem., 23, 4147-4152. (DOI: 10.1021/ic00193a009)

[98] Narula, C. K., Noeth, H. (1985) Contribution to the chemistry of boron. 150. Competition between adduct and cation formation in reactions between diorganylborane derivatives and pyridine or lutidines. Inorg. Chem., 24, 2532-2539. (DOI: 10.1021/ic00210a014)

[99] Narula, C. K., Noeth, H. (1985) Competition between adduct and cation formation in reactions between diorganylborane derivatives and pyridine or lutidines. Inorg. Chem., 16, 2532-2539. (DOI: 10.1021/ic00210a014)

[100] Narula, C. K., Nöth, H. (1984) A novel trico-ordinated boronium salt: 1,3-dimethyl-2-phenanthridin-5-yl-1,3,2-diazaborolidinium trifluoromethansesulphonate. J. Chem. Soc. Chem. Commun., 1023-1024. (DOI: 10.1039/C39840001023)

[101] Jutzi, P., (1987) Boronium and Borenium Salts and Neutral Adducts from (Pentamethylcyclopentadienyl) boron Halides and Nitrogen Bases. Krato, B., Hursthouse, M., Howes, A. J. (1987) Boronium- und Boreniumsalze sowie neutrale Addukte aus (Pentamethylcyclopentadienyl)borhalogeniden und Stickstoffbasen. Chem. Ber., 120, 1091-1098. (DOI: 10.1002/cber.19871200705)

[102] Kuhn, N., Kuhn, A., Lewandowski, J., Speis, M. (1991) 1,3,2-Diazaborinium-Verbindungen — neue Heteroaren-Kationen des Bors. Chem. Ber, 124, 2197-2201. (DOI: 10.1002/cber.19911241009)

[103] Vidovic, D., Reeske, D., Findlater, M., Cowley, A. H. (2008) Synthesis and structures of boron dihalides supported by the C_6F_5-substituted β-diketiminate ligand $[HC(CMe)_2(NC_6F_5)_2]^-$. Dalton Trans., 2293–2297. (DOI: 10.1039/B719722E)

[104] Bonnier, C., Parvez, M., Sorensen, T. S., Piers, W. E. (2008) Borenium cations derived from BODIPY dyes. Chem. Commun., 4593–4595. (DOI: 10.1039/B808739C)

[105] Chen, J., Lalancette, R. A., Jäkle, F. (2013) Synthesis and Lewis acid properties of a ferrocene-based planar-chiral borenium cation. Chem. Commun., 49, 4893-4895 (DOI: 10.1039/C3CC41556B).

[106] Mondal, R., Otten, E. (2018) Reactivity of Two-Electron-Reduced Boron Formazanate Compounds with Electrophiles: Facile N–H/N–C Bond Homolysis Due to the Formation of Stable Ligand Radicals. Inorg. Chem., 57, 9720-9727. (DOI: 10.1021/acs.inorgchem.8b00079)

[107] Cade, I. A, Ingleson, M. J. (2014) Syn-1,2-Carboboration of Alkynes with Borenium Cations. Chem. Eur. J., 20, 12874-12880. (DOI: 10.1002/chem.201403614]

[108] Parveen, D., Yadav, R. K., Mondal, B., Dallon, M., Sarazin, Y., Roy, D. K. (2024) Bis (diiminate)-based boron difluoro complexes: effective synthon for bis (borenium) cations. Dalton Trans., 53, 14139-14143. (DOI: 10.1039/D4DT02050B)

[109] Katzman, B. D., Maar, R. R., Cappello, D., Sattler, M. O., Boyle, P. D., Staroverov, V. N., Gilroy, J. B. (2021) A strongly Lewis-acidic and fluorescent borenium cation supported by a tridentate formazanate ligand. Chem. Commun., 57, 9530-9533. (DOI: 10.1039/D1CC03873G)

[110] Davis Jr., J. H., Madura, J. D. (1996) Synthesis and computational evaluation of a boronium ion analogue of the tropane ring system. Tetrahedron Lett., 37, 2729-2730. (DOI: 10.1016/0040-4039(96)00372-3)

[111] Biani, F. F. D., Gmeinwieser, T., Jäkle, F., Zanello, P. (1997) Multistep Redox Processes and Intramolecular Charge Transfer in Ferrocene-Based 2,2'-Bipyridylboronium Salts. Organometallics, 16, 4776-4787. (DOI: 10.1021/om970345z)

[112] Jenkins, H. A. Dumaresque, C. L. Clyburne, J. A. C. (2002) The coordination chemistry of o,o'-i-Pr2C6H3-bis(imino)acenaphthene to group 13 trihalides. Can. J. Chem., 80, 1398-1403. (DOI: 10.1139/v02-084)

[113] Jutzi, P., Buchner, W. (1979) 1-Halogen-2,3,4,5,6-pentamethyl-2,3,4,5,6-pentacarba-nido-hexaboran(6)-Kationen, ein neuer nido-Carbaboran-Typ. Chem. Ber., 112, 2488-2493. (DOI: 10.1002/cber.19791120717)

[114] Greiwe, P., Bethäuser, A., Pritzkow, H., Kühler, T., Jutzi, P. Siebert, W. (2000) Borane-stabilized Boranediyls (Borylenes): Neutral nido-1-Borane-2,3,4,5,6-pentamethyl-2,3,4,5,6-pentacarbahexaboranes(6) Eur. J. Inorg. Chem. 2000, 1927-1929. (DOI: 10.1002/1099-0682)

[115] Holtmann, U., Jutzi, P., Kühler, T., Neumann, B., Stammler H. G. (1999) Reaction of Decamethylsilicocene with Group 13 Element Halides: Insertions, Rearrangements, and Eliminations. Organomettallics, 18, 5531-5538. (DOI: 10.1021/om9906114)

[116] Suenaga, K., Ito, S., Tanaka, K., Chujo, Y. (2022) Modulation of properties by Ion Changing Based on Lumininescent Ionic Salts consisting of Spirobi(boron ketoiminate). Molecules,

[117] Watson, E. R., Boyle, P. D., Ragogna, P. J. Gilroy, J. B. (2025) Ligand protonation leads to highly fluorescent boronium cations. Chem. Sci., 16, 2258-2264. (DOI: 10.1039/D4SC06392A)

[118] Arduengo, A. J., Harlow, R. L., Kline, M. (1991) A stable crystalline carbene J. Am. Chem. Soc., 113, 361-363. (DOI: 10.1021/ja00001a054)

[119] Igau, A., Grützmacher, H., Baceiredo, A., Bertrand, G. (1988) Analogous .alpha.,.alpha.'-bis-carbenoid, triply bonded species: synthesis of a stable .lambda.3-phosphino carbene-.lambda.5-phosphaacetylene. J. Am. Chem. Soc., 110, 6463-6466. (DOI: 10.1021/ja00227a028)

[120] Kato, T., Gornitzka, H., Baceiredo, A., Savin, A., Bertrand, G. (2000) On the Electronic Structure of (Phosphino)(silyl)carbenes: Single-Crystal X-ray Diffraction and ELF Analyses. J. Am. Chem. Soc., 122, 998-999. (DOI: 10.1021/ja9939542)

[121] Merceron-Saffon, N., Baceiredo, A., Gornitzka, H., Bertrand, G. (2003) Synthesis of Carbenes Through Substitution Reactions at a Carbene Center. Science, 301, 1223.(DOI:10.1126/science.1086860)

[122] Vignolle, J., Cattoën, X., Bourissou, D. (2009) Stable Noncyclic Carbenes. Chem. Rev., 109, 3333-3384. (DOI: 10.1021/cr800549j)

[123] Harder, S. (2012) Molecular early main group metal hydrides: synthetic challenge, structures and applications. Chem. Commun., 48, 11165-11177. (DOI: 10.1039/C2CC33478J)

[124] Williams, A., Ibrahim, I.T. (1981) Carbodiimide chemistry: Recent advances. Chem. Rev. 81 589–636. (DOI: 10.1021/cr00046a004)

[125] Wilkinson, G., Gillard, R. D., McCleverty, J. A. (1987) Comprehensive coordination chemistry. The synthesis, reactions, properties and applications of coordination compounds. V.3. Main group and early transition elements. Oxford, U.K., 2, 20.1.

[126] Harder, S. (2020) Early main group metal catalysis. Concepts and reactions, Wiley-VCH, Weinheim, Germany.

[126] Roesky, H. W., Singh, S., Jancik, V., Chandrasekhar, V. (2004), A paradigm change in assembling oh functionalities on metal centers. Acc. Chem. Res., 37, 969–981. (DOI: 10.1021/ar0402154)

[127] Cramer, C. J., Tolman, W. B. (2007) Mononuclear Cu–O_2 complexes: Geometries, spectroscopic properties, electronic structures, and reactivity. Acc. Chem. Res., 40, 601–608. (DOI: 10.1021/ar700008c)

[128] Tan, X., Wang, H. (2022) Recent advances in borenium catalysis. Chem. Soc. Rev., 51, 2583-2600. (DOI: 10.1039/D2CS00044J)

[129] Stephan, D. W. (2016) The broadening reach of frustrated Lewis pair chemistry. Science, 354, 6317. (DOI: 10.1126/science.aaf7229)

[130] McArthur, D., Butts, C. P., Lindsay, D. M. (2011) A dialkylborenium ion via reaction of N-heterocyclic carbene–organoboranes with Brønsted acids-synthesis and DOSY NMR studies. Chem. Commun., 47, 6650-6652, (DOI: 10.1039/C1CC10767D)

[131] Chen, J., Lalancette, R. A. (2013) Synthesis and Lewis acid properties of a ferrocene-based planar-chiral borenium cation. Chem. Commun., 49, 4893-4895. (DOI: 10.1039/C3CC41556B)

[132] Koelle, P., Noeth, H. (1985) The chemistry of borinium and borenium ions. Chem. Rev., 85, 399-418. (DOI: 10.1021/cr00069a004)

[133] Farrell , J. F., Hatnean, J. A., Stephan, D. W. (2012) Activation of Hydrogen and Hydrogenation Catalysis by a Borenium Cation. J. Am. Chem. Soc., 134, 15728-15731. (DOI: 10.1021/ja307995f)

[134] Martin, D., Melaimi, M., Soleilhavoup, M., Bertrand, G. (2011) A Brief Survey of Our Contribution to Stable Carbene Chemistry. Organometallics, 30, 5304-5313. (DOI: 10.1021/om200650x)

[135] Palucki, M., Buchwald, S. L. J. (1997) Palladium-Catalyzed α-Arylation of Ketones. J. Am. Chem. Soc., 119, 11108-11109. (DOI: 10.1021/ja972593s)

[136] Hamann, B. C., Hartwig, J. F. (1997) Palladium-Catalyzed Direct α-Arylation of Ketones. Rate Acceleration by Sterically Hindered Chelating Ligands and Reductive Elimination from a Transition Metal Enolate Complex. J. Am. Chem. Soc., 119, 12382-12383. (DOI: 10.1021/ja9727880)

[137] Lavallo, V., Canac, Y., DeHope, A., Donnadieu, B., Bertrand, G. (2005) A Rigid Cyclic (Alkyl)(amino)carbene Ligand lead to Isolation of Low-Coordinate Transition Metal Complexes. Angew. Chem., Int. Ed., 44, 7236. (DOI: 10.1002/anie.200502566)

[138] Nolan, S. P. (2011) The Development and Catalytic Uses of N-Heterocyclic Carbene Gold Complexes. Acc. Chem. Res., 44, 91-100. (DOI: 10.1021/ar1000764)

[139] Gorin, D. J., Sherry, B. D., Toste, F. D. (2008) Ligand Effects in Homogeneous Au Catalysis. Chem. Rev., 108, 3351-3378. (DOI: 10.1021/cr068430g)

[140] De Vries, T. S., Prokofjevs, A., Vedejs, E. (2012) Cationic Tricoordinate Boron Intermediates: Borenium Chemistry from the Organic Perspective. *Chem. Rev.*, 112, 4246-4282. (DOI: 10.1021/cr200133c)

[141] Eisenberger, P., Bestvater, B. P., Keske, E. C., Crudden, C. M. (2015) Hydrogenations at Room Temperature and Atmospheric Pressure with Mesoionic Carbene-Stabilized Borenium Catalysts. Angew. Chem. Int. Ed., 54, 2467-2471. (DOI: 10.1002/anie.201409250)

[142] Guisado-Barrios, G., Soleilhavoup, M., Bertrand, G. (2018) 1H-1,2,3-Triazol-5-ylidenes: Readily Available Mesoionic Carbenes. Acc. Chem. Res., 51, 3236-3244. (DOI:10.1021/acs.accounts.8b00480)

[143] Vivancos, Á., Segarra, C., Albrecht, M. (2018) Mesoionic and Related Less Heteroatom-Stabilized N-Heterocyclic Carbene Complexes: Synthesis, Catalysis, and Other Applications. *Chem. Rev.*, 118, 9493-9586. (DOI: 10.1021/acs.chemrev.8b00148)

[144] Clarke, J. J., Maekawa, Y., Nambo, M., Crudden, C. M. (2021)Borenium-Catalyzed Reduction of Pyridines through the Combined Action of Hydrogen and Hydrosilane. Org. Lett., 23, 6617-6621. (DOI: 10.1021/acs.orglett.1c01892)

[145] Farrell, J. M., Eisenberger, P., Melen, R. L., Crudden, C. M., Stephan, D. W. (2016) Chiral carbene–borane adducts: precursors for borenium catalysts for asymmetric FLP hydrogenations. Dolton, Trans., 45, 15303-15316. (DOI: 10.1039/C6DT02202B)

[146] Mercea, D. M., Howlett, M. G., Piascik, A. D., Scott, D. J., Steven, A., Ashley, A. E., Fuchter, M. J. (2019)Enantioselective reduction of N-alkyl ketimines with frustrated Lewis pair catalysis using chiral borenium ions. Chem. Commun., 55, 7077-7080. (DOI: 10.1039/C9CC02900A)

[147] Colling, M., Braunschweig, H. (2003) The Chemistry of Borylene Complexes. Eur. J. Inorg. Chem., 393-403. (DOI: 10.1002/ejic.200390054).

[148] Englert, U., Kollann, C., Braunschweig, H. (1998) Synthesis and Structure of the First Terminal Borylene Complexes. Angew. Chem. Int. Ed., 37, 3179-3180. (DOI: 10.1002/(SICI)1521-3773).

[149]Dahcheh, F., Martin, D., Stephan, D. W., Bertrand, G. (2014) Synthesis and Reactivity of a CAAC–Aminoborylene Adduct: A Hetero-Allene or an Organoboron Isoelectronic with Singlet Carbenes. Angew. Chem. Int. Ed., 53, 13159-13163. (DOI: 10.1002/anie.201408371).

[150] Ledet, A. D., Hudnall, T. W. (2016) Reduction of a diamidocarbene-supported borenium cation: isolation of a neutral boryl-substituted radical and a carbene-stabilized aminoborylene. Dalton Trans., 45, 9820-9826. (DOI: 10.1039/C6DT00300A).

[151] Légaré, M. N., Chabot, G. B., Dewhurst, R. D., Engels, B., Braunschweig, H. (2018) Nitrogen fixation and reduction at boron. Science, 359. 871. (DOI: 10.1126/science.aaq1684)

[152] Lin, Y. J., Liu, W. C., Liu, Y. H., Lee, G. H., Chien, S. Y., Chiu, C. W. (2022) A linear Di-coordinate boron radical cation. Nat. Commun., 13, 7051. (DOI: 10.1038/s41467-022-34900-7).

[153] Kushvaha, S. K., Mishra, A., Roesky, H. W. Mondal, K. C. (2022) Recent Advances in the Domain of Cyclic (Alkyl)(Amino) Carbenes. Chem Asian J., 17, e202101301. (DOI: 10.1002/asia.202101301)

[154] Neeve, E. C., Geier, S. J., Mkhalid, I. A. I., Westcott, S. A., Marder, T. B. (2016) Diboron(4) Compounds: From Structural Curiosity to Synthetic Workhorse. Chem. Rev., 116, 9091-9161. (DOI: 10.1021/acs.chemrev.6b00193)

[155] Melaimi, M., Jazzar, R., Bertrand, G. (2017) Cyclic (Alkyl)(amino)carbenes (CAACs): Recent Developments. Angew. Chem. Int. Ed., 56, 10046-10068 (DOI: 10.1002/anie.201702148)

[156] Zhu, H., Inoue, S. (2025) N-Heterocyclic carbene-phosphinidenes in main-group chemistry. Chem., 102649. (DOI: 10.1016/j.chempr.2025.102649)

[157] Paris, M., Hass, M. (2025) N-Heterocyclic Carbene Stabilized Bisacylgermylenes. Chem. Eur. J., 31, e20250170. (DOI: 10.1002/chem.202501707)

[158] Nesterov, V., Reiter, D., Bag, P., Frisch, P., Holzner, R., Porzelt, A., Inoue, S. (2018) NHCs in Main Group Chemistry. Chem. Rev., 118, 9678-9842. (DOI: 10.1021/acs.chemrev.8b00079)

[159] Zhu, H., Chai, J., Stasch, A., Roesky, Herbert W., Blunck, T., Vidovic, D., Magull, J., Schmidt, H.-G., Noltemeyer, M. (2004) Reactions of the Aluminum(I) Monomer LAl [L = HC{(CMe)(NAr)}2; Ar = 2,6-iPr2C6H3] with Imidazol-2-ylidene and Diphenyldiazomethane. Eur. J. Inorg. Chem., 2004, 4046-4051. (DOI: 10.1002/ejic.200400159)

[160] Sarazin, Y., Carpentier, J.-F. (2015) Discrete cationic complexes for ring-opening polymerization catalysis of cyclic esters and epoxides. Chem. Rev., 115, 3564-3614. (DOI: 10.1021/acs.chemrev.5b00033)

[161] Bochmann, M. (2010) The chemistry of catalyst activation: The case of group 4 polymerization catalysts. Organometallics, 29, 4711-4740. (DOI: 10.1021/om1004447)

[162] Reed, C.A. (2010) H^+, CH_3^+, and R_3Si^+ carborane reagents: When triflates fail. Acc. Chem. Res., 43, 1, 121-128. (DOI: 10.1021/ar900159e)

[163] Swamy, V. S. V. S. N., Pal, S., Khan, S., Sen, S. S. (2015) Cations and dications of heavier group 14 elements in low oxidation states. Dalton Trans., 44, 12903-12923. (DOI: 10.1039/C5DT01912E)

[164] Fang, H., Wang, Z., Fu, X. (2017) Beyond carbocations: Synthesis, structure and reactivity of heavier Group 14 element cations. Coord. Chem. Rev., 344, 214-237. (DOI: 10.1016/j.ccr.2016.11.017)

[165] Braunschweig, H., Krummenacher, I., Légaré, M.-A., Matler, A., Radacki, K., Ye, Q. (2017) Main-group metallomimetics: Transition metal-like photolytic co substitution at boron. J. Am. Chem. Soc., 139, 1802-1805. (DOI: 10.1021/jacs.6b13047)

[166] Gompper, R. Schaefer, H. (1967) Ketenderivate, XII. Beiträge zur Chemie der Dithiocarbonsäureester und Ketenmercaptale. Chem. Ber., 100, 591-604. (DOI: 10.1002/cber.19671000228)

[167] Crocker, R. D., Nguyen, T. V. (2016) The Resurgence of the Highly Ylidic N-Heterocyclic Olefins as a New Class of Organocatalysts. Chem. Eur. J., 22, 2208-2213. (DOI: 10.1002/chem.201503575)

[168] Roy, M. M. D., Reward, E(2017) Pushing Chemical Boundaries with N-Heterocyclic Olefins (NHOs): From Catalysis to Main Group Element Chemistry. Acc. Chem. Res., 50, 2017-2025. (DOI: 10.1021/acs.accounts.7b00264)

[169] Maji, B., Mayr, H.(2012) Structures and Reactivities of O-Methylated Breslow Intermediates. Angew. Chem. Int. Ed., 51, 10408-10412. (DOI: 10.1002/anie.201204524)

[170] Ghadwal, R. S. (2016) Carbon-based two-electron σ-donor ligands beyond classical N-heterocyclic carbenes. Dalton Trans., 45, 16081-16095. (DOI: 10.1039/C6DT02158A)

[171] Wang, Y. W., Abraham, M. Y., Gilliard, R. J. Jr., Sexton, D. R., Wei, P., Robinson, G. H. (2013) N-Heterocyclic Olefin Stabilized Borenium Cations. Organometallics, 32, 6639-6642. (10.1021/om400539z)

[173] Rivard, E. (2016) Group 14 inorganic hydrocarbon analogues. Chem. Soc. Rev., 45, 989-1003. (10.1039/C5CS00365B)

[174] Doddi, A., Peters, M., Tamm, M. (2019) N-Heterocyclic Carbene Adducts of Main Group Elements and Their Use as Ligands in Transition Metal Chemistry. Chem. Rev., 119, 6994–7112. (10.1021/acs.chemrev.8b00791)

[175] Arduengo, A. J., Harlow, R., Kline, M. A. (1991) Stable Crystalline Carbene. *J. Am. Chem. Soc.*, *113*, 361-363. (DOI: 10.1021/ja00001a054)

[176] Herrmann, W. A., Köcher, C. (1997) N-Heterocyclic Carbenes. Angew. Chem. Int. Ed., 36, 2162-2187. (DOI: 10.1002/anie.199721621)

[177] Mahantesh, G., Sharma, D., Dandela, R., Dhayalan, V. (2023) Synthetic Strategies of N-Heterocyclic Olefin (NHOs) and Their Recent Application of Organocatalytic Reactions and Beyond. Chem. Eur. J., 29, e202302106. (10.1002/chem.202302106)

[178] Enders, D., Niemeier, O., Henseler, A. (2007) Organocatalysis by N-Heterocyclic Carbenes. Chem. Rev., 107, 5606-5655. (DOI: 10.1016/j.ccr.2016.11.017)

[179] Jacobs, E., Nguyen, T. V., (2025) N-Heterocyclic Carbenes and N-Heterocycles as Synthetic Reagents and Building Blocks. Chem. Eur. J. 31, e202402339. (DOI: 10.1002/chem.202402339)

[180] Krachko, T., Slootweg, C. (2018) N-heterocyclic Carbene-Phosphinidene Adducts: Synthesis, Properties and Applications. Eur. J. Inorg. Chem., 20, 2734-2754. (DOI: 10.1002/ejic.201800459)

Chapter 2

Synthesis and characterisation of Schiff base chelated mono and binuclear boron complexes: Role of spacers in variation of photoluminescence properties
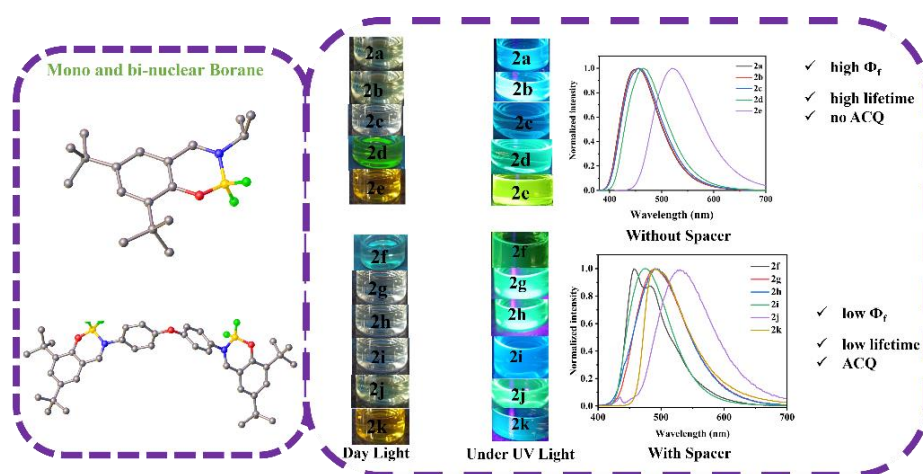
2.1 Introduction

Functional materials, mainly defined as any chemical system with useful physical and chemical properties, have gained remarkable attention over the years owing to their potential application in numerous fields. *[1-3]* A very young and popularized strategy for designing novel, functional material is to incorporate the boron atom into π-conjugate scaffolds. The benefit of this approach lies in the fact that boron is inherently electron-deficient and therefore imparts many unique features to the resulting B-doped molecules. For instance, the empty pz orbital of boron can participate in π-conjugation, thereby enhancing or tuning the photophysical properties of such compounds and making them useful as luminescent materials. *[4-7]*

In recent decades, organoboron-based fluorophores have emerged as compatible functional dyes with diverse photophysical and electrochemical properties, leading to the advancement in this research area. *[7]* In recent research, the main focus area is to develop multi-boron coordinated scaffolds because of their unique photophysical properties. Boron coordinated with scaffold-like BOPHY, BOMIPY, and BOPPY exhibit high thermal and photochemical stability, strong absorption, and tunable fluorescence. These compounds have attracted significant attention for some time now, thanks to their dynamic application in organic light-emitting diodes (OLEDs) *[8-11],* laser dyes [12-14], fluorescence imaging probes *[15-17],* photosensitizer dyes in photodynamic therapy *[18-22],* and also in solar cells.[23-29] Tetracoordinated fluorescent boron compounds are reported with different chelated bidentate ligands such as N, N-, N, O-, O-O, and O-S like dipyrromethenes,*[30-35]* quinolate,*[36-40]* diketonate,*[41-44]* sub-phthalocyanine,[45-49] thioketonate.*[50-55]* hydrazine-bispyrrole N, N-chelating (BOPHY),*[56,57]* dipyrrinato, and ligand-based difluroborane complexes are most studied because of their excellent optical properties, like high fluorescence quantum yields, high photo and chemical stability, and molar extinction coefficient.*[58]* So far, the development of efficient luminescent dyes for use in solid and aggregate

states has been a key focus in current research. Numerous captivating molecules with intriguing properties such as aggregation-induced emission (AIE), mechanochromism, and tunable emission based on solvent polarity have been discovered.*[59,60]* Boron complexes received valuable attention in the field of stimuli-responsive materials with applications in different areas.*[61-64]* Although BODIPYs have been studied in depth over the years, they have some limitations in their application, like exhibiting very low or no fluorescence in the solid state occasioned by aggregation-caused emission quenching (ACQ), aggregation-induced energy (AIE) transfer, and self-absorption that results in a small Stokes shift. In most of the above-stated applications, it is required for the fluorophore to be present in a self-gathered state. However, due to the ACQ phenomenon, most fluorescent organic molecules tend to become less emissive upon conglomeration. That setback of less emissiveness can be overcome by designing a molecule that exhibits aggregation-induced emissions.
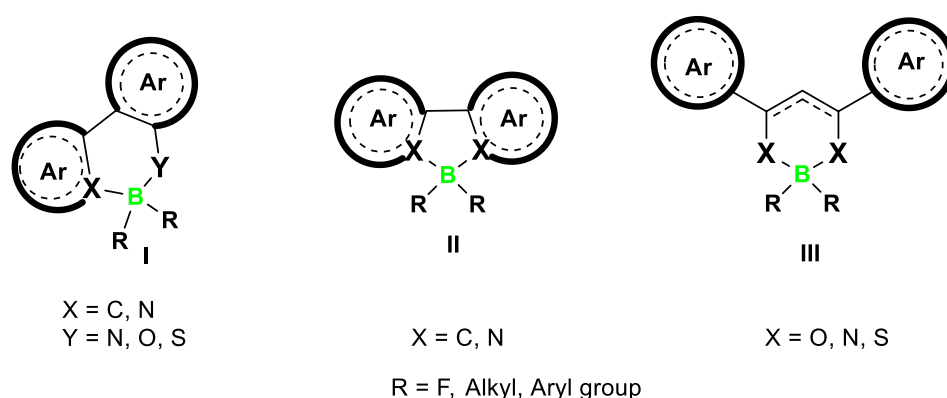

Figure 2.1 General representation of N-N, N-O, N-S, and O-O bidentate ligands based on organoboron compounds.

Organoboron compounds have great potential in the areas of luminescence, which has attracted researchers to develop a new class of ligands that achieve favorable optical properties in solid as well as in solution states.*[15]* To overcome paucity related to the rigid and planar BODIPY dyes, the boron complexes of Schiff base ligands with N-O donors were introduced to prepare four-coordinated complexes with difluoroboranes. In this context, salicylaldimine-based boron dyes prove
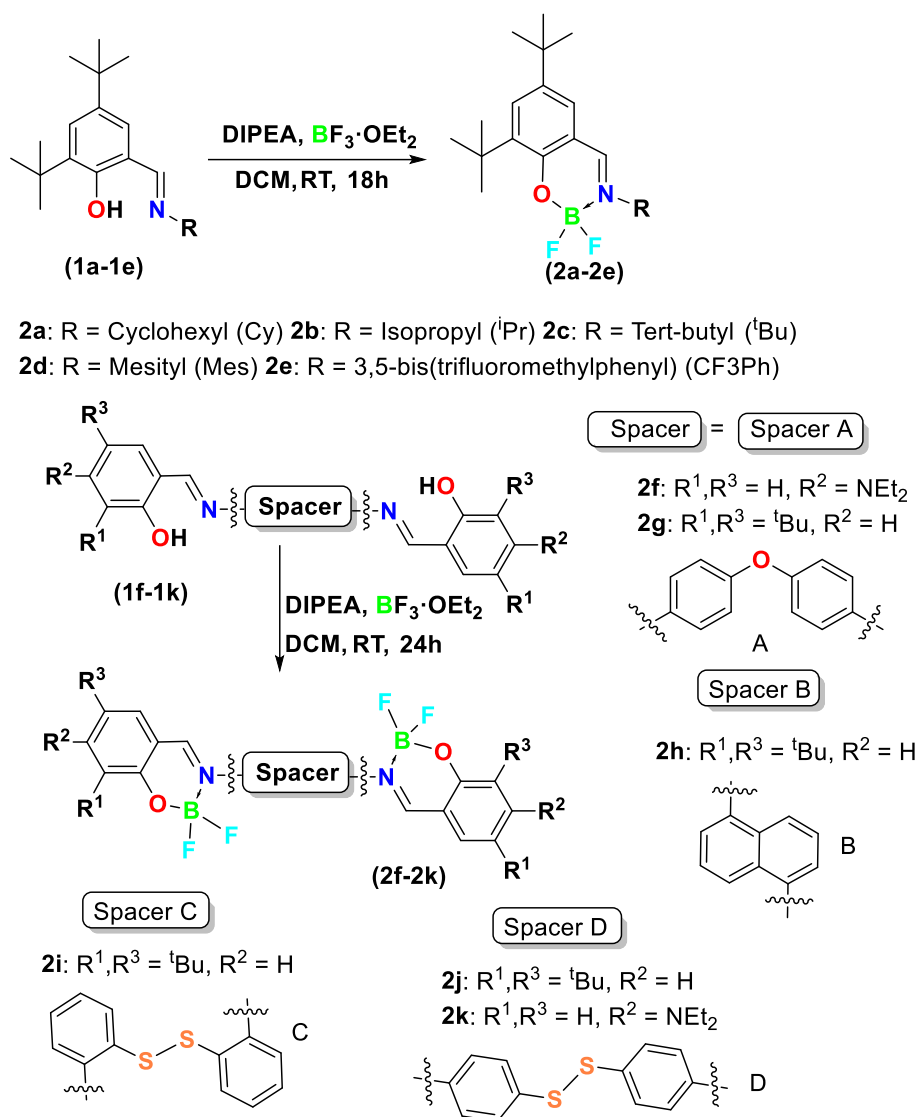
themselves as a next-generation photo-functional material. Mainly, N-O ligands are derived from salicylaldimine, oxime, or hydroxamic acid derivatives. These ligands coordinated with the Lewis acidic boron center to facilitate the chelated boron complexes with unique electronic architectures. These ligands not only provide easy synthetic modularity and flexibility but also facilitate the alternative root for the formation of the donor-acceptor architectures that help in the intramolecular charge transfer (ICT), resulting in red-shifted absorption and emission maxima and enhanced solvatochromic properties. Interestingly, the incorporation of an oxygen atom brings additional stability to the boron center and enhances stimulus-responsive luminescence via dynamic B-O interactions. *[55-60]*

Here, we report a rational design and synthesis of several mono- (**2a-2e**) and bi-nuclear (**2f-2k**) boron complexes having different substitutions and spacers. The complexes were synthesized in high yields and characterized by mass, NMR spectroscopy in solution, and solid-state structures of a few complexes (**2b**, **2e** and **2g**) were also undertaken. Further, we studied the photophysical, electrochemical and stimuli responsive properties of those boron complexes. Although **2a-2k** are inactive towards solvatochromism, mechanochromism, sulphide-bridged binuclear boron complexes **2i-2k** showed aggregate-caused quenching (ACQ) in the mixture of THF/water.

2.2 Results and Discussion

2.2.1 Synthesis of mono and bi-nuclear boron complexes

To facilitate the mono and bi-nuclear boron complexes, we focused on the synthesis of ligands. Ligands were prepared by simple condensation between aldehydes and amines by following previously reported procedures. All ligands were comprehensively analyzed by 1H, $^{13}C\{1H\}$ NMR and (HRMS) high-resolution mass spectrometry. Mononuclear boron difluoride complexes **2a-2k** were synthesized by deprotonating the ligands **1a-1k** with diisopropylethylamine (DIPEA) followed by the addition of $BF_3 \cdot OEt_2$ at room temperature, as shown in Scheme 1.

2a: R = Cyclohexyl (Cy) **2b**: R = Isopropyl (^{i}Pr) **2c**: R = Tert-butyl (^{t}Bu)
2d: R = Mesityl (Mes) **2e**: R = 3,5-bis(trifluoromethylphenyl) (CF3Ph)

Spacer = Spacer A

2f: R^1, R^3 = H, R^2 = NEt$_2$
2g: R^1, R^3 = ^{t}Bu, R^2 = H

A

Spacer B

2h: R^1, R^3 = ^{t}Bu, R^2 = H

B

Spacer C

2i: R^1, R^3 = ^{t}Bu, R^2 = H

C

Spacer D

2j: R^1, R^3 = ^{t}Bu, R^2 = H
2k: R^1, R^3 = H, R^2 = NEt$_2$

D

Scheme 2.1 Synthesis of mono and bi-nuclear boron complexes (**2a-2k**).

After quenching the reaction and extracting the compounds in dichloromethane (DCM), they were purified by column chromatography, yielding **2a-2k** in very good yields as colourless pale-yellow solids. Complexes were soluble in dichloromethane, acetonitrile, dioxane, toluene, and THF but partly soluble in saturated hydrocarbons and alcohols. They were characterized by FT-IR, ^{1}H, ^{13}C NMR, and hetero nuclear NMR (^{11}B,^{19}F) and mass spectrometry. The ^{1}H NMR spectra of ligands **1a-1k** showed a resonance for the imino CH proton in between 8.5 ppm to 9.5 ppm, depending on the substituents. While in ^{13}C NMR spectra of amino C-atom resonance of the ligands ranges from (160 ppm to 169 ppm), they are slightly (~ 4 ppm) up-field shifted for

their respective BF$_2$ complexes. The disappearance of phenolic OH signal in ^{1}H NMR as well as in FT-IR spectra of the complexes **2a-2k** suggests the formation of B-O bond. The ^{11}B NMR chemical shifts of **2a-2k** range from 0.95 to 1.1 ppm as a triplet, which is characteristic of tetracoordinated difluoride boron complexes. In ^{19}F NMR, a multiplet approximately at -135 ppm was observed for these complexes. In the FT-IR spectra of the complexes **2a-2k**, the stretching frequency for the imine -C=N band are observed between 1649 to 1610 cm^{-1}.

2.2.2 Single crystal X-ray diffraction (SCXRD) analysis of mono and bi-nuclear boron complexes
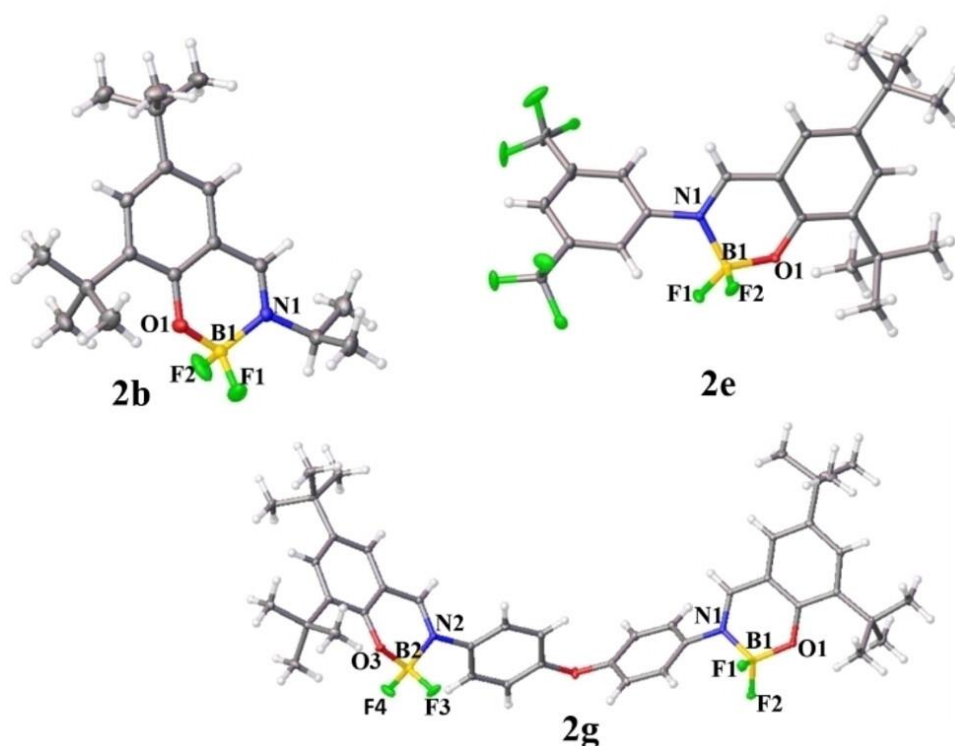
Figure 2.2 Crystal structure of **2b, 2e,** and **2g** borane.

Crystals of complexes **2b**, **2e**, and **2g** were obtained from acetonitrile, and single-crystal X-ray diffraction (SCXRD) analysis was performed on those crystals. All the complexes crystallized in a monoclinic system with different space groups, complex **2b** and **2e** in P21/c, whereas 2g in C2/c space groups. The solid-state structures of **2b** and **2e** showed the presence of a single boron centre, whilst two boron centers in **2g**, all having a distorted tetrahedral geometry around the boron atom. In these complexes, the Schiff base ligands chelated to the BF$_2$ units of the boron

center, forming a six membered ring in which the C-N bond lengths (**2b**: 1.283(3); **2e**: 1.3026(18), **2g**: 1.3003(14) Å) suggests that the imino groups retain the double bond character. As reflected in (**Table 2.1**), the B-F, B-O and B-N bond lengths are similar for these complexes, and they are all in the single bond range, respectively.

Table 2.1 Selected bond lengths [Å] and angles [º] for complexes **2b**, **2e**, and **2g**.

Parameters	2b	2e	2g
B1-O1	1.422(3)	1.4531(19)	1.4555(15)
B1-N1	1.569(3)	1.5834(19)	1.5925(16)
B1-F1	1.345(3)	1.368(2)	1.3706(16)
B1-F2	1.386(4)	1.388(2)	1.3706(16)
B1-F1-F2	109.2(2)	111.36(14)	111.41(8)
B1-F1-N1	110.1(2)	109.90(14)	109.90(12)
B1-F2-O1	109.7(2)	106.50(13)	111.622(14)
B1-N1-O1	110.96(19)	108.43(12)	108.042(15)

2.2.3 Crystal packing of complexes

As depicted in **Figure 2.3** and **Figure 2.74,** the crystal packing structures of **2b**, **2e,** and **2g** are influenced by intermolecular C–H···F, C–F···π, C–H···π, and lone pair···π interactions. In **2b**, there are two types of C–H···F interactions present. One is between the imine C–H and F of the BF$_2$ unit with a distance of 2.32 Å (angle 155º), and another one between isopropyl C–H and F of the BF$_2$ unit with a distance of 2.56 Å. According to the conditions given by Dunitz and Taylor for designation as hydrogen bonds,*[67]* i.e. the H···F–C interaction should be substantially shorter than the sum of the van der Waals radii (ca. 2.55 Å) and preferably no longer than ca 2.2–2.3 Å, with obtuse X–H–F angles. Similarly, the C–H···F interaction is observed in complex **2e**, where distances are 2.23 (angle 155º) and 2.54 Å, respectively. In addition, in **2e,** there are C–F···π$_{Ar}$ and C–H···π$_{Ar}$ (π$_{Ar}$ = π system of aromatic ring) interactions. For C–F···π$_{Ar}$ interactions, Prasana and Row reported a

statistical study of CSD in 2000, where they showed that the C–F⋯π_{Ar} nonvalent contacts affected the molecular conformation and the crystal packing, and the distance between F and the carbon atom of the aromatic system amounts to be 3.33 Å.[68] This is in accordance with the distances of 2.98 and 3.14 Å in **2e**. In the crystal packing diagram of complex **2g,** along with C–H⋯F (2.39 Å; angle 136º) and C–F⋯π_{Ar} (3.14 Å), there is lone pair⋯ πAr interaction between the lone pair of the bridged oxygen and the π bond of the aromatic ring (distance 3.15 Å).[69] In the crystal packing of **2g,** two acetonitrile molecules are present within the cavity of the complex along with two additional acetonitrile molecules shared with adjacent crystal units, resulting in a cross-shaped arrangement **Figure 2.75**.
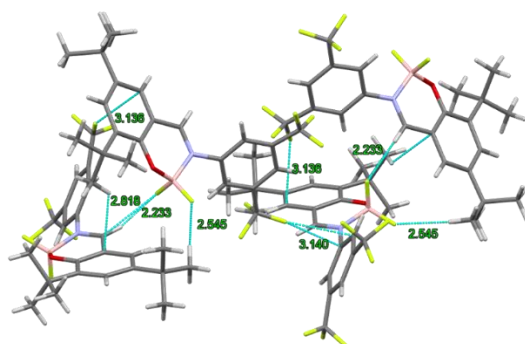
Figure 2.3 Crystal structure packing of **2e**, dotted line showing the noncovalent interactions.

2.2.4 Photophysical study

All the synthesized ligands **1a-1k** were non-emissive, whereas after complexation with the BF₂ unit, the fluorescence efficiency of the resulting complexes increased significantly. This is due to the incorporation of the BF₂ unit into the ligand skeleton, which makes the system rigid and might reduce the loss of energy via vibrational motions and increase the emission proficiency. UV-visible absorption and emission spectra of N-O chelated mono- and bi-nuclear boron difluoride complexes **2a-2h** were explored in different solvents. The photophysical properties of these mono- and bi-nuclear difluoroboron complexes are summarized in **Table 2.2** Complexes **2a-2d**, show strong absorption

between 360 to 380 nm in toluene, however; on varying the solvent polarity (toluene to acetonitrile) along with the presence of absorption band at around 370 nm, another band at a lower wavelength of 280 nm was observed. This might be due to the fact that the polar solvent stabilizes the relative energy of the orbital, thereby generating two feasible electronic transitions. Interestingly, the absorption bands **2e** and **2f** are red-shifted (**2e**: 400 nm and **2f**: 410 nm). The occurrence of relatively higher energy absorption bands for **2a-2d** might be the lack of conjugation in those complexes. On the contrary, for **2f,** although only one absorption band appeared in the low energy region, its emission spectrum is blue-shifted at 450 nm, along with one shoulder observed at 475 nm.[63-64] On varying the solvent polarity from toluene to DCM to acetonitrile to dioxane there is a decrease in absorption maxima band which suggests that the ground state is more polar than excited state, therefore, the polar solvents stabilize ground states more than the excited states making an overall increase in the energy gap between excited and ground state resulting in blue shift.*[70]*
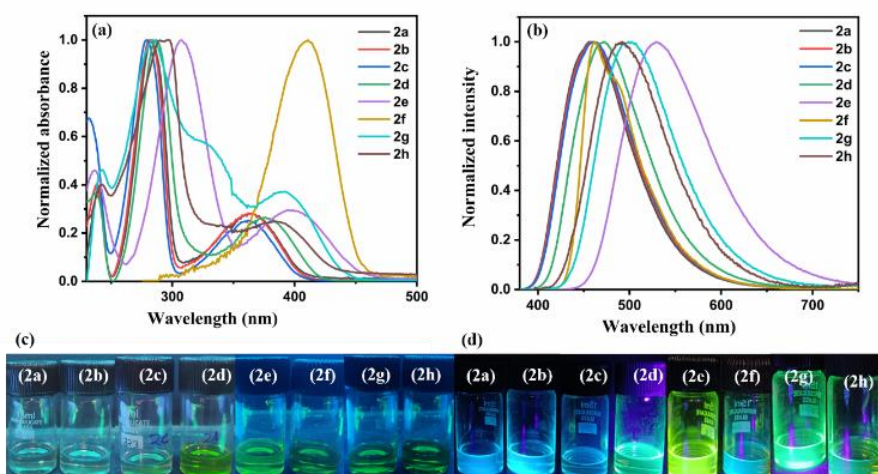

Figure 2.4 (a) Absorption spectra of **2i-2h** in DCM, (b) emission spectra of complexes **2a-2h** in DCM, (c) photograph under daylight in DCM, and (d) photograph under UV light in DCM.

However, in the case of binuclear complexes, there is not much change in the absorption and emission spectra when the solvent polarity is

changed (toluene to acetonitrile), confirming the absence of ground-state charge transfer in the synthesized BF$_2$ complexes. *[71-73]* Binuclear boron difluoride complexes **2f-2h** show a strong emission band at 457 nm, 495 nm, and 488 nm, respectively

Table 2.2 Maximum absorption (λabs) and emission (λemi) wavelengths, Stokes shift, quantum efficiency (ΦF), average fluorescence lifetime (τav) in DCM

Complex	λ_{abs} (nm)	λem (nm)	Stokes Shifts (nm)/ cm^{-1}	τ_{ave} (ns)	ϕ_f
2a	283, 363	458	95/5754	7.3	28
2b	281, 363	459	96/5761	8.0	29
2c	278, 364	461	97/5780	8.6	33
2d	287, 378	472	94/5268	6.1	20
2e	307, 397	529	132/6285	5.9	21
2f	410	462, 486	76/3814	0.2	5
2g	283, 339, 391	499	108/5535	1.3	7
2h	295, 385	492	107/5648	0.9	2
2i	314, 328, 380	449	69/4044	2.5	3
2j	292, 323, 395	505	110/5550	7.8	2
2k	408	477	69/3545	1.8	2

The emission spectra of complex **2e** appeared at low low-energy region (520 nm) in comparison to **2d** (465 nm). This may be due to the presence of CF$_3$ groups on the phenyl ring of **2e**. There is a significant difference between the maximum absorption and emission band as a result of a large Stokes shift, which was noted for these complexes, making them suitable for microscopy applications. *[74-76]* Complex **2e** has the highest Stokes shift (130 nm) among the synthesized complexes **Table**

2.2. In general, complexes having a large Stokes shift are due to the contribution of intramolecular charge transfer (ICT) in the excited state. Fluorescence decay study is investigated in toluene, THF, DCM, and dioxane. The fluorescence decay time follows the trends observed for the fluorescence quantum yield. Complex **2b** has the highest quantum yield and the highest fluorescence decay time in acetonitrile, while complex **2h** has the lowest quantum yield and fluorescence decay time **Table 2.2**.
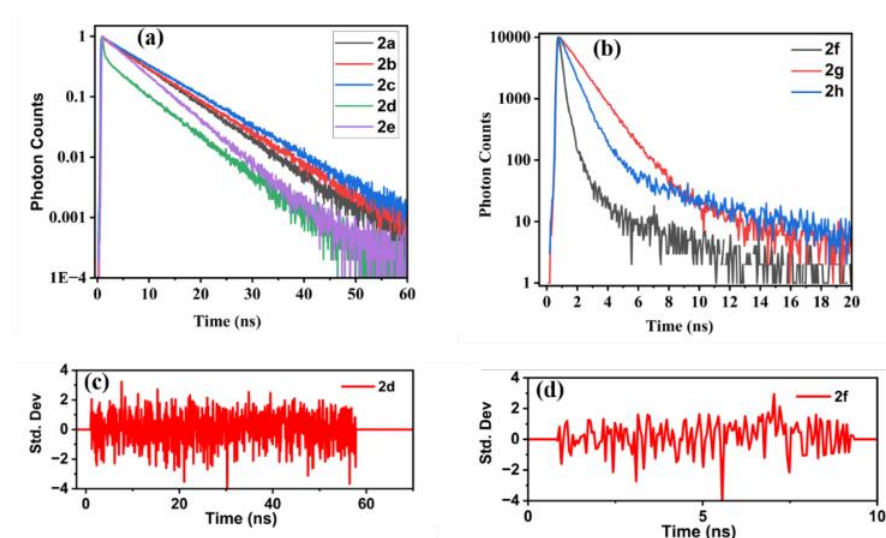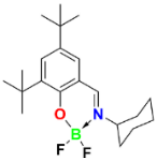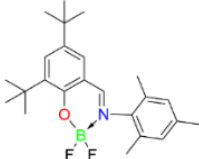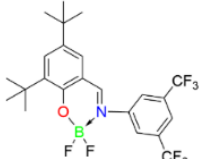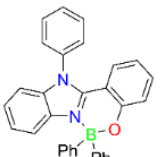
Figure 2.5 Fluorescence decay (a) mono BF_2 Complexes, (b) bi-nuclear boron complexes in DCM.

The absorption spectra of disulfide spacer-based complexes **2i** and **2j** were recorded at about 380 nm, like the other binuclear boron complexes **2f-2h**, whereas complex **2k** shows a lower energy absorbance at 406 nm. This red shift can be attributed to the presence of NEt_2 groups whose lone pair participates in the conjugations, making the higher wavelength absorption. The emission spectra of **2i-2k** were recorded in THF and it is observed at 448 nm for **2i**, 502 nm for **2j,** and 469 nm for **2k**, respectively **Figure 2.6a**. Emission of **2i** was observed at high energy, which might be due to the bulkiness of the tertiary butyl group present at the ortho position, whilst the emission of **2j** was observed at 502 nm, due to conjugation of auxochrome NEt_2 group present in the system.

95

Table 2.3 Comparison of optical properties of **2a**, **2d,** and **2e** vs BPh$_2$ counterpart in toluene.

Complex	λ_{abs} (nm)	λem (nm)	ϕ_f (%)
	363	455	30
	376	465	30
	300, 398	520	30
	356	440	30

The fluorescence quantum yields of these synthesized compounds are significantly greater than diphenyl borane complex, as shown in **Table 2.3**. Further, we aimed to collect the stimuli-responsive behaviour of the synthesized complexes. The optical properties of boron complexes were investigated in the condensed state. Firstly, we started our investigation of mono-nuclear boron complexes **2a**-**2e** and binuclear boron complexes **2f**-**2h**. Boron complexes **2a**-**2h** were inactive towards the external stimuli, properties like aggregate-induced emission (AIE), aggregate

caused quenching (ACQ), while disulfide spacer-based boron difluoride complexes **2i-2k** showed ACQ properties in the mixture of THF and water. Experiments were performed at 1.0×10^{-5} M, as the water percentage was increased, a significant decrease in emission was observed. Till water content (H$_2$O $\leq$ 60), emission intensity decreased slowly for **2i** and **2j,** but in the case of **2k,** emission intensity decreased drastically with the initial percentage of THF/Water mixture (90% THF, 10% water). For complexes **2i** and **2j** emission intensity drastically decreases when the water percentage reaches up to 90%. The ACQ phenomenon commonly comes from short-range molecular interactions, like π-π stacking, associated with the planarity of the molecular skeleton, force to the non-radiative relaxation pathways.
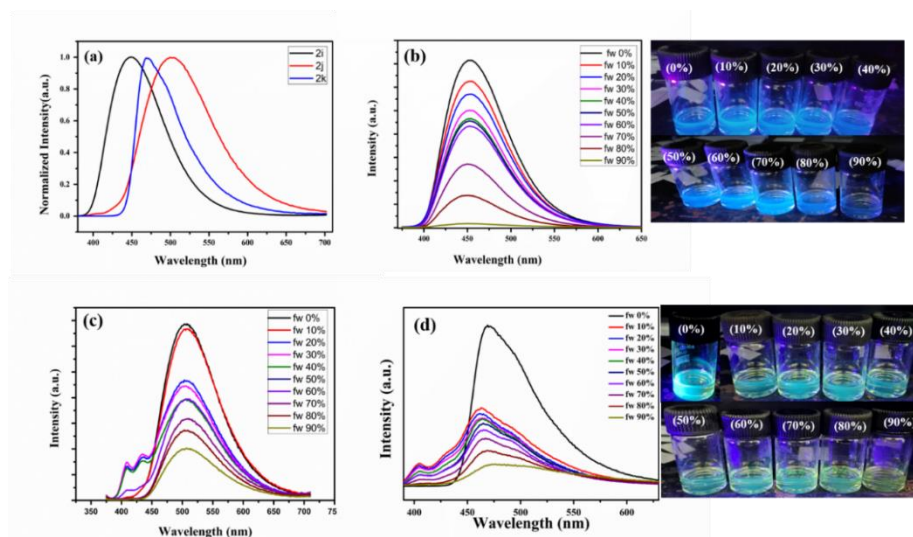
Figure 2.6 (a) Emission spectra of **2i-2k** in THF; (b), (c) and (d) ACQ graphs of **2i**, **2j** and **2k** in THF/H$_2$O, respectively.

2.3 DFT Studies on mono- (2a-2e) and binuclear (2f-2k) boron complexes

To understand the photophysical properties of the boron complexes **2a-2k**, theoretical calculations were conducted using the range-separated ω-B97XD functional *[80]* and a triple-zeta 6–311G(d) basis set[81,82] for ground-state geometry optimizations. Excited-state calculations utilized the τ-HCTHhybfunctional[83] and def2-TZVPP basis sets.[30] The electronic distribution and energy (in eV) of molecular orbitals for

mono-BF2 complexes **2a-2e** as well as bi-BF2 complexes **2f-2k** are presented in **Figure 2.7** and **Figure 2.9**, respectively. Computations for mono-BF$_2$ systems **2a-2e** reveal that the highest occupied molecular orbital (HOMO) is primarily located on the phenolate ligand moiety, whereas the lowest unoccupied molecular orbital (LUMO) is evenly distributed among phenolate and BF$_2$, containing a six-membered ring.
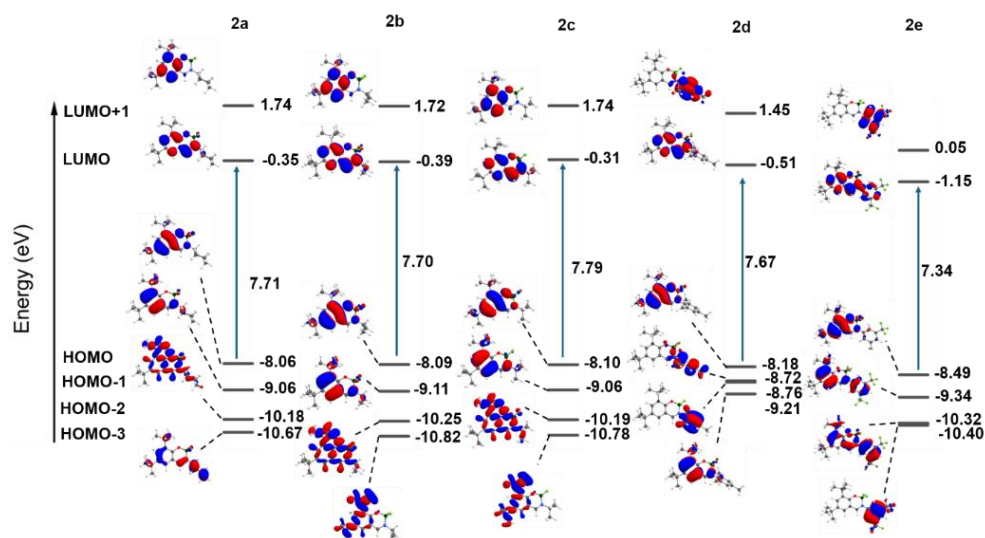

Figure 2.7 Electronic transitions of mono-BF$_2$ complexes **2a-2e** computed at the τ-HCTHhyb/def2-TZVPP(SMD: acetonitrile)//ω-B97XD/6-311G(d) level.

While the HOMO-1 orbital of **2a-2c** resides on the phenolate moiety, the HOMO-1 of **2d** can be found only on the mesityl moiety, and in **2e** it is evenly distributed between phenolate and $3,5$-$(CF_3)_2$-C_6H_3 ascribed to the π-accepting nature of $3,5$-$(CF_3)_2$-C_6H_3. Lastly, the LUMO + 1orbital of **2a-2c** is π* orbital of the phenolate moiety, whereas those of **2d** and **2e** are primarily centred on N-substituted mesityl or $3,5$-$(CF_3)_2$-C_6H_3 moieties, respectively. For complexes **2a-2f**, the first excitation (lowest in energy) results from the transition of electrons between HOMO and LUMO (**Figure 2.7**). The second excitation is associated with the transfer of electrons from HOMO-1→ LUMO for complexes **2a-2c** and **2e** or HOMO-3 → LUMO for complex **2d**. The electron-withdrawing -CF$_3$ substituents on the aromatic moiety (3,5-(CF3)2-

C6H3) of the imine exhibit lower LUMO energy in **2e** that resulted in decreased HOMO-LUMO gaps compared to that of **2d** ($E_{HOMO-LUMO}$ = 3.73 eV(**2d**) and 3.48 eV (**2e**)). This satisfactorily explains the experimentally observed red shift in the absorption spectra of **2e**. Comparison of the electrostatic potential surface plots between **2d** and **2e Figure 2.7** indeed shows effective electron delocalization in **2e** compared to **2d**, indicating efficient ICT in **2e**. From the optimized geometries, the dihedral angle between the BF_2-containing six-membered ring and the N-substituted aromatic rings was found to be 43.1° in **2e** and 90.8° in **2d**. The electronic charge distribution can also be understood from the LUMO and HOMO-1 orbitals of **2d** and **2e Figure 2.8**
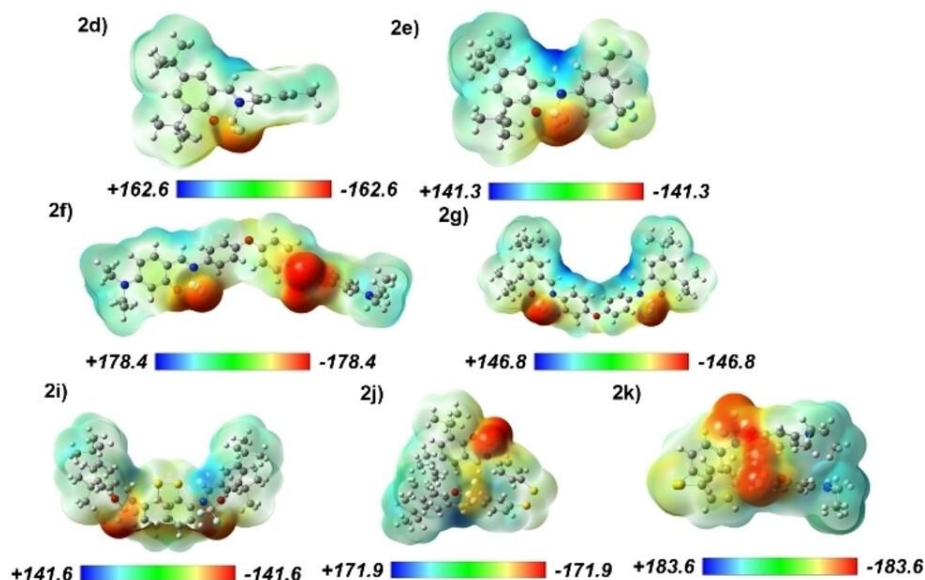
Figure 2.8 Electrostatic potential maps (isovalence=0.002).

The energy of the molecular orbitals of the bi-BF_2 complexes **2f-2k** using the time-dependent density functional theory (TD-DFT) revealed that the electron-donating substituent NEt_2 on the phenolate part increases the HOMO energies of **2f** and **2k** relative to other bi-BF_2 complexes **Figure 2.9**. This causes a lower HOMO-LUMO gap in **2f** (3.29 eV) and **2k** (2.96 eV), which explains the observed red shifts in these complexes. The HOMO of **2f** indeed show extended electron delocalization, including the participation of the lone pairs located on NEt_2, which can also be observed from the electrostatic potential maps

Figure 2.9. Among the disulfide spacer-based bi-BF$_2$ complexes, reduced HOMO-LUMO gaps (3.86 (**2i**), 3.35 (**2j**), and 2.96 eV(**2k**)) clearly explain their red shifts in the absorption spectra. The optimized geometries of **2i-2k** showed remarkable differences depending on the substitution pattern relative to the di-sulphide bond (ortho vs para). The substitution also impacts on the electronic charge distributions on **2i-2k**. Two sides of the **2j** and **2k** align parallel concerning the disulphide bondshinting at possible π-π interactions.
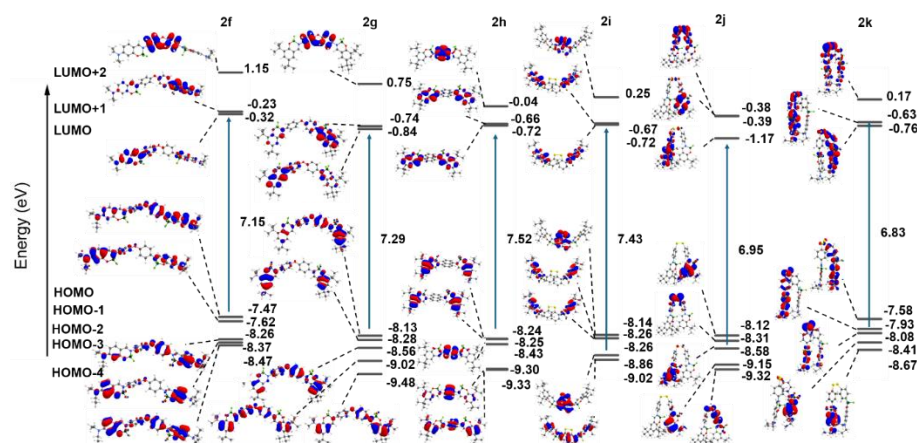
Figure 2.9 7. Electronic transitions of di-BF$_2$ complexes **2f-2k** computed at the τ-HCTHhyb/def2-TZVPP(SMD: acetonitrile)//ω-B97XD/6-311G(d) level.

For bi-BF$_2$ complexes **2f-2h**, the first excitation results from the transition of electrons between HOMO and LUMO. The second excitation is associated with the transfer of electrons from HOMO-1→LUMO+1 for complex **2f**, or HOMO-3→LUMO for complex **2g**, or HOMO-2→LUMO+2 for **2h**. Interestingly, the first excitation results from the transition of electrons between HOMO-2→LUMO for **2i** and **2j**, and between HOMO-1→LUMO+1 for **2k**. According to the electronic distribution, the transitions in the absorption process for **2a-2k** complexes are attributed to n-π* and π-π*-type transitions of the respective ligands. Further, **Table 2.4** summarizes a close correlation between the TD-DFT computed and experimentally measured absorption maxima with a maximum difference of 15 nm, as well as DFT (GIAO) calculated and experimentally measured ^{11}B NMR values. This complements the appropriate selection of the theoretical methods

to shed light on the electronic transitions in the mono and bi-BF$_2$ complexes.

Table 2.4 Experimentally observed and calculated ^{11}B NMR (GIAO-ωB97XD/6-311G*//ωB97XD/6-311G*), experimental (at room temperature in ACN) and calculated UV/vis data (at τHCTHhyb/def2-TZVPP-SMD//ωB97XD/6-311G*) **2a-2k**.

Complex	^{11}B (exp) ppm	^{11}B (cal.) ppm	λ(exp) nm	λ(exp) nm	HOMO-LUMO (eV)
2a	0.77	-0.91	359	278.4 (0.49)	7.71
2b	0.82	-0.95	363	355.9 (0.11)	7.70
2c	0.99	-0.79	364	274.4 (0.45)	7.79
2d	0.8	-0.72	371	277.7 (0.54)	7.67
2e	1.03	-0.55	389	391.7 (0.13)	7.34
2f	0.9	-0.66, -0.71	407	399.7 (1.19)	7.15
2g	1.02	-0.66, --0.71	382	394.8 (0.70)	7.29
2h	1.02	-0.95	377	378.5 (0.15)	7.52
2i		-1.09	371	383.4 (0.16)	7.43

2j	0.99	-1.19, -1.25	387	390.4 (0.1)	6.95
2k	0.88	-1.21, -1.58	404	399.8 (0.62)	6.83

2.4 Conclusions

In this work, we synthesized 3,5-Di-tert-butylsalicyladehyde, 5-Diethylaminosalicyaldehyde Schiff base-based mono and bis-boron complexes. All synthesized complexes were characterized by ^{1}H, ^{13}C, and heteronuclear NMR ^{11}B and ^{19}F, mass spectrometry, and X-ray analysis as well. The photo-physical properties of these complexes are fine-tuned by varying the substitutions on nitrogen as well as the spacer of these complexes. Two of the mono-BF2 complexes showed a large Stokes shift, while the disulfide spacer containing di-BF2complexes showed aggregate-caused quenching properties. These observations are supported by the DFT calculations explaining the effects due to the variation of the energies of the LUMO or HOMO orbitals, as well as significant intermolecular π-π interactions, respectively. Fluorescence decay and quantum yields of these complexes are recorded in different solvents, and the data showed that mononuclear complexes possess comparatively higher fluorescence decay times and quantum yields compared to binuclear boron complexes.

2.5 Experimental Section

General Methods

The reactions were performed under an argon atmosphere using standard Schlenk techniques or in the open air. Chemicals were purchased from Spectrochem, Sigma-Aldrich, and TCI and used as received. All the solvents were purified by distillation using the appropriate drying agents, deoxygenated using three freeze–pump–thaw cycles, and stored over molecular sieves under dry argon before use. The deuterated solvents used for NMR spectroscopy were deoxygenated by freeze–

pump–thaw cycles and stored under an argon atmosphere over molecular sieves. NMR chemical shifts are reported in ppm and coupling constants in Hz. ^{1}H, ^{11}B, ^{13}C, and ^{19}F NMR spectroscopy data were obtained at ambient temperature using a Bruker 500 NMR spectrometer (operating at 500 MHz for ^{1}H, 126 MHz for ^{13}C, 160 MHz for ^{11}B and 471 MHz for ^{19}F). ^{1}H NMR spectra were referenced via residual proton resonances of CDCl$_3$ (^{1}H, 7.26 ppm) and ^{13}C NMR spectra were referenced to CDCl$_3$ (^{13}C, 77.16 ppm) and BF$_3$·OEt$_2$ used as an internal standard used for ^{11}B NMR. Ligands 1a-1i were prepared by the previously reported procedure. [86-88] Bruker micrOTOF-Q II Daltonik was used to obtain HRMS spectrum. Photoluminescence (PL) spectra were recorded by using a Fluoromax-4 spectrofluorometer (HORIBA Jobin Yvon, model FM100) with an excitation and emission slit width at 5 nm. UV-Vis spectroscopy was performed on a 3 mL solution using the Varian UV−Vis spectrophotometer (Cary 100 Bio) in a quartz cuvette (1 cm × 1 cm). Cyclic voltammetry was performed using a C-H Instruments model CHI1103C in dichloromethane solvent using glassy carbon as the working electrode, Pt wire as the counter electrode, and a saturated calomel electrode (SCE) as the reference electrode. The scan rate was 100mV. A solution of Bu$_4$NPF$_6$ in dichloromethane (0.1 M) was used as the supporting electrolyte. The temperature was kept constant throughout each experiment at 25 °C. The crystal data collection was performed on a CCD Agilent Technologies (Oxford Diffraction) SUPER NOVA (Mo at home/near, Eos) diffractometer. Data for the compounds were collected at 293 K using graphite-monochromated MoK$_\alpha$ radiation. DFT calculations were implemented in the Gaussian 09 using the hybrid functional B3LYP in combination with the cc-pVDZ basis set for all atoms.

Synthesis Details

Synthesis and characterization of ligands

Ligands (**1a-1k**) were prepared by following the previously reported protocol with slight modification [86-88] in which a catalytic amount of AcOH was added and the reflux time was reduced to 18h. Two-neck

round bottom flask was charged with appropriate aldehydes, and corresponding mono- and bis-amines were added. Dry MeOH was added to it, and the reaction mixture was refluxed for 18h under an inert atmosphere. The yellow precipitate was washed with cold MeOH, dried under vacuum collected the product as a yellow solid in good yields (85-90%).

Note: Ligands **1a-1i** were previously reported, so we are providing the data of ligands **1j** and **1k** only.

Ligand 1j

3,5-Di-tert-butylsalicylaldehyde (377.90 mg, 1.61 mmol) and 4-aminophenyl disulfide (200 mg, 0.80 mmol).

^{1}H NMR (500 MHz, CDCl$_3$) δ 13.52 (s, 2H), 8.62 (s, 2H), 7.58 – 7.52 (m, 4H), 7.46 (d, J = 2.8 Hz, 2H), 7.27 – 7.22 (m, 5H), 7.21 (d, J = 2.8 Hz, 2H), 1.47 (s, 18H), 1.32 (s, 18H). 13C NMR (126 MHz, CDCl$_3$) δ 164.14, 158.45, 148.39, 140.87, 137.21, 135.09, 129.73, 128.48, 127.04, 122.12, 118.35, 35.26, 34.34, 31.60, 29.56. **LCMS:** Calculated for C$_{42}$H$_{53}$N$_2$O$_2$S$_2$ 681.3532 [M+H], found 681.3543.

Yield 70%.

Ligand 1k

4-(Diethylamino)salicylaldehyde (311.21 mg, 1.61 mmol) and 4-aminophenyl disulfide (200 mg, 0.80 mmol).

^{1}H NMR (500 MHz, CDCl$_3$) δ 13.71 (s, 2H), 8.47 (s, 2H), 7.58 (d, J = 8.5 Hz, 4H), 7.25 – 7.18 (m, 4H), 6.33 (d, J = 2.5 Hz, 1H), 6.31 (d, J = 2.5 Hz, 1H), 6.26 (d, J = 2.5 Hz, 2H), 3.47 (q, J = 7.0 Hz, 8H), 1.28 (t, J = 7.1 Hz, 12H). **^{13}C{^{1}H} NMR** (126 MHz, CDCl$_3$) δ 164.19, 160.76, 152.09, 148.79, 134.01, 133.77, 130.27, 121.68, 109.20, 104.03, 97.84, 44.75, 12.84. **LCMS** Calculated for C$_{36}$H$_{41}$N$_2$O$_2$S$_2$ 599.2506 [M+H], found 599.2509.

Yield 80%

General procedure of complex synthesis (2a-2k)

Boron difluoride complexes were synthesized by treating the ligands (1a-1k) with BF₃·OEt₂ and diisopropylethylamine in a stochiometric ratio of 1:3:3. In an oven dried two-neck round bottom flask ligand (1a-1k) and dry DCM was charged and stirred it for 10 minutes until a clear solution is obtained. In the continuous flow of argon current DIPEA and BF₃·OEt₂ were added into the reaction mixture. Further the reaction mixture was stirred at room temperature for 18h. The reaction was quenched by distilled water and the aqueous layer was washed with DCM. All the volatiles were dried and the complex was purified by column chromatography. (**Scheme 2.1**)

Complex 2a

1a (250 mg, 0.79 mmol), DIPEA (424.37 μL, 2.37 mmol) and BF₃·OEt₂ (263 μL, 2.37 mmol).

¹H NMR (500 MHz, CDCl₃) δ 8.26 (s, 1H), 7.63 (d, J = 2.4 Hz, 1H), 7.18 (d, J = 2.4 Hz, 1H), 3.86 (t, J = 12.2 Hz, 1H), 3.75 – 1.48 (m, 10H), 1.45 (s, 9H), 1.30 (s, 9H). **¹³C{¹H} NMR** (126 MHz, CDCl₃) δ 162.23, 155.90, 141.98, 139.20, 132.94, 125.34, 115.31, 60.79, 54.26, 35.27, 34.38, 33.64, 31.40, 29.45, 25.73, 25.37. **¹¹B NMR** (160 MHz, CDCl₃) δ 0.77 (td, J = 16.5, 4.5 Hz), -0.89. **¹⁹F NMR** (471 MHz, CDCl₃) δ -138.06**. FT-IR** (ν, cm⁻¹) 3090 (Ar-CH), 2960-2872 (Aliph-CH), 1610 (C=N), 1280 (C=C), 1245, 1120, 1024, 945, 823 (Aliph, C-C). **HRMS (ESI):** Calculated for C₂₁H₃₂BF₂NONa 386.2441 [M+Na], found 386.2448.

Yield 90%.

Complex 2b

1b (200 mg, 0.726 mmol), DIPEA (388 μL, 2.17 mmol) and BF₃·OEt₂ (241 μL, 1.37 mmol).

¹H NMR (500 MHz, CDCl₃) δ 8.27 (s, 1H), 7.64 (d, J = 2.5 Hz, 1H), 7.19 (d, J = 2.4 Hz, 1H), 4.28 (p, J = 6.7 Hz, 1H), 1.49 (d, J = 6.7 Hz, 6H), 1.46 (s, 9H), 1.31 (s, 9H). **¹³C{¹H} NMR** (126 MHz, CDCl₃) δ 162.03, 155.99, 142.02, 139.23, 133.01, 125.36, 115.31, 53.53, 35.27,

34.39, 31.39, 29.45, 22.98. ^{11}B NMR (160 MHz, CDCl$_3$) δ 0.82. ^{19}F NMR (471 MHz, CDCl$_3$) δ -138.28. **FT-IR** (ν, cm^{-1}) 3080 (Ar-CH), 2960-2872 (Aliph-CH), 1610 (C=N), 1280 (C=C), 1245, 1120, 1024, 945, 823 (Aliph, C-C). **HRMS (ESI):** Calculated for C$_{18}$H$_{28}$BF$_2$NONa 346.2128 [M+Na], found 346.2125.

Yield 88%.

Complex 2c

1c (300 mg, 1.03 mmol), DIPEA (555 μL, 3.10 mmol) and BF$_3$·OEt$_2$ (344.76 μL, 310 mmol).

^{1}**H NMR** (500 MHz, CDCl$_3$) δ 8.33 (s, 1H), 7.62 (d, J = 2.4 Hz, 1H), 7.19 (d, J = 1.0 Hz, 1H), 1.61 (s, 9H), 1.46 (s, 9H), 1.31 (s, 9H). ^{13}**C{^{1}H} NMR** (126 MHz, CDCl$_3$) δ 161.84, 155.97, 142.03, 139.12, 132.75, 125.78, 115.76, 61.50, 35.22, 34.41, 31.43, 29.72, 29.47. ^{11}**B NMR** (160 MHz, CDCl$_3$) δ 0.99. ^{19}**F NMR** (471 MHz, CDCl$_3$) δ -134.15. **FT-IR** (ν, cm^{-1}) 3080 (Ar-CH), 2960-2872 (Aliph-CH), 1610 (C=N), 1280 (C=C), 1245, 1120, 1024, 945, 823 (Aliph, C-C). **HRMS (ESI):** Calculated for C$_{19}$H$_{30}$BF$_2$NONa 360.2284 [M+Na], found 360.2292.

Yield 87%.

Complex 2d

1d (151 mg, 0.42 mmol), DIPEA (230 μL, 1.28 mmol) and BF$_3$·OEt$_2$ (142 μL, 1.28 mmol).

^{1}**H NMR** (500 MHz, CDCl$_3$) δ 8.12 (s, 1H), 7.74 (d, J = 2.4 Hz, 1H), 7.21 (d, J = 2.5 Hz, 1H), 6.96 (s, 2H), 2.32 (s, 3H), 2.25 (s, 6H), 1.51 (s, 9H), 1.33 (s, 9H). ^{13}**C{^{1}H} NMR** (126 MHz, CDCl$_3$) δ 168.04, 157.56, 142.37, 139.90, 138.89, 138.26, 134.36, 133.30, 129.45, 125.65, 115.52, 35.44, 34.46, 31.34, 29.51, 21.07, 18.22. ^{11}**B NMR** (160 MHz, CDCl$_3$) δ 0.80. ^{19}**F NMR** (471 MHz, CDCl$_3$) δ -137.43. **FT-IR** (ν, cm^{-1}) 3085 (Ar-CH), 2960-2872 (Aliph-CH), 1610 (C=N), 1280 (C=C), 1245, 1120, 1024, 945, 823 (Aliph, C-C). **HRMS (ESI):** Calculated for C$_{24}$H$_{32}$NOBF$_2$Na 422.2442 [M+Na], found 422.2433.

Yield 85%

Complex 2e

1e (250 mg, 0.56 mmol), DIPEA (300 μL, 1.68 mmol) and $BF_3 \cdot OEt_2$ (186.69 μL, 1.68 mmol).

^{1}H NMR (500 MHz, CDCl$_3$) δ 8.39 (s, 1H), 7.94 (s, 2H), 7.90 (s, 1H), 7.74 (d, *J* = 2.5 Hz, 1H), 1.41 (s, 9H), 1.26 (s, 9H). **^{13}C{^{1}H} NMR** (126 MHz, CDCl$_3$) δ 166.72, 158.68, 150.44, 141.39, 137.55, 133.17, 132.91, 129.69, 127.63, 124.34, 122.17, 121.67, 117.95, 35.31, 34.40, 31.57, 29.53. **^{11}B NMR** (160 MHz, CDCl$_3$) δ 1.03 (t, *J* = 14.7 Hz). **^{19}F NMR** (471 MHz, CDCl$_3$) δ -62.90, (d, *J* = 5.1 Hz), -133.78 (dd, *J* = 30.2, 18.7 Hz). **FT-IR** (ν, cm^{-1}) 3090 (Ar-CH), 2960-2872 (Aliph-CH), 1610 (C=N), 1280 (C=C), 1240, 1120, 1024, 940, 820 (Aliph, C-C). **HRMS (ESI):** Calculated for $C_{23}H_{24}BF_8NONa$ 516.1720 [M+Na] found 516.1729.

Yield 50%.

Complex 2f

1f (150 mg, 0.27mmol), DIPEA (145.94 μL, 0.81 mmol) and $BF_3 \cdot OEt_2$ (181.34 μL, 1.63 mmol)

^{1}H NMR (500 MHz, CDCl$_3$) δ 8.06 – 7.99 (s, 2H), 7.51 – 7.43 (m, 4H), 7.23 (d, *J* = 9.0 Hz, 2H), 7.08 – 7.00 (m, 4H), 6.36 (dt, *J* = 9.0, 2.2 Hz, 2H), 6.23 (q, *J* = 2.4 Hz, 2H), 3.45 (tt, *J* = 8.4, 4.2 Hz, 8H), 1.26 – 1.22 (m, 12H). **^{13}C{^{1}H} NMR** (126 MHz, CDCl$_3$) δ 161.90, 158.21, 156.40, 156.35, 138.99, 134.03, 124.87, 119.69, 106.79, 98.22, 45.31, 12.78. **^{11}B NMR** (160 MHz, CDCl$_3$) δ 0.90, (t, *J* = 34.9 Hz). **^{19}F NMR** (471 MHz, CDCl$_3$) δ -136.49 (dd, *J* = 33.0, 15.5 Hz). **FT-IR** (ν, cm^{-1}) 3080 (Ar-CH), 2960-2865 (Aliph-CH), 1610 (C=N), 1280 (C=C), 1240, 1120, 1024, 940, 820 (Aliph, C-C). **HRMS (ESI):** Calculated for $C_{34}H_{36}B_2F_4N_4O_3Na$ 669.2813 [M+Na] found 669.2817.

Yield 80%.

Complex 2g

1g (200 mg, 0.31 mmol), DIPEA (168 μL, 0.95 mmol) and BF$_3$.OEt$_2$ (210 μL, 1.89 mmol)

^{1}H NMR (500 MHz, CDCl$_3$) δ 8.41 (s, 2H), 7.74 (d, J = 2.4 Hz, 2H), 7.56 (d, J = 8.8 Hz, 4H), 7.29 (d, J = 2.4 Hz, 2H), 7.14 (d, J = 8.9 Hz, 4H), 1.50 (s, 18H), 1.33 (s, 19H). **^{13}C{^{1}H}** (126 MHz, CDCl$_3$). δ 163.14, 158.31, 156.08, 144.35, 140.75, 137.12, 128.09, 126.89, 122.67, 119.75, 118.46, 35.25, 34.34, 31.63, 29.58 **^{11}B NMR** (160 MHz, CDCl$_3$) δ 1.02 (t, J = 15.1 Hz).**^{19}F NMR** (471 MHz, CDCl$_3$) δ -135.11 (dd, J = 30.3, 18.9 Hz). **FT-IR** (ν, cm^{-1}) 3090 (Ar-CH), 2960-2870 (Aliph-CH), 1610 (C=N), 1280 (C=C), 1240, 1125, 1024, 940, 820 (Aliph, C-C). **HRMS (ESI):** Calculated for C$_{42}$H$_{52}$N$_2$B$_2$BF$_4$O$_3$Na 751.3830 [M+Na] found 751.38590.

Yield 80%

Complex 2h

1h (1g, 1.69 mmol), DIPEA (546.88 mg, 4.23 mmol) and BF$_3$·OEt$_2$ (600 mg, 4.23 mmol)

^{1}H NMR (500 MHz, CDCl$_3$) δ 8.40 (s, 2H), 8.00 (dd, J = 6.9, 2.8 Hz, 2H), 7.82 (d, J = 2.4 Hz, 2H), 7.66 – 7.60 (m, 4H), 7.28 (d, J = 2.4 Hz, 2H), 1.55 (s, 18H), 1.35 (s, 18H). **^{13}C NMR** (126 MHz, CDCl$_3$) δ 168.33, 157.89, 142.96, 140.01, 139.24, 135.32, 129.82, 126.96, 126.24, 124.36, 124.16, 115.15, 35.50, 34.53, 31.32, 29.53. **^{11}B NMR** (160 MHz, CDCl$_3$) δ 1.02. **^{19}F NMR** (471 MHz, CDCl$_3$) δ-133.82 (q) -136.74(q). **FT-IR** (ν, cm^{-1}) 3090 (Ar-CH), 2960-2872 (Aliph-CH), 1610 (C=N), 1280 (C=C), 1240, 1120, 1024, 940, 820 (Aliph, C-C). **HRMS(ESI): Calculated for** C$_{40}$H$_{48}$B$_2$F$_4$N$_2$O$_2$Na [M+Na] 709.3743 and found values 709.3751.

Yield 81%

Complex 2i

1i (100 mg, 0.14 mmol), DIPEA (156 μL, 0.88 mmol) and BF$_3$·OEt$_2$ (97.69 μL, 0.88 mmol).

¹H NMR (500 MHz, CDCl₃) δ 8.31 (d, J = 8.4 Hz, 2H), 7.80 (d, J = 8.1 Hz, 2H), 7.57 (dd, J = 11.3, 4.9 Hz, 4H), 7.46 (d, J = 7.8 Hz, 2H), 7.36 (d, J = 2.4 Hz, 2H), 7.18 (s, 2H), 1.45 (s, 19H), 1.29 (s, 19H). **¹³C{¹H} NMR** (126 MHz, CDCl₃) δ 170.35, 153.54, 143.88, 142.78, 140.30, 132.34, 129.33, 128.69, 127.09, 121.98, 120.83, 120.54, 120.51, 113.00, 35.59, 34.57, 31.39, 29.57. **¹¹B NMR** (160 MHz, CDCl₃) δ 2.28 – 0.37 (t). **¹⁹F NMR** (471 MHz, CDCl₃) δ -137.62 (dd, J = 26.9, 10.6 Hz). **FT-IR** (v, cm⁻¹) 3085 (Ar-CH), 2960-2865 (Aliph-CH), 1610 (C=N), 1280 (C=C), 1240, 1120, 1024, 940, 825 (Aliph, C-C). **LC-MS (ESI):** calculated for $C_{44}H_{53}B_2F_4O_2S_2N_3$ [M+CH3CN] 817.3710 and found values 717.4729.

Yield 60%

Complex 2j

1j (100 mg, 0.14 mmol), DIPEA (156 μL, 0.88 mmol) and BF₃·OEt₂ (97.69 μL, 0.88 mmol).

¹H NMR (500 MHz, CDCl₃) δ 8.40 (s, 2H), 7.74 (d, J = 2.5 Hz, 2H), 7.59 (d, J = 8.7 Hz, 4H), 7.50 (d, J = 8.6 Hz, 4H), 7.29 (d, J = 2.4 Hz, 2H), 1.48 (s, 18H), 1.32 (s, 18H). **¹³C{¹H} NMR** (126 MHz, CDCl₃) δ 164.10, 157.40, 142.84, 141.73, 139.68, 137.73, 134.89, 128.43, 126.23, 124.49, 115.79, 35.36, 34.47, 31.30, 29.44. **¹¹B NMR** (160 MHz, CDCl₃) (t) δ 0.99. **¹⁹F NMR** (471 MHz, CDCl₃) δ -134.93 (d, J = 26.0 Hz). **FT-IR** (v, cm⁻¹) 3080 (Ar-CH), 2960-2872 (Aliph-CH), 1610 (C=N), 1280 (C=C), 1240, 1125, 1024, 940, 830 (Aliph, C-C). **LC-MS (ESI):** calculated for $C_{44}H_{53}B_2F_4O_2S_2N_3$ [M+CH3CN] 817.3710 and found values 717.4729.

Yield: 60%

Complex 2k

1k (100 mg, 0.16 mmol), DIPEA (178 μL, 1.00 mmol) and BF₃.OEt₂ (112.66 μL, 1.00 mmol).

¹H NMR (500 MHz, CDCl₃) δ 8.01 (d, J = 5.8 Hz, 2H), 7.61 – 7.48 (m, 4H), 7.44 (d, J = 8.4 Hz, 4H), 7.21 (d, J = 9.1 Hz, 2H), 6.35 (dd, J = 9.1, 2.4 Hz, 2H), 6.21 (d, J = 2.4 Hz, 2H), 3.44 (q, J = 7.1 Hz, 8H), 1.23 (t, J = 7.1 Hz, 12H). **¹³C{¹H} NMR** (126 MHz, CDCl₃) δ 162.03, 158.04, 156.53, 142.61, 136.08, 134.18, 128.86, 124.03, 106.99, 98.18, 45.35, 12.79. **¹¹B NMR** (160 MHz, CDCl₃) δ 0.88 (t, J = 17.2 Hz). **¹⁹F NMR** (471 MHz, CDCl₃) δ -136.30 (dd, J = 34.0, 15.4 Hz). **FT-IR** (ν, cm⁻¹) 3090 (Ar-CH), 2960-2872 (Aliph-CH), 1610 (C=N), 1280 (C=C), 1240, 1120, 1024, 940, 820 (Aliph, C-C). **LC-MS (ESI):** calculated for C₃₄H₃₆B₂F₄O₂S₂N₄ [M+Na] 717.2306 and found values 717.2360. **Yield**: 65%

Spectroscopic details of ligands and complexes
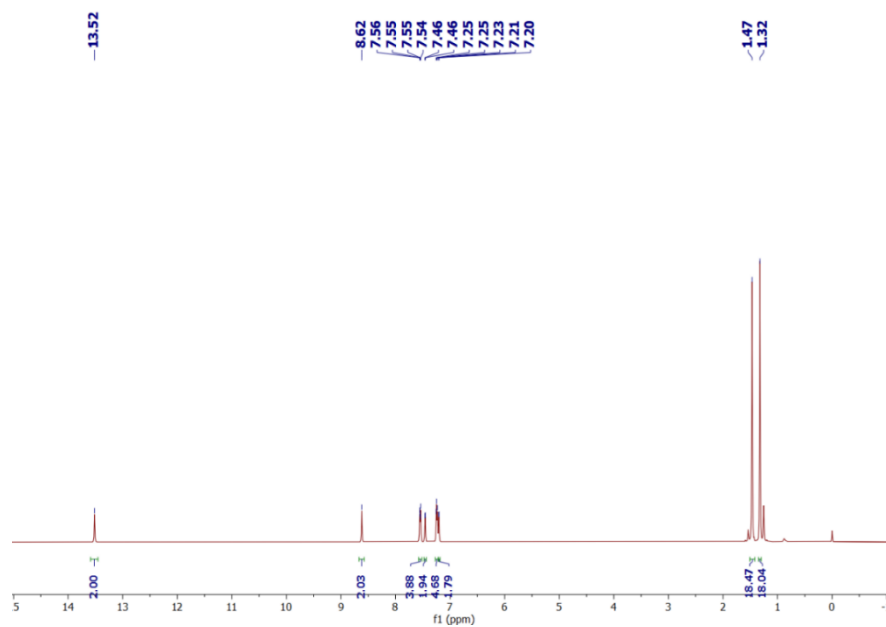
Figure 2.10 ^{1}H NMR of ligand **1j**.
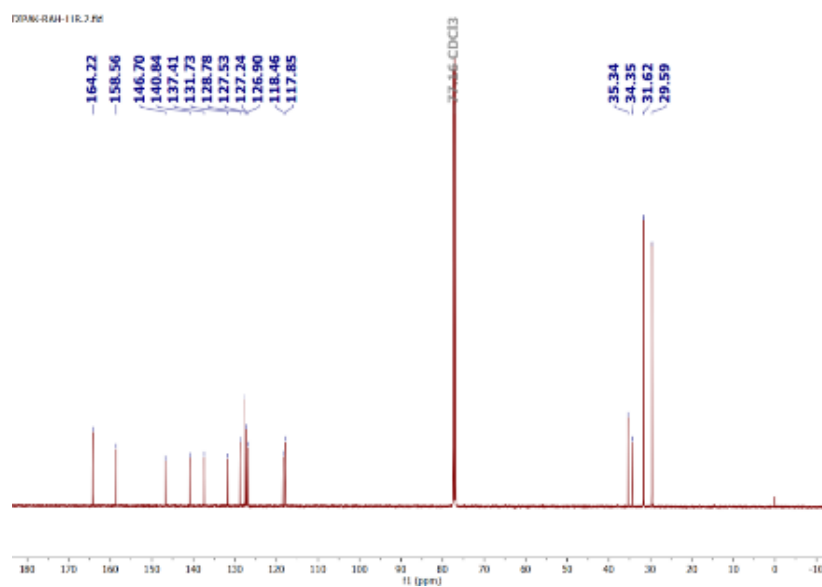
Figure 2.11 ^{13}C {^{1}H} NMR of ligand **1j**.
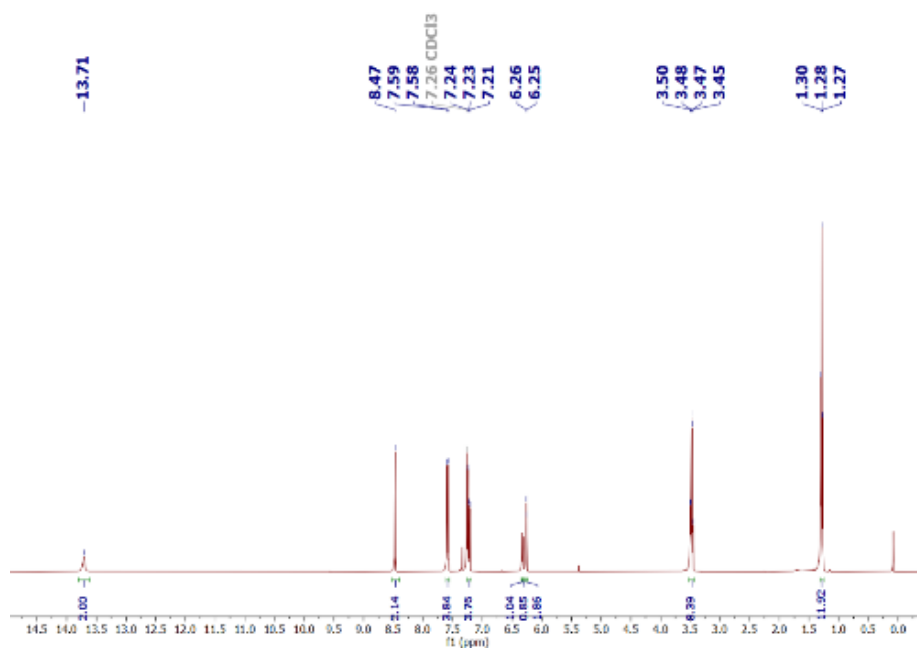
Figure 2.12 ^{1}H NMR of ligand **1k**.
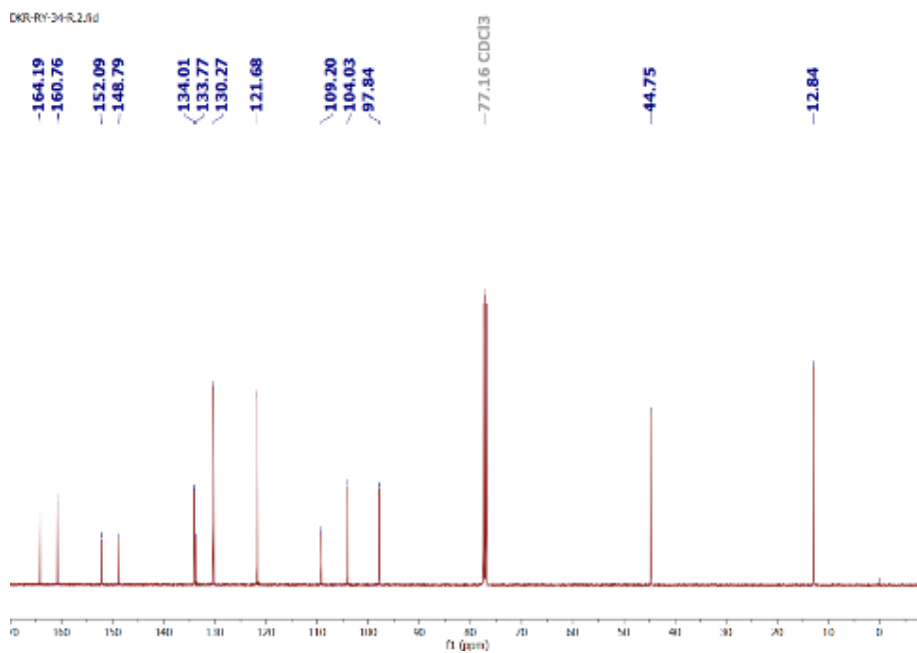
Figure 2.13 ^{13}C{^{1}H} NMR of ligand **1k**.
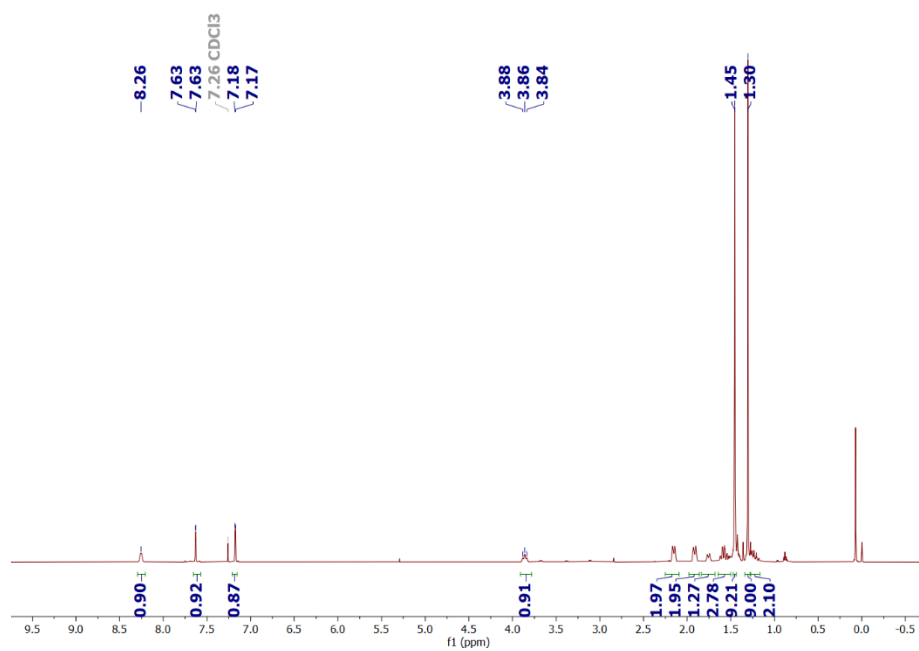
Figure 2.14 ^{1}HNMR of complex **2a**.
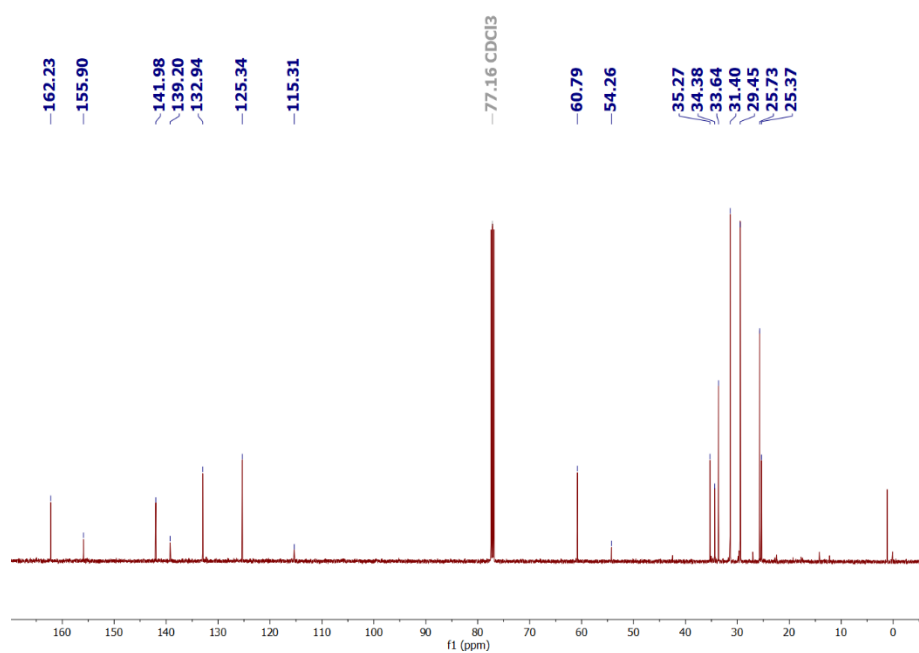
Figure 2.15 ^{13}C{^{1}H} NMR of complex **2a**.

0.78
0.76
0.66
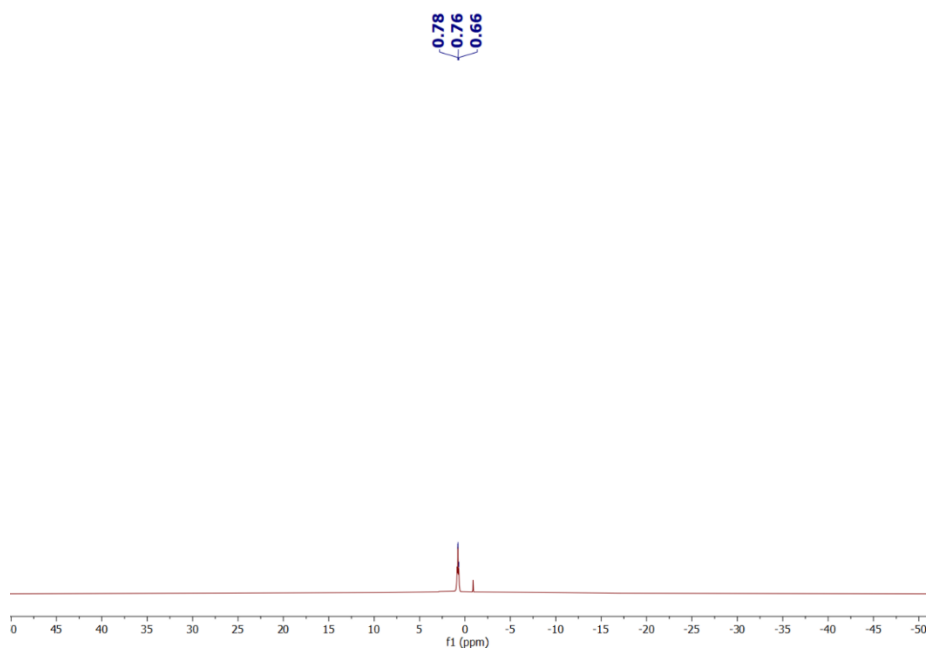
Figure 2.16 ^{11}B NMR of complex **2a**.

-138.06
-138.09
-138.13
-138.16
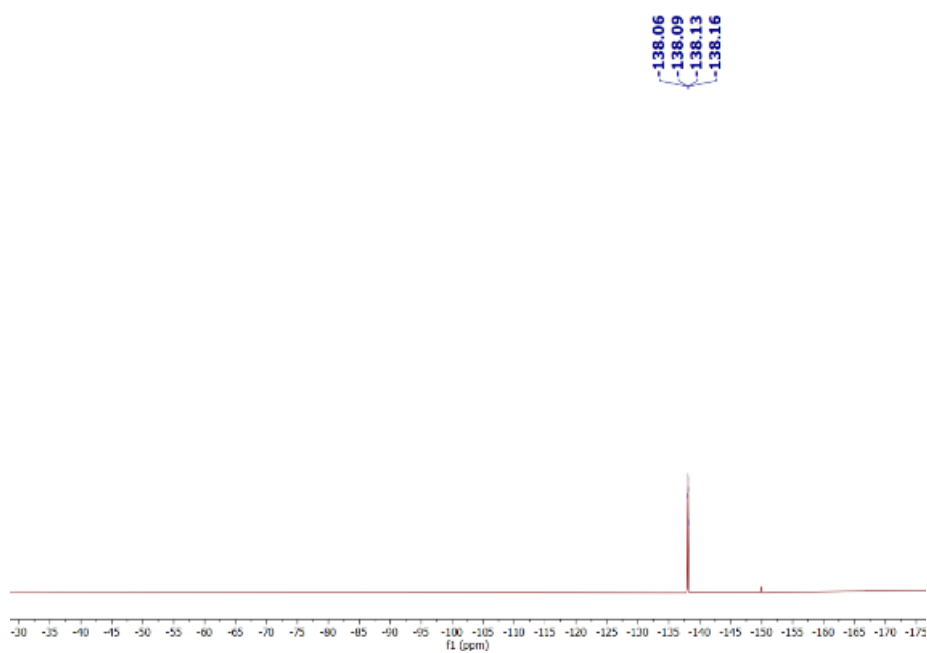
Figure 2.17 ^{19}F NMR of complex **2a**.
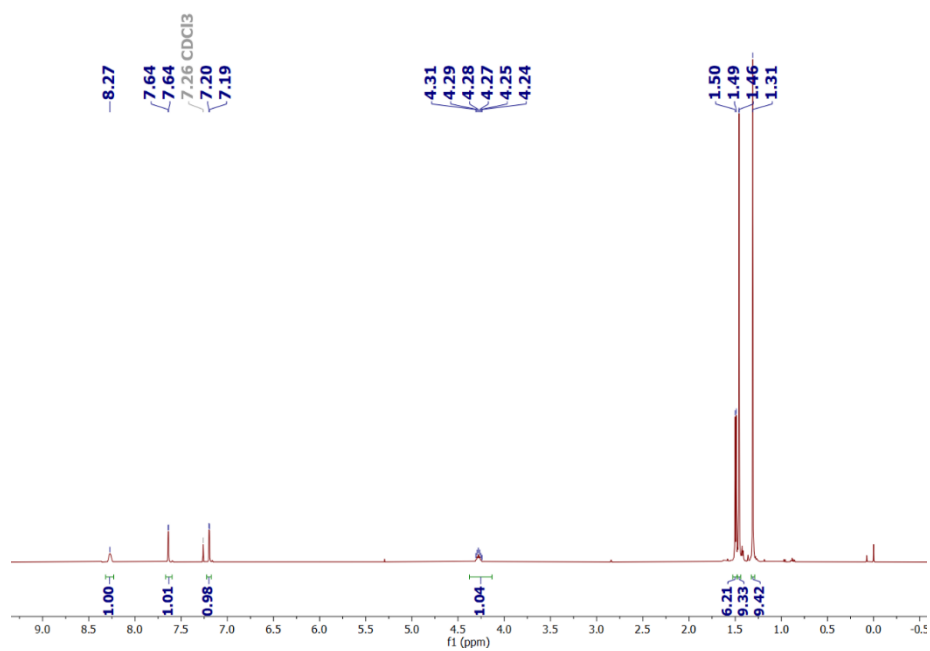
Figure 2.18 ¹H NMR of complex **2b**.
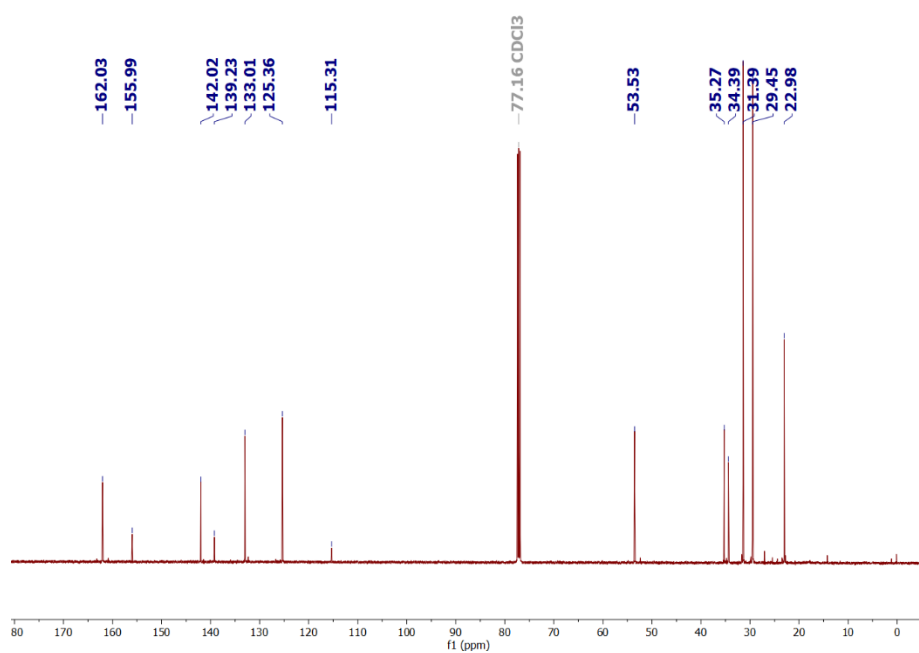
Figure 2.19 ¹³C{¹H} NMR of complex **2b**.

0.88
0.81
0.78

50 45 40 35 30 25 20 15 10 5 0 -5 -10 -15 -20 -25 -30 -35 -40 -45 -50
f1 (ppm)
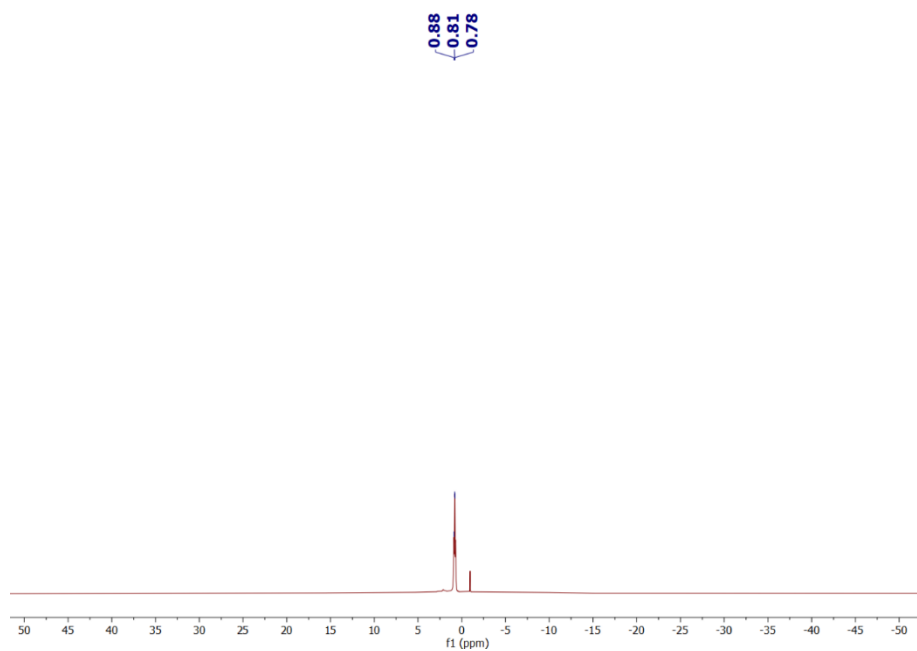
Figure 2.20 ^{11}B NMR of complex **2b**.

-138.28
-138.31
-138.35
-138.38

-30 -35 -40 -45 -50 -55 -60 -65 -70 -75 -80 -85 -90 -95 -100 -105 -110 -115 -120 -125 -130 -135 -140 -145 -150 -155 -160 -165 -170 -175
f1 (ppm)
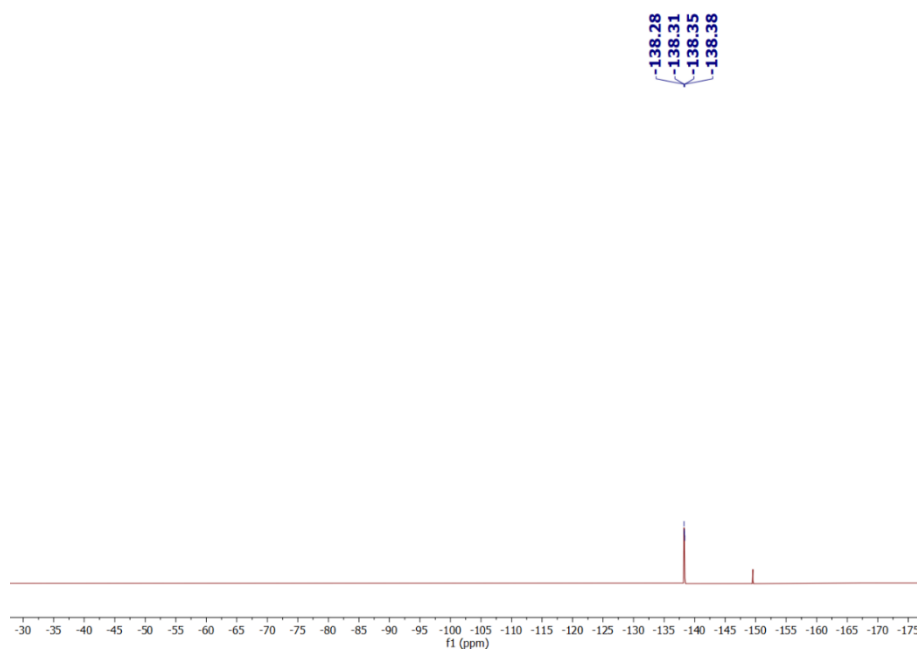
Figure 2.21 ^{19}F NMR of complex **2b**
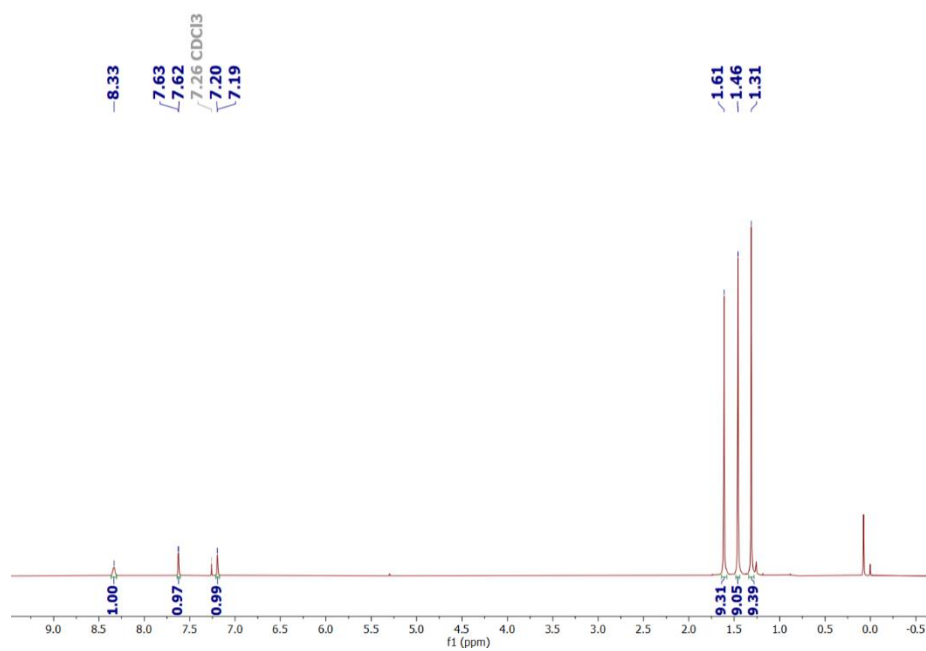
Figure 2.22 ¹H NMR of complex **2c**.
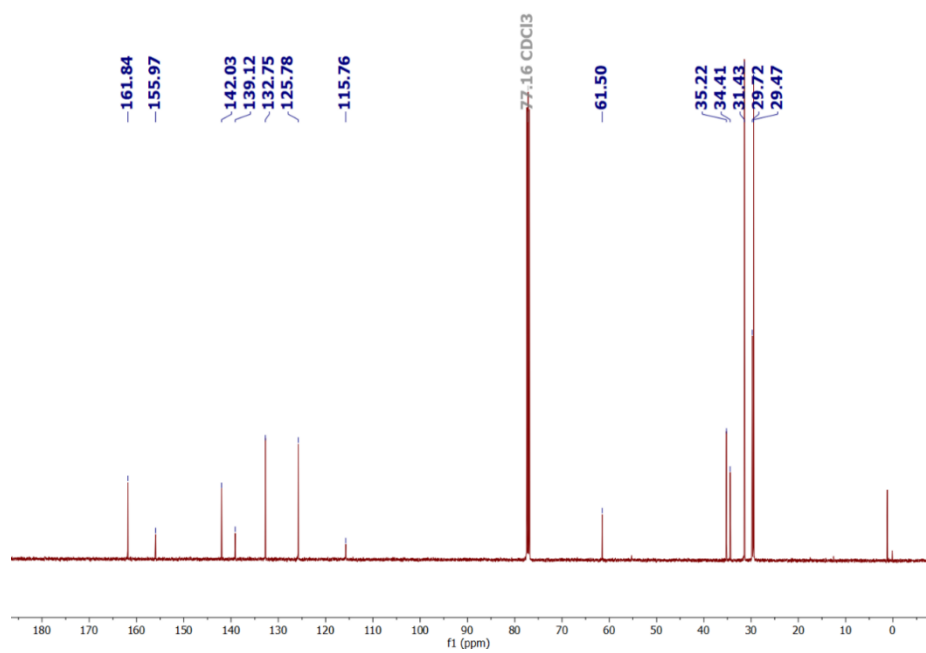
Figure 2.23 ¹³C{¹H} NMR of complex **2c**.

117

1.11
0.99
0.88

50 45 40 35 30 25 20 15 10 5 0 -5 -10 -15 -20 -25 -30 -35 -40 -45 -50
f1 (ppm)
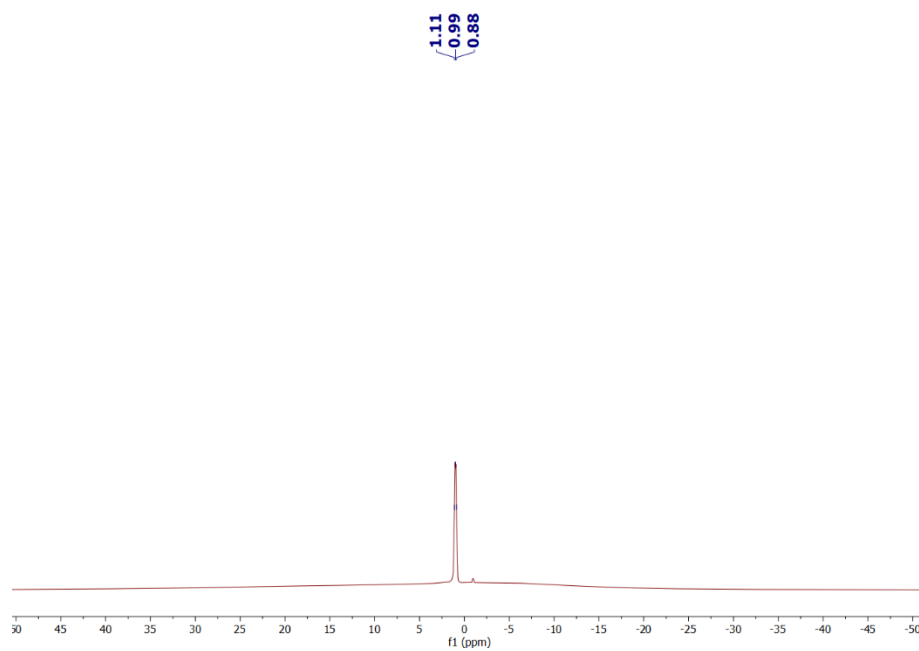
Figure 2.24 ^{11}B NMR of complex **2c**.

-138.06
-138.09
-138.13
-138.16

-30 -35 -40 -45 -50 -55 -60 -65 -70 -75 -80 -85 -90 -95 -100 -105 -110 -115 -120 -125 -130 -135 -140 -145 -150 -155 -160 -165 -170 -175
f1 (ppm)
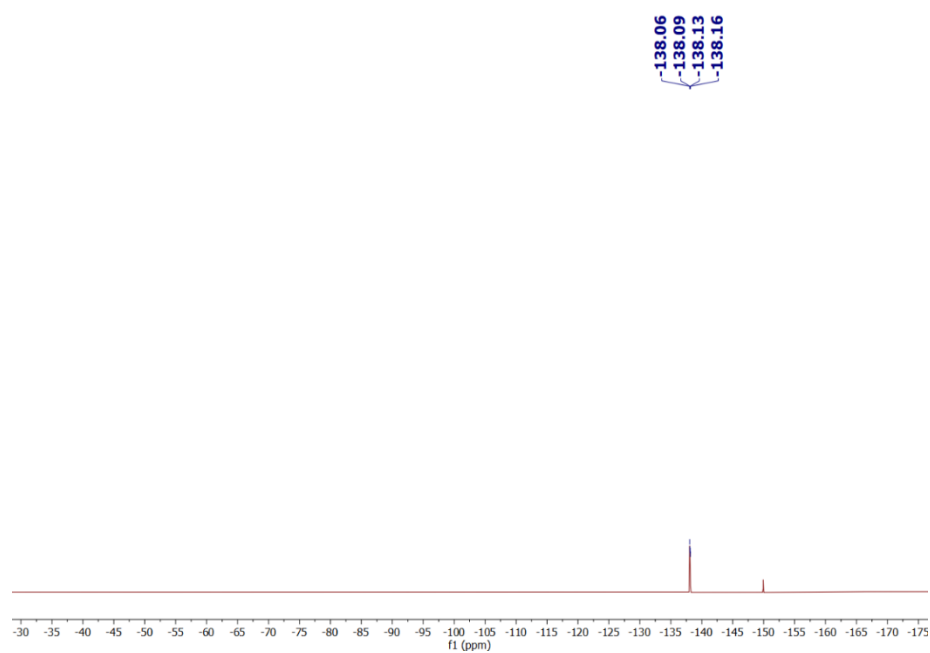
Figure 2.25 ^{19}F NMR of complex **2c**.

118
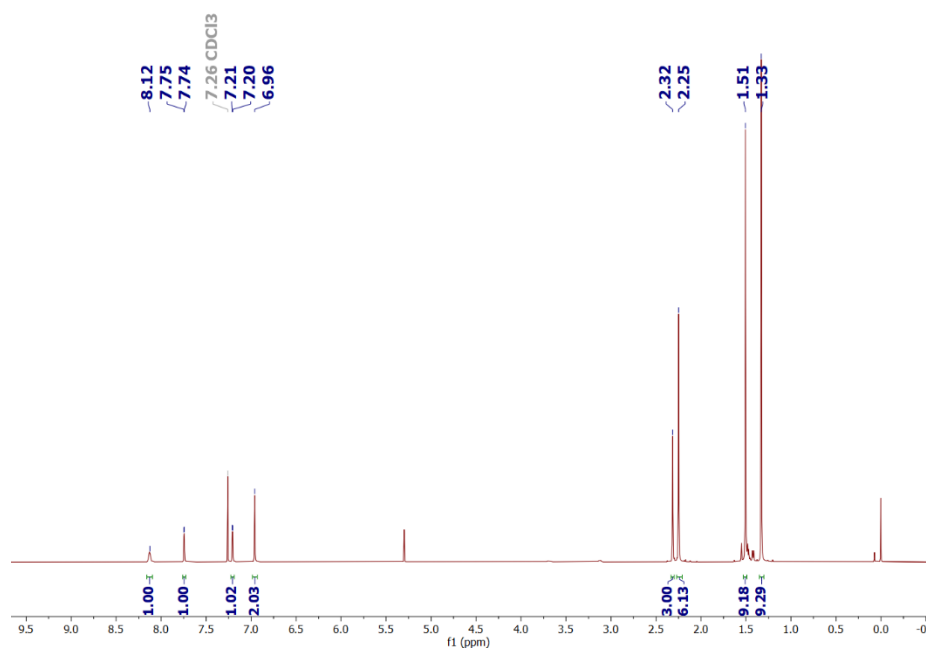
Figure 2.26 ^{1}H NMR of complex **2d**.
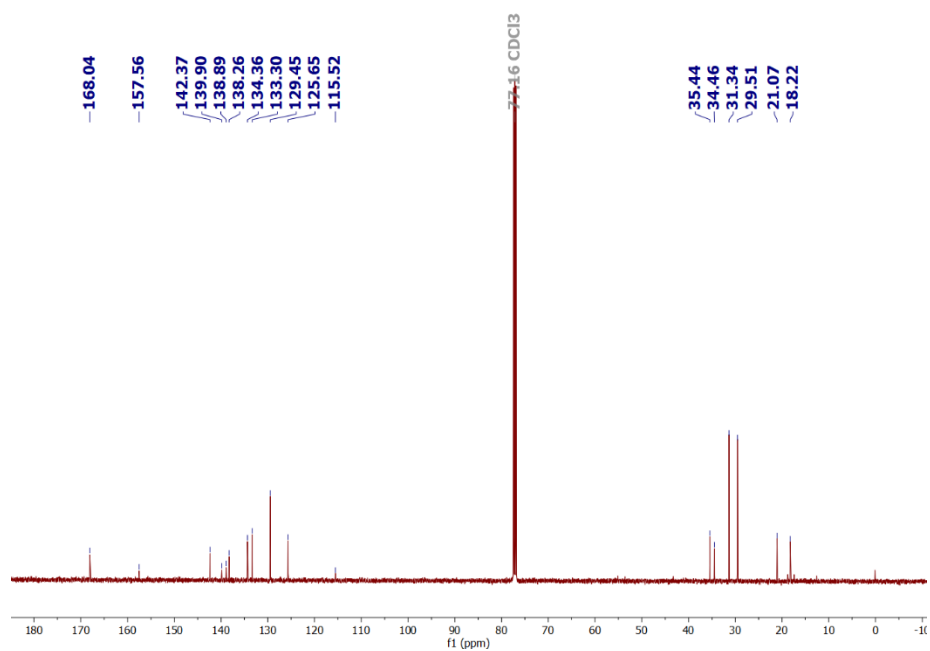
Figure 2.27 ^{13}C{^{1}H} NMR of complex **2d**
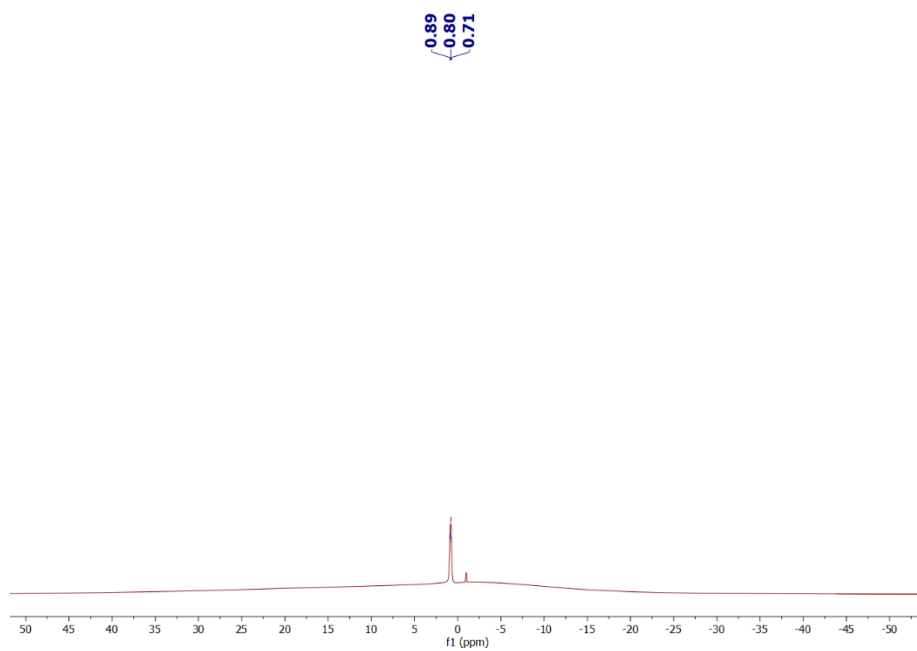
Figure 2.28 ^{11}B NMR of complex **2d**.
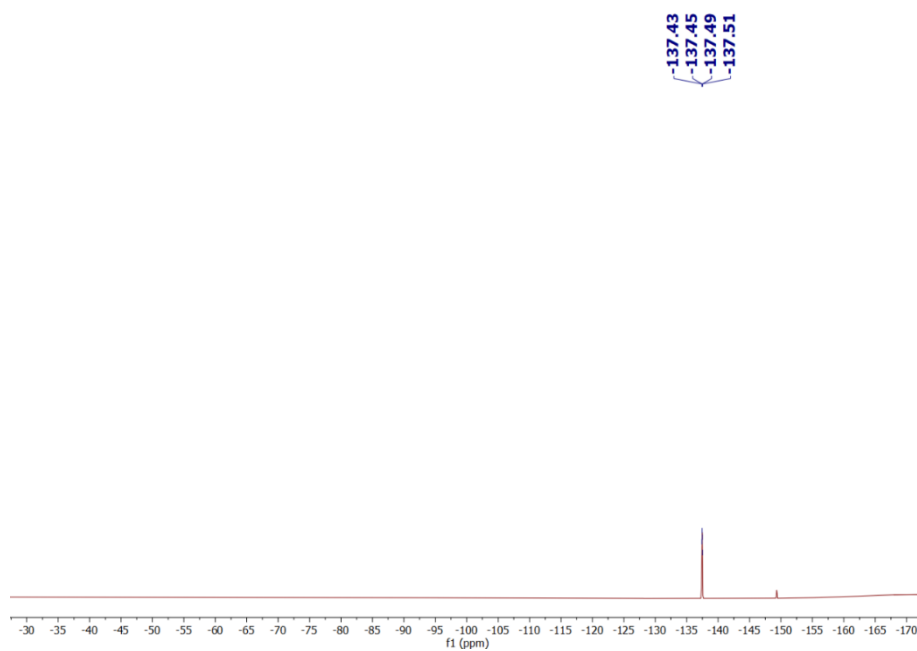
Figure 2.29 ^{19}F NMR of complex **2d**.
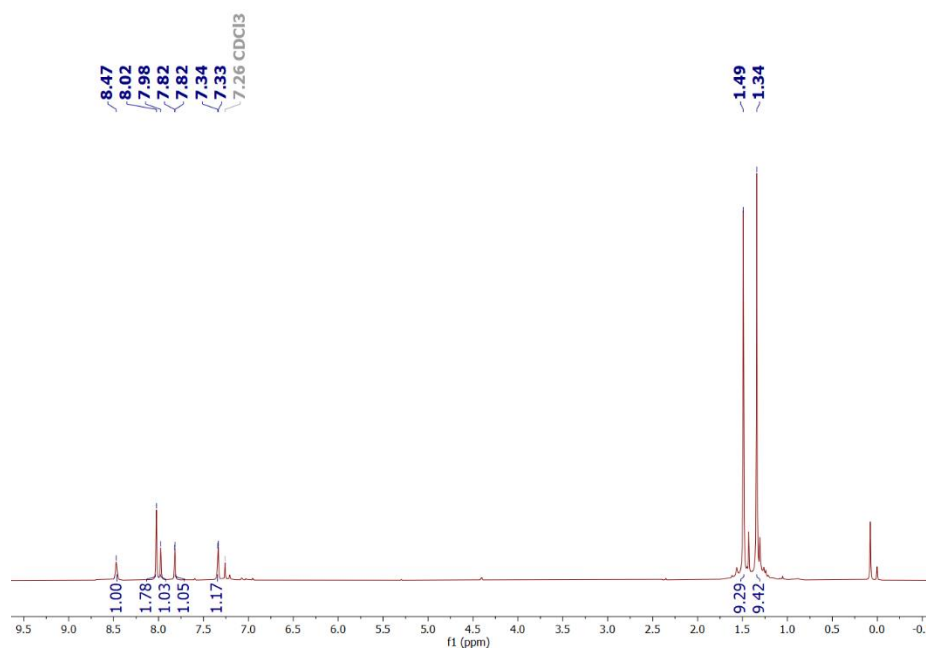
Figure 2.30 ^{1}H NMR of complex **2e**.
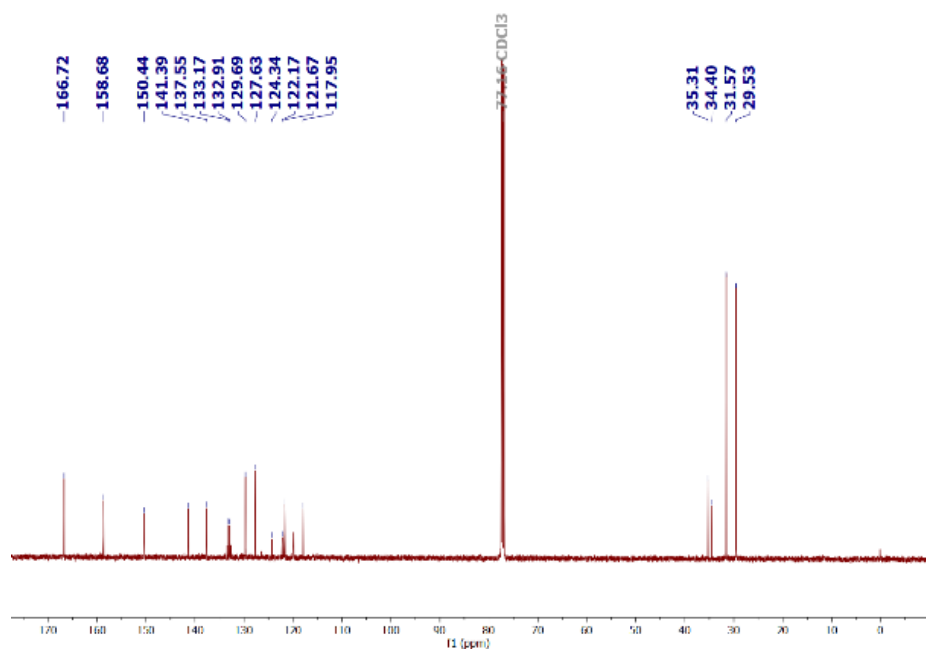
Figure 2.31 ^{13}C{^{1}H} NMR of complex **2e**.

1.12
1.03
0.94

-62.90
-63.16
-63.26
-63.28

-133.79
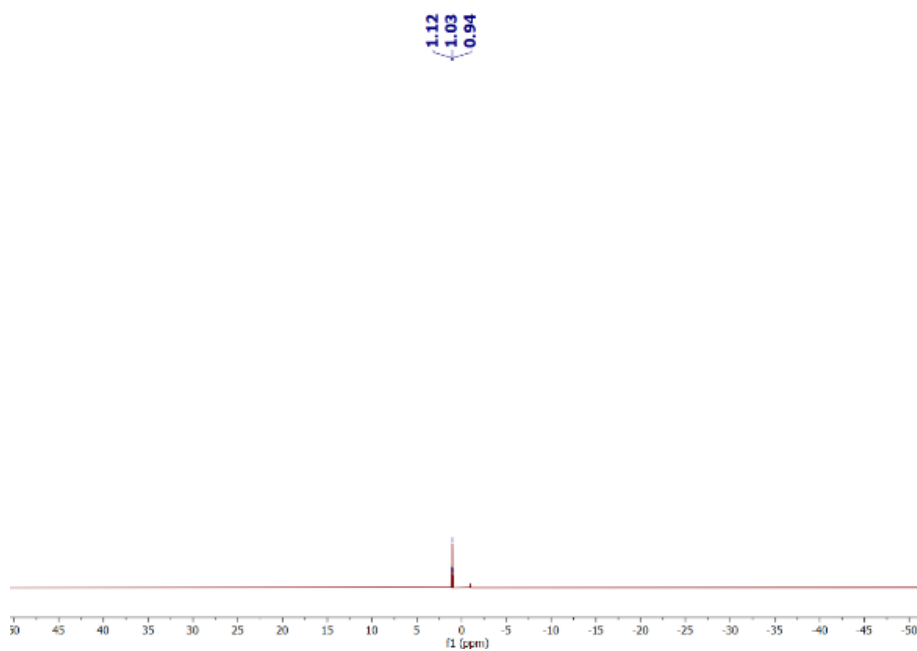
Figure 2.32 ^{11}B NMR of complex **2e**.
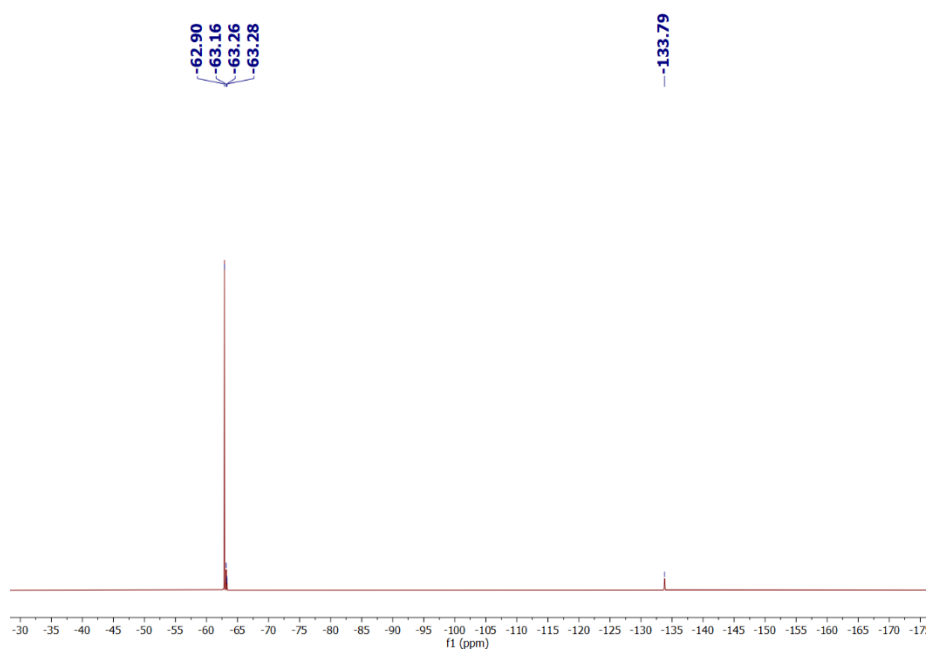
Figure 2.33 ^{19}F NMR of complex **2e**.
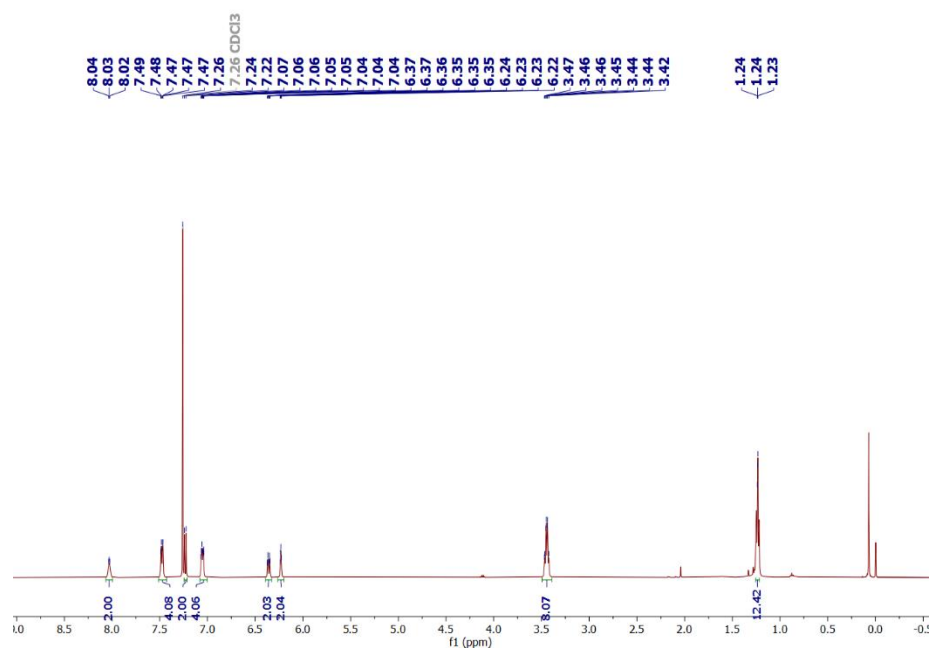
Figure 2.34 ^{1}H NMR of complex **2f**.
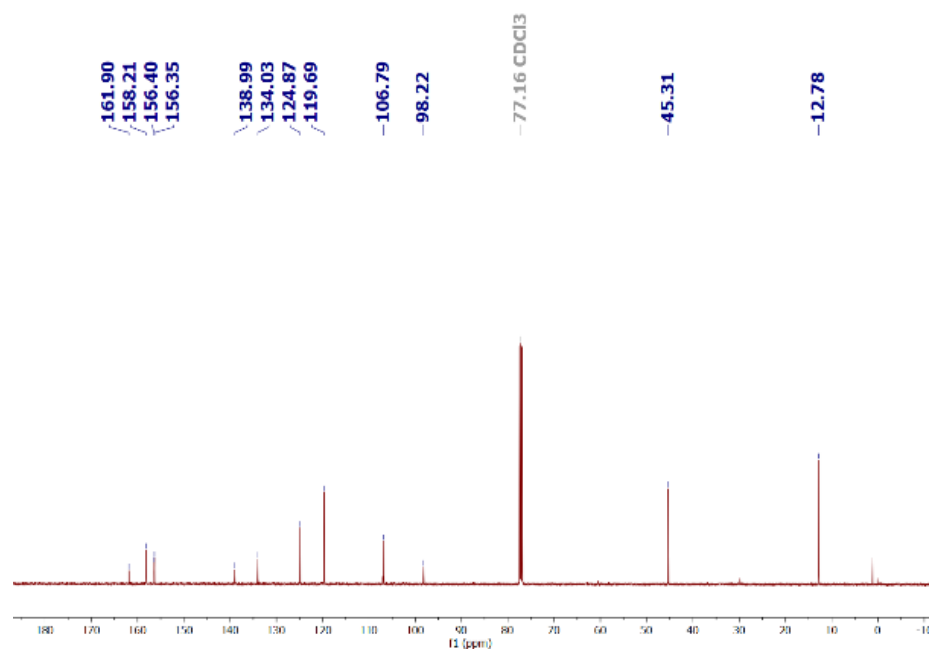
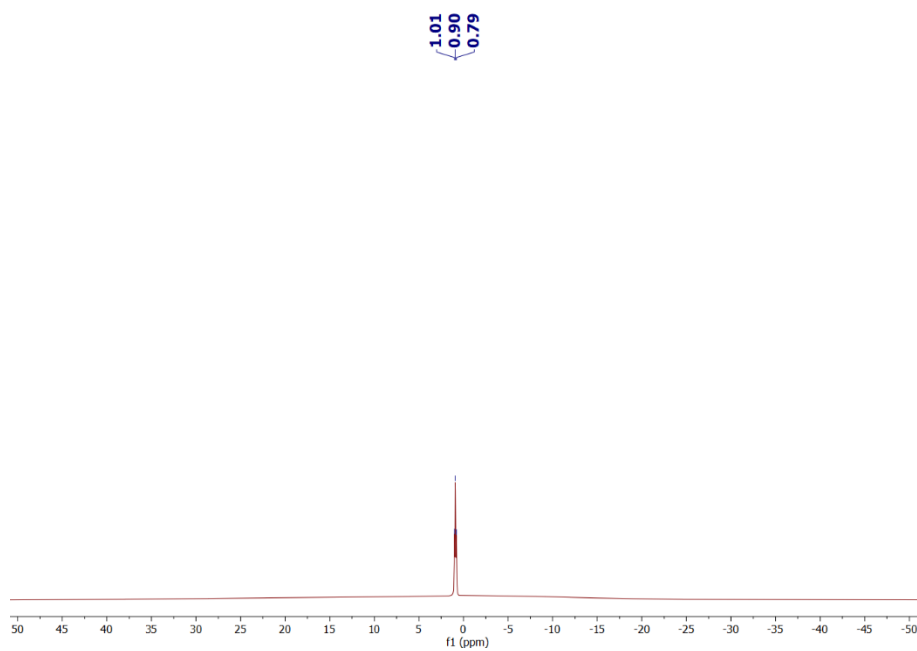**Figure 2.35** ^{13}C{^{1}H} NMR of complex **2f**.

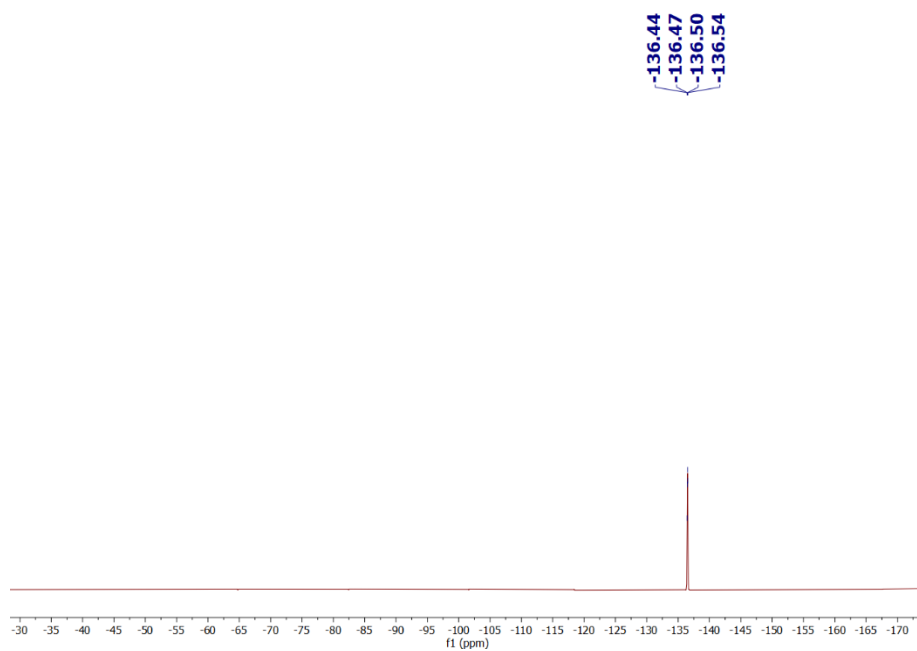**Figure 2.36** ^{11}B NMR of complex **2f**.

Figure 2.37 ^{19}F NMR of complex **2f**.
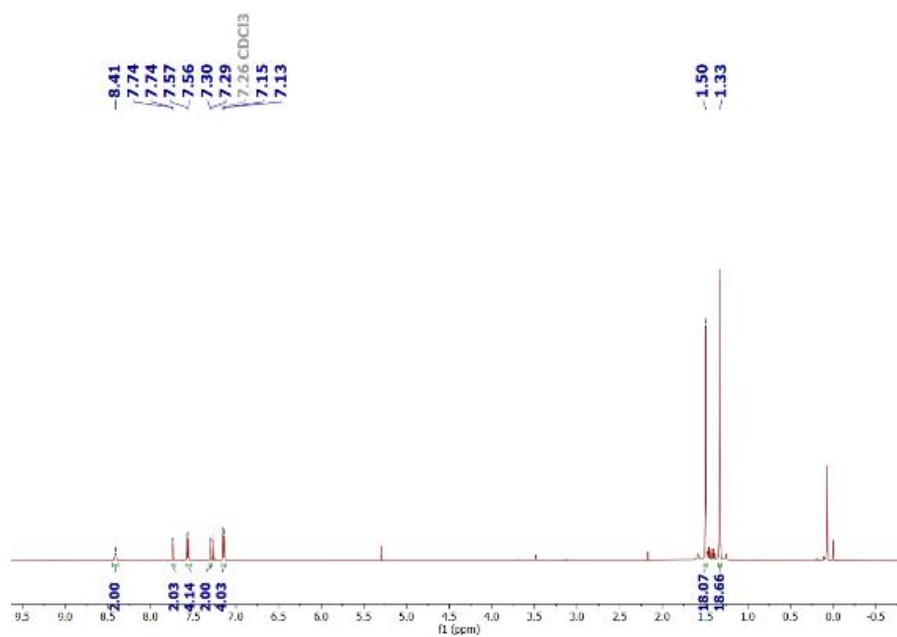
Figure 2.38 ¹H NMR of complex **2g**.
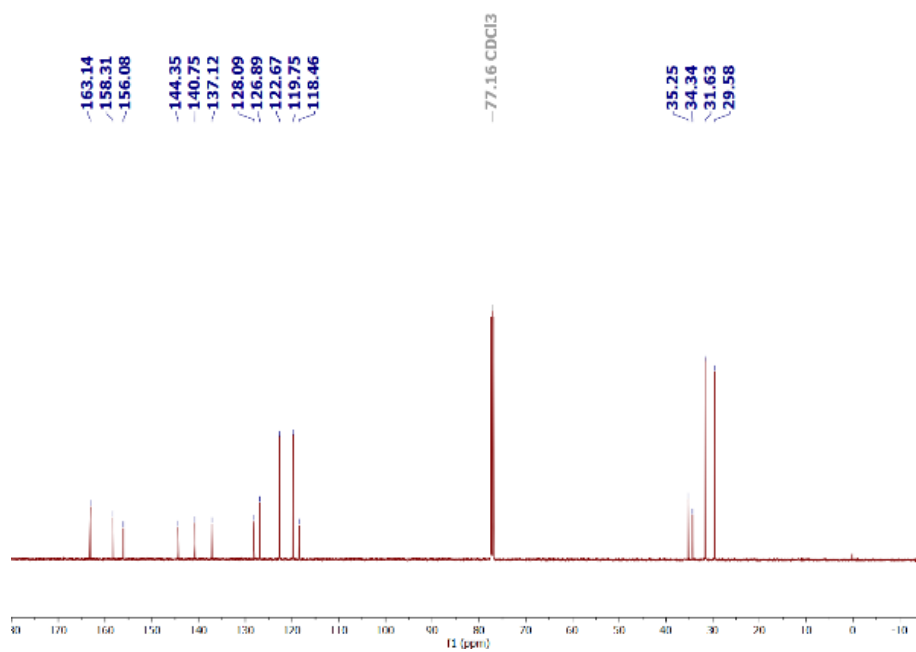
Figure 2.39 ¹³C{¹H} NMR of complex **2g**.

1.11
1.02
0.92
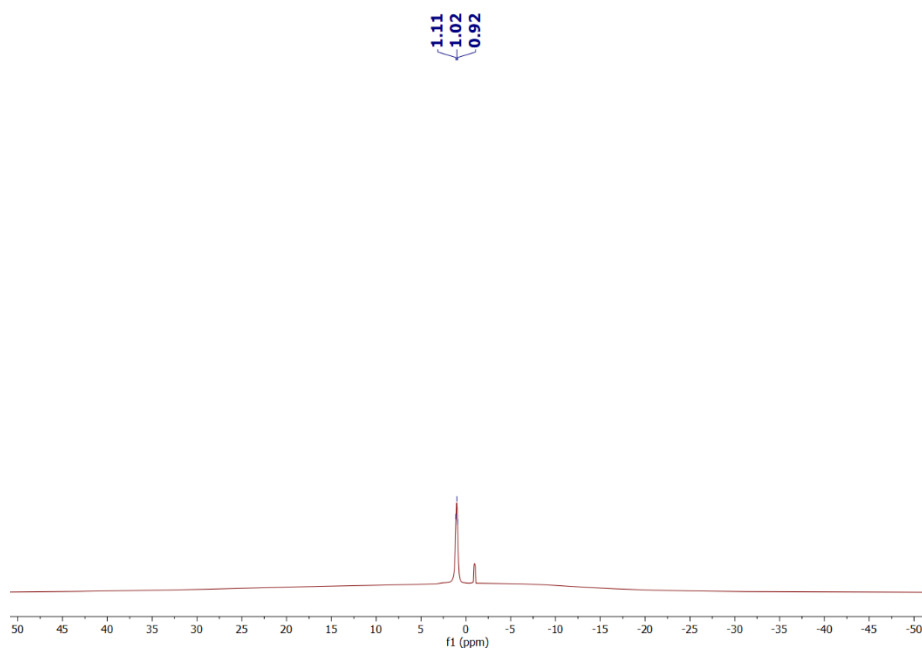
Figure 2.40 ^{11}B NMR of complex **2g**.

-135.06
-135.12
-135.17
-135.23
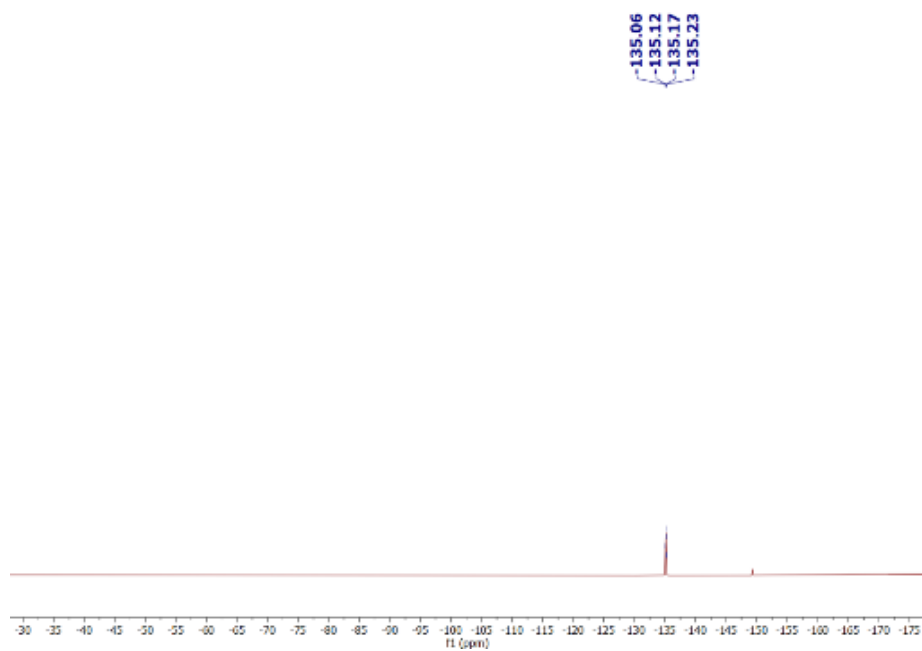
Figure 2.41 ^{19}F NMR of complex **2g**.
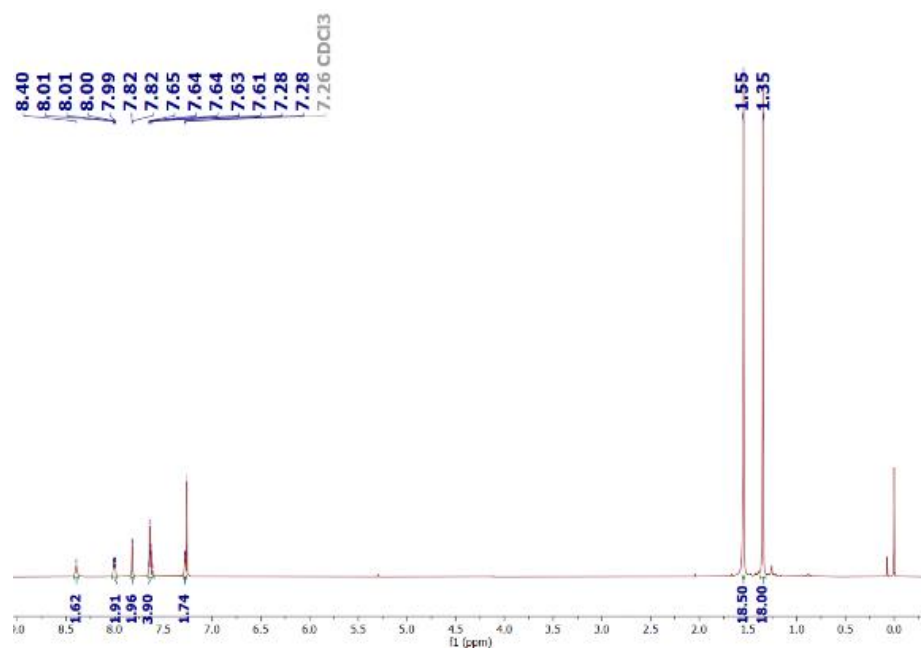
Figure 2.42 ^{1}H NMR of complex **2h**.
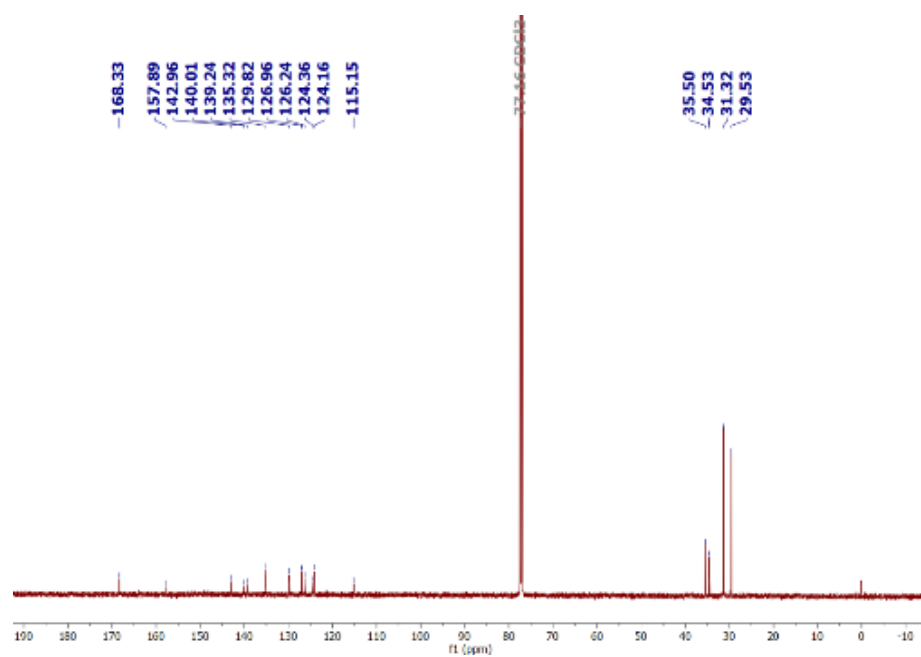
Figure 2.43 ^{13}C{^{1}H} NMR of complex **2h**.
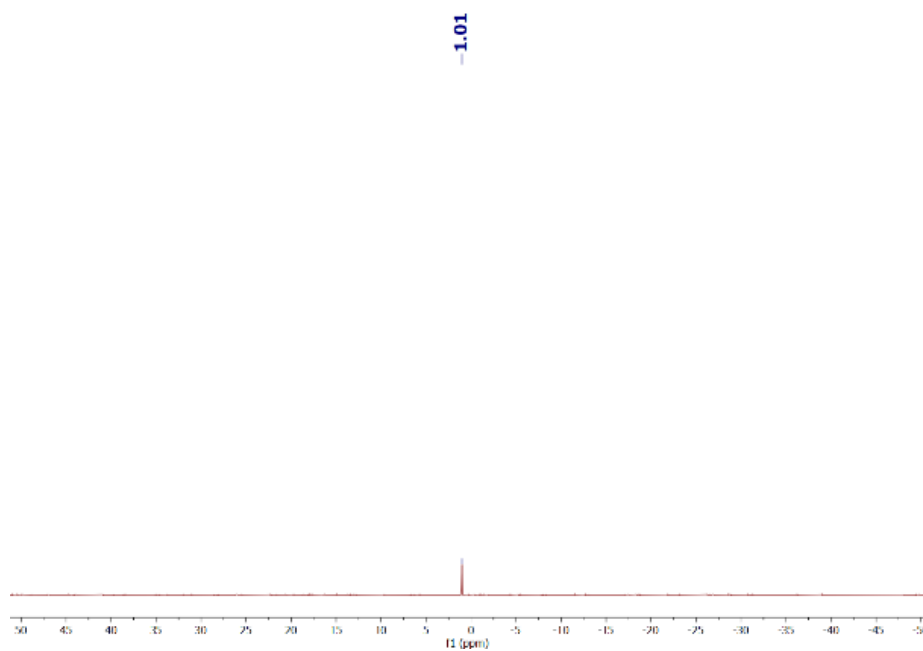
Figure 2.44 ^{11}B NMR of complex **2h**.
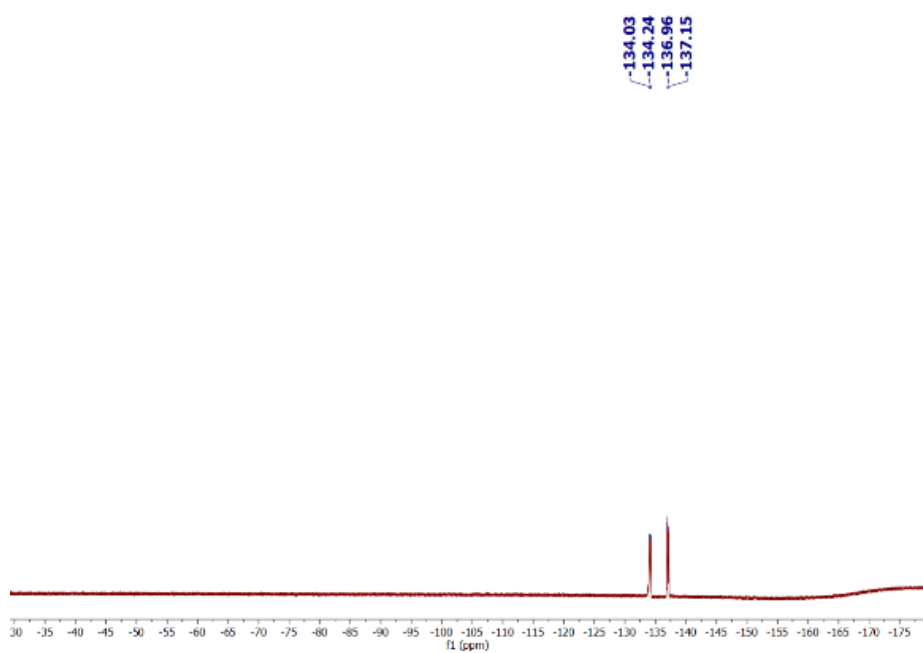
Figure 2.45 ^{19}F NMR of complex **2h**.
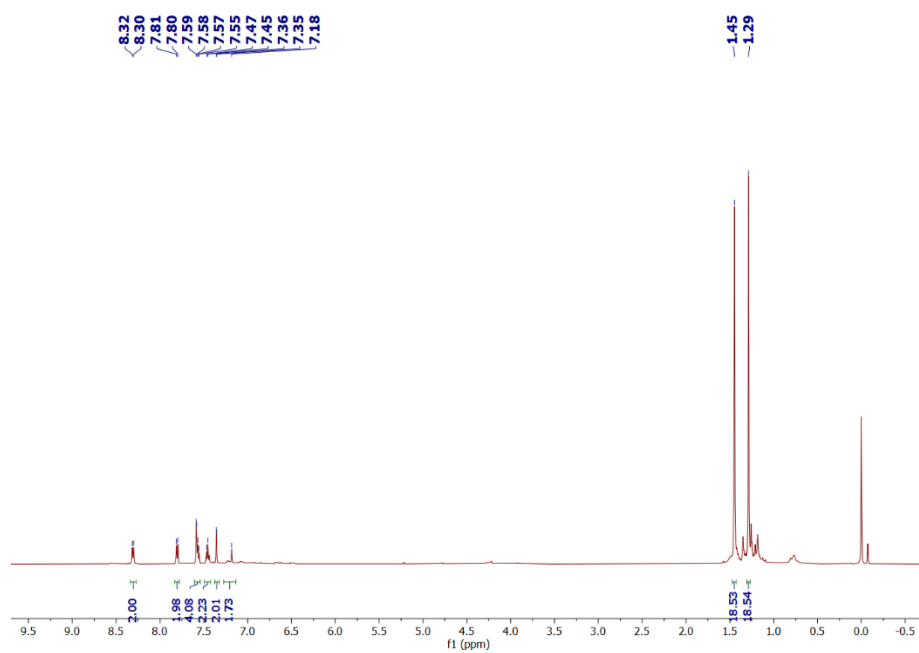
Figure 2.46 [^1]H NMR of complex **2i**.
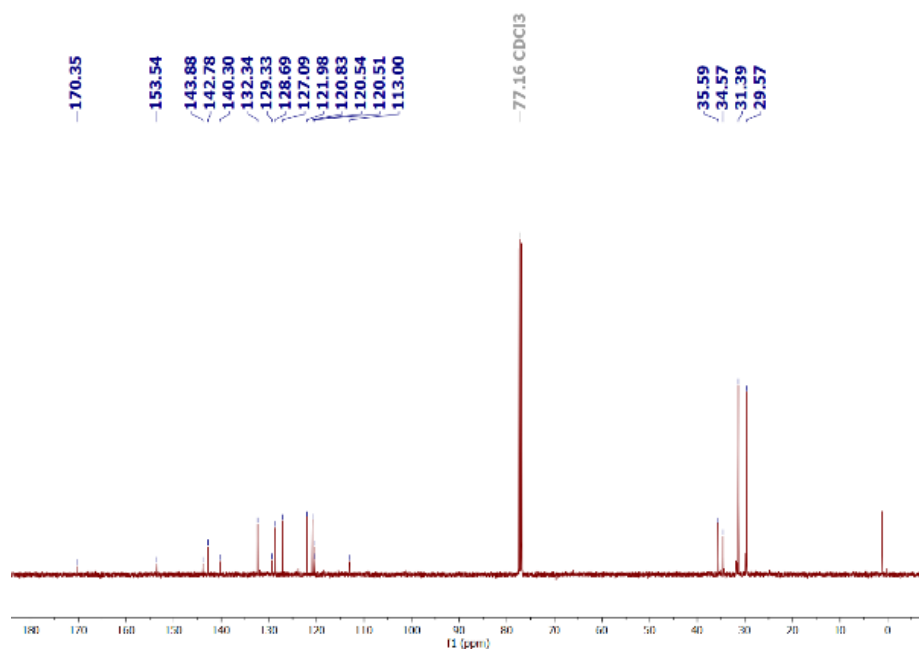
Figure 2.47 [^13]C{[^1]H} NMR of complex **2i**.

1.43
1.33
1.23
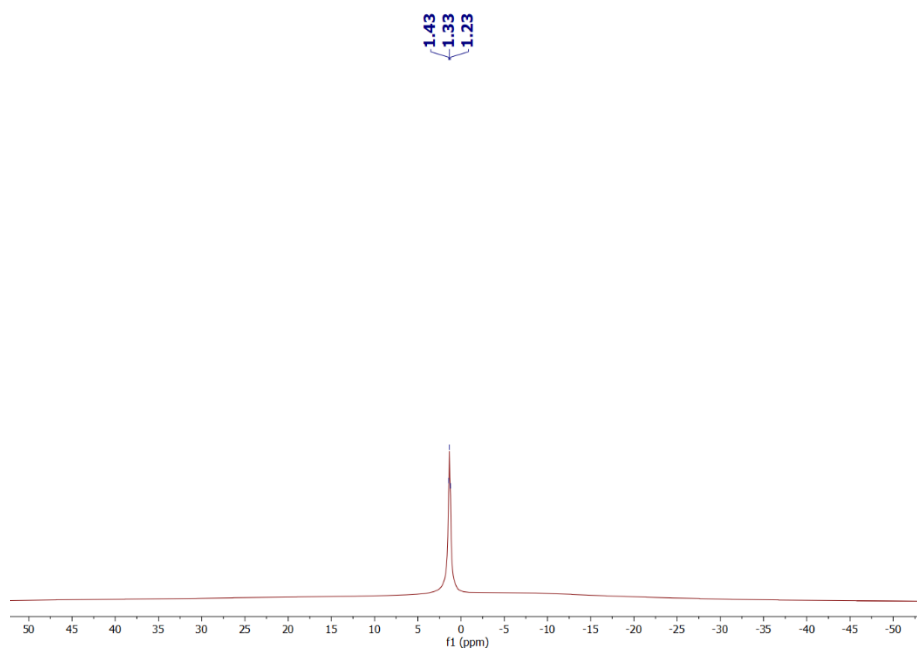
Figure 2.48 ^{11}B NMR of complex **2i**.

137.58
-137.61
-137.64
-137.66
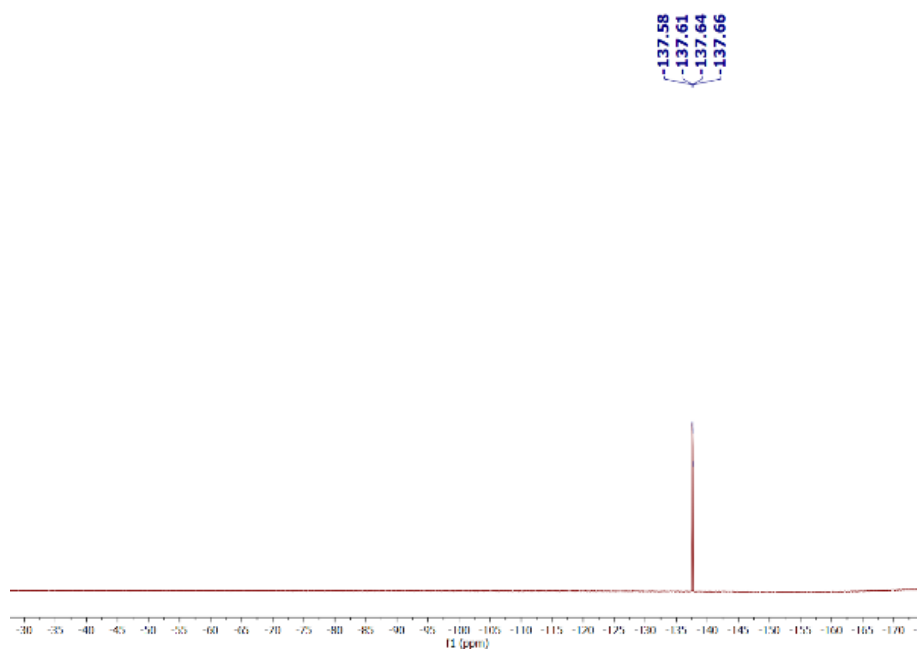
Figure 2.49 ^{19}F NMR of complex **2i**.

Figure 2.50 [^1]H NMR of complex **2j**.
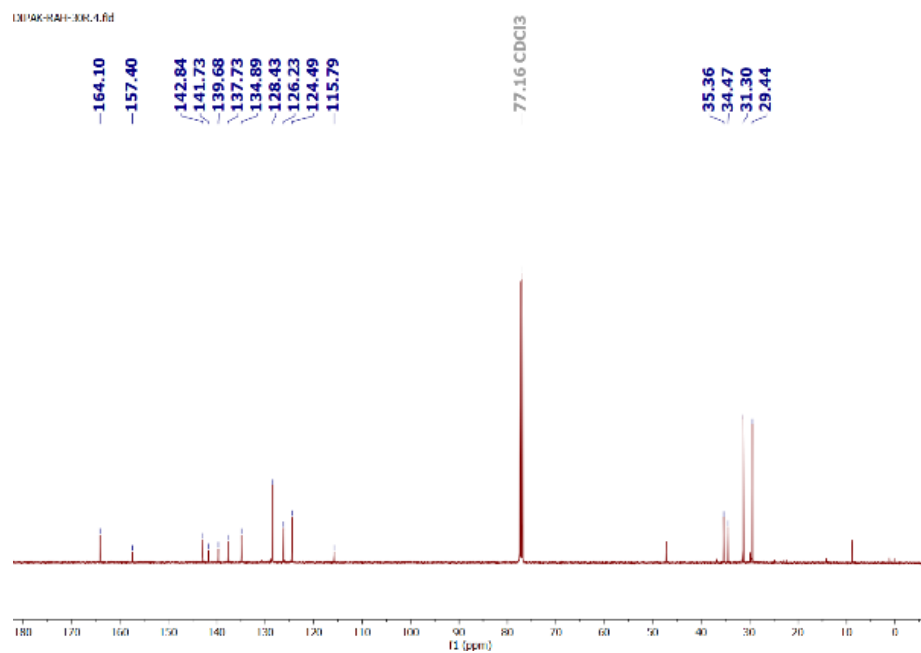
Figure 2.51 [^13]C{[^1]H} NMR of complex **2j**.
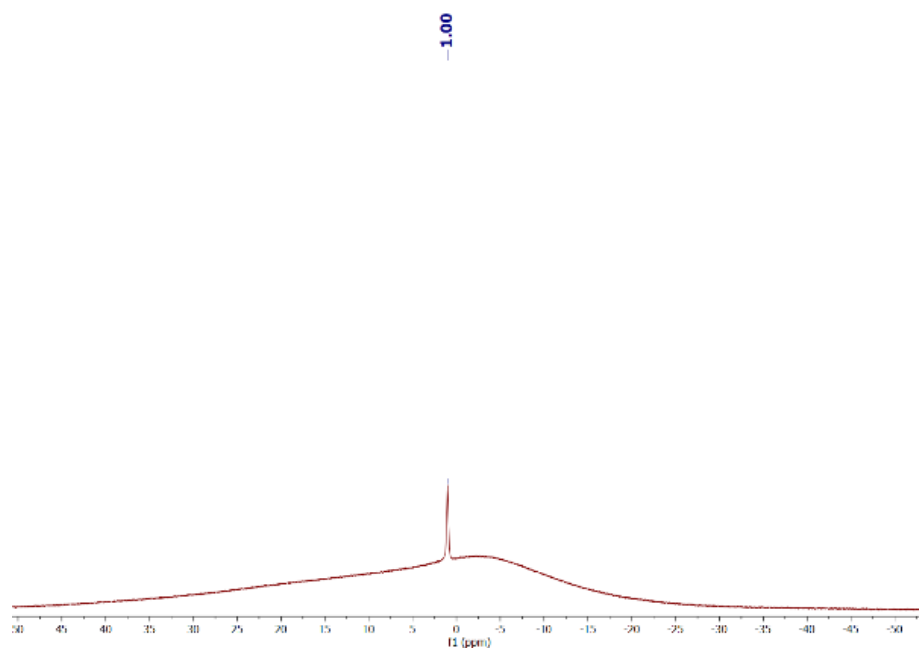
Figure 2.52 ^{11}B NMR of complex **2j**
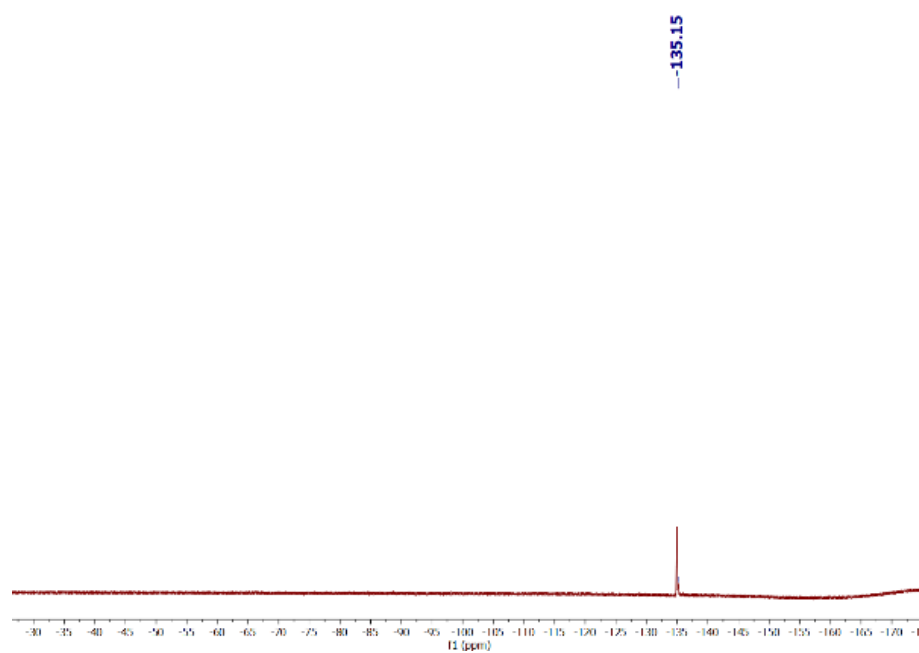
Figure 2.53 ^{19}F NMR of complex **2j**.
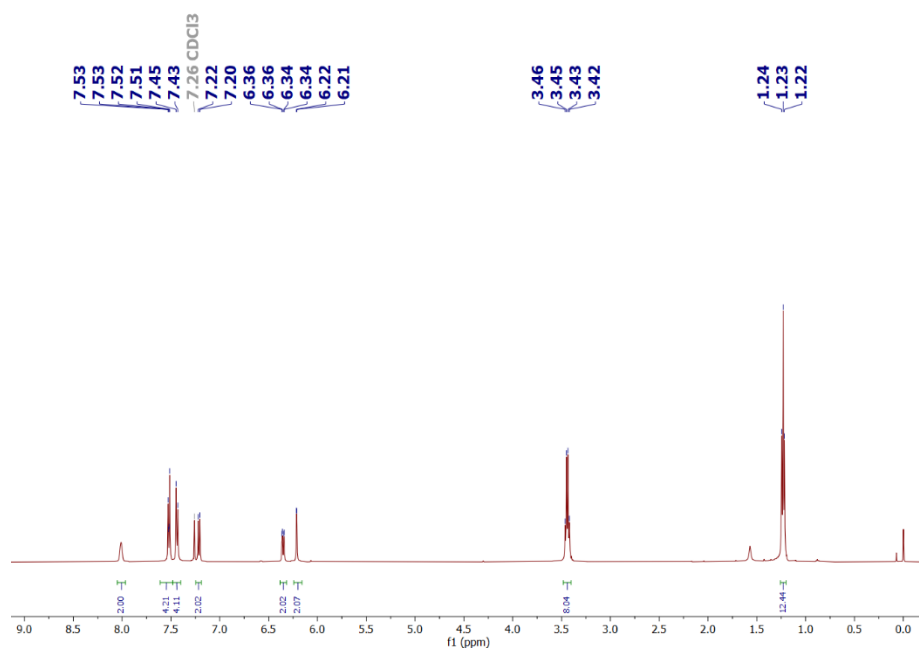
Figure 2.54 ^{1}H NMR of complex **2k**.
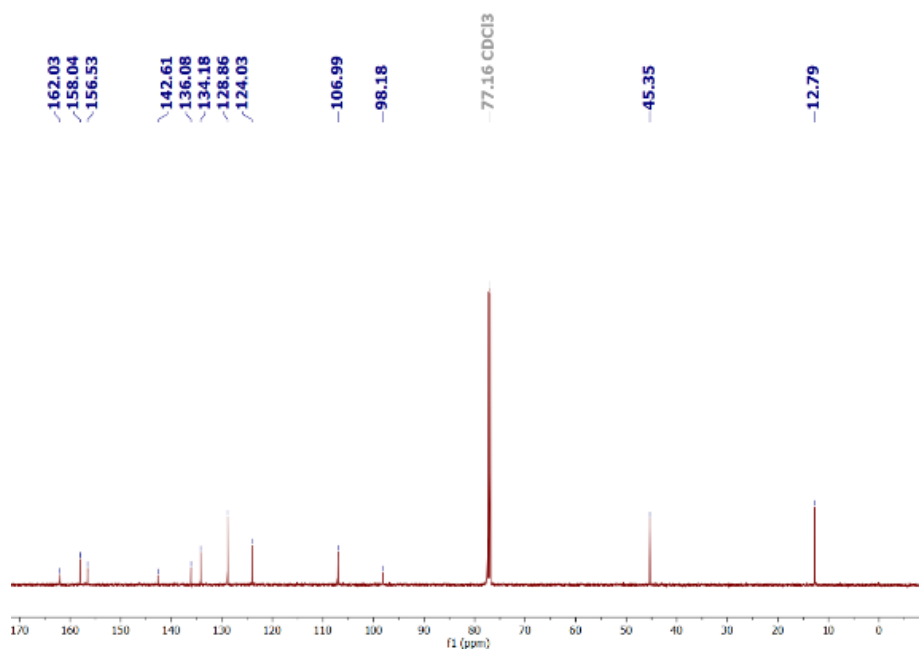
Figure 2.55 ^{13}C{^{1}H} NMR of complex **2k**.
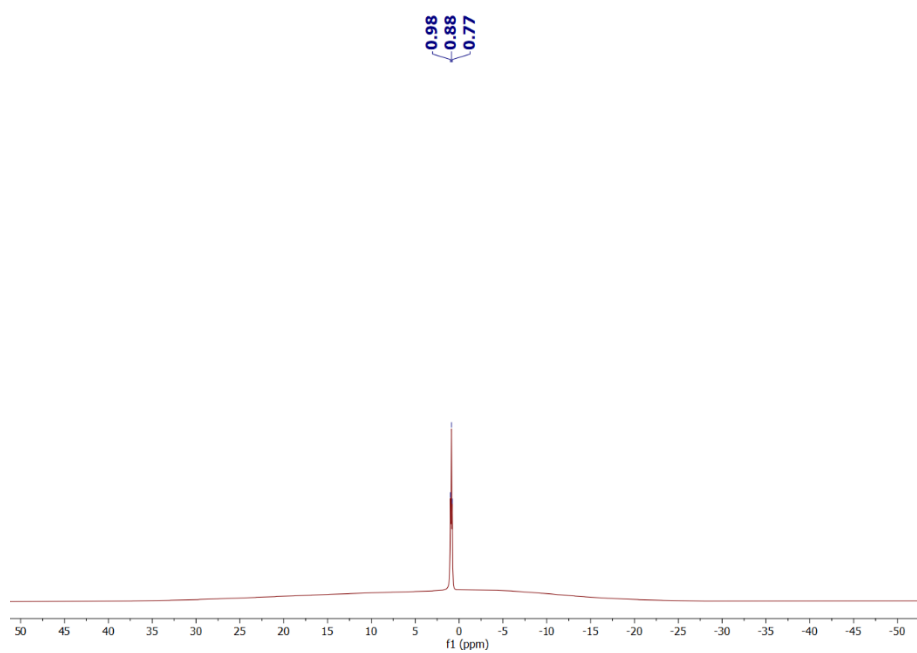
Figure 2.56 ^{11}B NMR of complex **2k.**
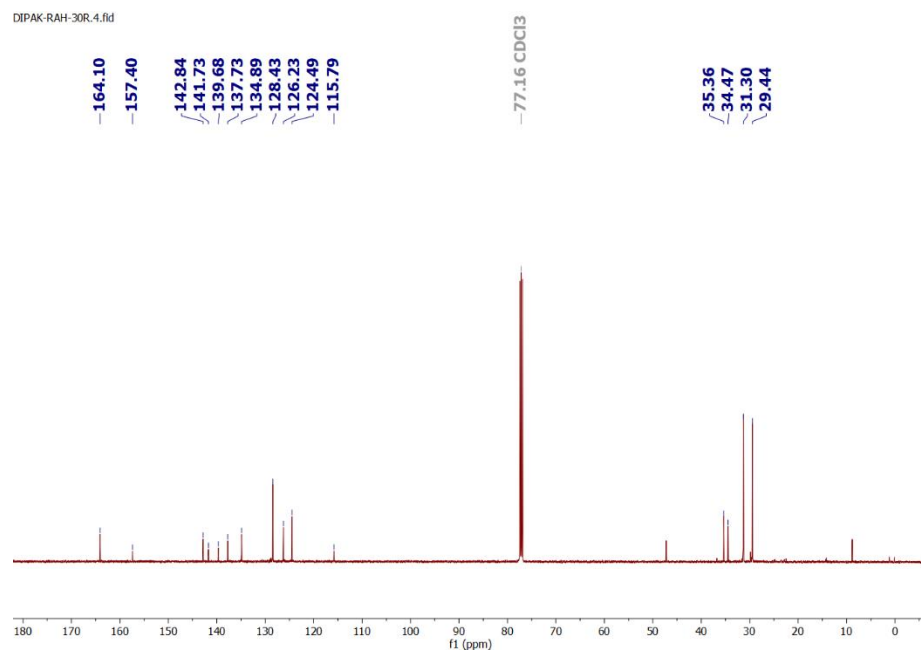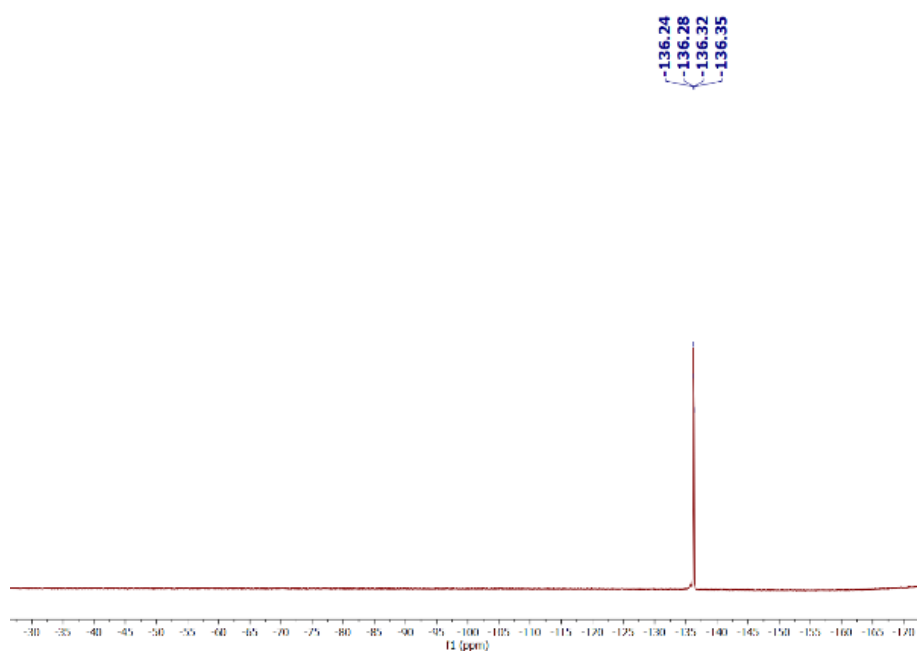

Figure 2.57 ^{19}F NMR of complex **2k**.

Table 2.5 Photophysical data of Complexes (**2a-2k**) in toluene

Sample	λ_{abs} (nm)[a]	λem (nm)[b]	Stokes Shifts (nm)[c]	τ_{ave} (ns)	ϕ_f
2a	363	455	92	6.2	30
2b	358	456	98	6.9	21
2c	363	456	93	7.3	33
2d	376	465	89	4.6	19
2e	300, 398	520	122	5.9	20
2f	407	457, 483	76	0.3	4
2g	327, 391	490	99	0.9	6
2h	298, 385	490	105	0.5	3
2i	310, 320, 390	450	60	2.4	7
2j	326, 395	505	110	7.1	2
2k	404	468	64	1.4	4

Table 2.6 Photophysical data of complexes (**2a-2k**) in DCM

Sample	λ_{abs} (nm)[a]	λem (nm)[b]	Stokes Shifts (nm)[c]	τ_{ave} (ns)	ϕ_f
2a	283, 363	458	95	7.3	28
2b	281, 363	459	96	8.0	29
2c	278, 364	461	97	8.6	33
2d	287, 378	472	94	6.1	20
2e	307, 397	529	132	5.9	21
2f	410	462, 486	76	0.2	5
2g	283, 339, 391	499	108	1.3	7
2h	295, 385	492	107	0.9	2
2i	314, 328, 380	449	69	2.5	3
2j	292, 323, 395	505	110	7.8	2
2k	408	477	69	1.8	2

Table 2.7 Photophysical data of complexes (**2a-2k**) in acetonitrile

Sample	λ_{abs} (nm)[a]	λem (nm)[b]	Stokes Shifts (nm)[c]	τ_{ave} (ns)	ϕ_f
2a	278, 359	457	98	7.2	28
2b	277, 358	459	101	7.4	30
2c	275, 360	462	102	8.1	29
2d	282, 371	472	101	6.1	23
2e	302, 389	472	83	5.0	13
2f	407	460,484	77	-	2
2g	281, 318, 382	495	113	1.3	8
2h	280, 377	488	111	0.8	4
2i	311, 324, 371	455	84	3.2	8
2j	287, 318, 387	518	131	8.2	2
2k	404	461	60	2.6	3

Table 2.8 Photophysical data of complexes (**2a-2k**) in dioxane

Sample	λ_{abs} (nm)[a]	λem (nm)[b]	Stokes Shifts (nm)[c]	τ_{ave} (ns)	ϕ_f
2a	277, 361	456	95	7.1	30
2b	277, 361	455	94	7.7	31
2c	276, 359	457	98	8.3	36
2d	283, 374	465	91	5.5	20
2e	299, 391	521	130	6.8	19
2f	-	457, 481	-	-	7
2g	322, 385	490	105	0.9	6
2h	295, 376	483	107	0.6	3
2i	290, 323, 392	451	59	2.6	24
2j	290, 323, 392	509	117	1.3	15
2k	401	461	60	3.7	5

[a]Absorption maximum, [b] emission maximum, [c] Stokes shift calculated by using longest wavelength absorption maximum and emission maximum, [τ_{ave}] life time and [ϕ_f] fluorescence quantum yield using coumarin 153 in ethanol as standard ($\phi f = 0.72$).

Table 2.9 Fluorescence decay parameters (λ_{ex}= 408 nm, λ_{em} 490 nm) the decay times (τ_1 and τ_2) and respective fractional contributions (α_1 and α_2, mentioned in parentheses), the quality of fitting (χ^2) are shown.

Complex	Solvents	Decay time (ns)		X^2
		τ_1	τ_2	
2a	ACN	3.6 (6.6)	7.5 (93.4)	1.01
	DCM	3.8 (2.1)	7.4 (97.9)	1.1
	Toluene	1.6 (3)	6.4 (97)	1.03
	Dioxane	3.6 (3.6)	7.2 (96.4)	1.1
2b	ACN	1.7 (7.2)	7.9 (92.8)	1.07
	DCM	1.1 (3)	8.2 (97)	1.09
	Toluene	1.5 (2.1)	7 (97.9)	1.01
	Dioxane	3.9 (4.4)	7.9 (95.6)	1.1
2c	ACN	1.6 (6.3)	8.5 (93.7)	1.06
	DCM	4.4 (4.2)	8.8 (95.8)	1.1
	Toluene	3.7 (4.9)	7.5 (95.1)	1.1
	Dioxane	4.2 (3.2)	8.4 (96.8)	1.08
2d	ACN	1.8 (14.1)	6.8 (85.9)	1.02
	DCM	0.9 (7.7)	6.5 (92.3)	1.07
	Toluene	1.6 (6.7)	4.8 (93.3)	1.09
	Dioxane	2.8 (1.1)	5.5 (98.9)	1.09
2e	ACN	2.6 (3.5)	5.1 (96.5)	1.15
	DCM	3 (3)	6 (97)	1.04
	Toluene	3.2 (4.8)	6.2 (95.2)	1.06
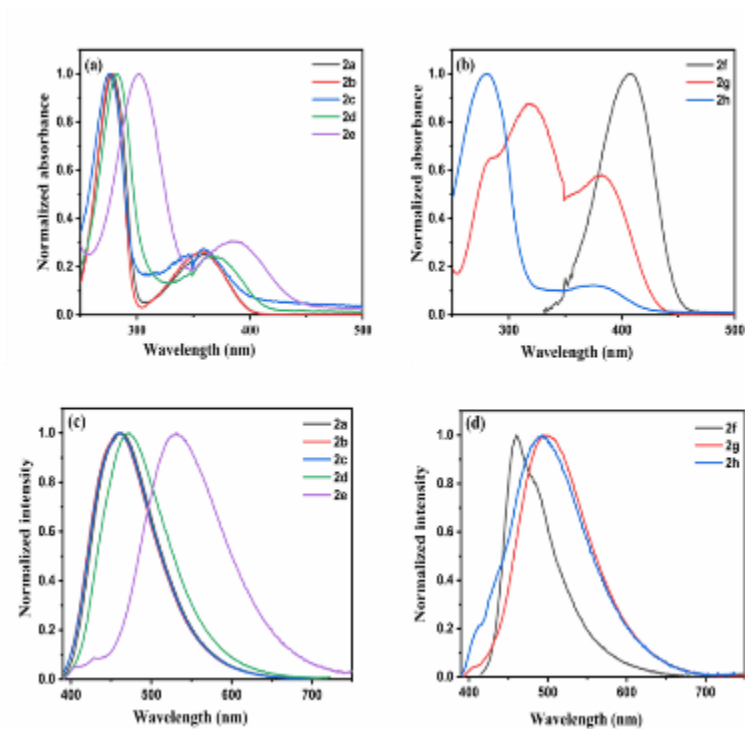
Figure 2.58 (a), (b) absorption spectra of complexes (**2a-2h**) and (c), (d) emission spectra of Complexes (**2a-2h**) in acetonitrile
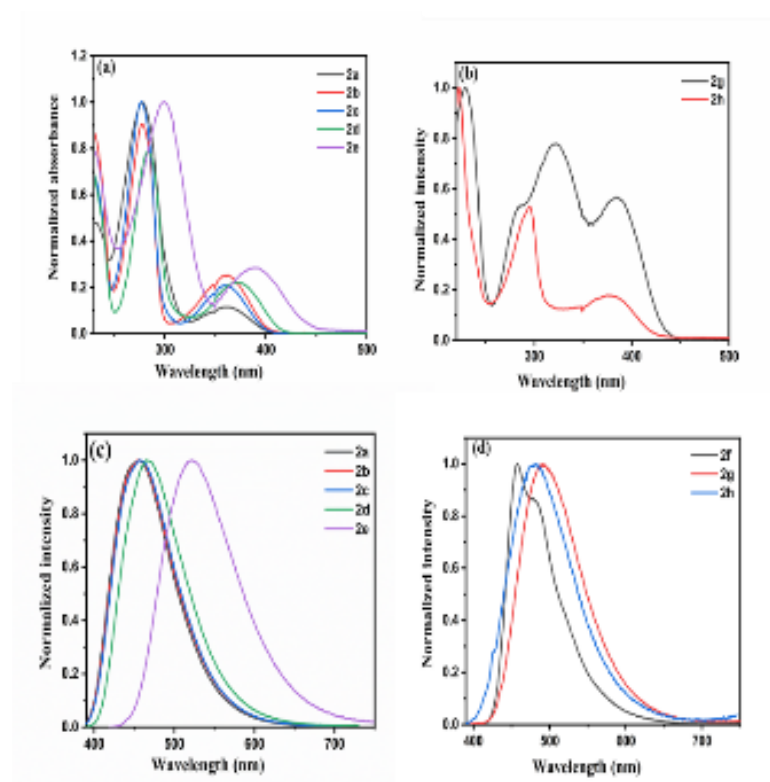
Figure 2.59 (a), (b) absorption spectra of complexes (**2a-2h**) and (c), (d) emission spectra of Complexes (**2a-2h**) in dioxane.
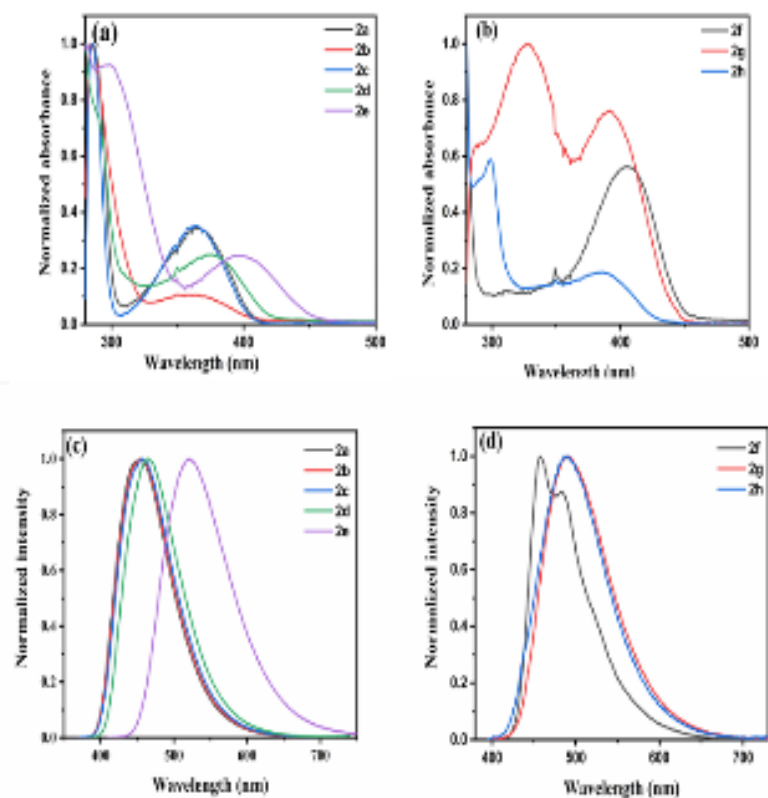
Figure 2.60 (a), (b) absorption spectra of complexes (**2a-2h**) and (c), (d) emission spectra of Complexes (**2a-2h**) in toluene.
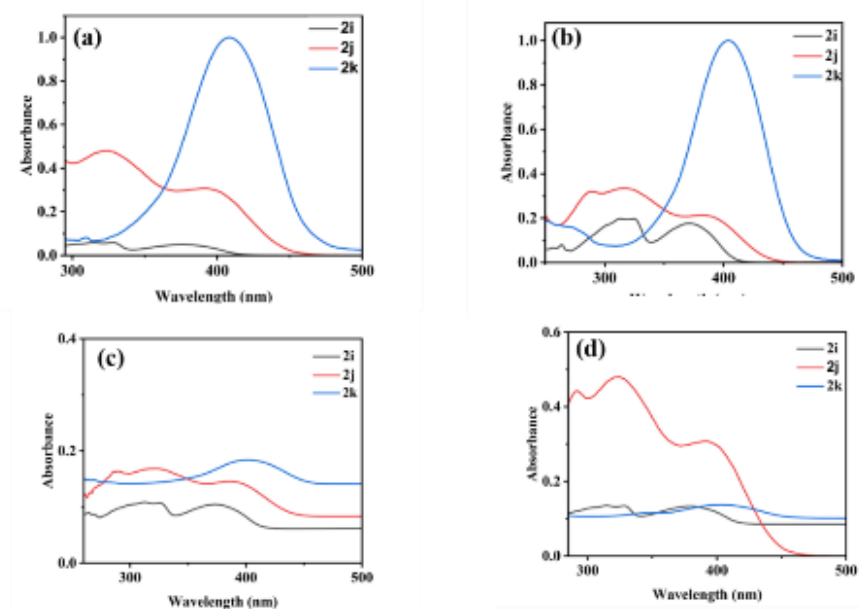
Figure 2.61 Absorption spectra of complexes (**2i-2k**) in (**a**) DCM, (**b**) acetonitrile, (**c**) dioxane, and (**d**) toluene.
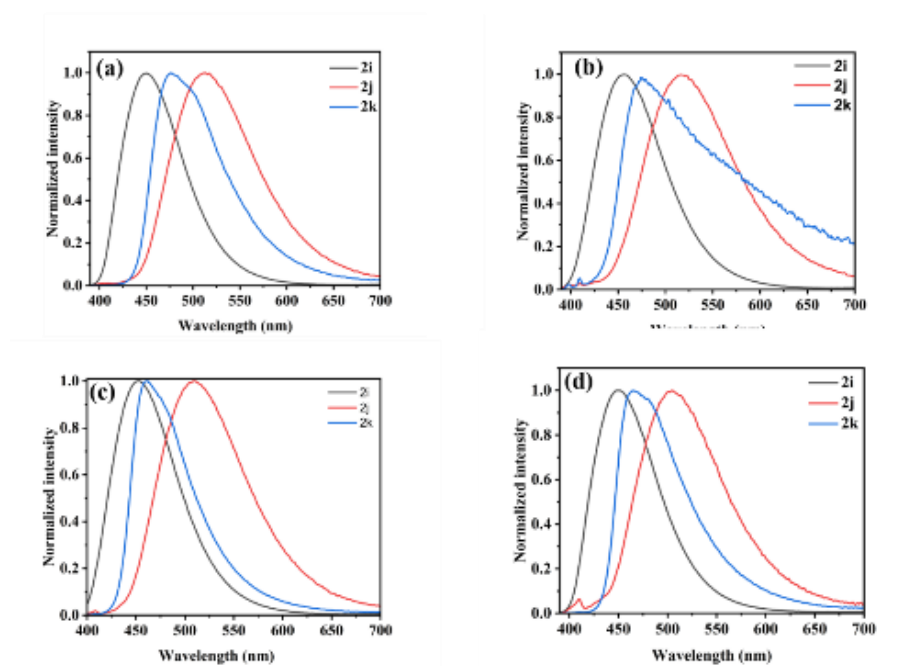
Figure 2.62 Emission spectra of complexes (**2i-2k**) in (**a**) DCM, (**b**) acetonitrile, (**c**) dioxane, and (**d**) toluene.
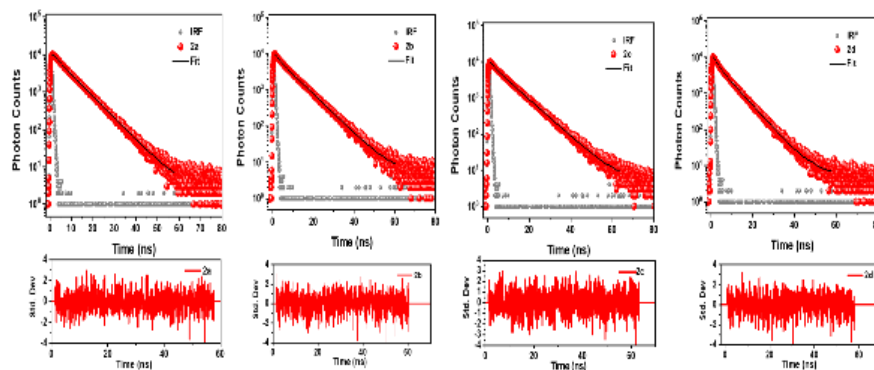
Figure 2.63 Decay curve of complex (**2a-2d**) in acetonitrile
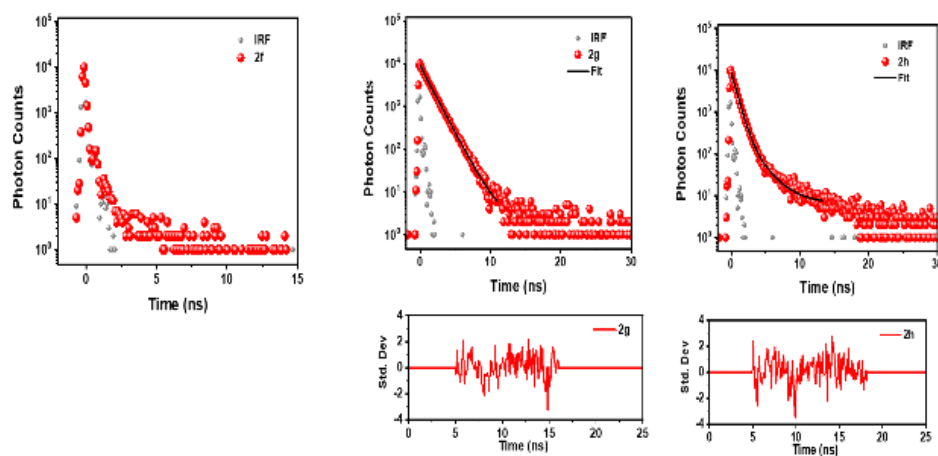
Figure 2.64 Decay curve of complexes (**2f-2h**) in acetonitrile
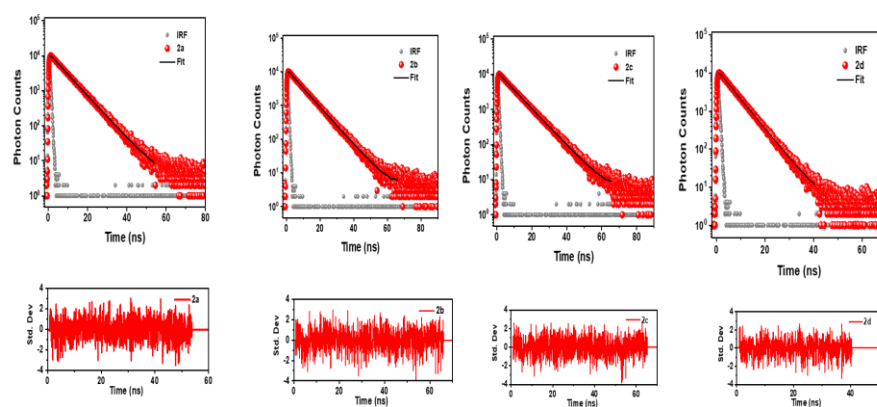
Figure 2.65 Decay curve of complex (**2a-2d**) in Dioxane.
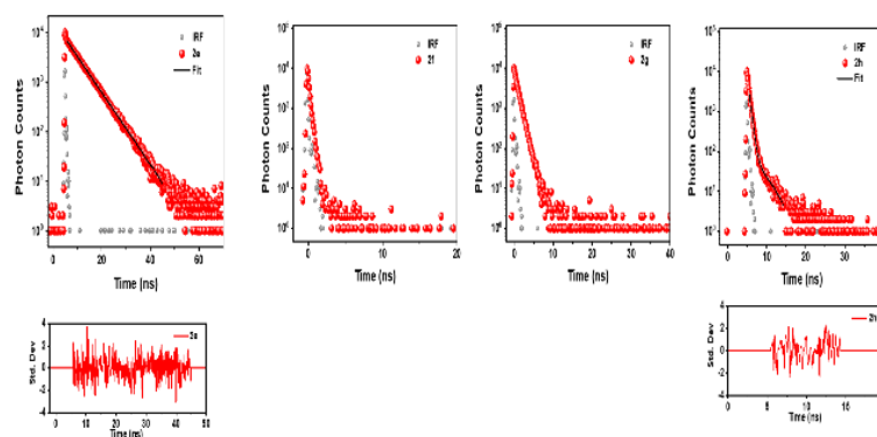
Figure 2.66 Decay curve of complexes (**2f-2h**) in dioxane.
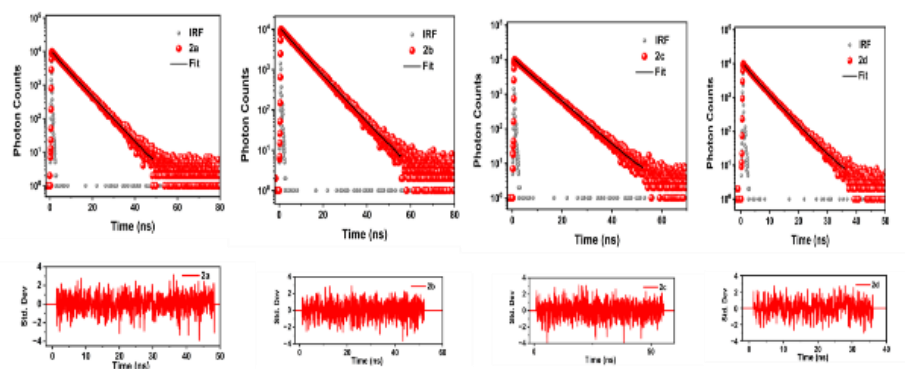
Figure 2.67 Decay curve of complexes (**2a-2d**) in toluene.
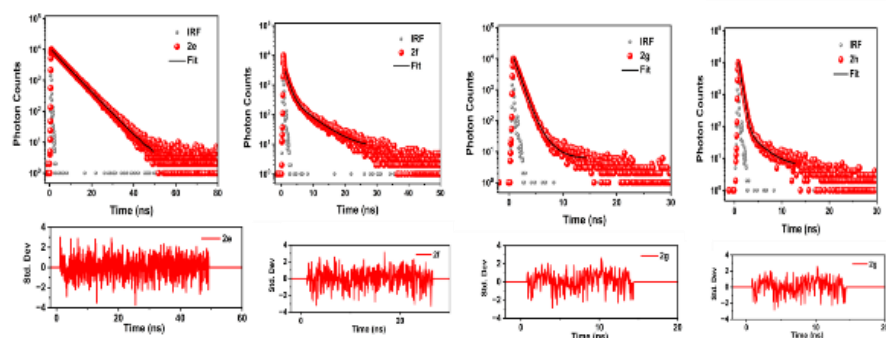
Figure 2.68 Decay curve of complexes (**2e-2h**) in toluene.
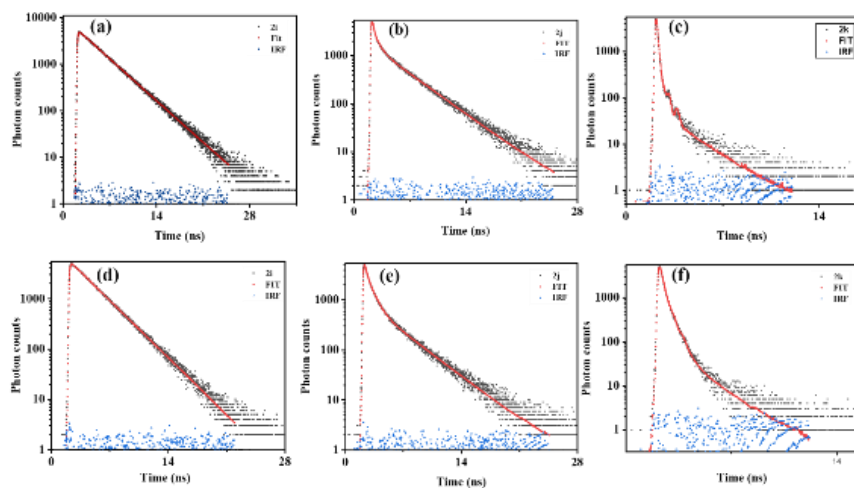
Figure 2.69 Decay curve of complexes (**2i-2k**) in acetonitrile (**a**), (**b**), (**c**) and in DCM (**d**), (**e**), and (**f**).
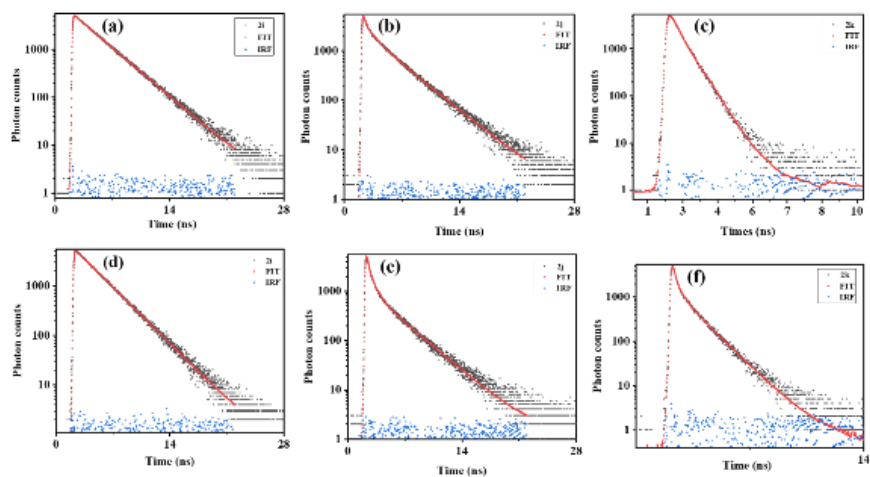
Figure 2.70 Decay curve of complexes (**2i-2k**) in dioxane (**a**), (**b**), (**c**) and in toluene (**d**), (**e**), and (**f**).
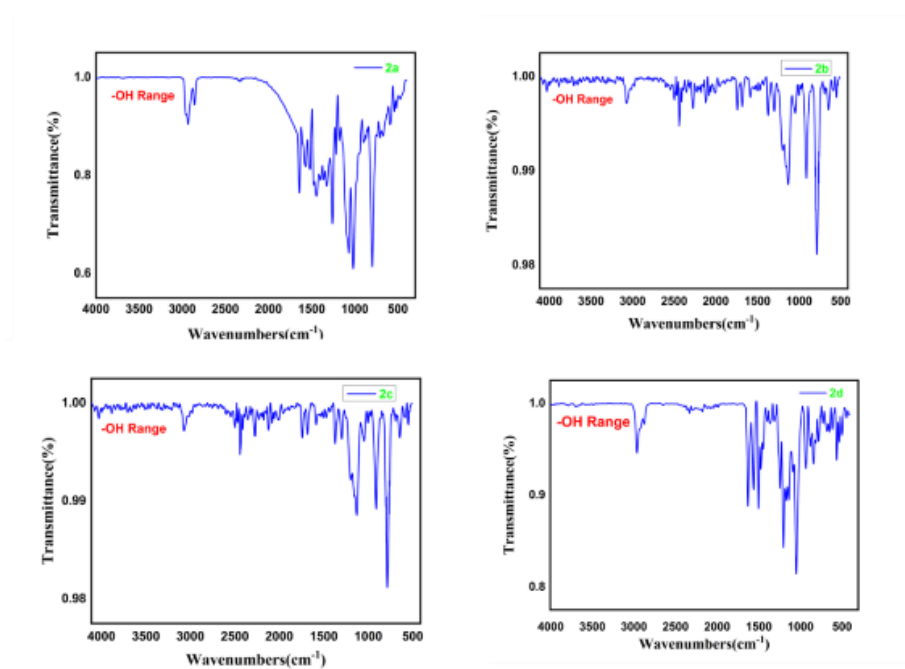
Figure 2.71 FT-IR spectrum of Complexes (**2a-2d**).
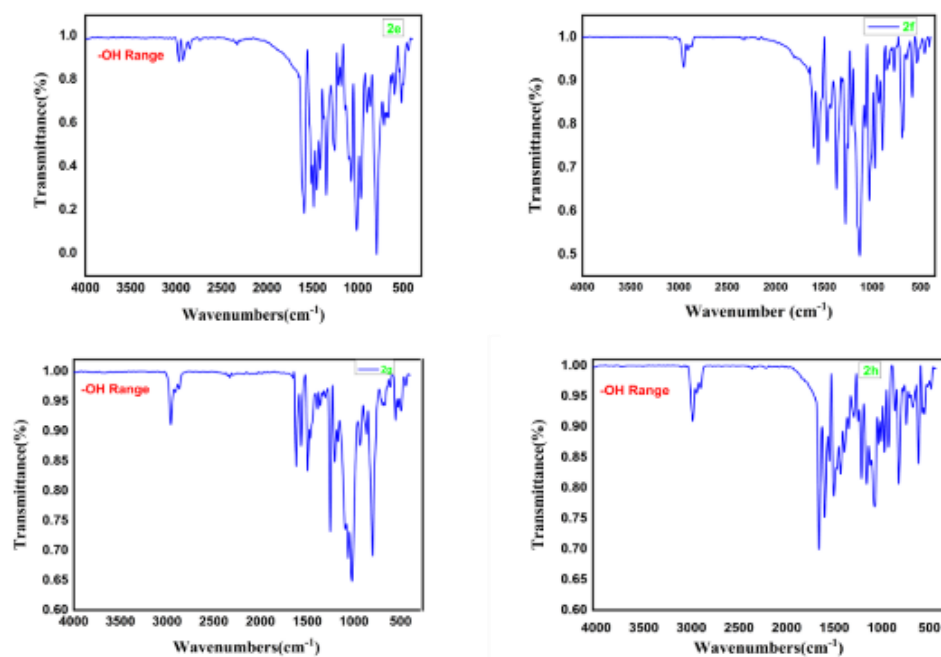
Figure 2.72 FT-IR spectrum of Complexes (**2e-2h**).
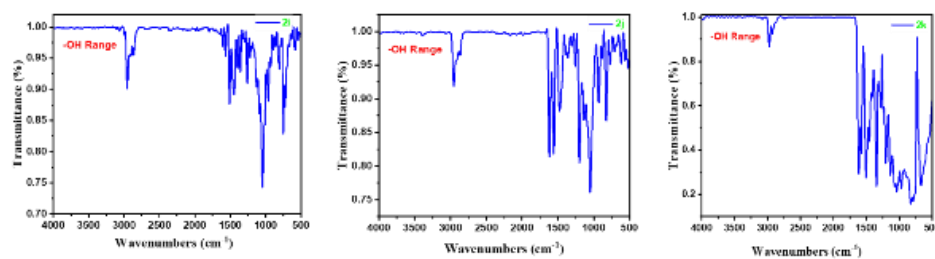
Figure 2.73 FT-IR spectrum of Complexes (**2i-2k**).
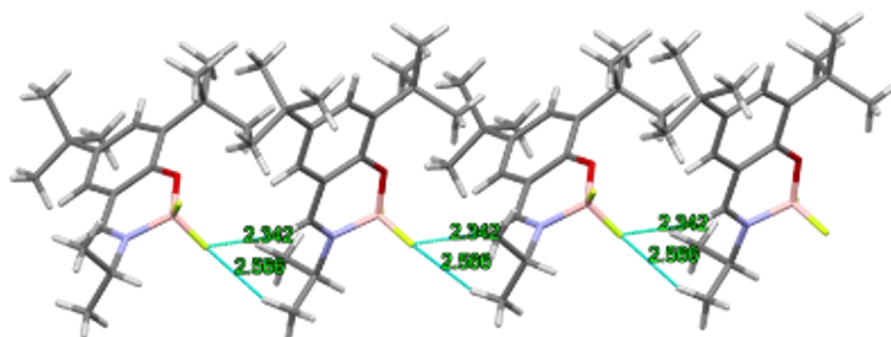
Figure 2.74 Crystal Packing of complex **2b** in a linear fashion
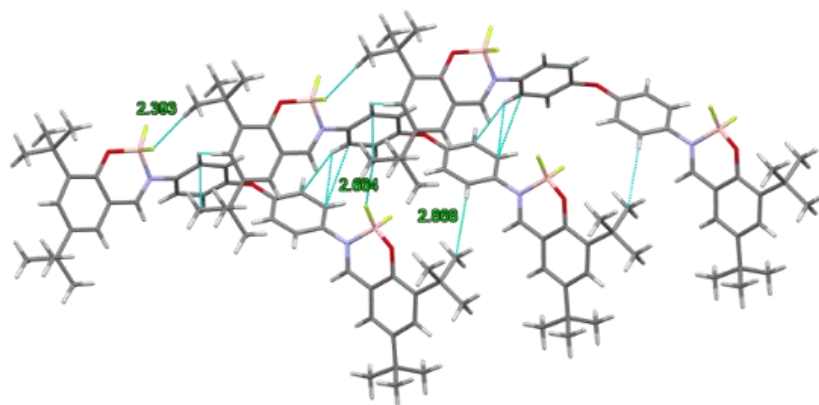
Figure 2.75 Crystal structure packing of complex 2g and intermolecular non-covalent interactions.

Crystallographic details:

The crystal data were collected on a SuperNova, Dual, Cu at home/near, Eos diffractometer. The crystal was kept at 293(2) K during data collection. Using Olex2 [89], the structure was solved with the SHELXT [90] structure solution program using Intrinsic Phasing and refined with the SHELXL [91] refinement package using Least Squares minimization. The structures were solved by direct methods and refined by full-matrix least squares, based on $F2$, using SHELXL Crystal structures were refined using Olex2-1.0 software. All non-hydrogen atoms were refined anisotropically.

Table 2.10 Crystallographic data for compounds 2a, 2b, and 2g

Complex	2b	2e	2g
Molecular Formula	$C_{18}H_{28}BF_2NO$	$C_{23}H_{24}BF_8NO$	$C_{43}H_{51}B_2F_4N_2O_3$
Formula weight	323.22	493.24	748.98
Temperature/K	293	100	100
Crystal system	monoclinic	monoclinic	monoclinic
Space group	P2$_1$/c	P2$_1$/c	C2/c

a/Å	15.0930(1)	20.3291(7)	34.2510(10)
b/Å	10.4321(7)	10.0250(3)	8.3848(2)
c/Å	12.2805(9)	11.9009(4)	30.5640(9)
$\alpha/°$	90	90	90
$\beta/°$	102.710(7)	104.2900(10)	112.7270(10)
$\gamma/°$	90	90	90
Volume/Å^3	1886.2(2)	2350.35(13)	8096.1(4)
Z	4	4	8
ρ_{calc}g/cm^3	1.138	1.394	1.229
Crystal size/mm3	$0.3 \times 0.2 \times 0.2$	$0.27 \times 0.18 \times 0.15$	$0.35 \times 0.3 \times 0.25$
Radiation	Mo Kα (λ = 0.71073)	Mo Kα (λ = 0.71073)	Mo Kα (λ = 0.71073)
Reflections collected	17818	95215	153571
Independent reflections	3317	5843	10120
R_{int}	0.0725	0.0354	0.0386
R indexes [I>=2σ (I)]	0.0845	R_1 = 0.0571	0.0491
wR$_2$	0.1947	0.1175	0.1125
Goodness-of-fit on F^2	1.102	1.040	1.031
CCDC No.	2379978	2379973	2379953

References:

[1] Sasabe, H., Kido, J. (2011) Multifunctional Materials in High-Performance OLEDS: Challenges for Solid-State Lighting. Chem. Mater., 23, 621-630. (DOI: 10.1021/cm1024052)

[2] Sirringhaus, H. (2014) Organic Field-Effect Transistors: The Path Beyond Amorphous Silicon. Adv. Mater., 26, 1319 -1335. (DOI: 10.1002/adma.201304346)

[3] Chen, F. C. (2019) Emerging Organic and Organic/Inorganic Hybrid Photovoltaic Devices for Specialty Applications: Low-Level-Lighting Energy Conversion and Biomedical Treatment. Adv. Opt. Mater., 7, 1800662. (DOI: 10.1002/adom.201800662)

[4] Entwistle, C. D., Marder, T. B. (2002) Boron Chemistry Lights the Way: Optical Properties of Molecular and Polymeric Systems. Angew. Chem., Int. Ed., 41, 2927-2931. (DOI: 10.1002/1521-3773)

[5] Entwistle, C. D., Marder, T. B. (2004) Application of Three-Coordinate Organoboron Compounds and Polymers in Optoelectronics. Chem. Mater., 16, 4574-4585. (DOI: 10.1021/cm0495717)

[6] Jäkle, F. (2006) Lewis acidic organoboron polymers. Coord. Chem. Rev., 250, 1107-1121. (DOI: 10.1016/j.ccr.2006.01.007)

[7] Mellerup, S. K., Wang, S. (2019) Boron-based stimuli responsive materials. Chem. Soc. Rev., 48, 3537-3549. (DOI: 10.1039/C9CS00153K)

[8] Chou, P. T., Chi, Y. (2007) Phosphorescent Dyes for Organic Light-Emitting Diodes. Chem. Eur. J., 13, 380. (DOI: 10.1002/chem.200601272)

[9] Uoyama, H., Goushi, K., Shizu, K., Nomura, C, Nomura, H., Adachi, C. (2021) Highly efficient organic light-emitting diodes from delayed fluorescence. Nature, 492, 234. (DOI: 10.1038/nature11687)

[10] Kagatikar, S., Sunil, D., Electron, J. (2021) Schiff Bases and Their Complexes in Organic Light Emitting Diode Application. Mater., 50, 6708. (DOI: 10.1007/s11664-021-09197-9)

[11] Tang, W. C., Vanslyke, A. S. (1987) Organic electroluminescent diodes. Appl. Phys. Lett., 51, 913. (DOI: 10.1063/1.98799)

[12] Kuehne, C. J. A., Gather, C. M. (2016) Organic Lasers: Recent Developments on Materials, Device Geometries, and Fabrication Techniques. Chem. Rev., 116, 12823. (DOI: 10.1021/cr200263w)

[13] Esnal, I., Escamilla, V. I., Durán, A, F, C. G., Benavides, A. U., Mendiola, L. M. B., López-Arbeloa, L., Bañuelos, J., García-Moreno, I., Costela, A., Cabrera, E. P. (2013) Blue-to-Orange Color-Tunable Laser Emission from Tailored Boron-Dipyrromethene Dyes. Chem. Phys. Chem., 14, 4134. (DOI: 10.1002/cphc.201300818)

[14] Mowatt, C., Morris, M. S., Song, H, M., Wilkinson, D. T., Friend, H. R., Coles, J, H. (2010) Comparison of the performance of photonic band-edge liquid crystal lasers using different dyes as the gain medium. J. Appl. Phys., 107,, 043101. (DOI: 10.1063/1.3284939)

[15] Zhao, J., Chen, J., Ma, S., Liu, Q., Huang, L., Chen, X., Lou, K., Wang, W. (2018) Recent developments in multimodality fluorescence imaging probes. Acta Pharm. Sin., 8, 320. (DOI: 10.1016/j.apsb.2018.03.010)

[16] Zhu, H., Fan, J., Du, X., Peng, X. (2016) Formaldehyde in biological systems: Involving sources, related diseases and reaction-based fluorescent detection. Acc. Chem. Res., 49, 2115. (DOI: 10.1016/j.trac.2023.117298)

[17] Loudet, A., Burgess, K. (2007) BODIPY Dyes and Their Derivatives: Syntheses and Spectroscopic Properties. Cem. Rev., 10,4891. (DOI: 10.1021/cr078381n)

[18] Dougherty, T. J., Gomer, C. J., Henderson, B. W., Jori, G., Kessel, D., Korbelik, M., Moan, J., Peng, Q. (1998) Photodynamic therapy. J. Natl. Cancer Inst., 90, 889. (DOI: 10.1093/jnci/90.12.889)

[19] Awuah, S. G., You, Y. (2012) Boron dipyrromethene (BODIPY)-based photosensitizers for photodynamic therapy. RSC Adv., 2, 11169. (DOI : 10.1039/C2RA21404K)

[20] Lim, S. H., Thivierge, C., Sliwinska, P. N., Han, J., Bergh, H. V. D., Wagnieres, G., Burgess, K., Lee, B. H., Med, J. (2010) In vitro and in vivo photocytotoxicity of boron dipyrromethene derivatives for photodynamic therapy. J. Med. Chem., 53, 2865. (DOI: 10.1021/jm901823u)

[21] Raza, Md. K., Gautam, S., Howlader, P., Bhattacharyya, A., Kondaiah, P., Chakravarty, A. R. (2018) Glucose-Appended Platinum(II)-BODIPY Conjugates for Targeted Photodynamic Therapy in Red Light. Inorg. Chem., 57, 14374. (DOI: 10.1021/acs.inorgchem.7b02249)

[22] Frimannsson, D. O., Grossi, M., Murtagh, J., Paradisi, F., O'Shea, D. F. (2010) Light Induced Antimicrobial Properties of a Brominated Boron Difluoride (BF2) Chelated Tetraarylazadipyrromethene Photosensitizer. J. Med. Chem., 53, 7337. (DOI: 10.1021/jm100585j)

[23] Qiao, F., Liu, A., Zhou, Y., Xiao, Y., Yang, P. O. (2009) High-Entropy Approach vs. Traditional Doping Strategy for Layered Oxide Cathodes in Alkali-Metal-Ion Batteries: A Comparative Study. Mater. Sci., 44, 1283. (DOI: 10.1016/j.ensm.2025.104295)

[24] Miao, J., Wang, Y., Liu, J., Wang, L. (2022) Organoboron molecules and polymers for organic solar cell applications. Chem. Soc. Rev., 51, 153. (DOI: 10.1039/D1CS00974E)

[25] Landi, A., Padula, D., Peluso, A. (2024) Fast Nonradiative Decay Paths in Organic Solar Cells: Implications for Designing More Efficient Photovoltaic Systems. ACS Appl. Energy Mater., 7, 707. (DOI: 10. 1021/acsaem.3c02790)

[26] Chen, L. X. (2019) Organic Solar Cells: Recent Progress and Challenges. ACS Energy Lett., 4, 2537. (DOI: 10.1021/acsenergylett.9b02071)

[27] Coropceanu, V., Chen, X. K., Wang, T., Zheng, Z., Brédas, J. L. (2019) Charge-transfer electronic states in organic solar cells. Nat. Rev. Mater., 4, 689. (DOI: 10.1038/s41578-019-0137-9)

[28] Sharma, D., Agrawal, A., Pradhan, R., Keshtov, M. L., Singhal, R., Liu, W., Zhu, X., Mishra, A. (2021) Correlation of Functional Coumarin Dye Structure with Molecular Packing and Organic Solar Cells Performance. ACS Appl. Energy Mater., 4, 11537. (DOI: 10.1002/solr.202300487)

[29] Tong, Y., Xu, B., Ye, F. (2024) Recent Progress of Solution-Processed Thickness-Insensitive Cathode Interlayers for High-Performance Organic Solar Cells. Adv. Funct. Mater., 34, 2310865. (DOI: 10.1002/adfm.202422023)

[30] Kaur, P., Singh, K. (2019) Recent advances in the application of BODIPY in bioimaging and chemosensing. J. Mater. Chem., 7, 11361. (DOI: 10.1039/C9TC03719E)

[31] Arroyo, I. J., Hu, R., Merino, G., Tang, B. J., Cabrera, E. P. (2009) The smallest and one of the brightest. Efficient preparation and optical description of the parent borondipyrromethene system. J. Org. Chem., 74, 5719. (DOI: 10.1021/jo901014w)

[32] Mahanta, C. S., Ravichandiran, V., Swain, S. P. (2023) Metal-free synthesis of selenoesters directly from carboxylic acids using bifunctional selenoureas under batch and continuous-flow conditions. ACS Appl. Bio Mater., 6, 2995. (DOI: 10.1039/D3CC02872K)

[33] Kumar, A., Kim, D., Kumar, S., Mahammed, A., Churchill, D.G., Gross, Z., (2023) Milestones in corrole chemistry: historical ligand syntheses and post-functionalization. Chem. Soc. Rev., 52, 573. (DOI: 10.1039/D1CS01137E)

[34] Jin, C., Yang, X., Zhao, W., Zhao, Y., Wang, Z., Tan, J. (2024) Bridging biodegradable metals and biodegradable polymers: A comprehensive review of biodegradable metal–organic frameworks for biomedical application. Chem. Soc. Rev., 52, 573. (DOI: 10.1016/j.pmatsci.2025.101526)

[35] Singh, R. S., Paitandi, R. P., Gupta, R. K., Pandey, D. S. (2020) Interaction of ferrocene appended Ru(II), Rh(III) and Ir(III) dipyrrinato complexes with DNA/protein, molecular docking and antitumor activity. Coord. Chem. Rev., 414, 213269. (DOI: 10.1016/j.ejmech.2014.06.052)

[36] Cui, Y., Liu, Q., Bai, D., Jia, W. (2005) Organoboron compounds with an 8-hydroxyquinolato chelate and its derivatives: substituent effects on structures and luminescence. S. Wang, Inorg. Chem., 44, 601. (DOI: 10.1021/ic0489746)

[37] Pandey, P., Walawalkar, M. G., Murugavel, R. (2024) Luminescent 8-hydroxyquinoline derived tin(IV) complexes. J. Organomet. Chem., 1007, 123023. (DOI: 10.1016/j.jorganchem.2024.123023)

[38] Galindo, M. E. C., Velázquez, B. A. R., Luna, R. A. J., Martínez, I. I. P., Ursúa, M. A. S., Ferrara, J. G. T. (2023) Advances in the management of type 2 diabetes in adults. Inorganics, 11, 94. (DOI: 10.1136/bmjmed-2022-000372)

[39] Boyet, M., Chabaud, L., Pucheault, M. (2023) Recent Advances in the Synthesis of Borinic Acid Derivatives. Molecules, 28, 2660. (DOI: 10.3390/molecules28062660)

[40] Parra, A. F., Contreras, R. (2000) Boron coordination compounds derived from organic molecules of biological interest. Coord. Chem. Rev., 196, 254. (DOI:10.1016/S0010-8545(99)00053-3)

[41] Nagai, A., Kokado, K., Nagata, Y., Arita, M., Chujo, Y. (2008) Luminescent alternating boron quinolate–fluorenecopolymers exhibiting high electron mobility. J. Org. Chem., 73, 8605. (DOI: 10.1039/B924729G)

[42] Chen, P. Z., Niu, L. Y., Chen, Y. Z., Yang, Q. Z. (2017) Bridging biodegradable metals and biodegradable polymers: A comprehensive review of biodegradable metal–organic frameworks for biomedical application. Coord. Chem. Rev., 350, 196. (DOI: 10.1016/j.pmatsci.2025.101526)

[43] Tanaka, K., Chujo, Y. (2015) Recent progress of optical functional nanomaterials based on organoboron complexes with β-diketonate, ketoiminate and diiminate. NPG Asia Mater., 7, e223. (DOI: 10.1038/am.2015.118)

[44] Parveen, D., Yadav, R. K., Mondal, B., Dallon, M., Sarazin, Y., Roy, D. K., (2024) Bis(diiminate)-based boron difluoro complexes: effective synthon for bis(borenium) cations. Dalton Trans., 53, 14139. (DOI: 10.1039/d4dt02050b)

[45] Claessens, C. G., Rodriguez, D. G., Torres, T. (2002) Subphthalocyanines: Singular Nonplanar Aromatic CompoundsSynthesis, Reactivity, and Physical Properties. Chem. Rev., 102, 835. (DOI: 10.1021/ol8023677)

[46] Hamad, O. A., Kareem, R. O., Omer, P. K. (2024) Recent Developments in Synthesize, Properties, Characterization, and Application of Phthalocyanine and Metal Phthalocyanine. Chem. Rev., 6, 39. (DOI: 10.48309/JCR.2024.412899.1250)

[47] Kolomeychuk, F. M., Safonova, E. A., Polovkova, M. A., Sinelshchikova, A. A., Martynov, A. G., Shokurov, A. V., Kirakosyan, A., Efimov, N. N., Yu, A., Tsivadze., Gorbunova, Y. G. (2021) Switchable Aromaticity of Phthalocyanine via Reversible Nucleophilic Aromatic Addition to an Electron-Deficient Phosphorus(V) Complex. J. Am. Chem. Soc., 143, 14053. (DOI: 10.1021/jacs.1c05831)

[48] Mizrahi, A., Bukurosh, E., Vestfrid, J., Bender, T. P., Gross, Z. (2020) Exploring the Synthesis and Electronic Properties of Axially Substituted Boron Subphthalocyanines with Carbon-Based Functional Groups. Inorg. Chem., 59, 2641. (DOI: 10.1002/ejic.202000525)

[49] Li, X., Zheng, B.D., Peng, X. H., Li, S. Z., Ying, J. W., Zhao, Y., Huang, J. D., Yoon, J. (2019) Phthalocyanines as medicinal photosensitizers: Developments in the last five years. Coord. Chem. Rev., 379, 147. (DOI: 10.1016/j.ccr.2017.08.003)

[50] Tamgho, I., Hasheminasab, A., Engle, J. T., Nemykin, V. N., Ziegler, C. J., Am. J. (2014) A New Highly Fluorescent and Symmetric Pyrrole–BF2 Chromophore: BOPHY. Chem. Soc., 136, 5623. (DOI: 10.1021/ja502477a)

[51] Yu, C., Jiao, L., Zhang, P., Feng, Z., Cheng, C., Wei, Y., Mu, X., Hao, E. (2014) Highly fluorescent BF2 complexes of hydrazine-Schiff base linked bispyrrole. Org. Lett., 16, 3048. (DOI: 10.1021/ol501162f)

[52] Zhang, G., Wang, M., Parvanova, P.B., Fronczek, F. R., Smith, K. M., Vicente, M. G. H. (2022) Investigations on the Synthesis, Reactivity, and Properties of Perfluoro-α-Benzo-Fused BOPHY Fluorophores. Chem. Eur., 28, e202200421. (DOI: *28*, e202200421)

[53] Wang, J., Boens, N., Jiao, L., Hao, E. (2020) Aromatic [b]-fused BODIPY dyes as promising near-infrared dyes. Org. Biomol. Chem., 18, 4135. (DOI: 10.1039/D0OB00790K)

[54] Wu, Q., Yu, C., Wei, Y., Mu, X., Hao, E., Jiao, L.(2016) Synthesis, structure and properties of thiophene-fused BODIPYs and azaBODIPYs as near-infrared agents. J. Org. Chem., 81, 11316. (DOI: 10.1039/C6NJ01011C)

[55] Swavey, S., Quinn, J., Coladipietro, M., Cox, K. G., Brennaman, M. K. (2017) Tuning the photophysical properties of BODIPY dyes through extended aromatic pyrroles. RSC Adv., 7, 173. (DIO: 10.1039/C6RA26331C)

[56] Murali, A. C., Nayak, P., Nayak, S., Das, S., Senanayak, S. P., Venkatasubbaiah, K., (2023) Boron-Thioketonates: A New Class of S,O-Chelated Boranes as Acceptors in Optoelectronic Devices. Angew. Chem. Int. Ed., 62, e202216871. (DIO: 10.1002/anie.202216871)

[57] Murali, A. C., Nayak, P., Panda, R., Venkatasubbaiah, K. (2023) Boron-Thioketonates: A New Class of S,O-Chelated Boranes as Acceptors in Optoelectronic Devices. ACS Appl. Opt. Mater., 1, 1033. (DIO: 10.1002/anie.202216871)

[58] Loudet, A., Burgess, K. (2007) BODIPY Dyes and Their Derivatives: Syntheses and Spectroscopic Properties. Chem. Rev., 107, 4891. (DIO: 10.1021/cr078381n)

[59] Montoya, M. M., Alcaraz, A. G., Ferao, A. E., Bautista, D., Curiel, D. (2023) Insight into the Stokes shift, divergent solvatochromism and aggregation-induced emission of boron complexes with locked and unlocked benzophenanthridine ligands. Dyes and Pigm., 209, 110924. (DIO: 10.1016/j.dyepig.2022.110924)

[60] Wu, Y., Lu, H., Wang, S., Li, Z., Shen, Z. (2015) Asymmetric boron-complexes containing keto-isoindolinyl and pyridyl groups: solvatochromic fluorescence, efficient solid-state emission and DFT calculations. J. Mater. Chem., 3, 12281. (DIO: 10.1039/C5TC03084F)

[61] Sun, T., Cheng, D., Chai, Y., Gong, J., Sun, M., Zhao, F. (2019) Bridging biodegradable metals and biodegradable polymers: A comprehensive review of biodegradable metal–organic frameworks for biomedical application. Dyes and Pigm., 170,107619. (DIO: 10.1016/j.pmatsci.2025.101526)

[62] Mellerup, S. K., Wang, S. (2019) Boron-based stimuli responsive materials. Chem. Soc. Rev., 48, 3537. (DIO: 10.1039/C9CS00153K)

[63] Kubota, Y., Tsuzuki, T., Funabiki, K., Ebihara, M., Matsui, M. (2010) Synthesis and fluorescence properties of a pyridomethene-BF2 complex. Org. Lett., 12, 4010. (DIO: 10.1021/ol101612z)

[64] Ma, X., Sun, R., Cheng, J., Liu, J., Gou, F., Xiang, H., Zhou, X. (2016) Fluorescence Aggregation-Caused Quenching versus Aggregation-Induced Emission: A Visual Teaching Technology for Undergraduate Chemistry Students. J. Chem. Educ., 93, 345. (DIO: 10.1021/acs.jchemed.5b00483)

[65] Suenaga, K., Tanaka, K., Chujo, Y. (2017) Front Cover: Design and Luminescence Chromism of Fused Boron Complexes Having Constant Emission Efficiencies in Solution and in the Amorphous and Crystalline States (Eur. J. Org. Chem. 35/2017), Issue 35. J. Org. Chem., 35, 5191. (DIO: 10.1002/ejoc.201701191)

[66] D'Aléo, A., Gachet, D., Heresanu, V., Giorgi, M., Fages, F.(2012) Two-photon excited fluorescence of BF_2 complexes of curcumin analogues: toward NIR-to-NIR fluorescent organic nanoparticles. Chem. Eur. J., 18, 12764. (DIO: 10.1039/c4tc00543k)

[67] Dunitz, J. D., Taylor, R. (1997) Organic Fluorine Hardly Ever Accepts Hydrogen Bonds. Chem. Eur. J., 3, 89. (DIO: 10.1002/chem.19970030115)

[68] Prasanna, M. D., Row, T. N. G. (2000) C–halogen···π interactions and their influence on molecular conformation and crystal packing: a database study. Cryst. Eng.,   3, 135.   (DIO: 10.1016/S1463-0184(00)00035-6)

[69] Jain, A., Ramanathan, V., Sankararamakrishnan, R. (2009) Effect of trehalose on protein structure. Protein Sci., 18, 595. (DIO: 10.1002/pro.3)

[70] Reichardt, C. (1994) Solvatochromic Dyes as Solvent Polarity Indicators. Chem. Rev., 94, 2319. (DIO: 10.1021/cr00032a005)

[71] Pavlovich, V. S. (2012) Solvatochromism and Nonradiative Decay of Intramolecular Charge-Transfer Excited States: Bands-of-Energy Model, Thermodynamics, and Self-Organization. Chem Phys Chem., 13, 4081. (DIO: 10.1002/cphc.201200426)

[72] Marini, A., Muñoz-Losa, A,, Biancardi, A., Mennucci, B. (2010) What is solvatochromism?. J. Phys. Chem. B., 114, 17128. (DIO: 10.1021/jp1097487)

[73] Winget, P., Bredas, J. L. (2011) Phosphonic Acid Modification of Indium−Tin Oxide Electrodes: Combined XPS/UPS/Contact Angle Studies. J. Phys. Chem. C., 115, 10823. (DIO: 10.1021/jp710893k)

[74] Wang, J., Ding, T., Nie, C., Wang, M., Zhou, P., Wu, K. (2020) J. Am. Chem. Soc., 142, 4723. (DIO: 10.1021/jp710893k)

[75] Sednev, M. V., Belov, V. N., Hell, S. W. (2015) Fluorescent dyes with large Stokes shifts for super-resolution optical microscopy of biological objects: a review. Methods Appl. Fluoresc., 65, 211. (DIO: 10.1088/2050-6120/3/4/042004)

[76] Calvo, C. S., Romero, F., González, I. L., Nishigaki, T. (2018) Robust Evaluation of Intermolecular FRET Using a Large Stokes Shift Fluorophore as a Donor. BioTechniques., 65, 211. (DOI: 10.2144/btn-2018-0041)

[77] Russegger, A., Borisov, S. M. (2021) Fluorescent 1-hydroxy-10-alkylacridin-9(10H)-one BF_2-chelates: Large Stokes shift and long emission decay times. Dyes Pigm., 184, 108816. (DIO: 10.1016/j.dyepig.2020.108816)

[78] Dai, J., Zhang, X. (2023) Chemical Regulation of Fluorescence Lifetime. Chem. Biomed. Imaging., 1, 796. (DIO: 10.1021/cbmi.3c00091)

[79] Bañuelos, J., Córdoba, J. A., Escamilla, I. V.,Hernández, A. A., Cabrera, E. P., Hu, R., Tang, B. Z., Esnal, I., Martínez, V., Arbeloa, I. L. (2011) Modulation of the photophysical properties of BODIPY dyes by substitution at their meso position. RSC. Adv., 1, 677. (DIO: 10.1039/C1RA00020A)

[80] Hong, Y., Lama, J. W. Y., Tang, B. Z. (2009) Aggregation-induced emission: phenomenon, mechanism and applications. Chem. Commun., 4332. (DIO: 10.1039/B904665H)

[81] Chai, J. D., Gordon, H. M., (2008) Long-range corrected hybrid density functionals with damped atom–atom dispersion corrections. Phys. Chem. Chem. Phys., 10, 6615. (DIO: 10.1039/B810189B)

[82] Krishnan, R., Binkley, J. S. Seeger, R., Pople, J. A. (1980) Self-consistent molecular orbital methods. XX. A basis set for correlated wave functions. J. Chem. Phys., 72, 650. (DIO: 10.1063/1.438955)

[83] Clark, T., Chandrasekhar, J., Spitznagel, G. W., Schleyer, P. V. R. (1983) Efficient diffuse function-augmented basis sets for anion calculations. III.† The 3-21+G basis set for first-row elements, Li–F. J. Comput. Chem., 4, 294. (DIO: 10.1002/jcc.540040303)

[84] Boese, A. D., Handy, N. C. (2002) New exchange-correlation density functionals: The role of the kinetic-energy density. J. Chem. Phys., 116, 9559. (DIO; 10.1063/1.1476309)

[85] Weigend, F., Ahlrichs, R. (2005) Balanced basis sets of split valence, triple zeta valence and quadruple zeta valence quality for H to Rn: Design and assessment of accuracy. Phys Chem Chem Phys., 7, 3297. (DIO: 10.1039/B508541A)

[86] Kasumov, V. T., Koksal, F., Sezer, A. (2005) Synthesis, structure and properties of ternary copper(II) complexes of ONO donor Schiff base, imidazole, 2,2′-bipyridine and 1,10-phenanthroline. Polyhedron. 24, 1203. (DIO: 10.1016/j.poly.2006.06.017)

[87] Kirk, S. M., Quilter, H. C., Buchard, A., Thomas, L. H., Kohn, K. G., Jones, M. D. (2016) Monomeric and dimeric Al(iii) complexes for the production of polylactide. Dalton Trans., 45, 13846. (DIO: 10.1039/C6DT02861F)

[88] Chu, Z., Huang, W. (2007) Synthesis of an E2-Ub-nucleosome conjugate to capture the E3 ligase PHF7-catalyzed H3K14 ubiquitination intermediate. J. Mol. Struct., 837, 15. (DIO: 10.1007/s11426-025-2697-6)

[89] Würth, C., Grabolle, M., Pauli, J., Spieles, M., Genger, U.R. (2013) Relative and absolute determination of fluorescence quantum yields of transparent samples. Nat. Protoc., 8, 1535. (DIO: 10.1038/nprot.2013.087)

[90] Rurack, K., Spieles, M. (2011) Fluorescence Quantum Yields of a Series of Red and Near-Infrared Dyes Emitting at 600−1000 nm. Anal. Chem., 83, 1232. (DIO: 10.1021/ac101329h)

[84] Dolomanov, O. V., Bourhis, L. J., Gildea, R. J., Howard, J. A. K., Mann, P. H. (2009) OLEX2: a complete structure solution, refinement and analysis program. J. Appl. Cryst., 42, 339. (DIO: 10.1107/S0021889808042726)

[91] Sheldrick, G. M. (2015) Crystal structure refinement with SHELXL. Acta Cryst., A71, 3. (DIO: 10.1107/S2053229614024218)

Chapter 3

Unveiling Borane Complexes with N-O Chelation: Synthesis, Reactivity, and Theoretical Perspectives
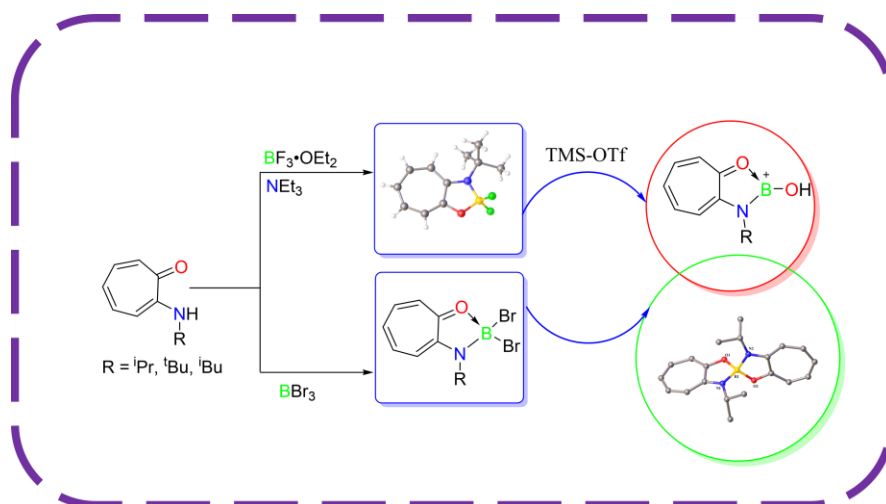
3.1 Introduction

The development of highly fluorescent organic fluorophores has drawn considerable attention due to their wide range of applications in material science and bioscience *[1-7]*. Among these, dyes featuring a BF_2 unit have become a privileged class of compounds that have rapidly grown in popularity over the past decade due to their tunable photophysical properties, photostability, and high fluorescence quantum yield *[8-12]*. Incorporating boron atoms into the π-conjugated frameworks of organic fluorophores is well known to enhance their photophysical properties significantly.*[13-15]* As a result, numerous boron complexes—most notably BODIPY dyes, which feature fluorescent BF_2 units coordinated by dipyrromethene ligands—have been extensively studied and explored for their potential applications in medical diagnostics.*[16-19]*, photodynamic therapy (PDT) *[20-22]*, solar cells, organic light-emitting diodes *[23-27]*, and many more. Different kinds of BODIPY analogues derived from dipyrromethene scaffolds have been dealt with in the above-described applications, whereas luminescent boron complexes based on aromatic ligands *[28-30]* have been developed to explore and expand their photo-functional properties. Namely, a few successful examples of four-coordinated boron complexes based on bidentate *[31,32]* and tridentate ligands *[33]*, which show luminescent properties and other unique properties like self-assembly *[34]*, aggregation-induced emission [35], aggregation-caused quenching *[36]*, and chiroptical properties *[37]*, have been reported.

The presence of the BF_2 unit in these dyes not only makes them good fluorophores, but they also become a starting point to synthesize Lewis acidic boron cations. The six-membered borane dyes chelated with N-N *[38]* and N-O *[39]* donor ligands are well explored and are derived from using aniline, indole, thiazole, quinoline, pyrimidine, isoindolin-1-one, imine, hydrazone, including BODYPI. Six-membered chelated borane chemistry has been extensively studied for its photophysical properties. Still, they also play a key role in the synthesis and isolation of various cationic and radical species. In 2008, W. E. Piers and co-workers

synthesized the borenium cation derived from BODIPY dyes upon treatment with fluoride abstracting reagent triethyl silyl perfluoro-tetraphenylborate [Et$_3$Si{B(C$_6$F$_5$)$_4$}].*[40]* In 2019, the Ryan group reported the isolation of oxoboranes through inert borane halide ion exchange, followed by hydrolysis of a formazanate-based borane dye.*[41]*
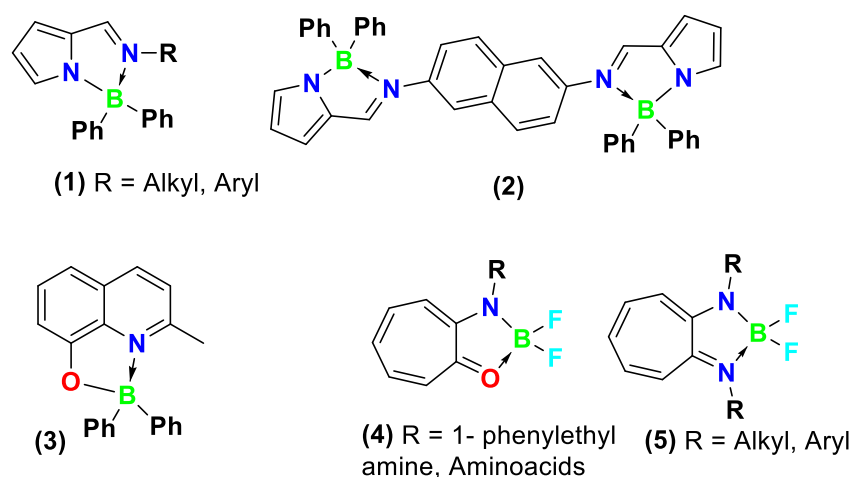

Figure 3.1 Previously reported five-membered boranes, 1) and 2) iminopyrrolyl ligand, 3) 8-hydroxy quinoline ligand, 4) and 5, ATIs N-O boranes, ATIs N-N boranes, respectively.

Electron-deficient complexes of boron, particularly boron cations, play a crucial role in catalysis due to their inherent Lewis acidity, enabling them to activate numerous substrates and facilitate a wide range of chemical transformations. Boron cations are utilized in diverse reactions, such as making a C-C bond, hydroborations, and hydrogenation reactions. They also know to be a part of FLPs, where a Lewis acidic boron species and a Lewis basic species are sterically prohibited from forming a simple adduct, enabling them to activate small molecules like H$_2$ and CO$_2$. Stephan and his team isolated the classical carbene-stabilized borenium cation as a catalyst for the FLP hydrogenation reaction. This ion reduced a wide range of imines and enamines using 1-5% catalyst loading at room temperature under 102 atm of H$_2$. Recently, Wang and his co-workers demonstrated that small carbene-stabilized borenium cation effectively participated in the C-C

bond cleavage of the cyclopropane at 80 °C under 80 bar of H_2. Denmark and his co-workers reported 2,6-lutidine-supported borenium cation [Lut-BBN]NTf_2 as an effective catalyst for hydrosilylation reactions in various ketones in the presence of 1.5 equiv. of $HSiEt_3$ at ambient temperature. Further, Crudden and his co-workers extended the Borenium-catalyzed hydrosilylations to the reduction of imines.

In recent decades, the domain of boron cation-based catalysts has witnessed remarkable growth, basically driven by the unique electronic features of boron cations. The inherent Lewis acidity at the boron center arises due to its formal positive charge serves as a key for their catalytic activities. Boron cations have been utilized across the range of catalytic transformation reactions, including C-C bond hydrogenolysis, hydrosilylations, C-H borylations, and hydroboration reactions. Moreover, boron-based catalysts, particularly borenium ions largely dependent on the electronic and steric factors governing their reactivity. For a better understanding of these effects, new boron-catalysed methodologies can be expected.

We focus on synthesizing the boron cations in six and five-membered ring systems, stabilized through the internal base donors. Our efforts led us to synthesize and characterize bis(borenium) dications containing a hydroxyl group, regarded as cationic borinic acid derivatives for the first time [9], whilst the six-membered N-O chelated borane complexes did not produce the boron cation. In search of isolating the boron cation in a five-membered scaffolds we found that aminotroponiminates (ATIs) boranes are useful precursors. Mono-nuclear N-N chelated ATI-boranes produce tri-coordinated borenium cations, while ethylene-bridged binuclear borane yeided the oxy-bridged bore(boro)nium cation. Upon comparing, we noticed that the five-membered ATI boranes yielded the tri-coordinated borenium cations in mild reaction conditions compared to the six-membered diiminate-based borane precursors.

Herein, we reported a series of 2-aminotropone-based borane complexes (**2l**–**2n**) that exhibit strong fluorescence in solution. Treatment of these

borane complexes with trimethylsilyl trifluoromethanesulfonate (TMS-OTf) results in the formation of mixtures of borenium and boronium cations in solution. In contrast, reacting 2-aminotropone with BBr₃ at room temperature selectively affords boronium cations (**4l-4n**). These cations were fully characterized using multinuclear NMR spectroscopy and single-crystal X-ray diffraction analysis.

5.2 Results and Discussion

5.2.1 Synthesis and characterization of 2-aminotropone boranes
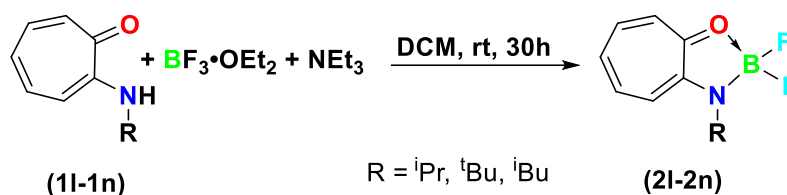
Scheme 3.1 Synthesis of 2-aminnotropone boranes (**2l-2n**)

For the synthesis of 2-aminotropone boranes, first, we focused on the synthesis of 2-aminotropone ligands by following the previously reported standard protocol. The purities of proligands were confirmed by comprehensive spectroscopic analysis, including ^{1}H NMR, ^{13}C{1H} NMR, and (HRMS) high-resolution mass spectrometry. Further, 2-aminotropone ligands were treated with BF₃·OEt₂ in the presence of triethylamine as a base in DCM to facilitate the 2-aminotropone borane complexes in good yields. The synthesized complexes exhibit good solubility in both polar and non-polar solvents. They have been systematically characterized using various spectroscopic techniques and high-resolution mass spectrometry. ^{1}H and ^{13}C{^{1}H} spectra show downfield shifts of approximately 0.2–0.5 ppm and 2–5 ppm, respectively, compared to the corresponding 2-aminotropone ligands, indicating deshielding upon complexation. In the ^{11}B NMR spectra, a triplet signal was observed between 5.60 and 5.70 ppm, while the ^{19}F NMR spectra showed a quartet between –124.5 and –135.6 ppm, indicating the presence of a BF₂ unit.

3.2.2 Single crystal X-ray diffraction (SCXRD) analysis of 2-aminotropone boranes

Crystals of compounds **2l-2n** were obtained from saturated solutions in a 2:1 DCM/hexane mixture, and their structures were confirmed by single-crystal X-ray diffraction (SCXRD) analysis. Complexes **2l** and **2n** are crystallized in the monoclinic system in the P2$_1$/n space group, but complex **2m** crystallizes in the triclinic system with the P-1 space group. As shown in Figure 21, the geometry around the boron is distorted tetrahedral, and Table 1 includes the selected geometrical parameters. The measured F1-B1-F2 bond angles of complexes **2l-2m** are ~109° confirming the tetrahedral arrangement around the boron centre. Interestingly BF$_2$ unit is coplanar with the C$_{ATI}$ backbone in all three complexes, adopting the confirmation that minimizes the steric repulsion. The C-C bond lengths of the C$_{ATI}$ backbone lie between single and double bonds, which indicates the delocalization of π electrons throughout the ring *[48].* **Figure 3.2 and Table 3.1**

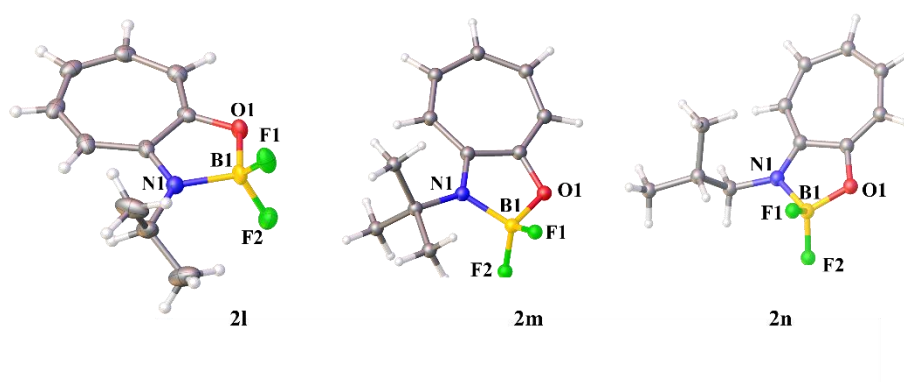**Figure 3.2** Crystal structure of 2-aminotropone boranes

Table 3.1 Selected bond lengths (Å) and bond angles (°) of complexes (**2l-2n**)

Selected bond length (Å) & bond angle (°)	2l	2m	2n
B1-N1	1.558(14)	1.5570(1)	1.561(12)
B1-O1	1.495(13)	1.471(2)	1.458(13)
B1-F1	1.378(15)	1.378(2)	1.350(13)
B1-F2	1.381(14)	1.378(2)	1.373(13)

| F1-B1-F2 | 109.665(9) | 110.01(13) | 108.8(11) |
| N1-B1-O1 | 99.698(9) | 100.53(11) | 100.2(10) |

3.2.3 Crystal packing of 2-aminotropne boranes

The non-covalent interactions are responsible for molecular assembly in 2-aminoropone borane complexes. The formation of a linear infinite chain in complex **2l** is due to the non-covalent interaction of C-H⋯F interaction between Lewis basic fluorine atom and the C_{ATI} hydrogen of the adjacent 2-aminotropone borane unit. The distances measured are 2.632 Å. Complex **2m** crystal packing propagates in the infinite molecular chain through one-dimensional head-to-tail packing of C_{ATI}-H⋯F and C_{6ATI}-H⋯O, with distances measured at 2.526 and 2.632 Å, respectively. In complex **2n**, another non-covalent interaction is observed, which allows the 2-aminotropone-borane unit to be arranged in an anti-parallel fashion **Figure 3.3**. The distance between two anti-parallel units is 7.137 Å, which ensures that there is no π-π interaction between them.
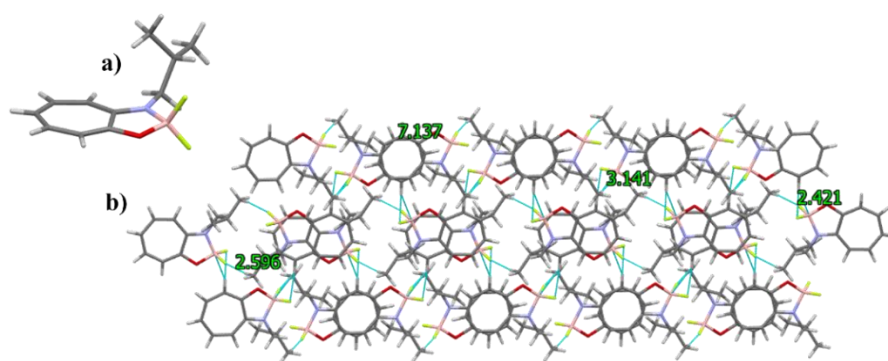
Figure 3.3 Crystal packing of **2n** borane

3.2.4 Photophysical study of 2-aminotropone boranes

2-Aminotropone ligands are non-emissive in solid as well as in solution, but their BF_2 complexes (**2l-2n**) are strongly blue emissive in solution. 2-Aminotropone boranes are emissive due to the chelation of the BF_2 unit with the ligand may allow the complete delocalization of π electrons through the rings and bring rigidity to the boranes. Absorption and

emission spectra of 2-aminotropone boranes were recorded in DCM, depicted in **Figure 3.4** The absorption spectra of 2-aminotropone borane **2l** exhibit three absorption bands at 392, 379, and 342 nm, mainly due to the π-π*, n-π*, and charge transfer in the 2- aminotropone borane residue. D. Curiel and his coworkers in 2012 reported very similar results in indolocarbazole-based borane fluorophores. They showed three absorption bands corresponding to the indolocarbazole unit's π-π, n-π, and intramolecular charge transfer.[54]
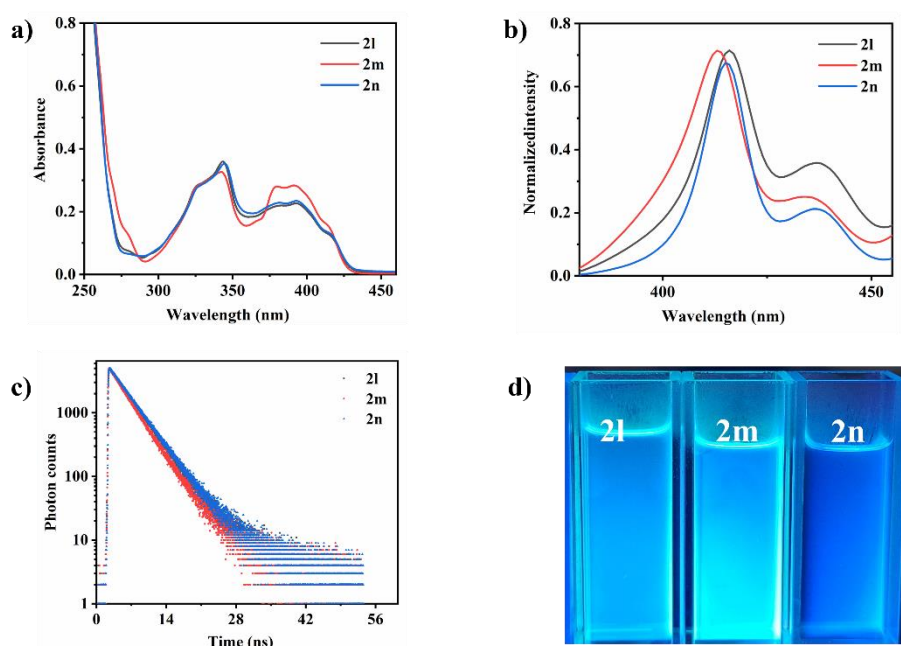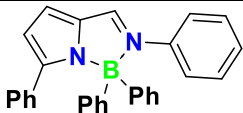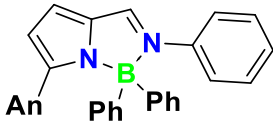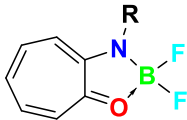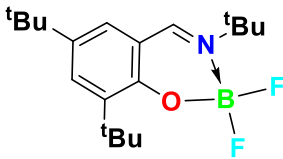

Figure 3.4 a) Absorption, b) emission spectra recorded in DCM, c) fluorescence decay plot, and d) photographs under UV light of complexes **2l-2n**.

The absorption spectra of complexes **2m** and **2n** also exhibit three bands similar to those observed for complex **2l**, suggesting that the substituents on the chromophores have minimal influence on their electronic transitions. Emission spectra were recorded in the DCM, and emission bands of all 2-aminoboranes appeared in a similar range. Photophysical parameters are tabulated in **Table 3.2** Emission spectra of complexes **2l-2m** show two distinct emission bands. The first emission bands were observed to appear at 414-416 nm, slightly higher energy reason in

contrast second bands appeared at slightly lower energy reason ranges (434 to 438 nm), **Figure 3.3**.

Table 3.2 Photophysical properties comparison of 2-aminotropon borane counterparts (An = Anthracene)

Compounds	Abs (λ_{abs})	Em (λ_{emi})	Stock shift (cm^{-1})	Lifetime(ns)
	416	480	64	3.93
	392	429	35	3.51
2c	392	438	46	3.91
	358	456	98	6.9

The fluorescence lifetimes of the 2-aminotropone borane complexes (**2l-2n**) are measured in DCM by using time-resolved fluorescence spectroscopy (TCSPC), excitation by 410 nm laser. The fluorescence decay graph is shown in Figure 3c. The substituents on the fluorophore significantly influence the fluorescence decay time of 2-aminotropone borane complexes. Steric bulk appears to play a key role, with complex **2n** exhibiting the longest lifetime, likely due to its less bulky isobutyl group compared to the tert-butyl and iso-propyl groups in other complexes. The observed lifetimes follow the descending steric order: tBu > iPr > iBu. This trend may also be attributed to the +I inductive effect of the isobutyl group, which increases electron density on the HOMO and reduces non-radiative decay pathways. Fluorescence decay time can be altered by changing the substituents on the fluorophore unit. Zang and coworkers reported a decrease in the fluorescence lifetime in

BODIPY-based fluorophores when introducing a chlorine atom.*[55]* Similar results reported by Kolhmaienen and his coworker found that in NBF_2O moieties, introducing an electron-withdrawing or releasing group decreases the fluorescence lifetime from 2.3 ns to 0.1 ns.*[56]*

Table 3.3 Photophysical parameters of 2-aminotropone borane complexes

Complex	Absorption(λ_{abs})	Emission(λ_{emi})	Stokes Shift(nm/cm^{-1})	ϕ_F	τ_F (ns)
2l	395, 379, 342	437, 415	42/2433	-	3.80
2m	394, 377, 344	436, 413	42/2444	-	3.44
2n	392, 379, 342	438, 417	46/2679	-	3.91

3.3.1 Synthesis of boron cations

Recently, our group synthesized a series of five-membered borenium cations that are stabilized by the C_2N_2 donor pockets of aminotroponimines (ATIs) ligands *[49]*. The C_2N_2 core of ATI ligands plays a vital role in facilitating the boron-centered cation. This might be possible due to the unique steric and electronic properties of the ATIs frameworks that help in isolating the electron-deficient borenium cations. In 2014, Ingelson and co-workers reported an N, O-chelated tricoordinate borenium cation by the treatment of quinolato boron chloride complexes with $AlCl_3$.*[50]* The groups of Bourissou and Jakle reported the five-membered borenium cations, stabilized by C, N, and C, P donors atoms respectively *[51,52]*. Inspired by previous reports, we aimed to synthesize N-O-chelated tricoordinate borenium cations. To this end, 2-aminotropone boranes were treated with trimethylsilyl trifluoromethanesulfonate (TMS-OTf) **Scheme 3.2** and the ^{11}B NMR spectrum showed two distinct signals at 21.6, 11.2 ppm along with the starting material at 6.10 ppm **Figure 3.21-3.23**   Even though we attempted several times with different reaction conditions to prepare a single compound, we were not only unable to prepare a single compound, but also the purification of these species was troublesome, and eventually resulted in a mixture of products. Therefore, we reasoned that the presence of oxygen in these N-O chelated ATI-BF$_2$ complexes

hampers the borenium cation formation, and the removal of fluoride might not be a viable path for the borenium cation isolation. In comparison, the N-N-chelated ATI-BF$_2$ complexes were very good precursors for the borenium cation formation. This difference may be attributed to two factors: steric and electronic effects. The substituents on the nitrogen atoms provide steric protection around the cationic boron centre, while the nitrogen's lone pair offers electronic stabilization by saturating the boron atom. In the case of N-O boranes, with sp^2 hybridized oxygen fails to provide steric and electronic saturation to the cationic boron centre.

2l-2n   **3a-3c**   **4a-4c**

3l: R = ^{i}Pr   4l: R = ^{i}Pr
3m: R = ^{t}Bu   4m: R = ^{t}Bu
3n: R = ^{i}Bu   4n: R = ^{i}Bu
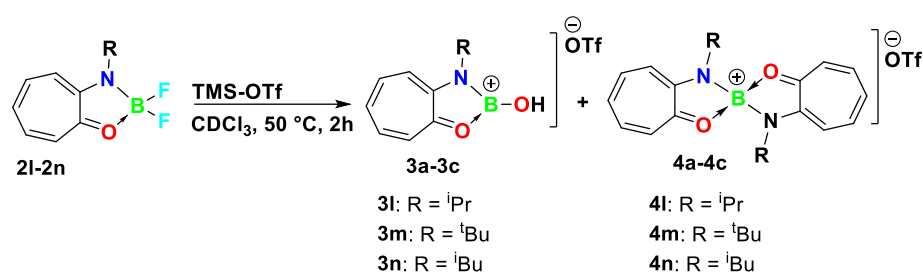
Scheme 3.2 Synthesis of borenium cations

In search of another precursor for the N,O-chelated borenium cation formation, we speculated that N, O-chelated ATI-BBr$_2$ complex might be a more amenable precursor for isolating the boron cation within the same ligand framework. We treated 2-aminotropone, **1l**, with boron tribromide in 1:1 ratio at room temperature in toluene. The reaction instantaneously resulted in a yellowish precipitate, which was washed with hexane several times to get **4l** as a light-yellow solid in 58% yield **Scheme 3.3**. The ^{11}B NMR of **4l** showed a sharp signal at 12.3 ppm is similar to the chemical shifts of several boronium cations *[53]*. This chemical shift, which is similar to the ^{11}B NMR observed during the fluoride abstraction of ATI-BF$_2$ complexes, hinted at the possibility of the formation of boronium cations **4l-4n** from **3l-3n** via ligand scrambling, common in borane chemistry.*[58]* reaction in case of In the ^{1}H NMR spectrum, three distinct sets of doublets were observed, each integrating for four protons (1.17 ppm to 1.47 ppm). This confirms

the presence of two 2-aminotropone units coordinated to a common boron centre. The appearance of three doublets, despite the apparent symmetry, indicates that the ligand environments are chemically non-equivalent-likely due to a diagonal arrangement around the boron atom. The HRMS data also supports the boronium cation formation.

4l: R = ^{i}Pr
4m: R = ^{t}Bu
4n: R = ^{i}Bu
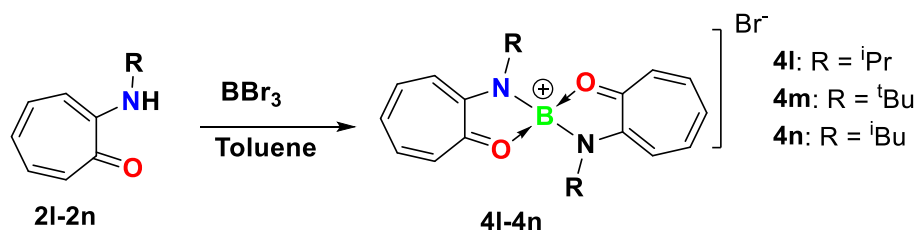
Scheme 3.3 Synthesis of boronium cations

3.3.2 Single crystal X-ray diffraction (SCXRD) analysis of boronium cation

Crystals were obtained from CDCl$_3$ solution at room temperature. Single crystal X-ray structure analysis discloses the identity of **4l** as a boronium cation where two ATI units are attached to the boron centre, resulting in a spirocyclic bora-oxazole type geometry **Figure 3.5**. The geometry around the boron atom is distorted tetrahedral, with the bond angle between 100-112°. The ATI-N,O units are perpendicular to each other with a dihedral angle of 84°. The nitrogen is covalently attached to boron with a distance of 1.543(6) Å. The B-O bond length (1.478(5) Å) is similar to the single bond distances.*[57]* The carbon-oxygen bond distance (1.328(5) Å) is slightly longer than the C-O double bond distance, evocative of another resonating structure of the compound **4l**. **Scheme 3.3**. Interestingly, the measured bond lengths between carbon-carbon atoms lie in between single and double bonds [(C$_1$-C$_7$ 1.442(6Å), C$_5$-C$_6$ 1.366(7Å), and C$_6$-C$_7$ 1404(6Å)], which indicates the complete delocalization of π electrons throughout the rigid backbone of the planer seven-membered ring.
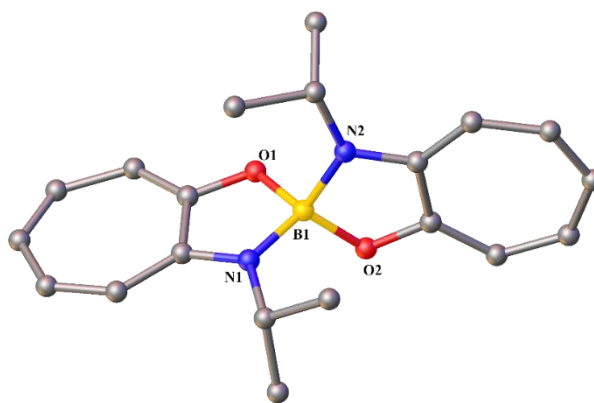
Figure 3. 5 Crystal structure of boronium cation **(xx)** Crystal structure boronium cation **4a**, hydrogen atoms, and counter anion are omitted for clarity. Selected bond length (Å) O1-B1 1.478(5), O2-B1 1.472(5), N1-B1 1.543(5), N2-B1 1.537(5) selected bond angles in (°) O2-B1-N1 111.6(3), O1-B1-N2 112.7(3), O2-B1-O1 113.5(3), O1-B1-N1 100.2(3), N2-B1-N1 100.2(3).

3.3.3 Photophysical study of boronium cations

We investigated the UV-Visible spectra of boronium cations (**4l-4n**) in DCM, which are all weakly emissive in the solution phase. The photophysical details are listed in **Table 3.4.** The emission and absorption maxima of the boronium cations (**4l-4n**) were observed to be similar to those of the neutral tetracoordinate BF_2 boranes. In absorption spectra, three absorption bands appear in boronium cations attributed π-π*, n-π*, and intramolecular charge transfer. Notably, the π-π* absorption bands in boronium cations shifted towards the blue region; this might happen due to the positive charge on the boron centers and perpendicular arrangement of both rings, which hampered the π-delocalizations. In emission spectra, two emission bands were observed, ranging from 416 nm to 445 nm. This is due to the formation of excimers. The formation of excimers depends on numerous factors such as temperature, pressure, geometry, and bite angles. *[67]* Interestingly, the bite angle of N-B-O in neutral boron complexes ranges [99.69(9) to 100.2(2)(°)] lower than the boronium cation, which is found around the boron center [O2-B1-N1 111.6(3), O1-B1-N2 112.7(3), (°)] respectively. The favorable geometric alignment of the aromatic cores

allows for efficient π-orbital overlap between adjacent molecules, thereby enhancing the likelihood of excimer formation in the excited state. Interestingly, we observed a higher Stokes shift in boronium cations (**2l, 2m**, to **4l, 4m**) respectively, while in the case of **2n** to **4n** decrease in Stokes shift was observed. This is the result of extended pi delocalization exhibiting higher absorption maxima in **4n** complex. **Figure 3.6**. T. Tsuno and his co-workers reported similar results in boron-based spiro chiral dyes. They observed that on changing the solvent polarity, the Stokes shift was significantly changed with negligible disturbance in photophysical intensities.*[68]* We recorded the fluorescence decay time of the boronium cations, which follows similar trends to neutral boranes.
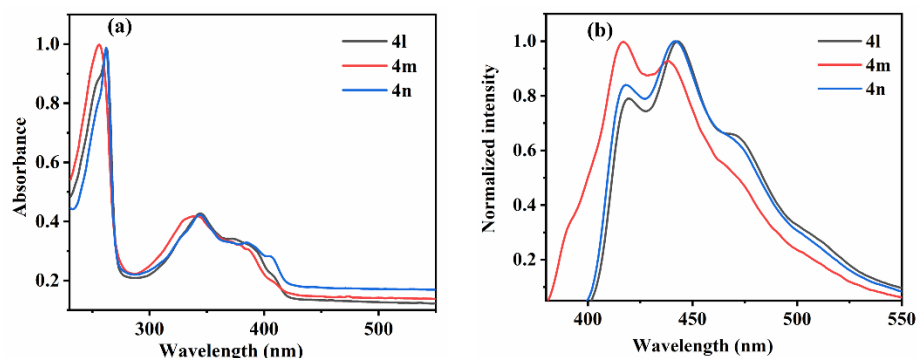

Figure 3.6 UV-Visible spectra of boronium cations (**4l-4n**)

Table 3.4 Photophysical outcomes of boronium cations

Complex	Absorption(λ_{abs})	Emission(λ_{emi})	Stokes Shift(nm/cm^{-1})	ϕ_F	τ_F (ns)
4l	397, 344, 262	442, 417	45/2564	-	1.24
4m	390, 336, 256	438, 416	48/2809	-	0.32
4n	405, 344, 261	441, 417	36/2015	-	1.23

3.4 DFT Studies on mono- and di-BF2 complexes and corresponding cationic species

To understand the photophysical properties of the boron complexes **2l-2n, 2a-Br₂**, cations **3l** and **4l** (anions are ignored), theoretical calculations were conducted using the range-separated ω-B97XD functional[24] and a triple-zeta 6-311G(d) basis set[25] for ground-state

172

geometry optimizations. Excited-state calculations were also performed at the aforementioned level of theory. The electronic distribution and energy (in eV) of molecular orbitals for BF_2-complex (**2l**) as well as cationic complexes (**3l** and **4l**), are presented in **Figure 3.5.** Computations on **3l** showed that the HOMO (highest occupied molecular orbital) and LUMO (lowest unoccupied molecular orbital) are primarily located on the aminotroponiminate moieties with similar HOMO-LUMO gap of 7.62 eV. While, HOMO describes the C-C-C-C extended π-interaction interaction along with electron localizations over the N centers of the aminotroponiminate moieties, LUMO describes corresponding anti-bonding interactions. However, corresponding cations **3l** showed relatively higher HOMO-LUMO gap of 8.12 eV compared to the neutral species due to the stabilizations of the corresponding HOMO orbitals. While HOMO of the mono-cationic **3l** revealed the extended C-C-C-C π-interactions as well as delocalization of the N based lone pairs to the empty p_z orbital located on B center, resulting in uneven N-B-N π delocalization. The uneven distribution of N-B-N π delocalization was due to the interference of the lone pair located in the -OH moiety attached to the B center. The degenerate orbitals HOMO and HOMO-1 of cationic **4l** are evenly distributed over the aminotroponiminate moieties, signifying the tetrahedral nature of the B center. The NBO (natural bond order) charge distribution (NBO charge: 0.46 (**2l**), and 0.57 (**4l**-cation)) and calculated ^{11}B-NMR values **Table 3.3** indeed corroborated satisfactorily with the observed ^{11}B NMR values. The B center becomes more de-shielded and accumulates more positive charge over it. The calculated ^{11}B NMR value of 24.1 ppm can satisfactorily be assigned to the transient cationic species **3l** which could not be isolated.
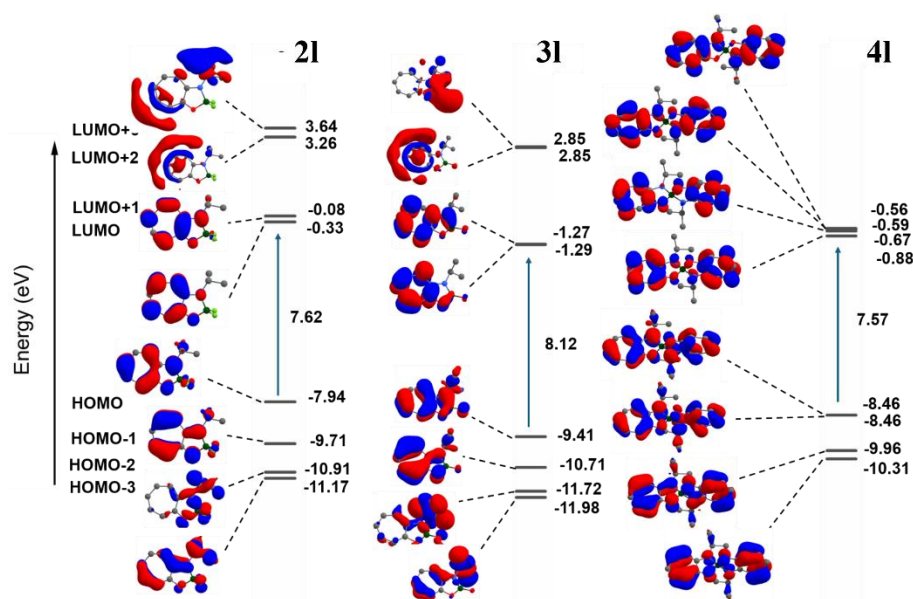
Figure 3.7 Electronic transitions of mono-BF$_2$ complexes (**3l** and **4l**) as well as di-BF2 complexes (**2l**) computed at the ϲ-HCTHhyb/def2-TZVPP(TD, SMD: dichloromethane)//ω-B97XD/6-311G(d) level.

For complexes **2l-2n** as well as **2l-Br₂**, the first excitation (lowest in energy) results from the transition of electrons between HOMO and LUMO **Figure 3.7**. The second excitation is associated with the transfer of electrons from HOMO→LUMO+1 for complexes. On the other hand, for the cationic complexes **3l** and **4l** the low energy excitations are either associated with transitions from HOMO→LUMO+1 (for **3l**) or a mixed transition consisting of HOMO/HOMO-1→LUMO/LUMO+1. According to the electronic distribution, the transitions in the absorption process are attributed to n→π* and π-π*-type transitions of the respective ligands. Further, **Table 3.3** summarizes that the calculated ^{11}B NMR were very close to the observed ^{11}B NMR, which validates the adoption of the computational methods to shed light on the electronic transitions in the di-BF$_2$ complexes as well as the related cationic species.

The standard enthalpies and Gibbs energies were calculated and shown in **Table 3.4** in order to shed light on the stepwise or direct formation of **4l** from **1l** and BBr₃. The results show that the direct formation of 4a starting from ligand 1a is a feasible process; however, stepwise formation through different intermediates can not be ruled out. Although

the BBr$_2$-adduct formation is apparently a feasible process, the results show that formation of the BBr-adduct and the product formation from it are endogenous and may involve slower pathways.

Table 3.5 Experimentally observed and calculated ^{11}B NMR (GIAO-ωB97XD/6-311G*//ωB97XD/6-311G*), experimental (at room temperature in ACN) and calculated UV/vis data (at ωB97XD/6-311G*-SMD) and corresponding orbital transitions for **2l-4l**

Complex	^{11}B NMR(exp) ppm	^{11}B NMR(cal) ppm	λ(exp) nm	λ(cal) ([a]f) nm	Transitions	E$_{HOMO-LUMO}$ (eV)	NBO Charge[c]
2l	6.09	4.60		340 (0.14)	HOMO→LUMO (96%)	7.62	0.46
				304 (0.31)	HOMO→LUMO+1 (91%)		
2m	5.98	4.61		340 (0.14)	HOMO→LUMO (96%)	7.60	0.45
				304 (0.31)	HOMO→LUMO+1 (91%)		
2n	5.97	4.66		339 (0.15)	HOMO→LUMO (96%)	7.63	0.48
				305 (0.30)	HOMO→LUMO+1 (91%)		
[b]**4l** (cation)	12.86	10.43		334 (0.12)	HOMO-1→LUMO (55%) HOMO→LUMO+1 (37%)	7.57	0.57
				311 (0.75)	HOMO-1→LUMO+2 (46%) HOMO→LUMO+3 (39%)		

[a](f = oscillator strength), [b]calculated only on the cationic part. [c]on B center

Table 3.6 Computed standard enthalpies ΔH°$_{298}$ and standard Gibbs free energies ΔG°$_{298}$ (in Kcal·mol-1), for the process of generating **4l** at ωB97XD/6-311G* level of theory.

Reaction	*ΔH^0*	*ΔG^0*

Ligand + BBr$_3$ = [BBr$_2$]$^-$ adduct+HBr	-31.04	-27.8
BBr$_2$-adduct + Ligand = BBr-adduct+HBr	19.48	23.35
BBr$_2$-adduct + Ligand = Pdt+HBr	1.42	4.71
BBr-adduct = Pdt	-18.06	-18.64
BBr$_3$ + 2x Ligand = Pdt + 2xHBr	-29.63	-23.09

3.5 Summary

In summary, we have synthesized a series of 2-aminotropone-based mononuclear borane complexes, all of which exhibit strong emission in solution. Attempts to generate tri-coordinated borenium cations by treating these boranes with a fluoride abstracting reagent were unsuccessful, likely due to the N-O-chelation failing to meet the steric and electronic requirements for borenium stabilization, unlike their N-N-chelated counterparts. Interestingly, treatment of 2-aminotropones with BBr$_3$ led to the formation of boronium cations, which were thoroughly characterized using various spectroscopic techniques and confirmed by single-crystal X-ray diffraction. The theoretical study also supported the feasibility of the formation of boronium cations.

3.6 Experimental Section

General Methods

The reactions were performed under an argon atmosphere using standard Schlenk techniques or in the open air. Chemicals were purchased from Spectrochem, Sigma-Aldrich, and TCI and used as received. All the solvents were purified by distillation using the appropriate drying

agents, deoxygenated using three freeze–pump–thaw cycles, and stored over molecular sieves under dry argon before use. The deuterated solvents used for NMR spectroscopy were deoxygenated by freeze–pump–thaw cycles and stored under an argon atmosphere over molecular sieves. NMR chemical shifts are reported in ppm and coupling constants in Hz. ^{1}H, ^{11}B, ^{13}C, and ^{19}F NMR spectroscopy data were obtained at ambient temperature using a Bruker 500 NMR spectrometer (operating at 500 MHz for ^{1}H, 126 MHz for ^{13}C, 160 MHz for ^{11}B and 471 MHz for ^{19}F). ^{1}H NMR spectra were referenced via residual proton resonances of CDCl$_3$ (^{1}H, 7.26 ppm) and ^{13}C NMR spectra were referenced to CDCl$_3$ (^{13}C, 77.16 ppm) and BF$_3$·OEt$_2$ used as an internal standard used for ^{11}B NMR. Bruker micrOTOF-Q II Daltonik was used to obtain HRMS spectrum. Photoluminescence (PL) spectra were recorded by using a Fluoromax-4 spectrofluorometer (HORIBA Jobin Yvon, model FM100) with an excitation and emission slit width at 5 nm. UV-Vis spectroscopy was performed on a 3 mL solution using the Varian UV−Vis spectrophotometer (Cary 100 Bio) in a quartz cuvette (1 cm × 1 cm). Cyclic voltammetry was performed using a C-H Instruments model CHI1103C in dichloromethane solvent using glassy carbon as the working electrode, Pt wire as the counter electrode, and a saturated calomel electrode (SCE) as the reference electrode. The scan rate was 100 mV. A solution of Bu$_4$NPF$_6$ in dichloromethane (0.1 M) was used as the supporting electrolyte. The temperature was kept constant throughout each experiment at 25 °C. The crystal data collection was performed on a CCD Agilent Technologies (Oxford Diffraction) SUPER NOVA (Mo at home/near, Eos) diffractometer. Data for the compounds were collected at 293 K using graphite-monochromated MoK$_\alpha$ radiation. *[59-61]* DFT calculations were implemented in Gaussian 09 using the hybrid functional B3LYP in combination with the cc-pVDZ basis set for all atoms.

Synthetic Details

General synthesis of ligands (1l-1n)

2-aminotrones (**1l-1n**) were reported by various groups, so we are not providing the synthetic details of them.

General procedure of 2-aminotropone boranes synthesis (2l-2n)

Aminotroponimine was dissolved in DCM and 10 equiv. of triethylamine was added under an inert atmosphere. To the resultant reaction mixture 10 equiv. of $BF_3 \cdot OEt_2$ was added dropwise and the mixture was left to stir at room temperature until reaction completion, as judged by TLC. The reaction mixture was quenched with DI water, and the product was extracted with DCM and purified by column chromatography to give yellow solids as pure products.

Complex 2l

Complex **2l** was prepared by using **1l** ligand (681 mg, 4.17 mmol), triethylamine (1689.5 mg, 16.70 mmol), and $BF_3 \cdot OEt_2$ (8889.1 mg, 62.6 mmol).

^{1}H NMR (500 MHz, CDCl$_3$) δ 7.64 – 7.56 (m, 1H), 7.47 (t, J = 10.1 Hz, 1H), 7.25 – 7.23 (m, 1H), 7.12 (d, J = 11.4 Hz, 1H), 7.05 (t, J = 9.8 Hz, 1H), 4.05 (sep, J = 6.6 Hz, 1H), 1.47 (d, J = 6.6 Hz, 6H). **^{13}C NMR** (126 MHz, CDCl$_3$) δ 167.62, 141.29, 139.66, 127.26, 118.78, 117.91, 46.95, 20.74. **^{11}B NMR** (160 MHz, CDCl$_3$) δ 6.09 (t, J = 20.1 Hz). **^{19}F NMR** (471 MHz, CDCl$_3$) δ -131.67 (dd, J = 39.9, 19.3 Hz). **HRMS (ESI):** Calculated for $C_{10}H_{13}BF_2NO$ 212.1052 [M+Na], found 212.1054.

Yield: 90%

Complex 2m

Complex **2m** was prepared by using **1m** ligand (2883.55 mg, 14.68 mmol), triethylamine (1114.11mg, 11.01 mmol), and $BF_3 \cdot OEt_2$ (929 mg, 6.54 mmol).

^{1}H NMR (500 MHz, CDCl$_3$) δ 7.57 (dd, J = 11.8, 9.0, 1.2 Hz, 1H), 7.53 – 7.43 (m, 2H), 7.24 (d, J = 2.9 Hz, 1H), 7.08 – 7.02 (m, 1H), 1.62 (s, 9H). **^{13}C NMR** (126 MHz, CDCl$_3$) δ 168.53, 139.95, 139.72, 127.29, 120.72, 119.12, 54.98, 28.18. **^{11}B NMR** (160 MHz, CDCl$_3$) δ 5.98 (t, J

= 20.3 Hz). ^{19}**F NMR** (471 MHz, CDCl$_3$) δ -128.45 (dd, J = 40.7, 19.9 Hz). **HRMS (ESI):** Calculated for C$_{11}$H$_{15}$BF$_2$NO 226.1209 [M+H], found 226.1208.

Yield: 80%

Complex 2n

Complex **2n** was prepared by using **1n** ligand (290 mg, 1.63 mmol), triethylamine (331.37 mg, 3.27 mmol), and BF$_3$·OEt$_2$ (929 mg, 6.54 mmol).

^{1}**H NMR** (500 MHz, CDCl$_3$) δ 7.64 – 7.57 (m, 1H), 7.48 (t, J = 10.2 Hz, 1H), 7.28 (d, J = 4.2 Hz, 1H), 7.14 (d, J = 11.4 Hz, 1H), 7.07 (t, J = 9.8 Hz, 1H), 3.42 (dd, J = 7.7, 3.1 Hz, 2H), 2.27 (sep, J = 13.9, 6.9 Hz, 1H), 1.01 (d, J = 6.7 Hz, 6H). ^{13}**C NMR** (126 MHz, CDCl$_3$) δ 167.57, 141.22, 139.61, 127.47, 118.91, 118.00, 51.36, 28.20, 20.84. ^{11}**B NMR** (160 MHz, CDCl$_3$) δ 5.97 (t, J = 18.7 Hz). ^{19}**F NMR** (471 MHz, CDCl$_3$) δ -137.92 (dd, J = 37.3, 18.2 Hz). **HRMS (ESI):** Calculated for C$_{11}$H$_{15}$BF$_2$NO 226.1209 [M+H], found 226.1208.

Yield: 85%

General procedure for borenium cation synthesis (3l-3n)

Trimethylsilyl triflate was dissolved in 2 mL of CDCl$_3$ and stirred for 5 minutes. Afterward, 2-aminoboranes were added to the solution in a J. Young NMR tube. The sealed tube was then heated at 50 °C for 6–8 hours. Upon completion of the reaction, the volatiles were removed under high vacuum, yielding greenish-yellow solids as the final product. (We are not isolated, pure products by this procedure; the findings of this procedure are mentioned)

Complex 3l

Complex **3l** was synthesized by using complex **2l** (15 mg, 0.071 mmol) and TMS-OTf (157.93 mg, 0.71 mmol)

^{11}B NMR (160 MHz, C$_6$D$_6$) δ 21.46 (borenium), 12.15 (boronium) and 6.35 (starting material). **FT-IR** (ν, cm^{-1}) 3550 (-OH), 3080 (Ar-CH), 1610 (C=N), 1245, 1150, 1024, 945 (Aliph C-C)

Complex 3n

Complex **3n** was synthesized by using complex **2n** (64 mg, 0.284 mmol) and TMS-OTf (631.54 mg, 2.84 mmol)

^{11}B NMR (160 MHz, C$_6$D$_6$) δ 22.17 (borenium), 11.71 (boronium) and 6.16 (starting material). **FT-IR** (ν, cm^{-1}) 3545 (-OH), 2980-2872 (Aliph-CH), 1618 (C=N), 1245, 1150, 1024, 945 (Aliph C-C)

General procedure for boronium cation synthesis (4l-4n)

In a flame-dried Schlenk tube, 2-aminotropone was dissolved in freshly distilled toluene under an inert atmosphere. To this solution, boron tribromide was added dropwise at room temperature. The resulting reaction mixture was stirred for 3 hours. Upon completion, all volatiles were removed under reduced pressure, and the resulting residue was washed several times with dry hexane to afford the desired white solid product.

Complex 4l

Complex **4l** was prepared by using ligand **1l** (100 mg, 0.61 mmol) and BBr$_3$ (612 μL, 0.61 mmol).

^{1}H NMR (500 MHz, CDCl$_3$) δ 8.15 (t, J = 10.4 Hz, 1H), 8.04 (m, 1H), 7.83 – 7.75 (m, 3H), 7.71 – 7.61 (m, 1H), 7.51 (d, J = 9.9 Hz, 4H), 7.19 – 7.12 (m, 1H), 4.27 (td, J = 18.6, 16.0, 9.4 Hz, 2H), 1.44 (d, J = 6.3 Hz, 4H), 1.35 (d, J = 6.3 Hz, 4H), 1.18 (d, J = 6.5 Hz, 4H). **^{11}B NMR** (160 MHz, CDCl$_3$) δ 12.46. **HRMS (ESI):** Calculated for C$_{20}$H$_{24}$BN$_2$O$_2$ 335.1930 [M], found 335.1930.

Yield: 58%

Complex 4m

Complex **4m** was prepared by using ligand **1m** (70 mg, 0.394 mmol) and BBr_3 (197 μL, 0.197 mmol).

^{11}B NMR (160 MHz, $CDCl_3$) δ 12.35. **HRMS (ESI):** Calculated for $C_{22}H_{28}BN_2O_2$ 363.2251 [M], found 363.2251.

Yield: 55%

Complex 4n

Complex **4n** was prepared by using ligand **1n** (100 mg, 0.565 mmol) and BBr_3 (370 μL, 0.37 mmol)

^{1}H NMR (500 MHz, $CDCl_3$) δ 8.18 (dd, J = 11.1, 9.3 Hz, 2H), 7.87 (d, J = 11.2 Hz, 2H), 7.77 (t, J = 10.2 Hz, 2H), 7.54-7.46 (m, 4H), 3.68 (dd, J = 13.9, 6.7 Hz, 2H), 2.93 (dd, J = 13.9, 8.4 Hz, 2H), 2.03 – 1.94 (m, 2H), 0.97 (d, J = 6.6 Hz, 6H), 0.91 (d, J = 6.6 Hz, 6H). **^{13}C NMR** (126 MHz, $CDCl_3$) δ 166.12, 160.99, 144.82, 141.12, 131.62, 121.76, 121.35, 51.50, 32.01, 28.21, 22.82, 20.88, 20.75. **^{11}B NMR** (160 MHz, $CDCl_3$) δ 12.83. **HRMS (ESI):** Calculated for $C_{22}H_{28}BN_2O_2$ 363.2251 [M], found 363.2251.

Yield: 65%

Computational details

All the calculations were carried out employing density functional theory (DFT) implemented in the Gaussian 09 (rev. E.01) program package. Geometry optimizations of all the species were carried out in the gas phase using the long-range dispersion corrected ωB97XD functional in combination with the 6-311G* basis set for all atoms. The X-ray crystallographic coordinates were used as the initial geometries, wherever available, for optimizing the ground-state geometries. Whereas, educated guess based on the experimental data, served as initial starting point where X-ray data were unavailable. The optimized geometries were confirmed as local minima on the potential energy surface by calculation of harmonic frequencies (all positive eigenvalues) at the same level of theory. Finally, the absorption spectra, were determined using TD-DFT calculations at the *aforementioned* level

based on the optimized geometries obtained. Solvent effects were addressed by using Truhlar's solvation model based on density (SMD) with acetonitrile as solvent. The combination of calculations used here found useful previously, demonstrating a good correlation with the experimental data.The gauge including atomic orbital (GIAO)method has been used to compute the [11]B chemical shifts. The NMR chemical shifts were calculated using ωB97XD and 6-311G* basis set on the optimized geometries. The ^{11}B NMR chemical shifts were calculated relative to B_2H_6 (B3LYP B shielding constant 90.43 ppm) and converted to the usual [$BF_3.OEt_2$] scale using the experimental δ ([11]B) value of B_2H_6, 16.6 ppm. *[60-66]*

Spectroscopic details of ligands and complexes
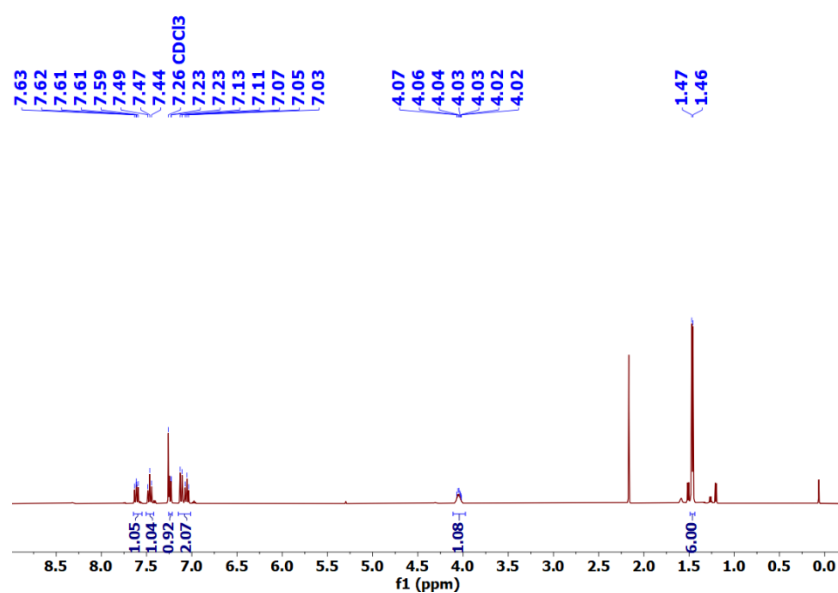
Figure 3.8 ^{1}HNMR of complex **2l**.
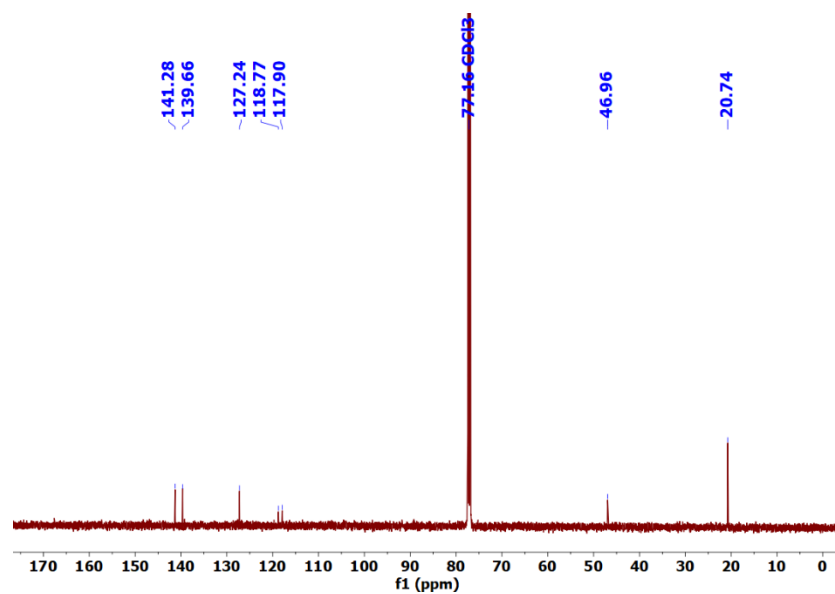
Figure 3.9 $^{13}C\{^1H\}$ NMR of complex **2l**.
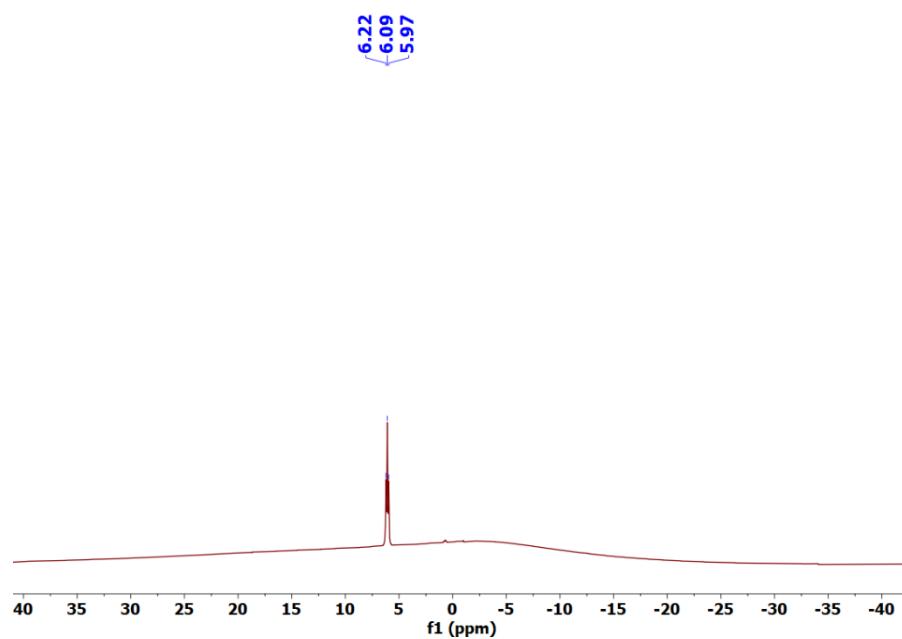
Figure 3.10 ^{11}BNMR of complex **2l**.
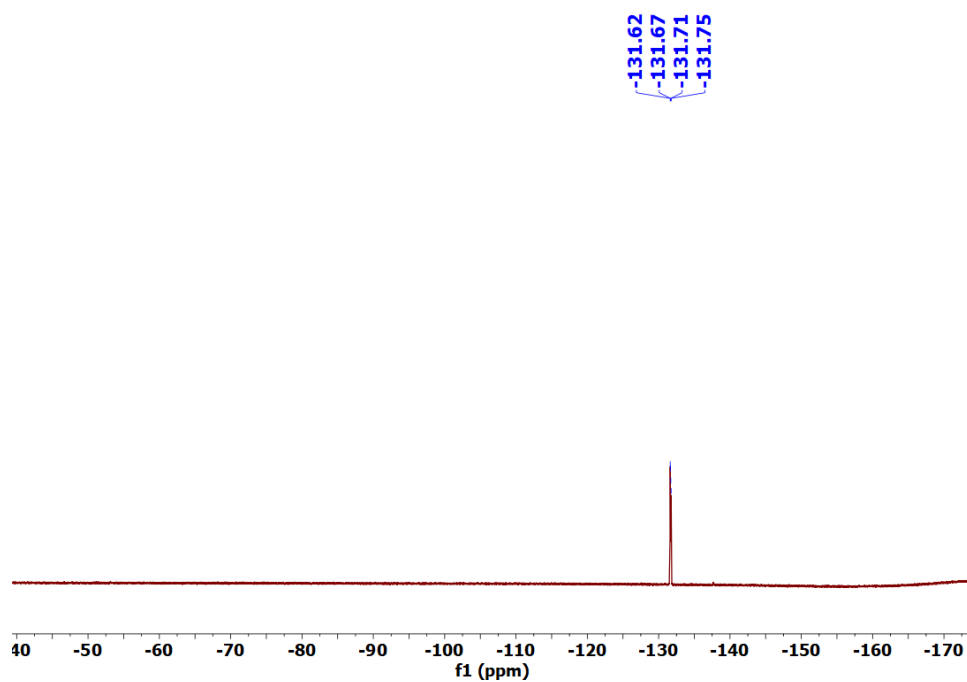
Figure 3.11 ^{19}FNMR of complex **2l**.
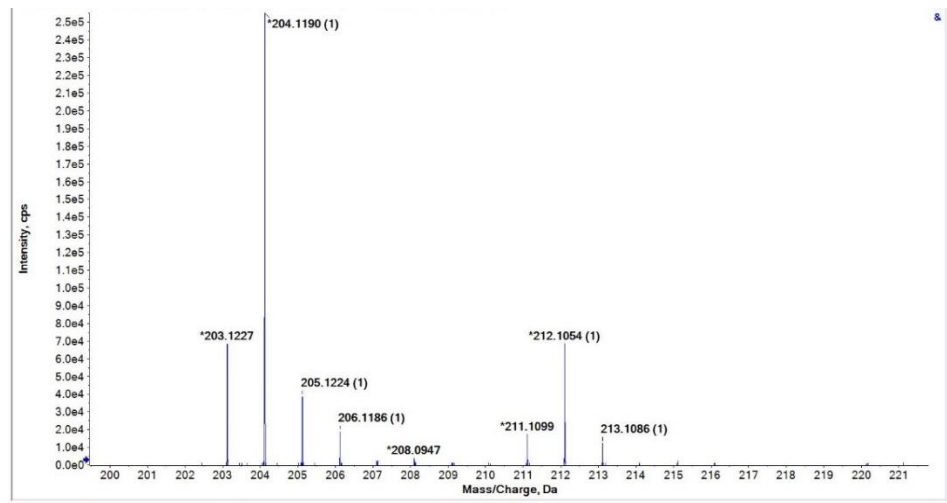
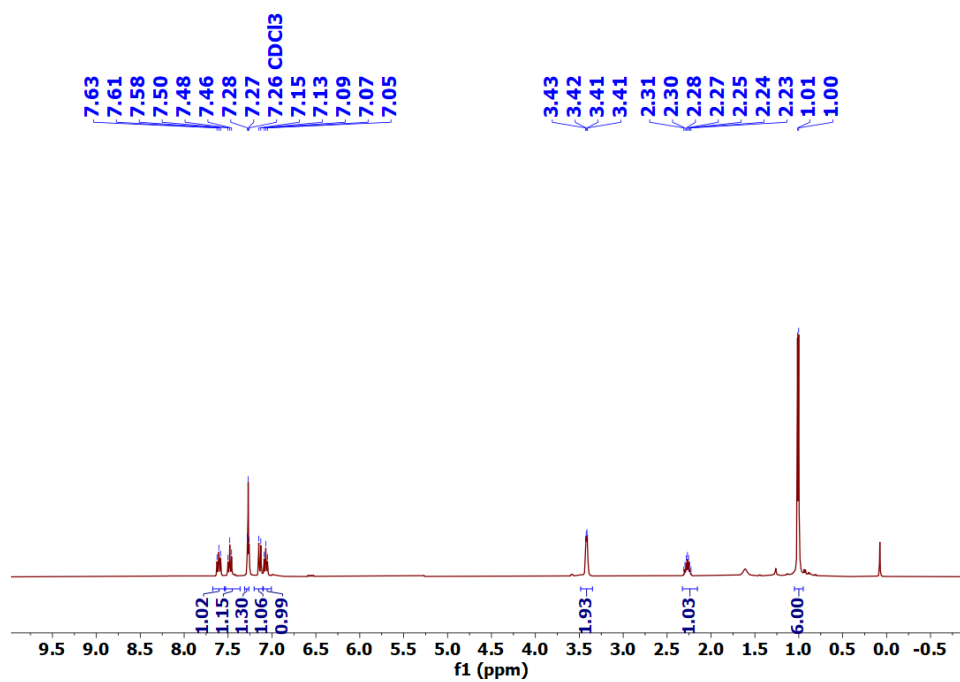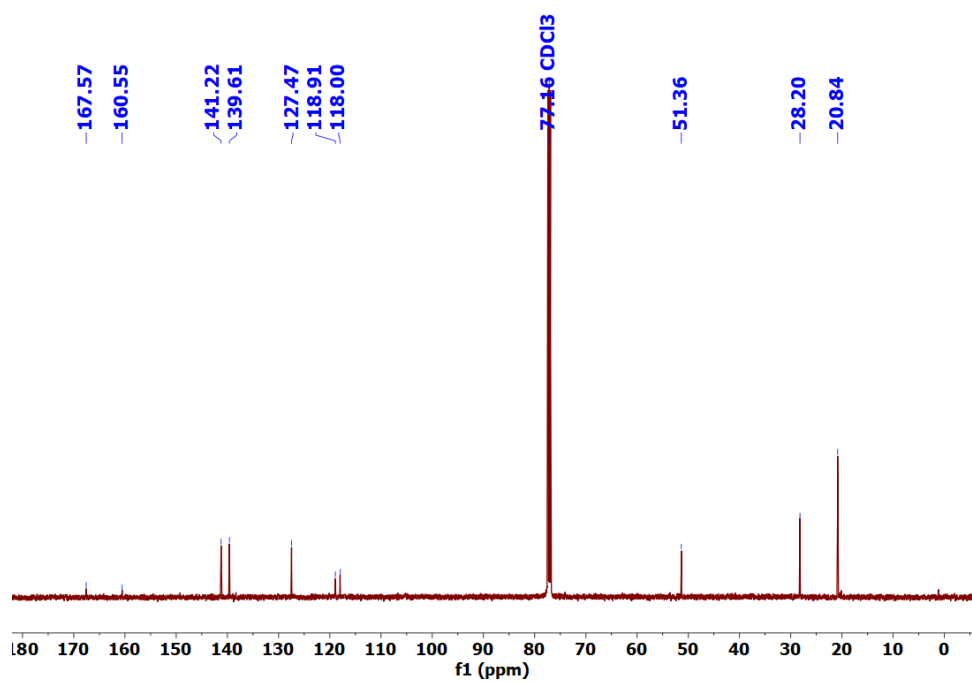**Figure 3.12** Mass spectra of complex **2l**.
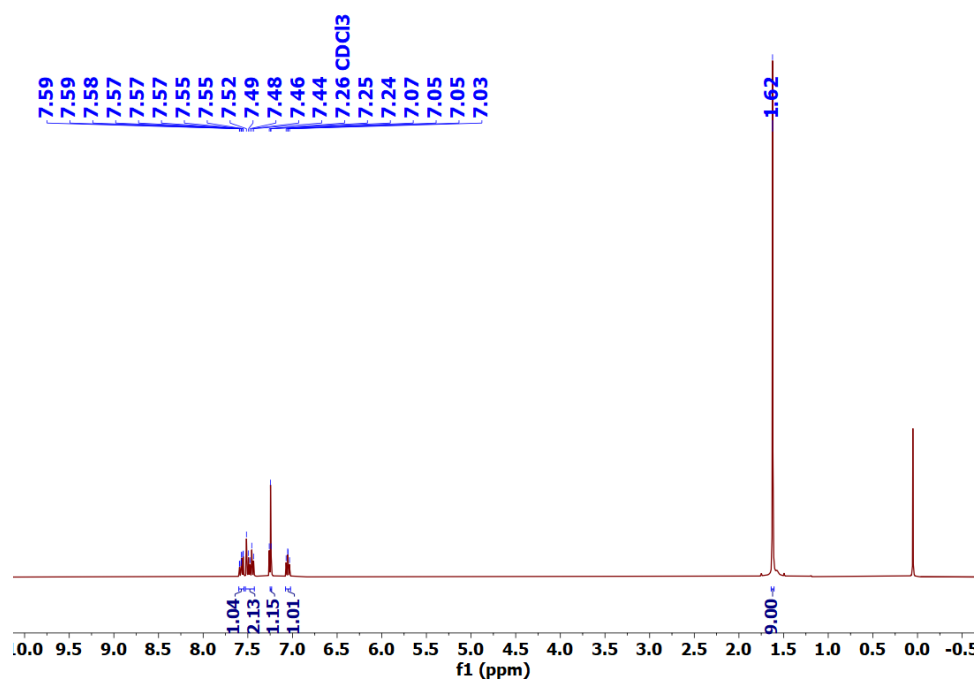
Figure 3.13 ^{1}HNMR of complex **2m**.
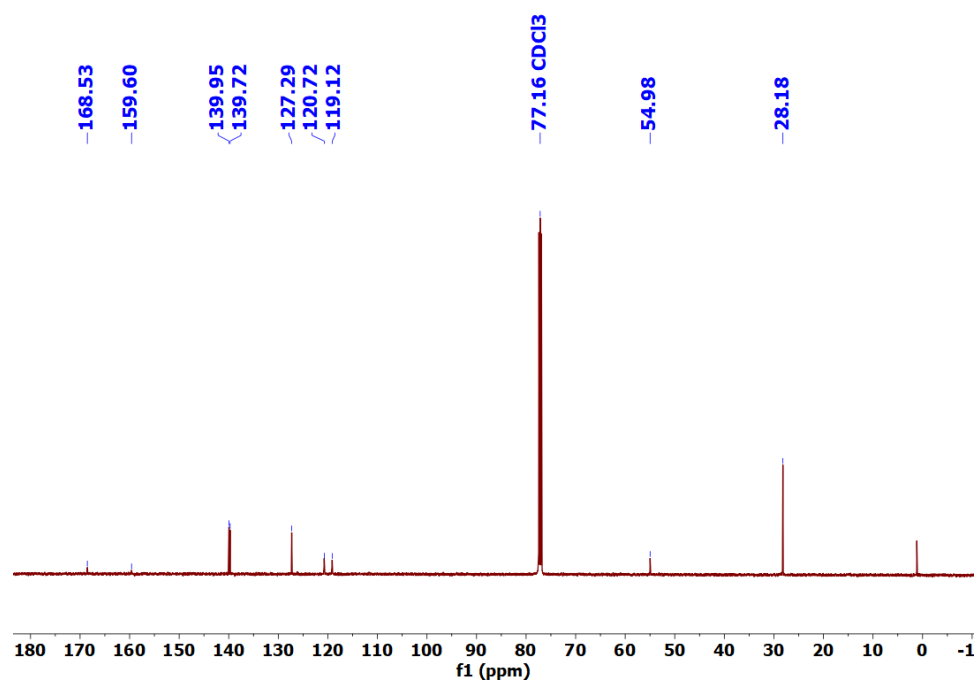
Figure 3.14 ^{13}C{^{1}H} NMR of complex **2m**.

185
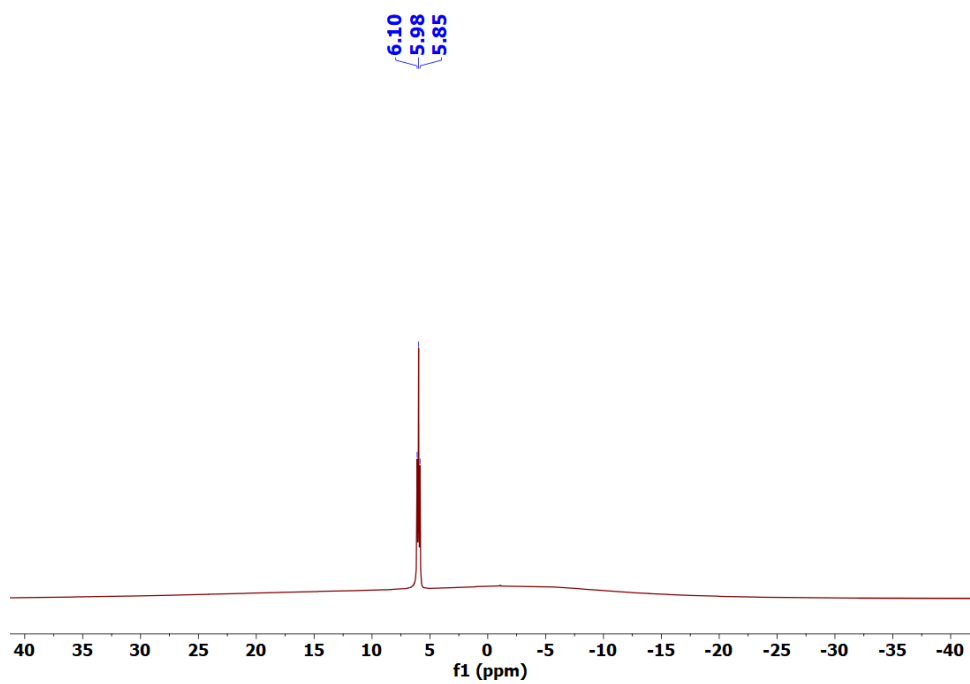
Figure 3.15 ^{11}BNMR of complex **2m**.
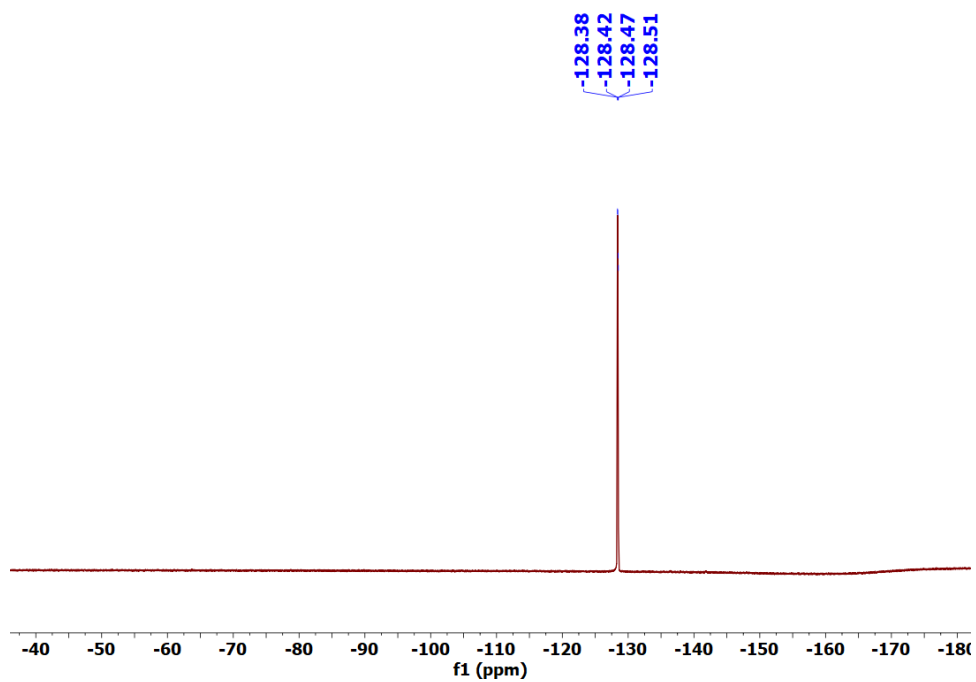
Figure 3.16 ^{19}F NMR of complex **2m**.
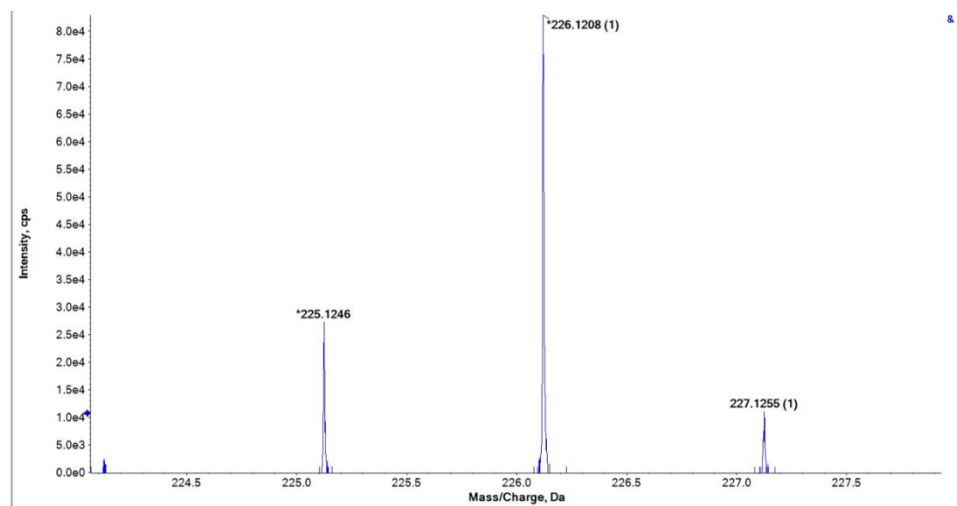
Figure 3.17 High-resolution mass spectra of complex **2m**.

Figure 3.18 ^{1}H NMR of complex **2n**.
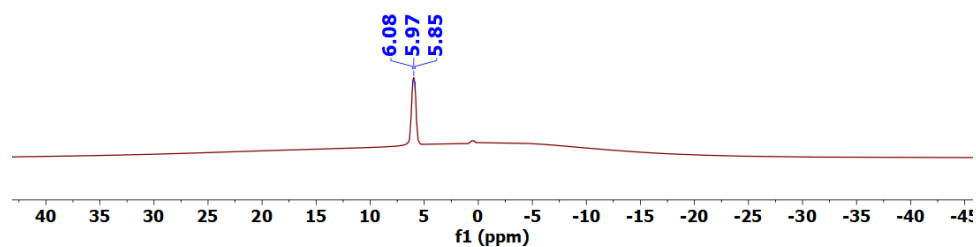
Figure 3.19 ^{13}C{^{1}H} NMR of complex **2n**.

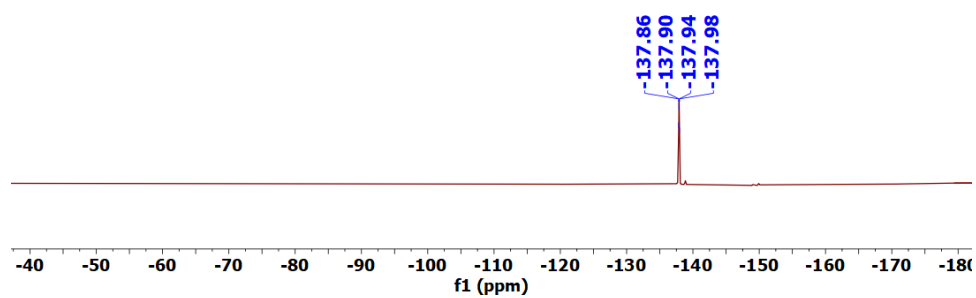**Figure 3.20** ^{11}B NMR of complex **2n**.

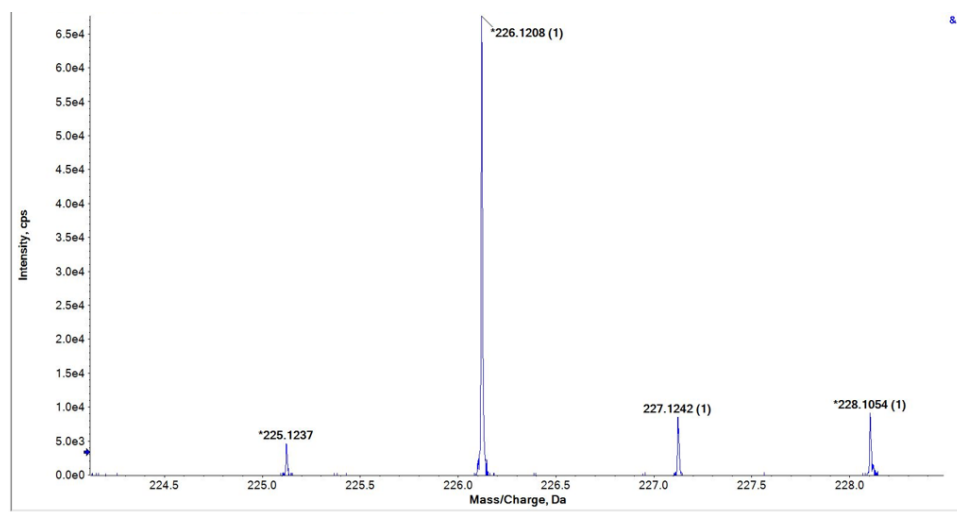**Figure 3.21** ^{19}F NMR of complex **2n**.

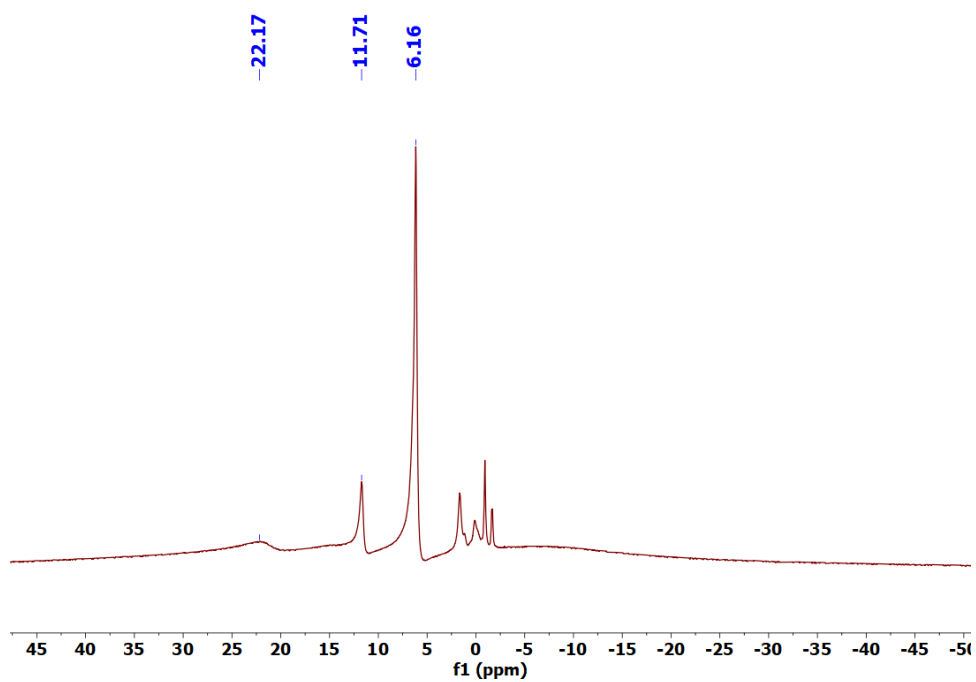**Figure 3.22** High-resolution mass spectra of complex **2n**.
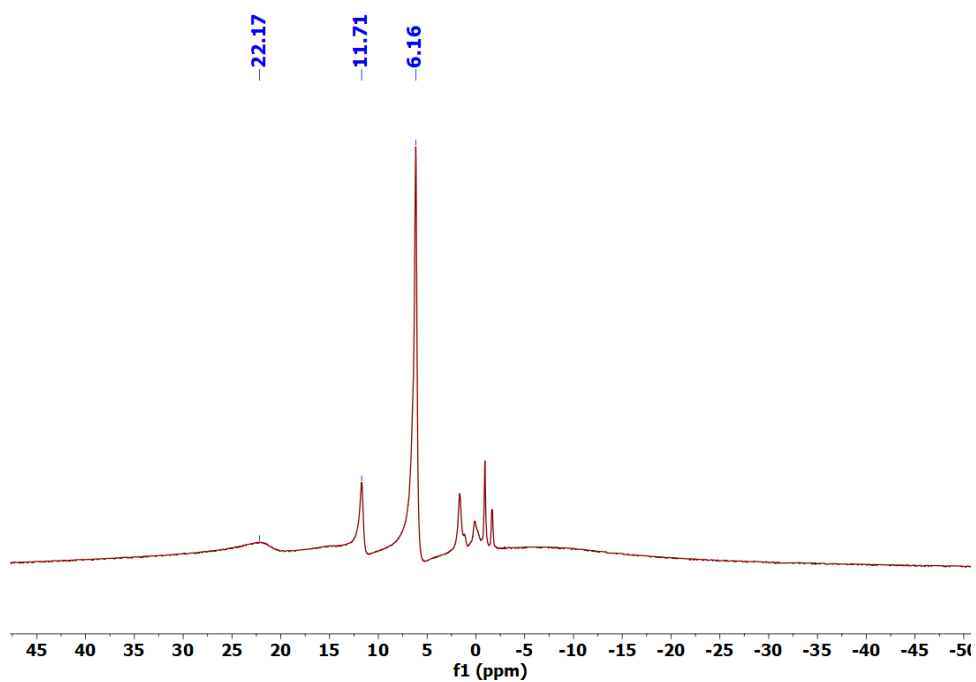
Figure 3.23 ^{11}B NMR of Complex **3l**.

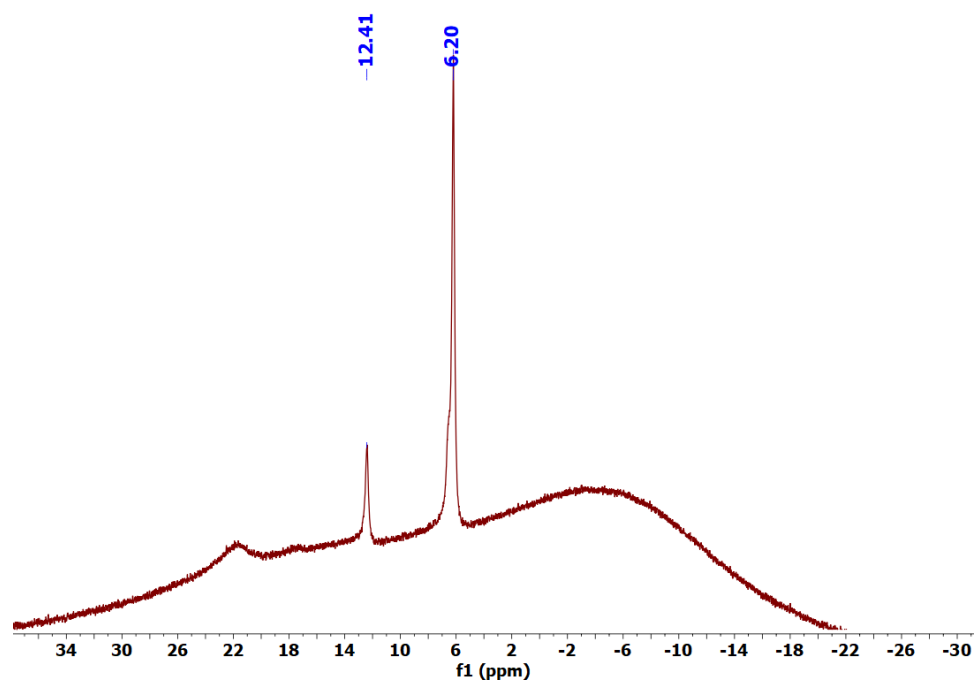**Figure 3.24** ^{11}B NMR of Complex **3m**.

Figure 3.25 ^{11}BNMR of complex **3n**.
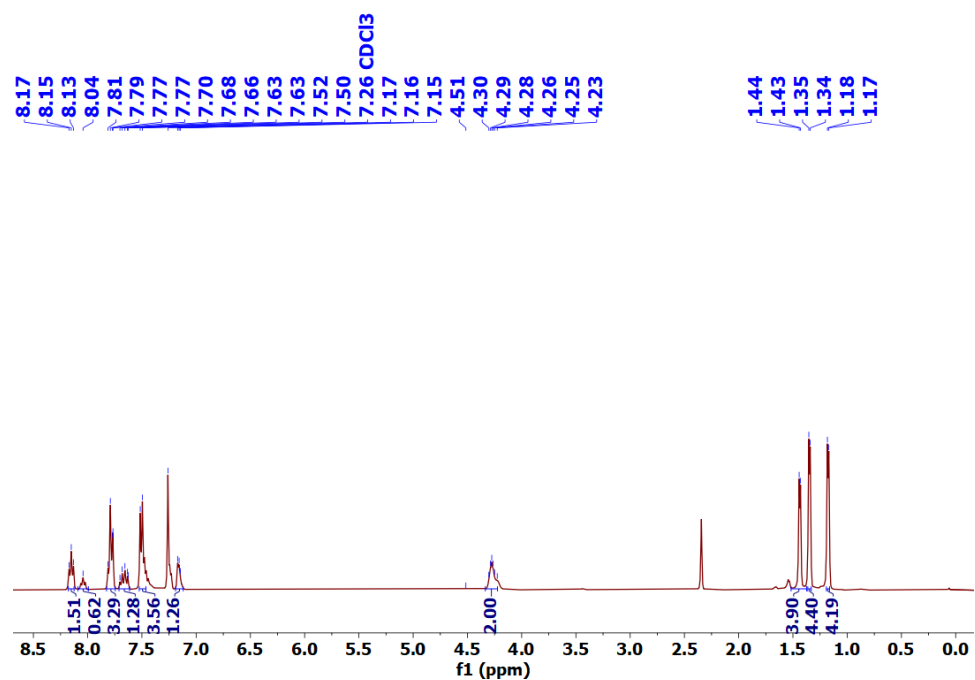
Figure 3.26 ^{1}HNMR of Complex **4l**.
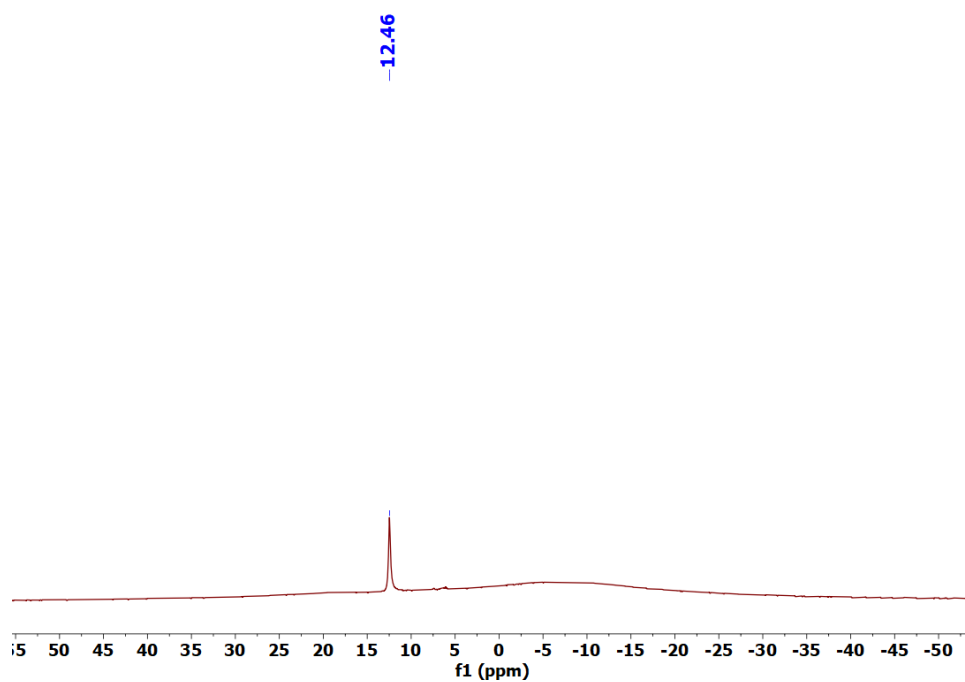
Figure 3.27 ^{11}BNMR of Complex **4l**.

m/z	Z	Abund	Diff (ppm)	Height %	Height % (Calc)	Ion Species	Formula
334.1958	1	962611	-1.10	23.13	23.52	M+	C20H24BN2O2
335.1930	1	4161603	0.42	100.00	100.00	M+	C20H24BN2O2
336.1956	1	849283	-1.10	20.41	22.18	M+	C20H24BN2O2
337.1981	1	88046	-1.93	2.12	2.78	M+	C20H24BN2O2

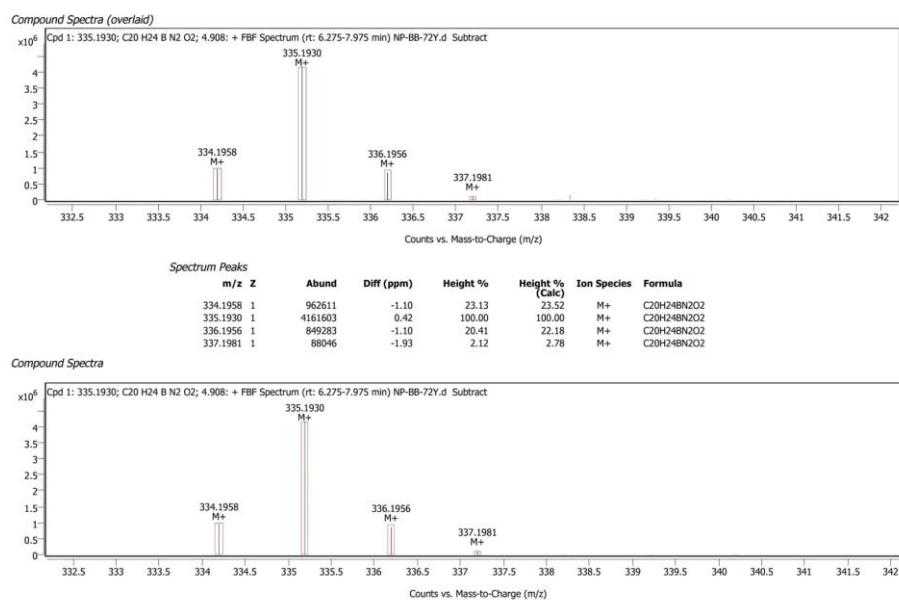**Figure 3.28** High-resolution mass spectra of complex **4l**.
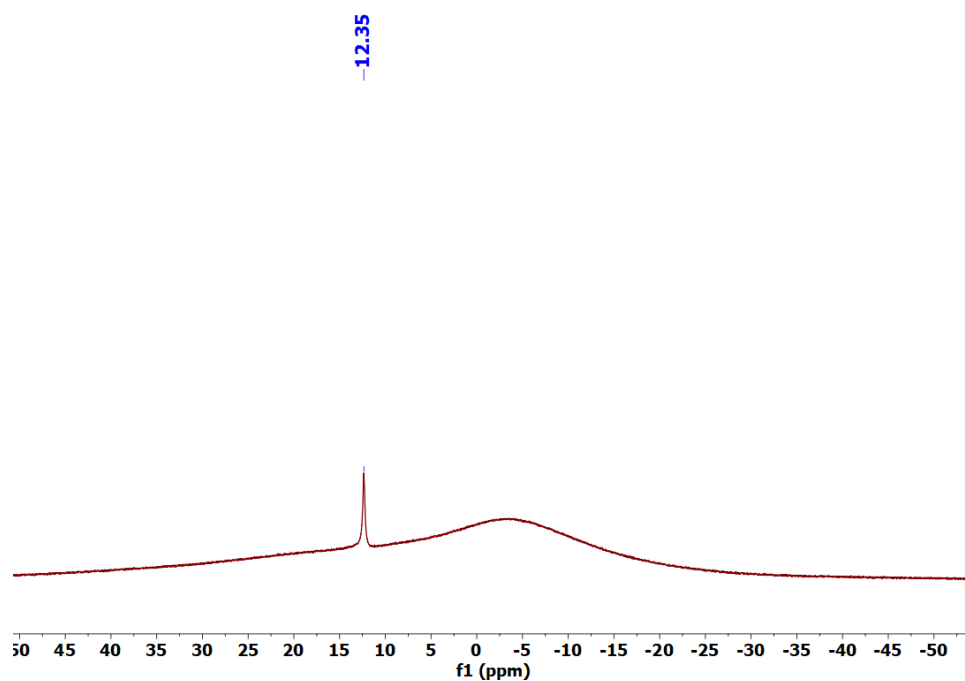
Figure 3.29 ^{11}BNMR of complex **4m**.
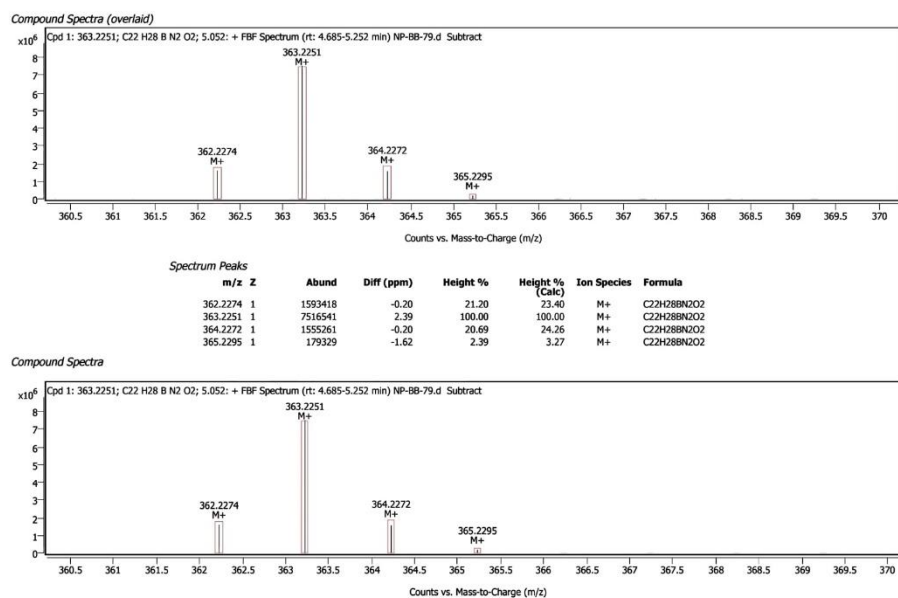
Figure 3.30 High-resolution mass spectra of complex **4m**.
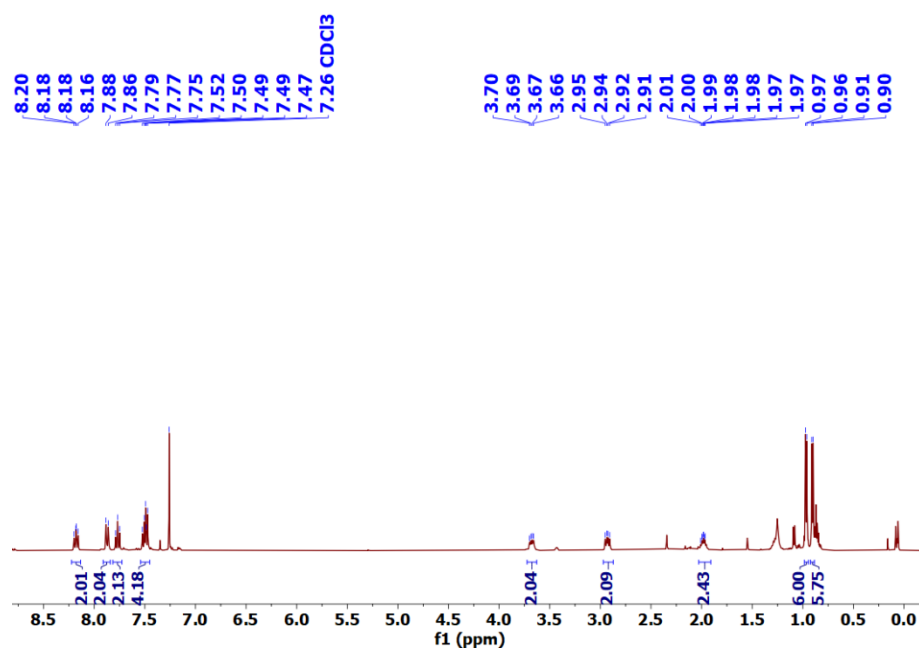
Figure 3.31 ^{1}HNMR of complex **4n**.

Figure 3.32 $^{13}C\{^1H\}$ NMR of complex **4n**.

194

Figure 3.33 ^{11}B NMR of complex **4n**.

Figure 3.34 High-resolution mass spectra of complex **4n**.

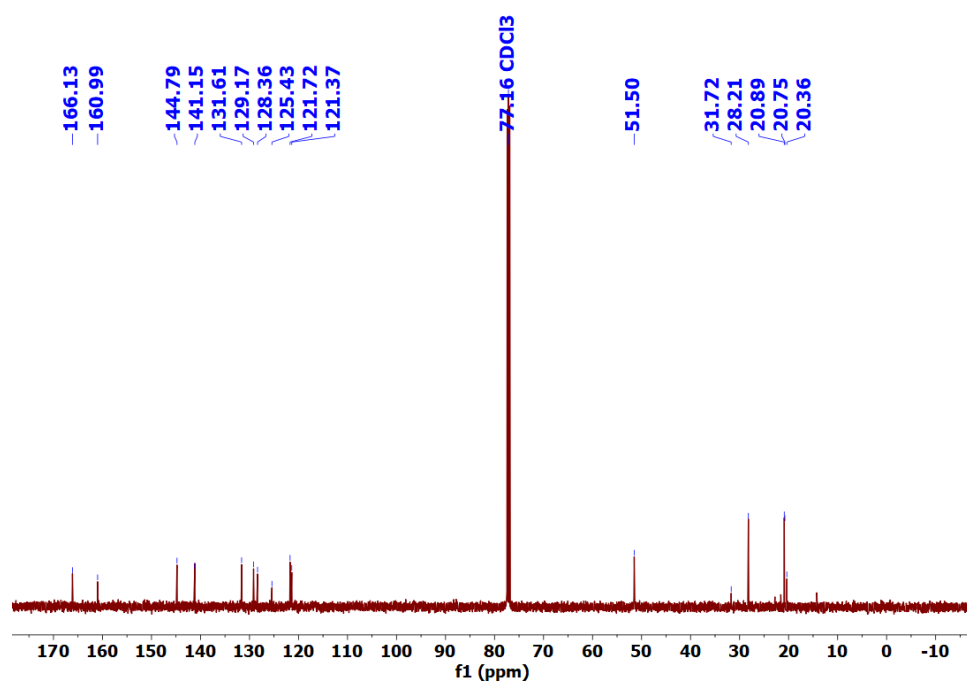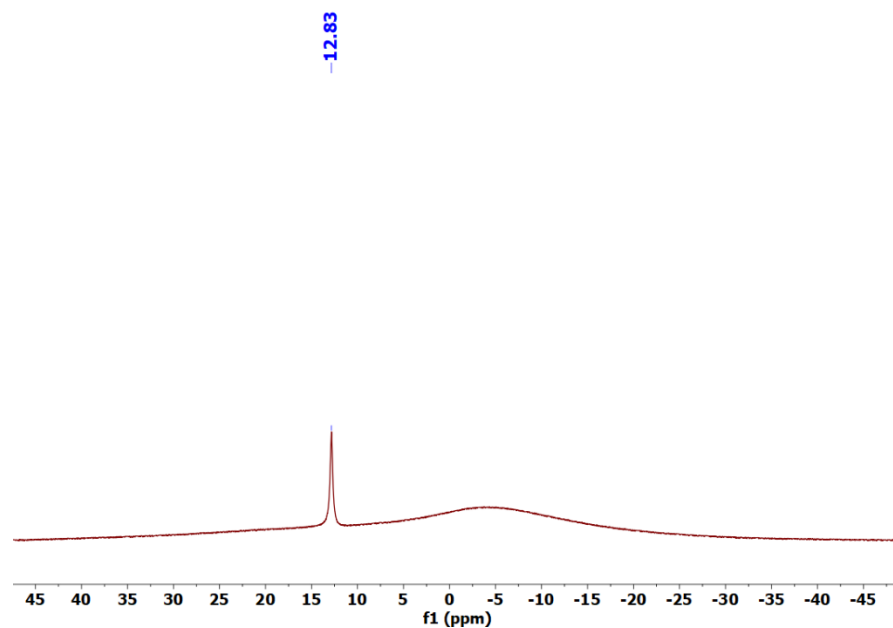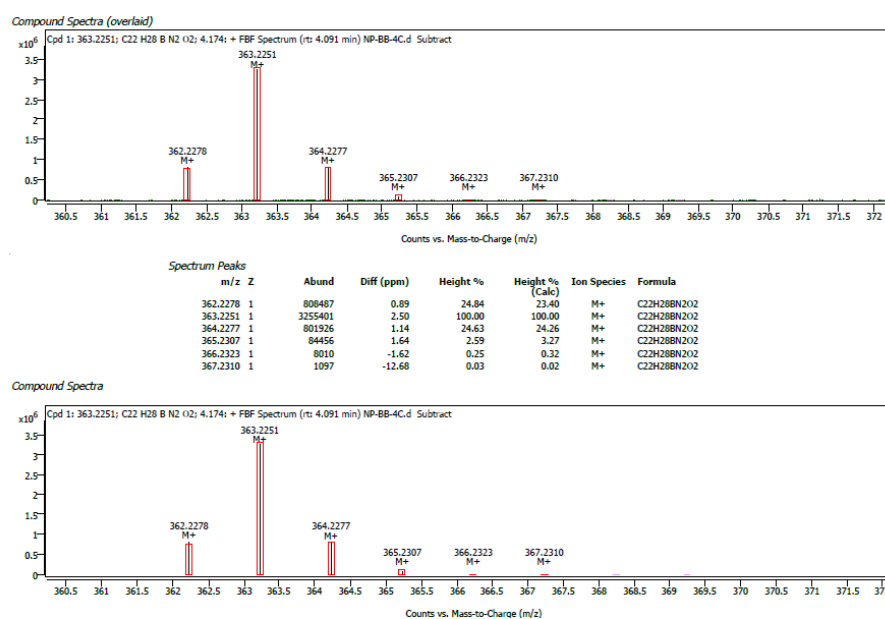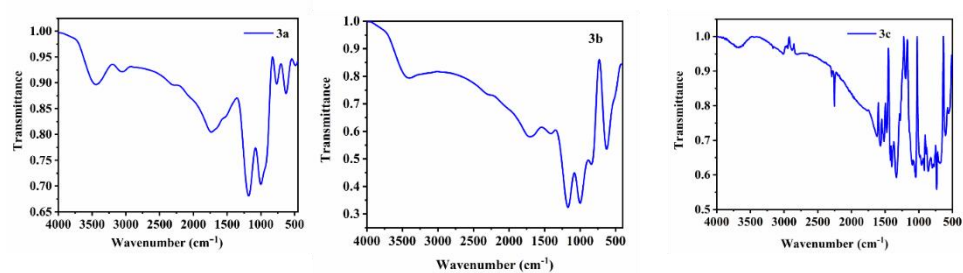**Figure 3.35** FT-IR spectra of complex **3l**, **3m** and **3n**.

195

Crystallographic Details

The crystal data were collected on a Super Nova, Dual, Cu at home/near, Eos diffractometer. The crystal was kept at 293(2) K during data collection. Using Olex2 [5], the structure was solved with the SHELXT [6] structure solution program using Intrinsic Phasing and refined with the SHELXL [7] refinement package using Least Squares minimization. The structures were solved by direct methods and refined by full-matrix least squares, based on $F2$, using SHELXL Crystal structures were refined using Olex2-1.0 software. All non-hydrogen atoms were refined anisotropically.

Table 3.7 Crystal data for Complex **2l, 2m, 2n** and **4l**

Chemical Compound	2l	2m	2n	4l
Empirical formula	$C_{10}H_{12}BF_2NO$	$C_{11}H_{14}BF_2NO$	$C_{11}H_{14}BF_2NO$	$C_{20}H_{24}BN_2O_2Br$
Formula weight (g·mol^{-1})	211.02	225.04	225.04	352.95
Temperature (K)	293 (2)	293(2)	293 (2)	293(2)
Radiation, λ (Å)	Mo-K_α, 0.71073	Mo-K_α, 0.71073	Mo-K_α, 0.7107	Mo-K_α, 0.7107
Crystal system	orthorhombic	Triclinic	Monoclinic	Triclinic
Space group	Fdd2	P-1	P2$_1$/c	P-1
Unit cell dimensions				
a (Å)	43.01(2)	7.0843(10)	10.280(4)	9.3519(6)
b (Å)	11.126(4)	9.0674(11)	9.100(3)	10.6218(9)
c (Å)	8.901(3)	9.9364(13)	12.729(3)	12.7373(7)
α (°)	90	76.236(11)	90	103.470(6)
β (°)	90	73.547(12)	96.21(3)	102.940(5)
γ (°)	90	67.870(12)	90	114.379(8)
Volume (Å^3)	4259(3)	560.82(14)	1183.8(7)	1045.00(14)
Z	16	2	4	2
Calculated density (g·m^{-3})	1.316	1.333	1.263	1.122
F(000)	1760	236.0	472.0	375.0
Reflections collected	11006	4554	8828	8534
Independent reflections	2568	2597	2812	4727

Refinement method	Full-matrix least-squares on F^2	Full-matrix least-squares on F^2	Full-matrix least-squares on F^2	Full-matrix least-squares on F^2
Goodness-of-fit on F^2	1.018	1.051	0.939	1.040
R_{int}	0.1277	0.0267	0.29	0.0660
R indices (all data)	$R_1 = 0.0981$, $wR^2 = 0.2992$	$R_1 = 0.0467$, $wR^2 = 0.1315$	$R_1 = 0.1392 wR^2 = 0.3334$	$R_1 = 0.1380$ $wR^2 = 0.1771$
CCDC Number	2447428	2447427	-	-

References:

[1] Yuan, L., Lin, W., Zheng, L. W. He., L., Huang, W. (2013) Far-red to near infrared analyte-responsive fluorescent probes based on organic fluorophore platforms for fluorescence imaging. Chem. Soc. Rev., 42, 622-661. (DOI: 10.1039/C2CS35313J)

[2] O oyama, Y., Harima, Y. (2009) Molecular Designs and Syntheses of Organic Dyes for Dye-Sensitized Solar Cells. Eur. J. Org. Chem. 290 3-293 4, (DOI:10.1002/ejoc.200990047)

[3] Li, L., Dong, X., Li, J. (2020) A short review on NIR-II organic small molecule dyes. Dyes and Pigments. 183, 108756. (DOI: 10875,10.1016/j.dyepig)

[4] Cai, Y., Si, W., Huang, W., Chen, P., Shao, J., Dong, X. (2018) Organic Dye Based Nanoparticles for Cancer Phototheranostics. Small 14(25):e1704247 (DOI: 10.1002/smll.201704247)

[5] Zhang, X. X., Yang, F., Zhao, X., Wu, Q., He, Le., Li, Z., Ren, T. X. (2024) Thermally Healable Electrolyte-Electrode Interface for

Sustainable Quasi-Solid Zinc-ion Batteries. Chem. Int. Ed. 63 e 202410666 (DOI: 10.1002/anie.202317457)

[6] Mishra, A., Bäuerle, P. (2012) Small Molecule Organic Semiconductors on the Move: Promises for Future Solar Energy Technology. 51, 9, 27, 2012 2020-2067. (DOI: 10.1002/anie.201102326)

[7] Zhao, M., Ren, F., Zhou, Y. (2024) Construction of Boron Difluoride Complexes with Asymmetric N,N'-Bidentate Ligands. Volume30, 46, 19, 2024 e202401784 (DOI: 10.1002/chem.202401784)

[8] Yadav, R. K., Parveen, D., Mondal, B., Roy, K. D. (2025) The Role of Spacers as a Probe in Variation of Photoluminescence Properties of Mono- and Bi-Nuclear Boron Compounds . Asian J. 20, e202401113. (DOI: 10.1002/asia.202401113)

[9] Parveen, D., Yadav , R. K., Mondal, B., Dallon, M., Sarazin, Y., Roy, D. K. (2024) Bis(diiminate)-based boron difluoro complexes: effective synthon for bis(borenium) cations. Dalton Trans., 53, 14139-14143. (DOI: 10.1039/D4DT02050B)

[10] Bismillah, A. N., Aprahamian, I. (2021) Fundamental studies to emerging applications of pyrrole-BF$_2$ (BOPHY) fluorophores. Chem. Soc. Rev. 50, 5631-5649. (DOI: 10.1039/d1cs00122a)

[11] Bodio, E., Goze, C. (2019) Investigation of B-F substitution on BODIPY and aza-BODIPY dyes: Development of B-O and B-C BODIPYs. Dyes and Pigments 160 700- 710 (DOI: 10.1016/j.dyepig.2018.08.062)

[12] Tikhonov, S. A., Vovna, V. I., Gelfand, N. A., Smushko, S. O., Fedorenko, E. V., (2016) Electronic Structure and Optical Properties of Boron Difluoride Dibenzoylmethane Derivatives. J. Phys. Chem. A 120 7361-7369. (DOI: 10.1021/acs.jpca.6b07242)

[13] Tolle, M. Sc. M., Fresia, M., Jones, P. G., indel, T. (2024) Fluorescent BF$_2$ Complexes Inspired by Ageladine A. ChemPhotoChem. 8 e202400065, (DOI: 10.1002/cptc.202400065)

[14] Yan, X., Zhu, P., Zhou, Z., Yang, H., Lan, H., Xiao, S. (2019) Aggregation-induced emission enhancement (AIEE)-active boron-

difluoride dyes with reversible mechanochromic fluorescence. RSC Adv
. 9 3587 2– 35877, (DOI: 10.1039/C9RA07437F)

[15] Yang, X. G., Yin, P. P., Wang, Q., Yang, S. Y., Li, Y., Gao, X.,
Song, J., Zhang, X. Y. (2024) A Review on Design Strategies for
Carbon Based Metal Oxides and Sulfides Nanocomposites for High
Performance Li and Na Ion Battery Anodes. Inorg. Chem. 63 17346-
17350. (DOI: 10.1002/aenm.201601424)

[16] Zhang, J., wang, N., Ji, X., Tao, Y., Wang, J., Zhoa, W. (2020)
BODIPY-Based Fluorescent Probes for Biothiols. Chem . Eur. J. 26
4172-4192, (DOI: 10.1002/chem.201904470)

[17] Hou, J. T., W u, M. Y., Li, K., Yang , J., Yu, K. K., Xie, Y. M.,
Yu, X. Q. (2014) Mitochondria-targeted colorimetric and fluorescent
probes for hypochlorite and their applications for in vivo imaging. Chem
.commun. 50 8640-8643, (DOI: 10.1039/c4cc02673j)

[18] Chevalier, A., Mercier, C., Saurel, L., Orenga, S., Renard, P. Y.,
Romieu, A. (2013) The first latent green fluorophores for the detection
of azoreductase activity in bacterial cultures. Chem. Commun., 49,
8815-8817. (DOI: 10.1039/C3CC44798G)

[19] Das, S., Dey, S., Patra, S., Bera, A., Ghosh, T., Prasad , B.,
Sayala, K. D., Maji, K., Bedi, A., Debnath, S. (2023) BODIPY-Based
Molecules for Biomedical Applications. Biomolecules 13 (12) 1723,
(DOI: 10.339 0/biom13121723)

[20] Ilhan, H., Şeker, M., Gülseren, G., Bakırc ı, Melike. E., Boyacı,
A. I., Cakmak, Y.   (2025) Nitric Oxide Activatable Photodynamic
Therapy Agents Based on BODIPY–Copper Complexes. ACS
Pharmacol. Transl . Sci.   8 (3)   679-689,   (DOI:
10.1021/acsptsci.4c00428)

[21] Mukherjee, N., Podder, S., Mitra, K., Majumdar, S., Nandi, D.,
Chakravarty, A. R. (2018) Targeted photodynamic therapy in visible
light by BODIPY-appended copper(II) complexes of vitamin B6 Schiff
base. Dalton Trans. 47 823-835 (DOI: 10.1039/C7DT03976J)

[22] Agostinis, P., Berg, K., Cengel, K. A., Foster, T. H., Girotti, A. W.,
Gollnick, S. O., Hahn, S. M., Hamblin, M. R., Juzeniene, A., Kessel,

D., Korbelik, M., Moan, J., Mroz, P., Nowis, D., Piette, J., Wilson, B. C., Golab, J. (2011) Photodynamic therapy of cancer: an update. J. C lin. 61 250-281, (DOI: 10.3322/caac.20114)

[23] Zubair,I., Khera, R. A., Naveed ,A., Iqbal, J. (2022) Designing the optoelectronic properties of BODIPY and their photovoltaic applications for high performance of organic solar cells by using computational approach. Materials Science in Semiconductor Processing 148 106812 (DOI: 10.1016/j.mssp.2022.106812)

[24] Coughlin, J. E., Henson, Z. B., Welch, G. C., Bazan, G. C. (2014) Design and Synthesis of Molecular Donors for Solution-Processed High-Efficiency Organic Solar Cells. Acc. Chem. Res. 47 257– 270. (DOI: 10.1021/ar400136b)

[25] Martinez, N. C. F., Lin, K. H., Kremer, K., Andrienko, D. (2022) Virtual Screening for Organic Solar Cells and Light Emitting Diodes. Adv. Sci. 9 2200825, (DOI: 10.1002/ad vs.202200825)

[26] Kordt, P., Holst, J. J. M. V., Helwi, M. A., Kowalsky, W., May, F., Badinski, A., Lennartz, C., Andrienko, D. (2015) Modeling of Organic Light Emitting Diodes: From Molecular to Device Properties. Adv. Funct. Mater. 25 1955-1971 (DOI: 10.1002/adfm.201403004)

[27] May, F., Helwi, M. A., Baumeier, B., Kowalsky, W., Fuchs, E., Lennartz, C., Andrienko, D. (2012) Design Rules for Charge-Transport Effic ient Host Materials for Phosphorescent Organic Light-Emitting Diodes, J. Am. Chem. Soc. 134 13818-13822. (DOI: 10.1021/ja305310r)

[28] Bai, G., Yu, C., Cheng, C., Hao, E., Wei, Y., Mu, X., Jiao, L. (2014) Syntheses and photophysical properties of BF_2 complexes of curcumin analogues. Org. Biomol. Chem. 12 1618-1626, (DOI: 10.1039/C3OB42201A)

[29] Yu, C., Jiao, L., Zhang , P., Feng, Z., Cheng, C., Wei, Y., Mu, X., Hao, E. (2014) Highly fluorescent BF2 complexes of hydrazine-Schiff base linked bispyrrole. Org. Lett. 1 6 113048–3051 (DOI: 10.1021/ol501162f)

[30] Zhao, M., Yuan, Z., Zhou, Y. (2024) 1-Azaazulene: A Ligand Moiety for Boron Difluoride (BF_2) Complexes To Achieve Long-

Wavelength Absorption. Org. Lett. 26 8837-8841. (DOI: 10.1021/acs.orglett.4c03270)

[31] Moshkina, T. N., Nosova, E. V., Lipunova, G. N., Valova, M. S., Taniya, O. S., Slepukhin, P. A., Charushin, V. N. (2015) Synthesis and luminescent prop erties of BF_2 complexes with N,O-b enzazine ligands, J. Fluor. Chem. 221 17-24, (DOI: 10.1016/j.jfluc hem.2015.04.010)

[32] Poddar, M., Misra, R. (2020) Recent advances of BODIPY based derivatives for optoelectronic applications. Chem. Rev . 421 213462, (DOI: 10.1016/j.ccr.2020.213462)

[33] Ohtani, S., Gon, M., Tanaka, K., Chujo, Y. (2020) The Desig n Strategy for an Ag greg ationand Crystallization-Ind uced Emission-Ac tive Molecule Based on the Introduc tion of Skeletal Distortion by Boron C omplexation with a Tridentate Ligand, Crystals, 10 615, (DOI: 10.33 90/cryst10070615)

[34] Cheng, H. B., Cao, X., Zhang, S., Zhang, K., Cheng, Y., Wang, J., Zhao, J., Zhou, L., Liang, X. J., Yoon, J. (2023) BODIPY as a Multifunctional Theranostic Reagent in Biomedicine: Self-Assembly, Properties, and Applications. Ad v. Mater. 35 2207546 , (DOI: 10.1002 /adma.202207546)

[35] Zheng, J., Huang, F., Li, Y., Xu, T., Xu, H., Jia, J., Ye, Q., Gao, J. (2015) The aggregation-induced emission enhancement properties of BF_2 complex isatin-phenylhydrazone: Synthesis and fluorescence characteristics. Dyes and Pigments, 113 502-509, (DOI: 10.1016/j.dyepig.2014.09.025)

[36] Yamaguchi, M., Ito, S., Hirose, A., Tanaka, K., Chujo, Y. (2017) Control of aggregation-induced emission versus fluorescence aggregation-caused quenching by bond existence at a single site in boron pyridinoiminate complexes. Mater. Chem. Front. 1, 1573-1579. (DOI: 10 .1039/C7QM00076F)

[37] Chen, C. H., Zheng, W. H. (2021) Planar chiral boron difluoride complexes showing circularly polarized luminescence. Org. Chem. Front 8, 6622-6627. (DOI: 10.1039/D1QO01202A)

[38] Killian, L., Lutz, M., Thevenon, A. (2024) A π-extended β-diketiminate ligand via a templated Scholl approach. Chem. Commun., 60, 6663-6666 (DOI: 10.1039/D4CC01627K)

[39] Li, X., Son, A. (2014) Efficient luminescence from easily prepared fluorine–boron core complexes based on benzothiazole and benzoxazole. Dyes and Pigments 107:182–187 (DOI: 10.1016/j.dyepig.2014.04.001)

[40] Vidovic, D., Reeske, G., Find later, M., Cowley, A. H. (2008) Synthesis and structures of boron dihalides supported by the C6F5-substituted β-diketiminate ligand [HC(CMe)2(NC6F5)2]⁻ Dalton Trans., 2008, 2293-2297 (DOI: 10.1039/B719722E)

[41] Maar, R. R., Hoffman, N. A., Staroverov, V. N., Gilroy, J. B. (2019) Oxoborane Formation Turns on Formazanate-Based Photoluminescence. 22;25(47):11015-11019. (DOI: 10.1002/chem.201902419)

[42] Mondol, R., Otten, E. (2018) Reactivity of Two-Electron-Reduced Boron Formazanate Compounds with Electrophiles: Facile N–H/N–C Bond Homolysis Due to the Formation of Stable Ligand Radicals. Inorg. Chem. 2018, 57, 16, 9720–9727. (DOI: 10.1021/acs.inorgchem.8b00079)

[43] Balachandra, C., Sharma, N. K. (2017) Novel fluorophores: Syntheses and photophysic al studies of boron-aminotrop onimines. Dyes and Pigment. . 137, 532-538 (DOI: 10.1016/j.dyepig.2016.10.051)

[44] Suresh, D., Gomes, C. S. B., Gomes, P. T., Paolo, R. E. D., Maçanita, A. L., Calhord a, M. J., Charas, A., Morgado, J., Duarte, M. T. (2012) Synthesis and properties of 2'-O,4'-C-ethyleneoxy bridged 5-methyluridine. (14):3702-5. (DOI: 10.1021/ol401566r)

[45] Suresh, D., Gomes, C. S. B., Lopes, P. S., Figueira, C. A., Ferreira, B., Gomes, P. T., Paolo, R. E. D., Maçanita, A. L., Duarte, M. T., Charas, A., Morgado, J., Viçosa, D. V., Calhorda, M. J. (2015) Luminescent Di- and Trinuc lear Boron Comp lexes Based on Aromatic Iminopyrrolyl Sp acer Lig ands: Synthesis, Charac terization, and Ap

plication in O LEDs. Chem. Eur. J 21, 9133-9149 (DOI: 10.1002/chem.201500109)

[46] Ikeshita, M., Itayama, H., Tanaka, K., Suzuki, D., Ono, J., Mai, J., Tsuno, T. (2025) Boron-Containing Chiral Spiro Molecules: Synthesis and Color-Tunable Circularly Polarized Luminescence. (26):9141-9146. (DOI: 10.1021/acs.joc.5c00971)

[47] Meyer, N., Löhnwitz, K., Zulys, A., Roesky, P. W., Dochnahl, M., Blechert, S. (2006) The reference provided appears to be a citation for a scientific article. Organometallics 25:3730–3734 (DOI: 10.1021/om060369i)

[48] Aléo, D., Felouat, A., Heresanu, V., Ranguis, A., Chaudanson, D., Karapetyan, A., Giorgi, M., Fages, F. (2014) Two-photon excited fluorescence of BF2 complexes of curcumin analogues: toward NIR-to-NIR fluorescent organic nanoparticles. J. Mater. Chem. C,2, 5208-5215. (DOI: 10.1039/C4TC00543K)

[49] Yadav , R. K., Parveen, D., Jangra P., Mondal, B., Roy, D. K. (2025) Synthesis, Characterization, and Reactivity of Aminotroponiminate-Based Difluoroboranes: A Pathway toward Bore(boro)nium Cations. Inorg. Chem (22):1078010791. (DOI:10.1021/acs.inorgchem.5c00451)

[50] Cade, A., Ingleson, M. J. (2014) syn-1,2-carboboration of alkynes with borenium cations. Chem. Eur. J. (40):12874-80. (DOI: 10.1002/chem.201403614)

[51] Chen, J., Lalancette, R. A., Jäkle, F. (2013) Synthesis and Lewis acid properties of a ferrocene-based planar-chiral borenium cation. Chem. Commun. 49, 4893-4895. (DOI: 10.1039/C3CC41556B)

[52] Devillard, M., Brousses, R., Miqueu K., Bouhadir, G., Bourissou, D. (2015) A Stable but Highly Reactive Phosphine-Coordinated Borenium: Metal-free Dihydrogen Activation and Alkyne 1,2-Carboboration. Angew. Chem. Int. Ed . 54, 5722– 5726 , (DOI: 10.1002/anie.201500959)

[53] Biani, F. F. D., Gmeinwieser, T., Herd tweck, E., JTkle, F., Laschi, F., Wag ner, M., Zanello, P. (1997) Multistep Redox Processes and Intramolecular Charge Transfer in Ferrocene-Based 2,2'-

Bipyridylboronium Salts. Organometallics 1997, 16, 22, 4776–4787. (DOI: 10.1021/om970345z)

[54] Curiel, D., Montoya, Usea, L., Espinosa, A., Orenes, R.A., Molina, P. (2012) Indolocarbazole-Based Ligands for Ladder-Type Four-Coordinate Boron Complexes. Org. Lett. 14, 13, 3360–336 (DOI: 10.1021/ol301339y)

[55] Zhang, X., Xiao, Y., Qi, J., Qu, J., Kim, B., Y ue, X., Belfield, K. D. (2013) Long-wavelength, photostable, two-photon excitable BODIPY fluorophores readily modifiable for molecular probes. J. Org. Chem. (18):9153-60. (DOI: 10.1021/jo401379g)

[56] Ośmiałowski, B., Zakrzewska, A., Jędrzejewska B., Grabarz, A., Zaleśny, A., Bartkowiak, E. (2015) Kolehmainen, Influence of Sub stituent and Benzoannulation on Photop hysical Properties of 1 - Benzoylmethyleneisoquinoline Difluorob orates. J. Org. Chem., 80 2072 -2080 (DOI: 10.1021/jo502244j)

[57] Chi, X., Itkis, M. E., Patrick, B. O., Barclay, T. M., Reed, R. W., Oakley, R. T., Cord es, A. W., Haddon, R. C. (1999) A phenalenyl-based neutral stable π-conjugated polyradical. Synthetic Metals 159(17):1772-1777. (DOI: 10.102 1/ja992040)

[58] Li, X., Song, Q. (2024) "Homoleptic" Tetracoordinate Boron Compounds. Inorg. Chem., 25, 5295-5314. (DOI: 10.1021/acs.inorgchem.4c00102)

[59] Dolomanov, O. V., Bourhis, L. J., Gildea, R. J., Howard, J. A. K., Mann, P. H. (2009) OLEX2: a complete structure solution, refinement and analysis program. J. Appl. Cryst. 42, 339. (DIO: 10.1107/S0021889808042726

[60] Sheldrick, G. M. (2015) Crystal structure refinement with SHELXL. Acta Cryst. A71, 3. (DIO: 10.1107/S2053229614024218)

[61] Chai, J. D., Head-Gordon, M. (2008) . Long-Range Corrected Hybrid Density Functionals with Damped Atom-Atom Dispersion Corrections. Phys. Chem. Chem. Phys., 10, 6615-6620. (DOI:)

[62] Marenich, A. V., Cramer, C. J., Truhlar, D. G. (2009) Universal Solvation Model Based on Solute Electron Density and on a Continuum Model of the Solvent Defined by the Bulk Dielectric Constant and

Atomic Surface Tensions. J. Phys. Chem., 113, 6378-6396. (DOI: 10.1021/jp810292n)

[63] Onak, T. P., Landesman, H. L., Williams, R. E., Shapiro, I. (1959) The B11 Nuclear Magnetic Resonance Chemical Shifts and Spin Coupling Values for Various Compounds. J. Phys. Chem., 63, 1533-1535. (DOI: 10.1021/j150579a601)

[64] Frisch, M. J., Trucks, G. W., Schlegel, Scuseria, G. E., Robb, M. A., Cheeseman, J. R., Scalmani, G., Barone, V., Mennucci, B., Petersson, G. A., Nakatsuji, A., Caricato, M., Li, X., Hratchian, H. P., Izmaylov, A. F., Bloino, J., Zheng, G., Sonnenberg, J. L., Hada, M., Ehara, M., Toyota, K., Fukuda, F., Hasegawa, J., Ishida, M., Nakajima, T., Honda, Y., Kitao, O., Nakai, H., Vreven, T., Montgomery, J. A., Peralta, J. R., Ogliaro, F., Bearpark, M., Heyd, J. J., Brothers, E., Kudin, K. N., Staroverov, V. N., Keith, T., Kobayashi, R., Normand, J., Raghavachari, K., Rendell, A., Burant, J. C., Iyengar, J. C., Tomasi, J., Cossi, M., Rega, N., Millam, J. M., Klene, M., Knox, J. E., Cross, J. B., Bakken, V., Adamo, C., Jaramillo, J., Gomperts, R., Stratmann, R. E., Yazyev, O., Austin, A. J., Cammi, R., Pomelli, C., Ochterski, J. W., Martin, R. L., Morokuma, K., Zakrzewski, V. G., Voth, G. A., Salvador, P., Dannenberg, J. J., Dapprich, S., Daniels, A. D., Farkas, O., Foresman, J. B., Ortiz, J. V., Cioslowski, J., Fox, D. J. (2013) Gaussian 09, Revision E.01. Gaussian, Inc., Wallingford CT.

[65] Landon, F. (1937) Théorie quantique des courants interatomiques dans les combinaisons aromatiques. J. Phys. Radium., 8, 397-409. (DOI: 10.1051/jphysrad:0193) [66] McWeeny, R. (1962) Perturbation Theory for the Fock-Dirac Density Matrix. Phys. Rev., 126, 1028. (DOI: 10.1103/PhysRev.126.1028)

[67] Mohammed, A. H. A., Benniston, A. C., Copley, G., Harriman, A., Howgego, D. (2011) Intramolecular Excimer Formation for Covalently Linked Boron Dipyrromethene Dyes. J. Phys. Chem. A, 115, 12111-12119. (DOI: 10.1021/jp2070419)

[68] Ikeshita, M., Ichinose, M., Ono, J., Suzuki, D., Imai, Y., Tsuno, T. (2025) Boron-Containing Chiral Spiro Molecules: Synthesis and Color-

Tunable Circularly Polarized Luminescence. J. Org. Chem. 90, 9141-9146. (DOI: 10.1021/acs.joc.5c00971)

Chapter 4

Synthesis, Characterization, and Reactivity of ATIs-Based Difluoroboranes: A Pathway Towards Bore(boro)nium Cation
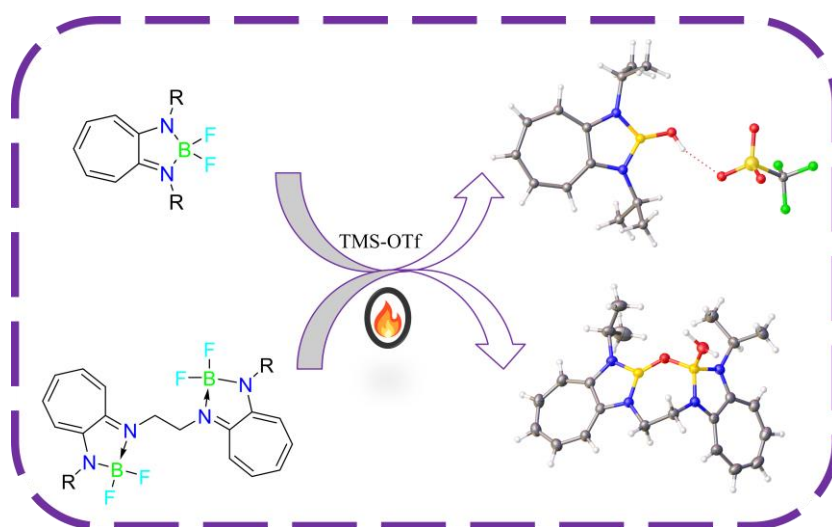
4.1 Introduction

Due to the presence of one vacant p-orbital in neutral three-coordinated boranes, to exhibit Lewis acidity, boranes play a crucial role in non-metallic catalytic processes. Boron, positioned at the top of Group 13 in the periodic table, occupies a unique position as a boundary element between metals and non-metals. This makes boron a versatile conditante in widespread applications in domains such as materials science, organic synthesis, optoelectronics, and medicinal chemistry. *[1-6]* Boron cations are highly reactive, exhibit higher Lewis acidity than their neutral borane counterparts. The presence of a formal positive charge on the boron center significantly enhances its electron deficiency, thereby increasing its electrophilicity. This heightened electrophilic character is directly correlated with the magnitude of the positive charge. Due to this, boron cations are more reactive than their neutral tri- or tetracoordinate boron counterparts. The evolution and stabilization of highly reactive boron cations have advanced notably, driven by the tailored ligands and counterions that dictate their stability and reactivity. *[7-10]* The pioneering work of the cationic boron complexes was done by Nöth and co-workers, who introduced their nomenclature based on the coordination number of the boron center. Four, three, and two-coordinated boron cations are termed boronium, borenium, and borinium, respectively.*[11-14]* Reactivity of borenium cation lies in between the more reactive di-coordinated and electronically saturated tetra-coordinated boron cations. Due to their unique stability and reactivity, borenium cations are used in various organic transformations, small molecule activations, and catalysis.*[15-18]* Many research groups investigated that borenium ions possess novel properties as a reagent that enhance electrophilic aromatic borylations, hydroboration of alkynes, and catalytic reductions of heteroaromatic compounds and different functional groups. *[19-35]*
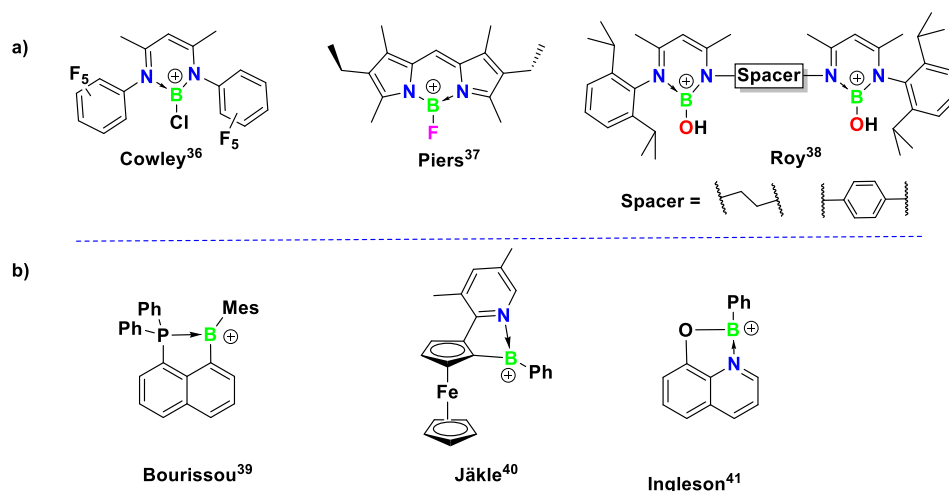
Figure 4.1 a) Previously reported six memberd borenium cations, b) five-membered borenium cations

Borenium cations in a six-membered framework resulted mostly in different ligand moieties like BODIPY, BDI, and formazanate. In 2008, Cowley and coworkers reported the six-membered borenium cations synthesized in a β-diketiminate scaffold,[36] and in the same year, Piers and co-workers also reported the BODIPY-based borenium cation, which was stabilized by intra-ligand N-donors.[37] Recently, our group reported the synthesis and isolation of bis(diiminate) scaffold-supported bis(borenium) cations.[38] Unlike the six-membered borenium cations, the five-membered rings containing a positively charged boron atom are very limited.[39] A few examples of five-membered borenium cations having ligands with O, N, and P atoms as donor moieties are listed in Figure 1. Jäkle and coworkers reported the five-membered borenium cation in the ferrocene derivative scaffold.[40] Bourissou and his group synthesized phosphorus-stabilized borenium cation on a naphthalene platform.[41] In 2014, Ingleson reported the quinolato borenium salts, a five-membered borenium cation stabilized by the NO donor ligand, prepared from quinolato boron-chlorides, reacting with aluminium trichloride.[42]

Aminotroponiminates (ATIs) have garnered broad interest as easily accessible ligands that readily form complexes with (semi-)metals across large sections of the periodic table. Due to their different

properties, such as (i) monoanionic, (ii) N, N-bidentate, (iii) redox-innocent under reducing conditions, (iv) chemically inert at their C7 backbone, (v) spectator ligands, they are becoming important for main group compounds. Aminotroponiminates can coordinate metals/semi-metals in two possible ways; one is through the nitrogen centers and another is via the C_7 backbone. Such multifaceted binding modes have enabled the formation of stable complexes across a wide range of main-group and transition-metal centers. The chemistry of ATIs ligands with heavier elements of group 13 elements, such as Al, Ga, and In, has been extensively explored, with both neutral and cationic complexes stabilized by the ATI ligands. ATI ligands were first introduced by Dias in main group chemistry and isolated the five-membered chelate complex with aluminum. Using these neutral aluminum complexes Jordan group synthesized a series of mono and binuclear aluminum cations. Notably, all aluminum complexes *[43-46]* were potent Lewis acids and underwent feasible β-H transfer to unsaturated substrates. This type of reaction is very crucial for polymerisation reactions. In 2002, the same research group synthesized the indium cations stabilized in ATIs' pockets. By coordinating metals/semi-metals through the nitrogen centers, ATIs may provide an opportunity to synthesize boron cations in a five-membered ring framework and offer insights into the stability and reactivities of borenium cations of different ring sizes.

In this work, we first synthesized a series of symmetrical and unsymmetrical mono- and bis-ATI ligands. Further ligands were treated with $BF_3 \cdot OEt_2$, which facilitates the highly fluorescent ATI-based boron complexes under the mild reaction conditions, which allowed us to achieve the borenium cations in a five-membered C_2N_2B core. Further, upon treatment with TMSOTF, the bis(ATI)-based boron difluoride yielded a rare bore(boro)nium cation in a unified molecular framework. All the complexes were characterized via multinuclear NMR spectroscopy, mass spectrometry, and single-crystal diffraction analysis in concert with DFT calculations.

4.2 Results and Discussion

4.2.1 Synthesis and characterization of ATIs boranes

a)

1o = R^1, R^2 = ^{i}Pr, **1p** = R^1, R^2 = ^{t}Bu
1q = R^1, R^2 = ^{i}Bu, **1r** = R^1 = ^{i}Pr, R^2 = ^{t}Bu

b)

1s   **2s**
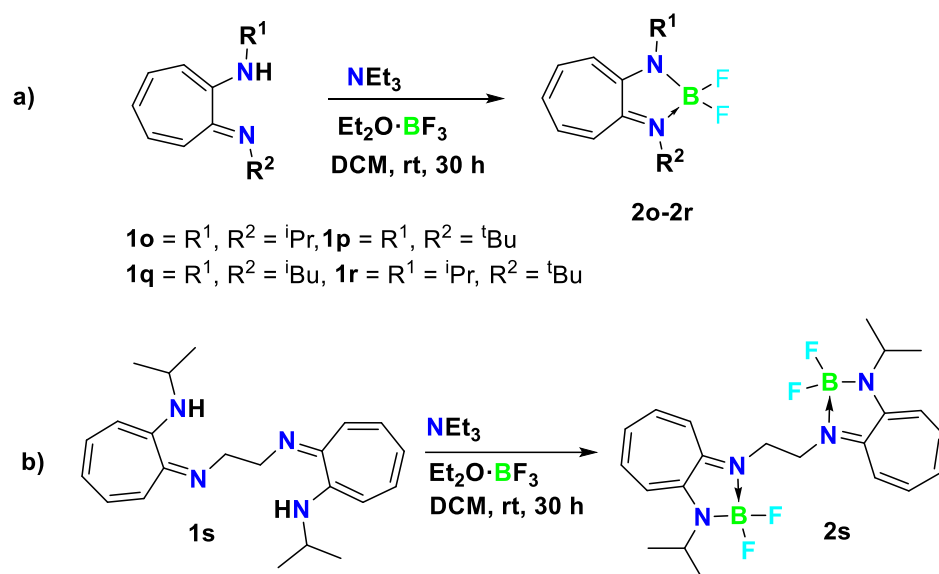
Scheme 4.1 Synthetic route of mono-binuclear ATIs boranes

In search of preparing boron cations in a five-membered ring, we were interested in synthesizing aminotroponiminates (ATIs) based-boranes as it provides boron to be in a C_2N_2B framework. Following the previous protocol, *[47,48]* as shown in Scheme 1, we synthesized several symmetrical and unsymmetrical ATI ligands (**1o-1r**) and characterized them by ^1H and $^{13}C\{^1H\}$ NMR and mass spectrometry. Along with the mono-ATIs, to achieve a compound with two borenium cations, we prepared an ethylene-bridged bis-ATI ligand **1s** in good yield. ATIs scaffold-based boranes **2o-2s** were synthesized by treatment of ATI ligands with a large excess of triethylamine and BF$_3$·OEt$_2$ in dry DCM **Scheme 4.1**. After stirring the reaction mixture overnight at room temperature, the product was extracted in DCM and purified by column chromatography in a mixture of hexane and ethyl acetate to isolate light yellow compounds. All the complexes are soluble in a range of organic solvents. Complexes **2o-2r** were characterized in solution by ^1H, $^{13}C\{^1H\}$, ^{11}B, ^{19}F NMR spectroscopy and mass spectrometry, and in the solid state, their molecular arrangements were ascertained via single-crystal X-ray diffraction analysis. A broad signal at 7.3 ppm to 7.5 ppm

in ^{1}H NMR for the ligands was absent in complexes **2o-2r,** confirming the complex formation. In ^{1}H NMR, **2o** showed a doublet at 1.46 ppm for the isopropyl methine proton, which is slightly downfield in comparison to **1o** (value), and in complex **2p**, a singlet at 1.61 ppm was observed for the tert-butyl group. The ^{11}B NMR of these complexes appeared between 5.3 to 5.9 ppm, which, to some extent, is downfield shifted from that of BDI-based six-membered BF_2 species (~1-3 ppm).*[49]* This might be partly due to the delocalization of nitrogen lone pair into the tropolone ring, which in turn reduces the electron density around the boron center or a reduced N-B-N bond angle of the sp^3 hybridized B center in ATI-BF_2 (~98°) compared to BDI-BF_2 (~110°) indicating less *s* and more *p* orbital contribution thereby making the B center in ATI-BF_2 comparatively more deshielded. The ^{19}F NMR of **2o-2r** showed signals between 125 ppm to 135 ppm, which is marginally different from the BDI-based six-membered BF_2 species.

4.2.2 Single crystal structure analysis of ATIs boranes (2o-2s)

Crystals of these complexes were grown from saturated pentane solutions at -20 °C. The solid-state structures, established by using single-crystal X-ray diffraction (SC-XRD) analysis, are shown in Figure 2. The crystals belong to the monoclinic crystal system and the boron atom is encompassed by four other atoms fitting in a distorted tetrahedron geometry. In complexes **2o**, **3p**, and **3r** the N1–B1–N2 bond angles were found to be 98° to 99°. The F1-B1-F2 bond angles around the BF_2 units in complexes **2o, 2p,** and **2r** are 108.4°, 108.5°, 110°.0 and 109.4 °, respectively, resembling BODIPY-based BF_2 complexes. The B1-N1 and B1-N2 bond lengths in all ATI-boron complexes are similar with a very marginal change according to the substituents, suggestive of the delocalization of 10π electrons through the ring. Selected bond lengths and bond angles are given in **Table 4.1**. The SC-XRD analysis of **2s** crystal unveils that it belongs to a monoclinic crystal system with a C2/c space group. As shown in **Figure 4.2**, both the ring planes of the dimeric ATI-BF_2 species are parallel to one another and the interplanar

distance is 1.962 Å. The bond distances and angles are quite similar to the monomeric species **2o-2r**. All efforts to grow good quality crystals of **2q** to perform SC-XRD analysis were unsuccessful; however, the SC-XRD study on these crystals of **2q** confirmed its connectivity **Figure 4.54**, and the identity and purity of the compound were confirmed by the spectroscopic data.
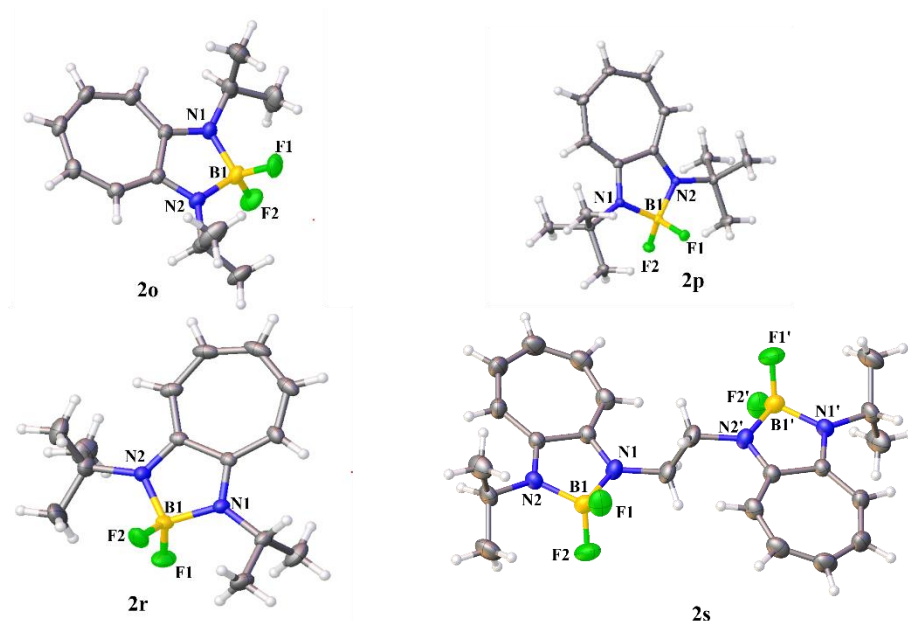

Figure 4.2 Crystal structure of the complex **2o, 2p, 2r,** and **2s**

Table 4.1 Selected bond angles (Å) and bond lengths (°) of complexes **2o**, **2p**, **2r**, and **2s**

Parameters	2o	2p	2r	2s
B1-N1	1.5413(19)	1.5489(13)	1.529(3)	1.541(2)
B1-N2	1.5413(19)	1.5477(14)	1.538(3)	1.533(2)
B1-F1	1.3929(19)	1.4104(12)	1.389(3)	1.392(2)
B1-F2	1.3877(19)	1.3908(12)	1.393(3)	1.390(2)
F1-B1-F2	108.46(12)	108.57(8)	109.4(2)	108.29(14)
N1-B1-N2	98.37(10)	99.67(8)	99.28(16)	98.26(12)

4.2.3 Crystal packing of ATIs boranes

The non-covalent interactions like C–H···F, C–F···π, B–F···F and C–H···π monitor the crystal structure packing in the unit cell. In **2o**, two types of intermolecular interactions were observed. One interaction is between methylene C-H and fluorine atom of the BF_2 unit; while the

π⋯π interaction is between the two parallel seven-membered rings, and the distance between the rings is (3.345 Å) (Figure 3; top). The non-coordinating interactions (π–π) in BODIPY derivatives were reported by Churchill and coworkers *[47],* and the distance between two parallel BODIPY units was observed as 3.69 Å. In complex **2p,** two types of contacts viz C–F⋯π (3.139 Å) and C–H⋯F (2.656 Å), are present, making this complex packed in a linear fashion **Figure 4.4**.
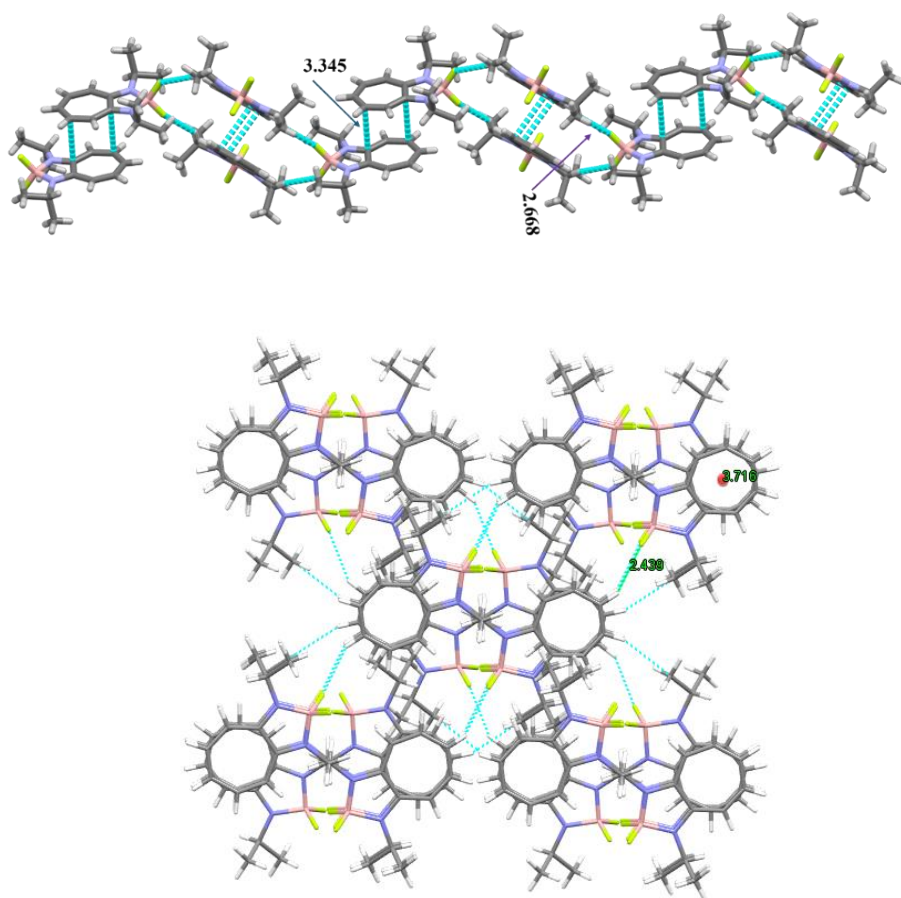
Figure 4.3 Crystal packing of complex **2o** and **2s**

In complex **2r** head to tail crystal packing is observed, where two C–H⋯F interactions are seen between the fluorine of BF_2 and the ATI hydrogen(s). The crystal packing of **2s** revealed C–H⋯F and π-π stacking interactions resulting in a layered-type structure. The π-π stacking interactions between the intermolecular tropylium units in **2s** is 3.716 Å. These complexes possess similar kinds of non-covalent

interactions like C–H⋯F, C–F⋯π, B–F⋯F, and C–H⋯π or π-π stacking interactions resulting in analogous photophysical properties.
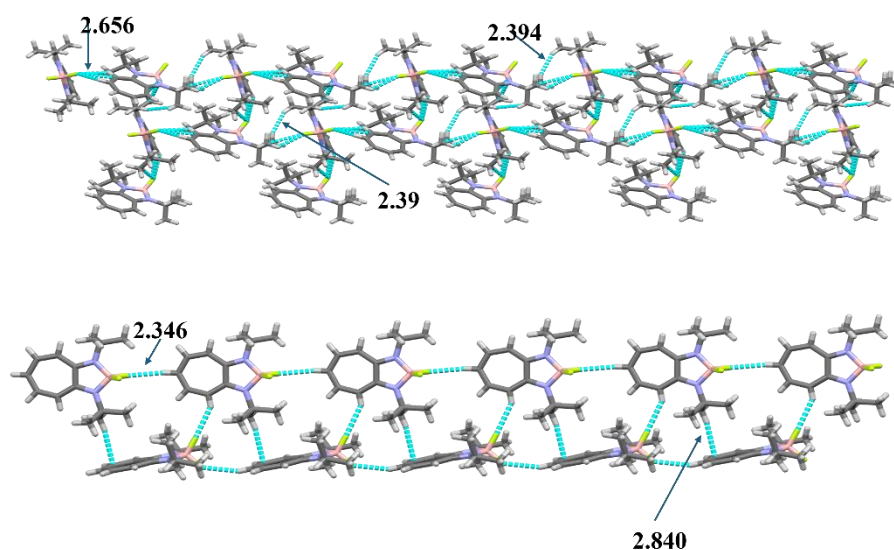
Figure 4.4 Crystal packing of complex **2p** top and **2r** bottom

4.2.4 Photophysical properties of ATIs boranes

All the synthesized ligands (**1o–1s**) were non-emissive, whereas after complexation with the BF_2 unit, the fluorescence efficiency of the resulting complexes (**2o-2s**) increased significantly. This might be due to the incorporation of the BF_2 unit into the ligand skeleton, which makes the system rigid, allowing the delocalization of the 10π electrons in the ring and might reduce the loss of energy via vibrational motions and increase the emission proficiency. Besides, the luminescence of ATIs borane complexes might be the result of electron delocalization over the entire molecule, favouring charge transfer transitions from ligand moieties to boron atom. As depicted in **Figure 4.5** and **Table 4.2**, we recorded the absorption and emission spectra of ATI-BF_2 complexes **2o-2s** in DCM. These complexes show three absorptions. The first absorption was observed around 270 nm, and the second and third absorptions are at 355 and 460 nm, respectively. In case of **2q,** the second and third absorptions are approximately 10 and 15 nm red-shifted compared to other complexes. The fluorescence lifetime depends on the various factors, like extended π bonds, polarity of the solvents, molecular interactions, excited state intramolecular proton transfer

(ESIPT), thermally activated delayed fluorescence (TADF) and substituents attached to the fluorophore. The fluorescence decay time of the ATI-BF$_2$ complexes **2o-2s** was recorded in DCM with a time-correlated single photon counting (TCSPC) spectrometer, which is found to be 1.7 ns to 2.8 ns **Table 4.2** and the lifetime of complex **2q** is comparatively higher than that of other complexes. This might be due to the presence of less bulky groups on the nitrogen atoms.*[48]*
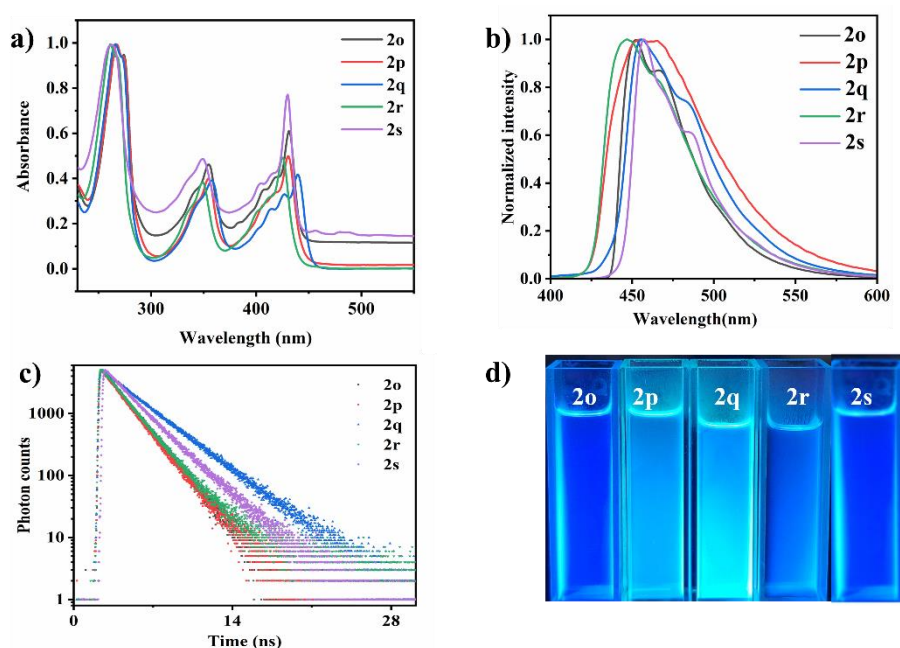

Figure 4.5 Photophysical study of complexes (**2o-2s**) in DCM. (a) Absorption (b) emission spectra in DCM (1 X 10^{-4} M) (c) decay plot of complexes in DCM (d) photograph under UV light.

Table 4.2 Photophysical outcomes of ATIs boranes (**2o-2s**)

Complex	Absorption(λ_{abs})	Emission(λ_{emi})	Stokes Shift(nm/cm^{-1})	τF (ns)
2o	431, 355, 267	468, 452	37/1834	1.76
2p	430, 354, 273	464, 453	34/1704	1.70
2q	445, 363, 271	484, 455	39/1810	2.80
2r	430, 356, 267	466, 447	36/1796	1.83
2s	434, 353, 264	487, 457	53/2507	2.28

4.3 Boron Cations: Synthesis and Characterization
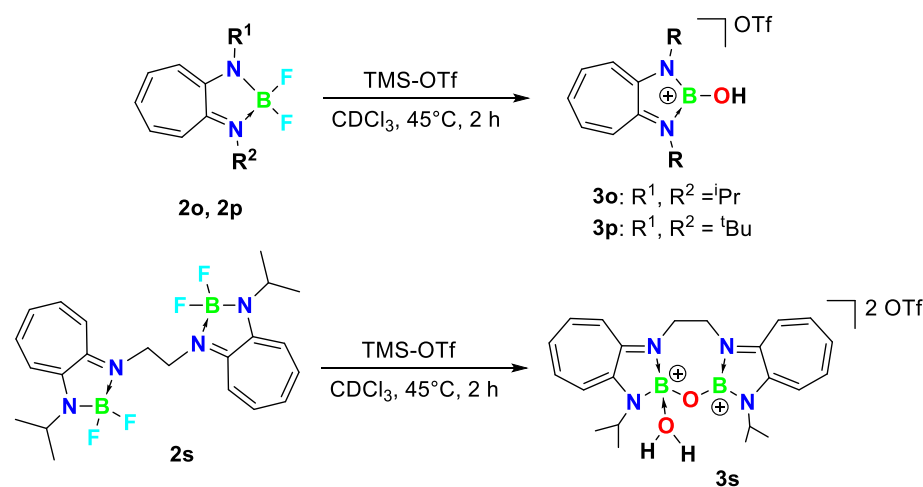
Scheme 4.2 Synthesis of borenium cations **(3o-3p)** and **(3s)**

With the ATI-BF$_2$ complexes in our hand, we went on to synthesize ATIs-based borenium cations, and considering the recent success of using trimethylsilyl triflate [TMS-OTf] as a fluoride abstracting reagent *[36]* we treated the ATI-BF$_2$ complex **2o** with TMSOTf at 45 °C for two hours (Scheme 2). That resulted in a new broad ^{11}B NMR signal at 24.6 ppm. This chemical shift hinted at the formation of a three-coordinate boron center. Similar to our observed chemical shift, the ^{11}B NMR of BDI-based borenium cations $[(C_{36}H_{54}N_4B_2O_2)]^{2+}$ and $[(C_{40}H_{54}N_4B_2O_2)]^{2+}$, appeared at 23 ppm and 21 ppm, *[38]* is suggestive of N, N-coordinated borenium cation formation. Solvents were evaporated under vacuum, and residues were washed with dry pentane, resulting in an off-white solid **3o**. As shown in Table 3, the ^{11}B NMR chemical shift values of the five-membered borenium cations are generally higher compared to the six-membered borenium cations. This might be attributed to the ring strain and subsequent hybridization of the B-center. With a more strained ring in five-membered borenium cations, the B-center possesses a lower amount of s-character compared to the six-membered borenium cation, which might lead to a downfield ^{11}B NMR chemical shift in the five-membered borenium cation.

4.3.1 Single-crystal structure analysis of boron cations

Single crystals of **3o** obtained at -20°C from CDCl₃ were analyzed via single-crystal X-ray diffraction. The solid-state structure depicted in **Figure 4.6** revealed that the hydroxyl group is attached to boron, and the geometry around the boron atom is trigonal planar.
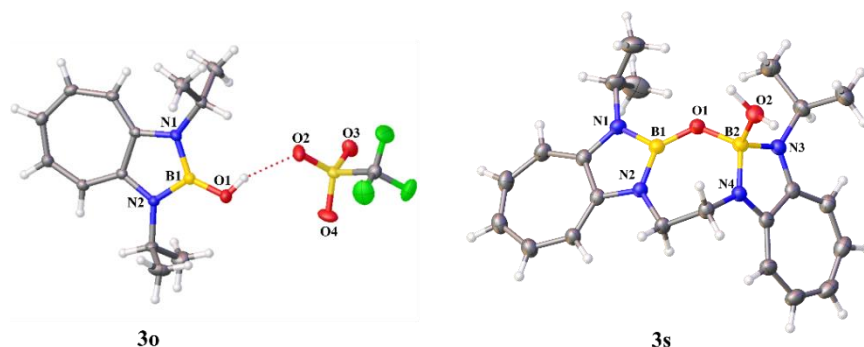
Figure 4.6 Crystal structure of complexes **3o** and **3s**. In **3s** counter anion is omitted for clarity, selected bond angles (°) and bond lengths (Å) (**3o**) B1-O1, 1.333(3), O1-H1, 0.82, N1-B1 1.448(3), N2-B1 1.452. (**3s**) B1-O1, 1.334, B2-O2, 1.444, B1-N1, 1.458, B1-N2, 1.456, N3-B2, 1.531, B2-N4, 1.336, B1-O1-B2, 130.9(2), B1-O1-N1, 124.6(2), B1-O1-N2, 130.751, B2-O1-O2, 105.2(2), O1-B2-N3, 116.8(2), O1-B1-N4, 114.273(19).

The B-N bond distances (B1-N1: 1.448(3) Å; B1-N2: 1.452(3) Å) is shorter than the neutral boron difluoride complex **2o** (B1-N1: 1.5413(19) Å; B1-N2: 1.5413(19) Å). This might be due to the electrostatic attraction between the positively charged boron atom and the electronegative nitrogen center. The B-O bond distance of 1.333(3) Å in **3o** is shorter than the B-O interatomic radii, confirming the cationic nature of the boron atom. A hydrogen bonding (interatomic distance 1.937 Å) between the OTf and OH bound to the boron atom indicates the presence of the OTf group stabilizing the hydroxyborenium cation.

After successful isolation of tri-coordinated borenium cation **3o**, we performed the reaction of TMSOTf with **2p-2r** by following a similar protocol. Although the reaction of **2p** and TMSOTf yielded the

borenium cation **3p**, complexes **2q** and **2r** produced a mixture of products that could not unable to purify. The ^{11}B NMR of **3p** showed a signal at 24.5 ppm, whereas the ^{19}F NMR revealed a peak at 78.3 ppm, confirming the free OTF as counter anion. The FT-IR spectrum possesses well well-defined O-H stretching frequency. *[49,50]*
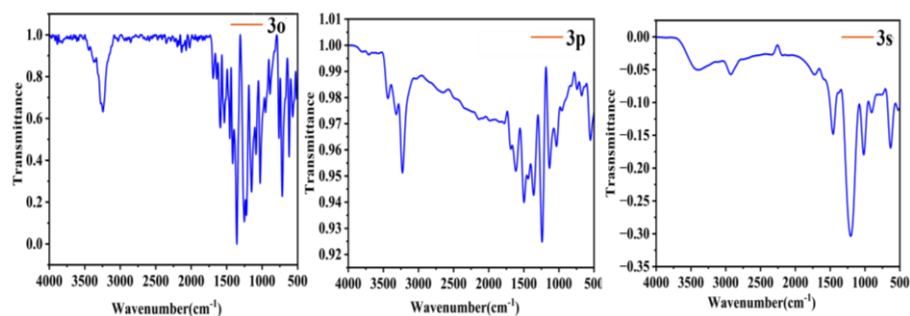
Figure 4.7 FT-IR spectrum of cations **3o**, **3p**, and **3s**

Subsequently, the reactivity of bis ATI-BF$_2$ complex **2s** with TMS-OTf was explored by following a similar procedure to generate the bis(borenium) cation. **2s** was treated with a slight excess of TMS-OTF in a J-Young NMR tube in CDCl$_3$ and heated at 45 ˚C for two hours. In the ^{11}B NMR data, two new singlets appeared with equal intensity at 8.5 ppm and another at 25.4 ppm, indicating both the boron atoms in different chemical environments. Crystals were grown from CDCl$_3$ solution and further analyzed by single-crystal structure X-ray diffraction study. Crystals are crystallized in P2$_1$/c space group in the monoclinic system. The solid-state structure revealed the presence of two boron centers in different environments and the presence of two OTf units, making the overall charge of the cationic unit two. The three coordinated boron center is attached to two nitrogen and a bridged oxygen atom, making it a borenium cation, whereas the four coordinated one is attached to two nitrogen, one bridged oxygen atom, along with a coordinated water molecule creating a boronium center. The geometry around the four coordinated boronium center is distorted tetrahedral and trigonal planar around the borenium cation. The bond length between B1-O1 is 1.334(3) Å whilst the distance between O1-B2 is 1.444(3) Å. This change in the B-O bond length might be due to the presence of the

differently coordinated boron atoms. The B-O bond distances are shorter than the neutral boroxine, demonstrating the cationic nature of the boron atoms. The measured distance between B2-O2 atoms is 1.522(3)Å, which is longer than that of neutral [52] B-O and cationic B-O bond distances, revealing the dative nature of the water molecule. Grubba and coworkers synthesized a NHC stabilized oxo-bridged bis(borenium) cations [53] and the B-O distances were 1.394(9) Å and 1.409(9) Å. Other reports on oxy bridged B-O-B borenium cation species stabilized by the cyclic porphyrin ligand having B-O bond distance 1.351(13) Å and 1.307(12) Å, were reported by the P. J. Brothers group.[54] These values are very similar to our ATI stabilized B-O-B boron cations. Both cationic boron atoms are separated by 2.527 Å and situated slightly (2.12 Å) above the seven-membered rings while the oxygen atom lies out of the plane. The crystal structure packing analysis of complex **3s** revealed the non-covalent interactions between the counter anion and aromatic ring hydrogens of the seven-membered ring **Figure 4.7**.
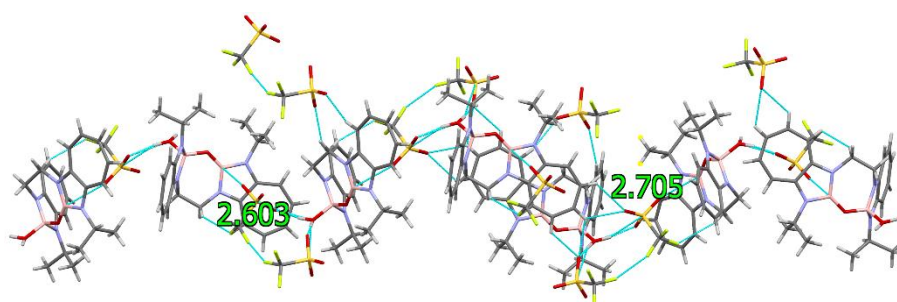
Figure 4.8 Crystal packing of complex **3s**.

A notable non-covalent interaction between (S-O···B; 3.080 Å) interaction is observed. The C-H$_{Ar}$···O interaction (2.654 Å) with a seven-membered ring and adjacent counter ion is detected **Figure 4.8**. Another non-coordinating interaction (1.660 Å) between a water molecule attached to the boronium ion and the oxygen atom of the triflate ion O-H···O is identified. The presence of OH or H_2O molecules in these obtained cations could be the result of the existence of TMSOH, an impurity found in TMSOTf, arising from hydrolysis with water/moisture. To check if the two hydrogens are bound to the

exocyclic oxygen (H_2O) and not to any of the other basic sites like (bridged O or Ns), we performed the variable temperature (VT) ^{1}H NMR study. We were unable to find any change in ^{1}H NMR precluding any tautomerization process **Figure 4.51**.
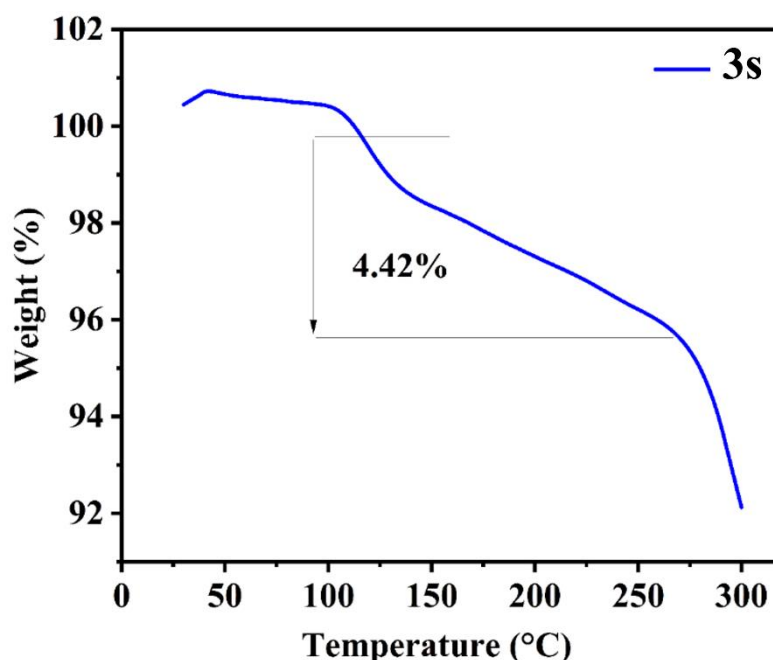
Figure 4.9 TGA graph of cation **3s**

Further, the TGA analysis was performed under an N_2 environment with N_2 flow rate (20 mL min^{-1}) with an increase in temperature of 10 °C min^{-1}. Initially, a slight increase in weight is observed due to the bouncy effect, and this effect is prominent at low temperatures; and as the temperature is increased, this effect is reduced. The first degradation step for complex **3s** appeared at 112 ˚C **Figure 4.9** with an approximate molecular weight loss of 4.40%, close to the calculated percentage molecular weight composition of the water molecule (4.45%) in complex **3s**.

4.4 DFT Studies on mono- and di-BF₂ complexes and corresponding cationic species

To understand the photophysical properties and electronic structures of the neutral boron complexes **2o**-**2s** and cationic species **3o** and **3s**

(anions are ignored), theoretical calculations were conducted using the range-separated ω-B97XD functional *[55]* and a triple-zeta 6-311G(d) basis set *[56]* for ground-state geometry optimizations and for excited-state calculations, the ɕ-HCTHhyb functional *[57,58]* and def2-TZVPP basis sets were utilized.*[59-67]* The electronic distribution and energy (in eV) of molecular orbitals (from TD-DFT) for mono-BF_2 complexes (**2o** and **3o**) as well as di-BF_2 complexes (**2s** and **3s**), are presented in **Figure 4.10**. Computations on **2o** and **2s** showed that the HOMO (highest occupied molecular orbital) and LUMO (lowest unoccupied molecular orbital) are primarily located on the aminotroponiminate moieties with similar HOMO-LUMO gaps (**2o**: 3.56 eV; **2s**: 3.42 eV). While HOMO describes the C-C-C allylic interaction along with an extended C-C-C-C π-interaction and electron localizations over the N centers of the aminotroponiminate moieties, LUMO defines corresponding anti-bonding interactions. The corresponding cations **3o** and **3s** showed relatively higher HOMO-LUMO gaps of 4.02 eV (**3o**) and 3.57 (**3s**) compared to the neutral species primarily due to the stabilizations of the corresponding HOMO orbitals. While HOMO of **3o** revealed the allylic C-C-C, N-B-N, and extended C-C-C-C π interactions, HOMO of di-cationic **3s** is unsymmetrically distributed. This unsymmetrical electronic distribution was due to the coordination of an H_2O molecule to one of the B-centers (boronium cation). The NBO (natural bond order) charge distribution (four connect B center: 1.21 and three connect B-center: 1.16) and calculated ^{11}B-NMR values **Table 4.3** indeed supported the dissimilar boron environments.
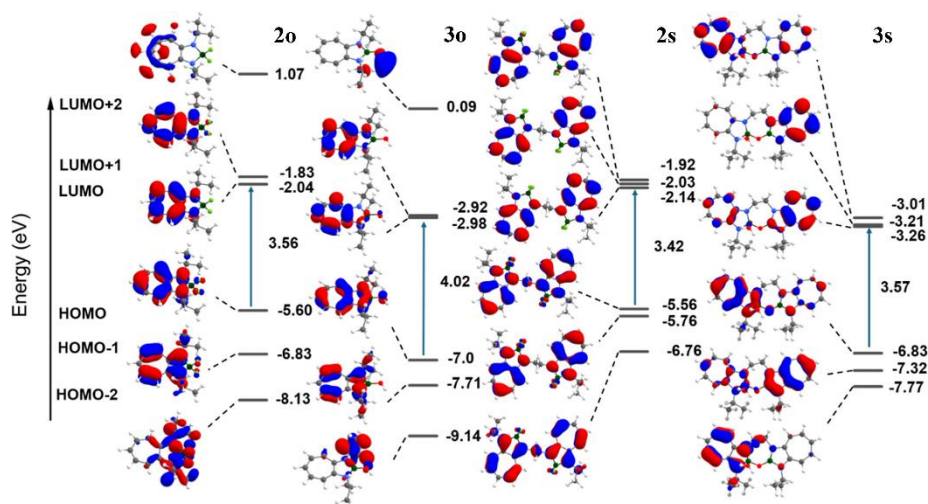
Figure 4.10 Electronic transitions of mono-BF$_2$ complexes (**2o** and **3o**) as well as di-BF$_2$ complexes (**2s** and **3s**) computed at the τ-HCTHhyb/def2-TZVPP(TD, SMD: dichloromethane)//ω-B97XD/6-311G(d) level.

For complexes **2o-2s**, the first excitation (lowest in energy) results from the transition of electrons between HOMO and LUMO (Figure 6). The second excitation is associated with the transfer of electrons from HOMO→LUMO+1 for complexes **2o-2r** or HOMO→LUMO+2 for complex **2s**. On the other hand, for the cationic complexes **3o** and **3s** the low-energy excitations are associated with transitions from HOMO→LUMO+1 as well as HOMO→LUMO. According to the electronic distribution, the transitions in the absorption process for **2o-2s** complexes are attributed to n→π* and π→π*-type transitions of the respective ligands. Further, **Table 4.3** summarizes close corroboration between the TD-DFT computed and experimentally measured absorption maxima as well as DFT (GIAO) calculated and experimentally measured ^{11}B NMR values. This complements the appropriate selection of the theoretical methods to shed light on the electronic transitions in the mono and di-BF$_2$ complexes and related cationic species.

Further, we have calculated a possible intermediate (**I**) containing two B-OH cationic centers that may rearrange into the formation of **3s**.

Flexible {-C_2H_4-} linkage may provide sufficient degrees of freedom to **I** so that both the B-OH moieties can come to proximity {BO(H)•••B(OH) = 3.09 Å} to rearrange into the formation of **3s** which is associated with ΔG of -10.1 kJ mol^{-1} calculated at ωB97XD/6-311G*. The driving force for this rearrangement could be the formation of an extra B-O bond (bond strength 536 kJ mol^{-1}) in **3s**. This partially supports the non-isolation of the desired di-cationic species **I**. **Figure 4.11**
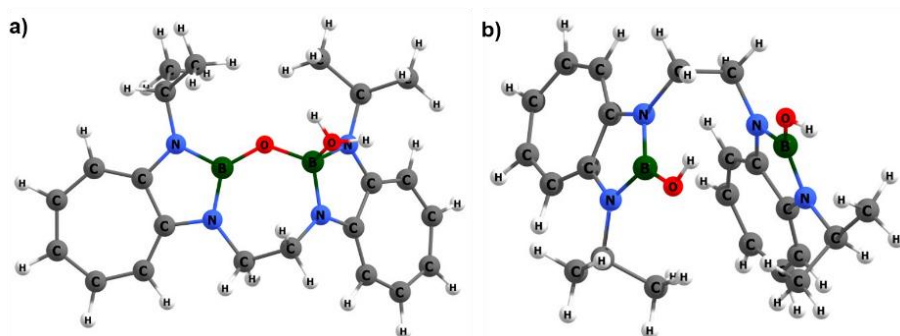
Figure 4.11 Optimized geometries of di-cationic (a) **3s** and (b) **I** (hypothetical intermediate) at ω-B97XD/6-311G(d) level.

Table 4.3 Experimentally observed and calculated ^{11}B NMR (GIAO-ωB97XD/6-311G*//ωB97XD/6-311G*), experimental (at room temperature in ACN) and calculated UV/vis data (at τHCTHhyb/def2-TZVPP-SMD//ωB97XD/6-311G*).

Complex	^{11}B (exp, ppm)	^{11}B(cal, ppm)	^{a}λ(exp, nm)	λ(cal, nm)	E_H-E_L (ev)
2o	5.9	4.2	431, 335, 267	367, 341, 254	3.56
2p	5.8	4.0	430, 354, 273	366, 340, 254	3.57
2q	5.2	4.0	445, 363, 271	368, 344, 254	3.55
2r	5.8	4.2	430, 356, 267	367, 341, 254	3.57
2s	5.7	4.1	434, 353, 264	394, 367, 352	3.42

3o	24.6	24.6	-	342, 335, 258	3.87
[b]**3s**	25.4, 8.8	21.9, 12.6[c]	-	345, 289, 258	3.86

[a]f = oscillatorstrength. [b]Calculatedonlyonthecationicpart. [c]Four-coordinated B-center.

4.5 Conclusions

In summary, in search of synthesizing five-membered borenium cations, we have synthesized a series of tetracoordinated difluoroboron complexes containing aminotroponiminate ligands. All synthesized complexes were characterized by using multinuclear NMR spectroscopy, mass spectrometry, and followed by single crystal X-ray diffraction analysis. All complexes are highly blue luminescent in solution. Further, they were treated with trimethylsilyl triflate, leading to the formation of tri-coordinated borenium cations. When bis(ATI)BF$_2$ complex **3s** was treated with TMS-OTf, it facilitated the formation of a seven-membered heterocyclic ring having two boron cations with different coordination environments. Theoretical calculations complement with the experimental findings and shed insight into the structure and bonding of the neutral BF$_2$ complexes as well as the cationic species.

4.6 Experimental Section

General Methods

The reactions were performed under an argon atmosphere using standard Schlenk techniques or in the open air. Chemicals were purchased from Spectrochem, Sigma-Aldrich, and TCI and used as received. All the solvents were purified by distillation using the appropriate drying agents, deoxygenated using three freeze–pump–thaw cycles, and stored over molecular sieves under dry argon before use. The deuterated solvents used for NMR spectroscopy were deoxygenated by freeze–pump–thaw cycles and stored under an argon atmosphere over molecular sieves. NMR chemical shifts are reported in ppm and coupling constants in Hz. ^{1}H, ^{11}B, ^{13}C, and ^{19}F NMR spectroscopy data were obtained at ambient temperature using a Bruker 500 NMR spectrometer (operating at 500 MHz for ^{1}H, 126 MHz for ^{13}C, 160 MHz for ^{11}B and 471 MHz for ^{19}F). ^{1}H NMR spectra were referenced via residual proton resonances of $CDCl_3$ (^{1}H, 7.26 ppm) and ^{13}C NMR spectra were referenced to $CDCl_3$ (^{13}C, 77.16 ppm) and $BF_3 \cdot OEt_2$ used as an internal standard for ^{11}B NMR. Bruker micrOTOF-Q II Daltonik was used to obtain the HRMS spectrum. Photoluminescence (PL) spectra were recorded by using a Fluoromax-4 spectrofluorometer (HORIBA Jobin Yvon, model FM100) with an excitation and emission slit width at 5 nm. UV-Vis spectroscopy was performed on a 3 mL solution using the Varian UV−Vis spectrophotometer (Cary 100 Bio) in a quartz cuvette (1 cm × 1 cm). Cyclic voltammetry was performed using a C-H instruments model CHI1103C in dichloromethane solvent using glassy carbon as the working electrode, Pt wire as the counter electrode, and saturated calomel electrode (SCE) as the reference electrode. The scan rate was 100mV. A solution of Bu_4NPF_6 in dichloromethane (0.1 M) was used as the supporting electrolyte. The temperature was kept constant throughout each experiment at 25 °C. The crystals data collections were performed on a CCD Agilent Technologies (Oxford Diffraction) SUPER NOVA (Mo at home/near, Eos) diffractometer. Data for the compounds were collected at 293 K using graphite-

monochromated MoK$_\alpha$ radiation. DFT calculations were implemented in the Gaussian 09 using the hybrid functional B3LYP in combination with the cc-pVDZ basis set for all atoms.

Synthetic Details

General synthesis of ligands (1o-1s)

Et$_3$·OBF$_4$ in DCM was added to the solution of 2-amino tropone in DCM and stirred it for 3h. After cooling the reaction to 0˚C, the appropriate amine was added. The reaction temperature slowly increased to room temperature, and further stirred it for 12h. All the volatiles were removed under reduced pressure. The residue was dissolved in 2N NaOH, and an aqueous layer was extracted in diethyl ether. The organic phase was dried over anhydrous MgSO$_4$. After evaporating the solvent, the compound was purified by column chromatography over basic alumina in hexane and ethyl acetate mixture to isolate the analytically pure product as yellow solid.

Ligands (**1o-1q**) have been previously reported, so we are not providing the data related to them.

Ligand 2r

¹H NMR (500 MHz, CDCl3) δ 6.76 – 6.61 (m, 2H), 6.54 (dd, *J* = 22.0, 11.1 Hz, 1H), 6.33 (d, *J* = 10.2 Hz, 1H), 6.07 (t, *J* = 9.2 Hz, 1H), 3.84 (sept., *J* = 12.7, 5.4 Hz, 1H), 1.46 (s, 9H), 1.19 (d, *J* = 6.2 Hz, 6H).**¹³C NMR** (126 MHz, CDCl$_3$) δ 137.40, 136.50, 128.38, 122.05, 109.14, 53.09, 27.66, 22.14. **LCMS (ESI):** Calculated for [C$_{14}$H$_{23}$N$_2$] 219.1856 [M+H] found 219.1854.

Yield: 80%

Ligand 2s

¹H NMR (500 MHz, CDCl$_3$) δ 6.81 – 6.66 (m, 4H), 6.47 (d, *J* = 11.3 Hz, 2H), 6.23 (d, *J* = 10.7 Hz, 2H), 6.13 (t, *J* = 9.3 Hz, 2H), 3.82 (sept., *J* = 6.3 Hz, 2H), 3.71 (s, 4H), 1.25 (dd, *J* = 6.4, 1.1 Hz, 12H). **¹³C NMR** (126 MHz, CDCl$_3$) δ 155.49, 150.33, 133.05, 132.29, 117.51, 116.70,

106.05, 51.21, 50.77, 29.34. **LCMS (ESI):** Calculated for [C$_{22}$H$_{31}$N$_4$] 351.2543[M+H] found 351.2539.

Yield: 50%

General procedure for ATI-difluoroboranes (2o-3s)

Aminotroponimine was dissolved in DCM and 10 equiv. of triethylamine was added under an inert atmosphere. To the resultant reaction mixture, 10 equiv. of BF$_3$·OEt$_2$ was added dropwise, and the mixture was left to stir at room temperature until reaction completion, as judged by TLC. The reaction mixture was quenched with DI water, extracted the product with DCM, and purified by column chromatography to give yellow solids.

Complex 2o

Complex **2o** was prepared by using **1o** (311 mg, 1.33 mmol), BF$_3$·OEt$_2$ (1901 mg, 13.39 mmol) and NEt$_3$ (1356 mg, 13.39 mmol)

^{1}H NMR (500 MHz, CDCl$_3$) δ 7.34 (t, J = 10.3 Hz, 2H), 6.81 (d, J = 10.9 Hz, 2H), 6.69 (t, J = 9.6 Hz, 1H), 4.18 – 4.01 (m, 2H), 1.46 (d, J = 6.7 Hz, 12H).**^{13}C NMR** (126 MHz, CDCl$_3$) δ 155.73, 137.94, 137.86, 121.48, 121.46, 121.35, 112.10, 46.50, 20.93. **^{11}B NMR** (160 MHz, CDCl$_3$) δ 5.97 (t, J = 35.0 Hz). **^{19}F NMR** (471 MHz, CDCl3) δ -124.72 (dd, J = 69.9, 34.7 Hz). **LCMS (ESI):** Calculated for [C$_{13}$H$_{19}$BF$_2$N$_2$Na] 275.1504 [M+Na] found 275.1693.

Yield: 82%.

Complex 2p

Complex **2p** was prepared by using **1p** (311 mg, 1.33 mmol), BF$_3$.OEt$_2$ (1901 mg, 13.39 mmol) and NEt$_3$ (1356 mg, 13.39 mmol)

^{1}H NMR (500 MHz, CDCl$_3$) δ 7.33 – 7.27 (m, 2H), 7.19 (d, J = 11.2 Hz, 2H), 6.67 (t, J = 9.3 Hz, 1H), 1.64 (s, 18H). **^{13}C NMR** (126 MHz, CDCl$_3$) δ 156.78, 136.46, 121.27, 115.35, 54.48, 28.86. **^{11}B NMR** (160 MHz, CDCl$_3$) δ 5.65 (t, J = 36.3 Hz). **^{19}F NMR** (471 MHz, CDCl3) δ -

116.50 (q, J = 72.7, 35.6 Hz). **LCMS (ESI):** Calculated for [$C_{15}H_{23}BF_2N_2Na$] 303.1817 [M+Na] found 303.1822.

Yield: 82%.

Complex 2q

Complex **2q** was prepared by using ligand **1q** (1500 mg, 6.45 mmol), BF$_3$·OEt$_2$ (6532 mg, 64.55 mmol) and NEt$_3$ (9161 mg, 64.55 mmol)

Yield: 78%.

^{1}H NMR (500 MHz, CDCl$_3$) δ 7.34 (t, J = 10.3 Hz, 2H), 6.82 (d, J = 10.7 Hz, 2H), 6.71 (t, J = 9.6 Hz, 1H), 3.39 (d, J = 4.2 Hz, 4H), 2.23 (sep, J = 7.1 Hz, 2H), 0.98 (d, J = 6.6 Hz, 12H). **^{13}C NMR** (126 MHz, CDCl$_3$) δ 156.73, 137.84, 121.84, 112.50, 50.83, 27.87, 20.93. **^{11}B NMR** (160 MHz, CDCl$_3$) δ 5.26 (t, J = 31.6 Hz). **^{19}F NMR** (471 MHz, CDCl$_3$) δ -137.11 (q, J = 31.7, 28.8 Hz). **LCMS (ESI):** Calculated for [$C_{15}H_{23}BF_2N_2Na$] 303.1817 [M+Na] found 303.1807.

Complex 2r

Complex **2r** was prepared by using ligand **1r**(200 mg, 0.91 mmol), BF$_3$·OEt$_2$ (1950 mg, 13.74 mmol) and NEt$_3$ (1390 mg, 13.74 mmol)

^{1}H NMR (500 MHz, CDCl$_3$) δ 7.32 (q, J = 9.9 Hz, 2H), 7.22 – 7.16 (m, 1H), 6.82 (d, J = 11.0 Hz, 1H), 6.69 (t, J = 9.4 Hz, 1H), 4.14 – 4.02 (m, 1H), 1.64 (s, 9H), 1.45 (d, J = 6.7 Hz, 6H). **^{13}C NMR** (126 MHz, CDCl$_3$) δ 156.51, 156.07, 137.86, 136.64, 121.39, 115.37, 112.17, 54.46, 46.51, 28.80, 20.90. **^{11}B NMR** (160 MHz, CDCl$_3$) δ 5.83 (t, J = 35.6 Hz). **^{19}F NMR** (471 MHz, CDCl$_3$) δ -120.44 (q, J = 71.3, 35.6 Hz). **LCMS (ESI):** Calculated for [$C_{14}H_{21}BF_2N_2Na$] 289.1661 [M+Na] found 289.1697.

Yield: 80%.

Complex 2s

Complex **2s** was prepared by using ligand **1s** (150 mg, 0.42 mmol), BF$_3$·OEt$_2$ (904.32 mg, 6.40 mmol), and NEt$_3$ (432.08 mg, 4.27 mmol)

^{1}H NMR (500 MHz, CDCl3) δ 7.31 (t, J = 10.2 Hz, 4H), 7.12 (d, J = 10.7 Hz, 2H), 6.82 (d, J = 10.9 Hz, 2H), 6.69 (t, J = 9.5 Hz, 2H), 4.10 (t, J = 6.9 Hz, 2H), 3.92 (s, 4H), 1.49 (d, J = 6.7 Hz, 12H).**^{13}C NMR** (126 MHz, CDCl$_3$) δ 138.55, 137.99, 122.60, 113.03, 112.52, 46.51, 40.97, 21.07. **^{11}B NMR** (160 MHz, CDCl$_3$) δ 5.74 (t, J = 33.8 Hz). **^{19}F NMR** (471 MHz, CDCl$_3$) δ -132.14 (dd, J = 67.0, 33.1 Hz). **LCMS (ESI):** Calculated for [C$_{22}$H$_{28}$B$_2$F$_4$N$_4$Na] 469.2336 [M+Na] found 469. 2390.

Yield: 65%.

General procedure for boron cation synthesis (3o, 3p, and 3s)

A mixture of ATI-BF$_2$ complex and trimethylsilyl triflate (TMS-OTf) in CDCl$_3$ was heated at 45 °C in a J-Young NMR tube for two hours. After that, all the volatiles were dried and washed with pentane. Finally, it was dissolved in CDCl$_3$ and kept at room temperature to get yellow crystals.

Complex 3o

Complex **3o** was prepared by using **2o** (66 mg, 0.13 mmol) and TMS-OTf (31.11 mg, 0.14 mmol) in CDCl$_3$

^{1}H NMR (500 MHz, CDCl$_3$) δ 8.25 – 8.03 (m, 4H), 7.80 (tt, J = 9.2, 1.4 Hz, 1H), 4.57 (sept, J = 7.1 Hz, 2H), 1.51 (d, J = 6.9 Hz, 12H). **^{13}C NMR** (126 MHz, CDCl$_3$) δ 154.18, 140.99, 134.80, 128.49, 123.41, 47.62, 21.21. **^{11}B NMR** (160 MHz, CDCl3) δ 24.64. **^{19}F NMR** (471 MHz, CDCl3) δ -78.33. **LCMS (ESI):** Calculated for [C13H20BN2O]$^+$ 231.1666 [M] found 231.1697. **FT-IR Data** (cm^{-1}) O-H, 3249, (Aliph-CH), 2960-2872, C=C 1580-1600, C=N 1270.

Yield: 28%

Complex 3p

Complex **3p** was prepared by using **2p** (20 mg, 0.07 mmol) and TMS-OTf (15.55 mg, 0.07 mmol) in CDCl$_3$

^{1}H NMR (400 MHz, CDCl$_3$) δ 8.08 (d, J = 11.0 Hz, 1H), 7.98 – 7.82 (m, 4H), 7.54 (t, J = 9.2 Hz, 1H), 1.72 (s, 18H**). ^{13}C NMR** (126 MHz, CDCl$_3$) δ 154.58, 141.00, 134.57, 123.44, 47.94, 21.46. **^{11}B NMR** (160

MHz, CDCl3) δ 24.50. **¹⁹F NMR** (471 MHz, CDCl$_3$) δ -78.32. **LCMS (ESI):** Calculated for [C$_{15}$H$_{24}$BN$_2$O]$^+$ 259.1964 [M] found 259. 1964. **FT-IR Data** (cm^{-1}) O-H, 3235, (Aliph-CH), 2960-2872, C=C 1580-1600, C=N 1270.

Yield: 20%

Complex 3s

Complex **3s** was prepared by using complex **2s** (18 mg, 0.04 mmol) and TMS-OTf (26.67 mg, 0.12 mmol) in CDCl$_3$

¹H NMR (500 MHz, CDCl$_3$) δ 8.33 – 8.10 (m, 4H), 7.93 (t, J = 9.4 Hz, 1H), 7.76 (d, J = 10.2 Hz, 1H), 7.69 (t, J = 10.4 Hz, 1H), 7.58 (d, J = 10.6 Hz, 1H), 7.29 (d, J = 10.9 Hz, 1H), 7.21 (t, J = 9.8 Hz, 1H), 4.68 (sep, J = 6.8 Hz, 1H), 4.57 (s, 2H), 4.24 (sep, J = 6.7 Hz, 1H), 4.05 (s, 2H), 1.73 (d, J = 6.9 Hz, 6H), 1.52 (d, J = 6.8 Hz, 6H). **¹¹B NMR** (160 MHz, CDCl$_3$) δ 17.26 (d, J = 2691.8 Hz). **¹⁹F NMR** (471 MHz, CDCl$_3$) δ -77.30. **LCMS (ESI):** Calculated for [C$_{22}$H$_{30}$B$_2$N$_4$O$_2$Na]$^+$ 427.2431 [M+Na] found 427.2431. **FT-IR Data** (cm^{-1}) O-H, 3240, (Aliph-CH), 2960-2872, C=C 1580-1600, C=N 1270.

Yield: 20%

Spectroscopic details of ligands and complexes
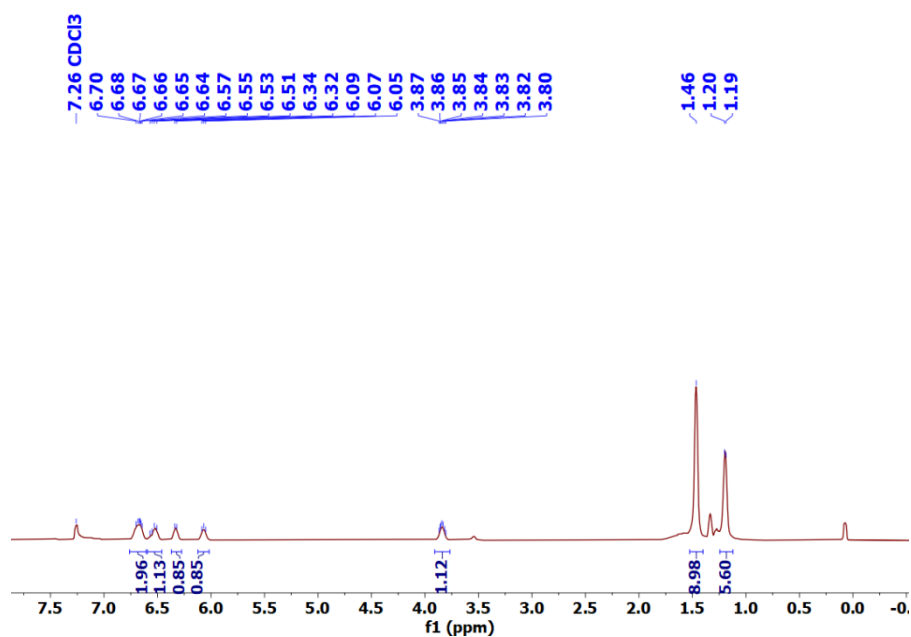
Figure 4.12 ^{1}HNMR of ligand **1r**.
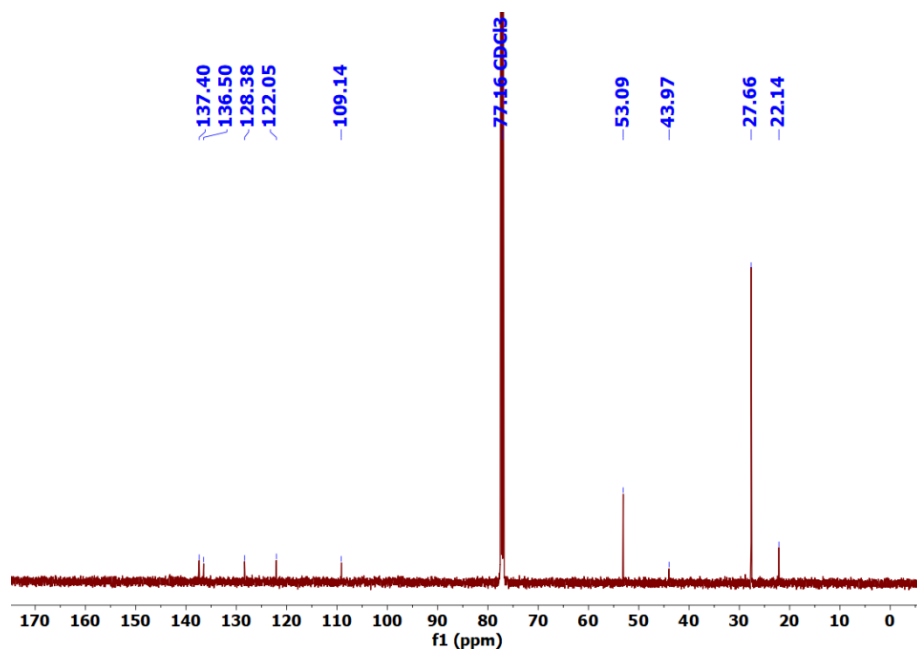
Figure 4.13[13]C{^{1}H} NMR of ligand **1r**.
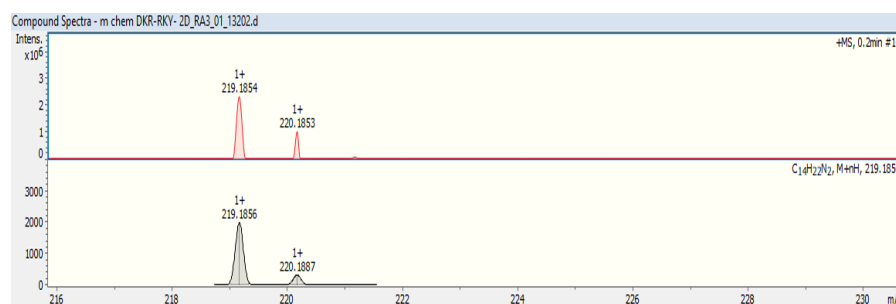
Figure 4.14 High-resolution mass spectra of the ligand **1r**.
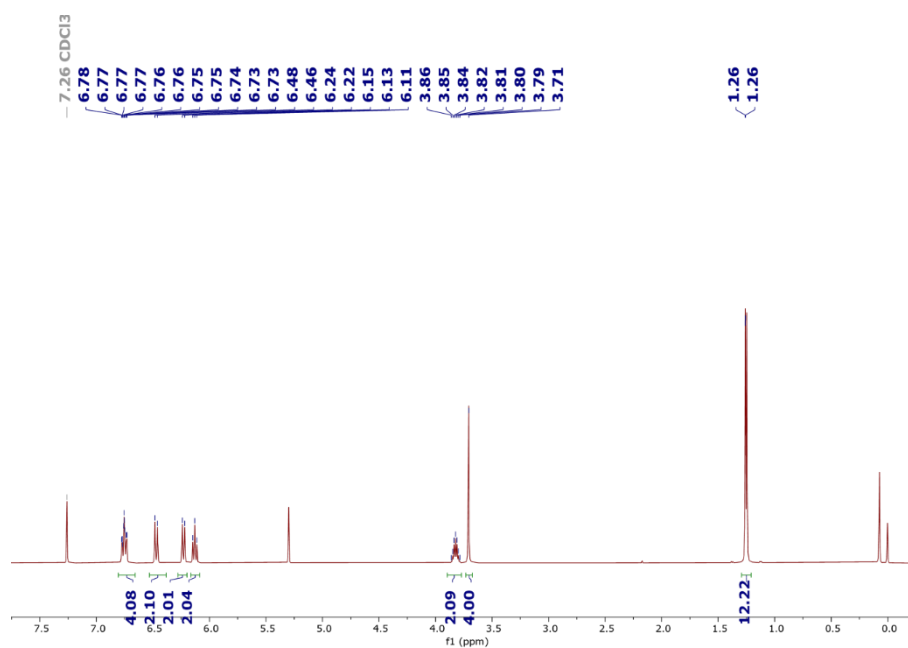
Figure 4.15 ¹HNMR of ligand 1s.
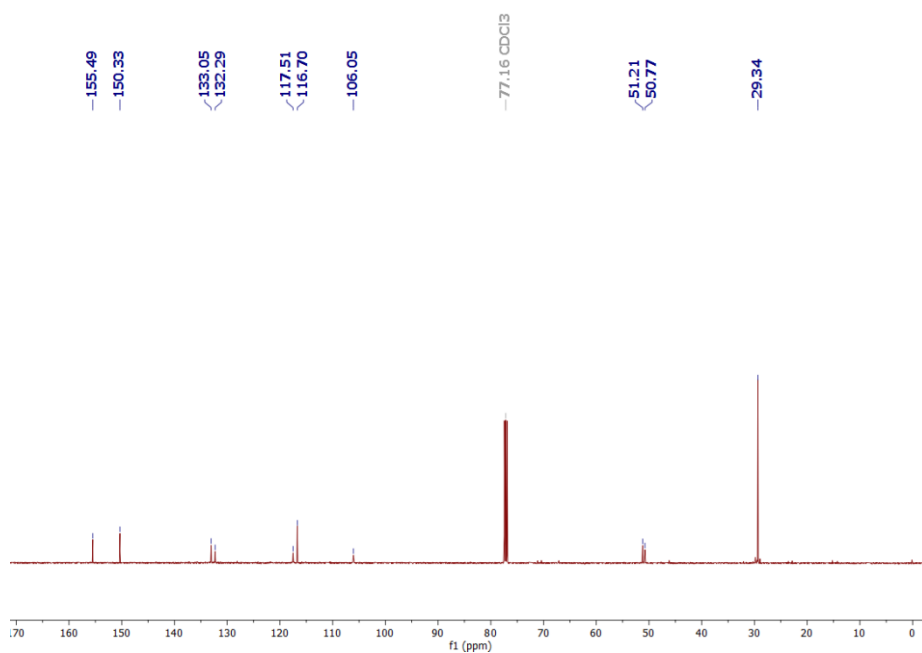
Figure 4.16 ^{13}C{^{1}H} NMR of ligand 1s.
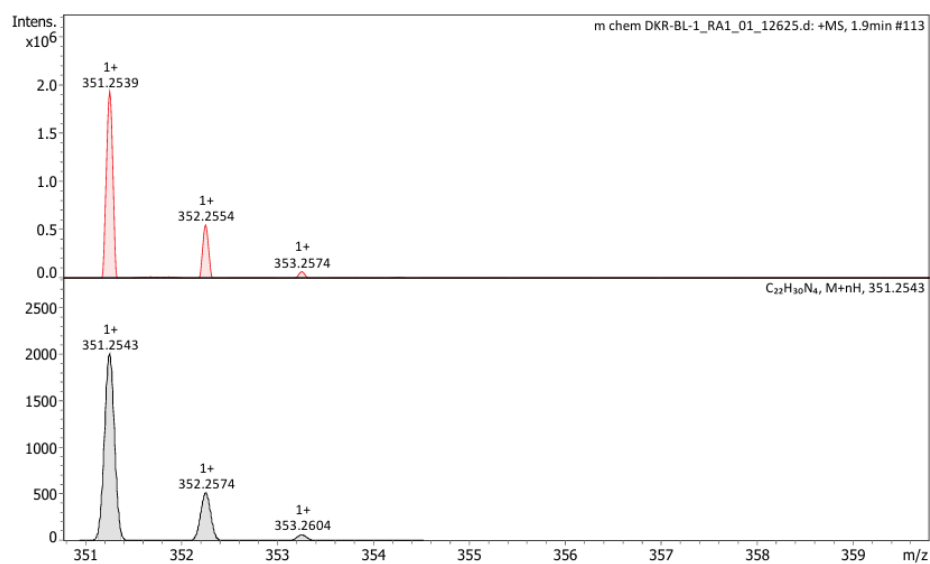
Figure 4.17 High-resolution spectra of ligand 1s.
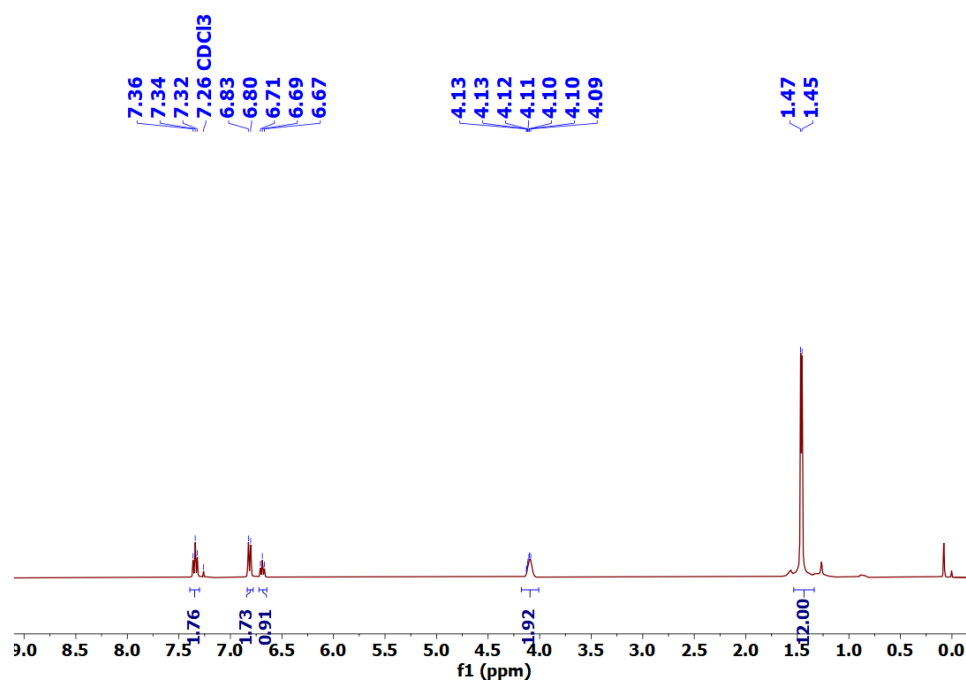
Figure 4.18 ^{1}H NMR of complex **2o**.
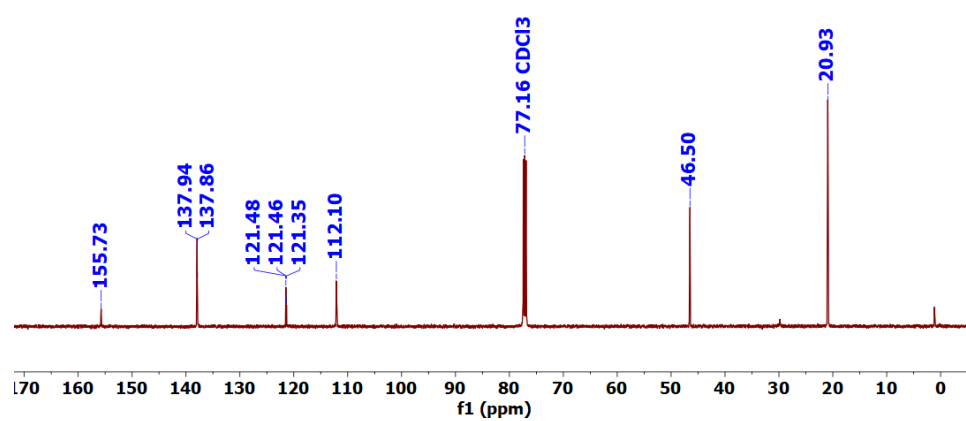
Figure 4.19 ^{13}C{^{1}H} NMR of complex **2o**.
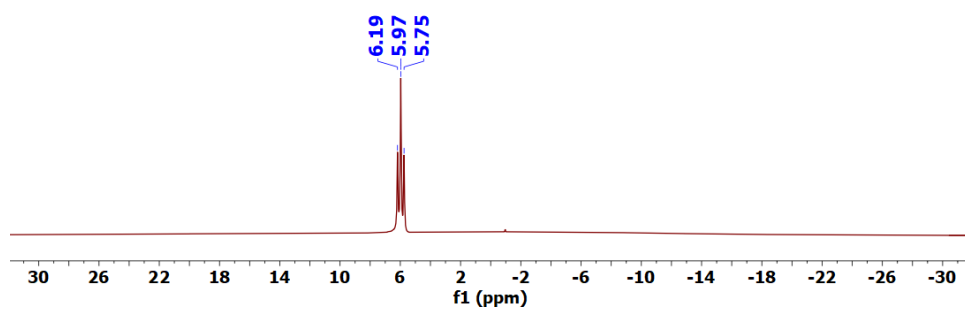
Figure 4.20 ^{11}B NMR of complex **2o**.
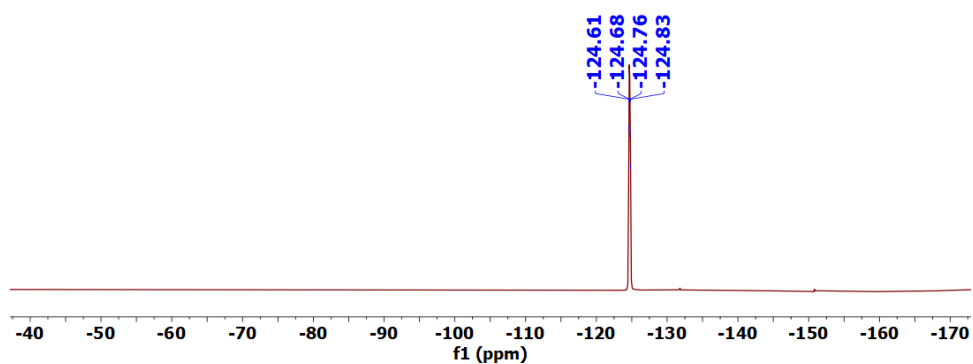
Figure 4.21 ^{19}FNMR of complex **2o**.
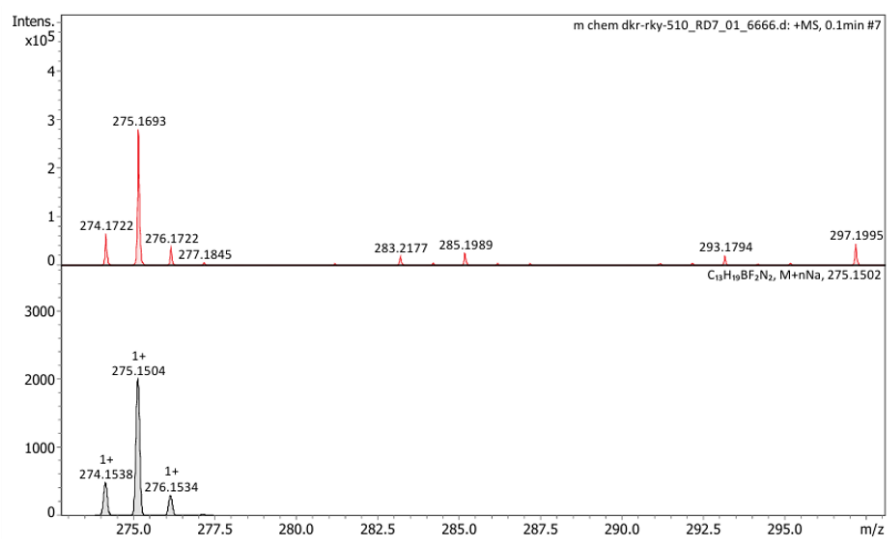
Figure 4.22 Mass spectrum of complex 2o.
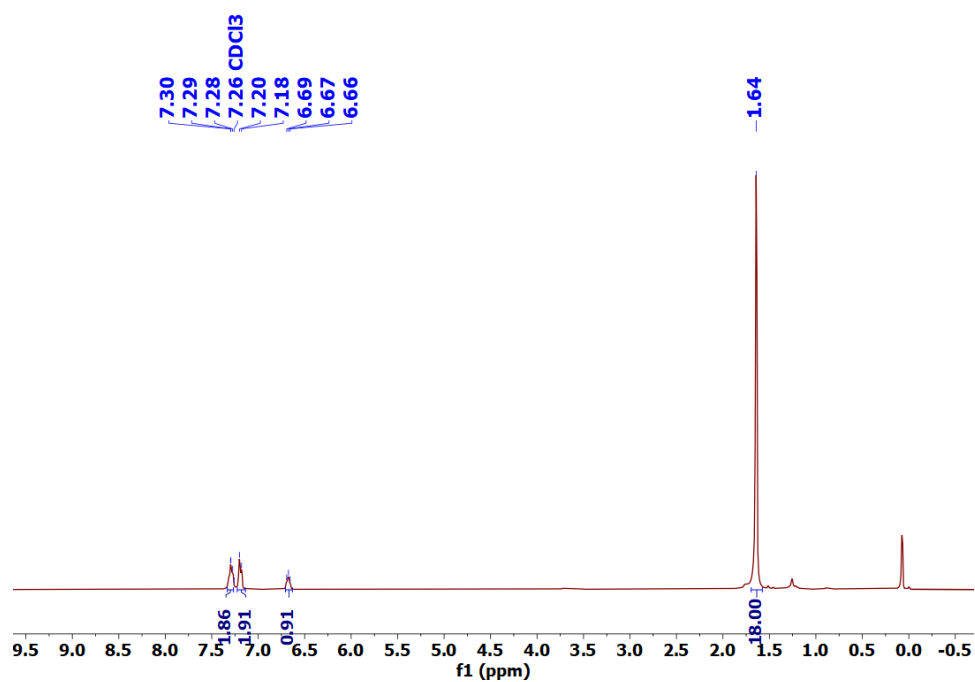
Figure 4.23 ^{1}H NMR of complex **2p**.
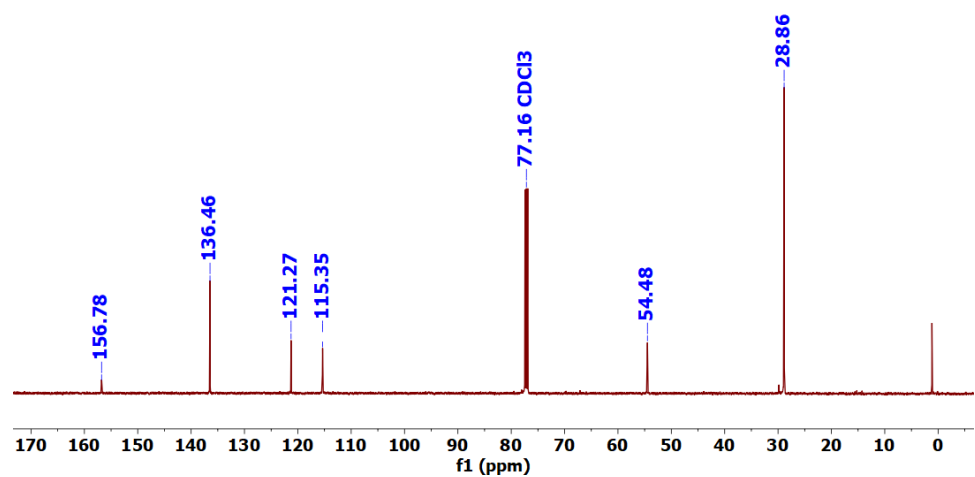
Figure 4.24 ^{13}C{^{1}H} NMR of complex **2p**.
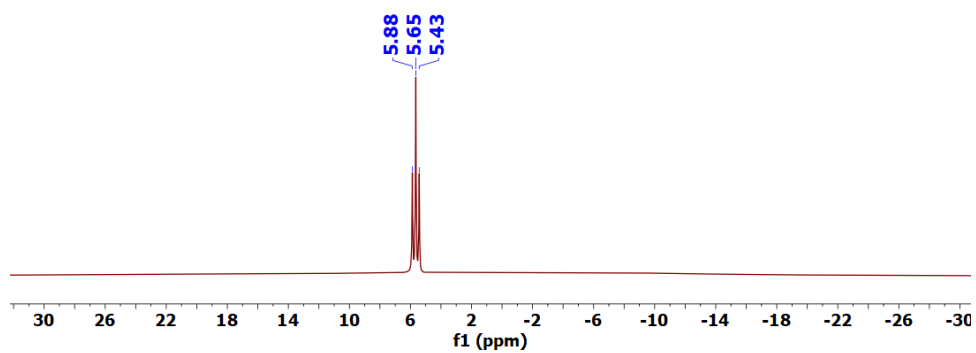
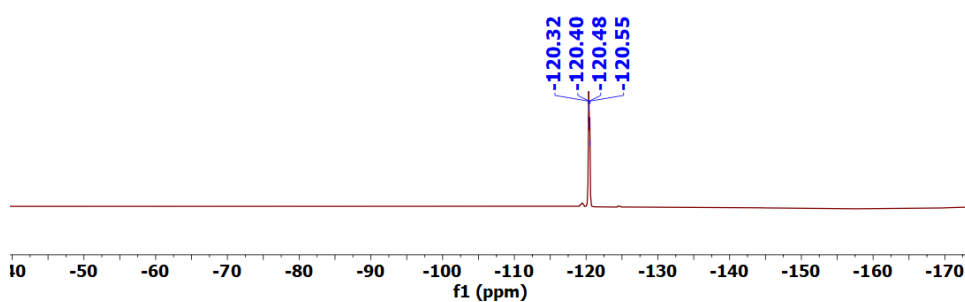**Figure 4.25** ^{11}B NMR of complex **2p**.
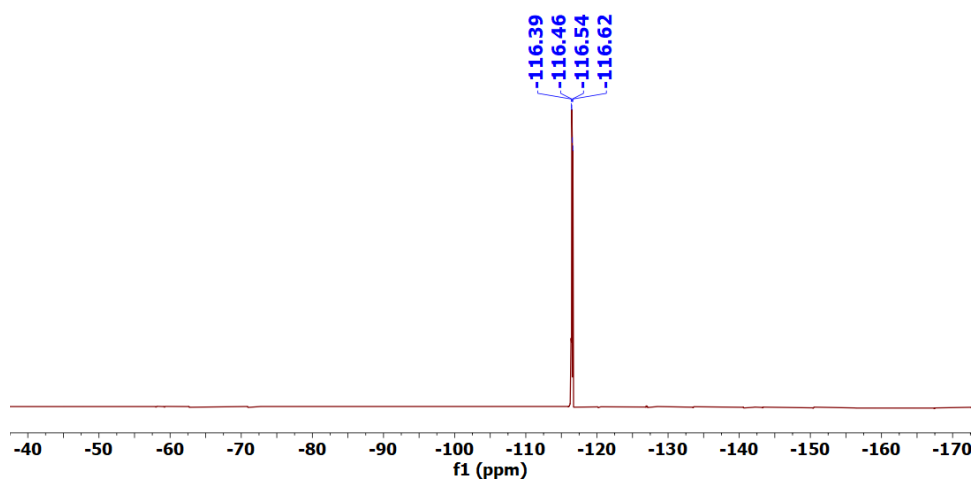
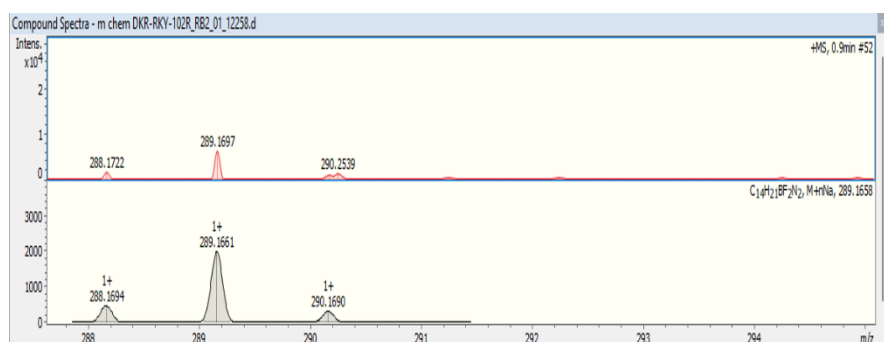**Figure 4.26** ^{19}F NMR of complex **2p**.
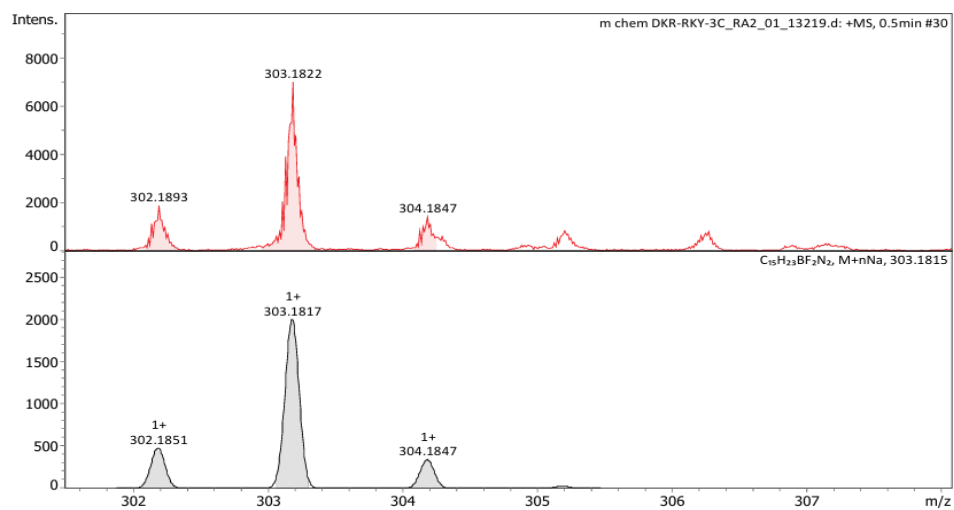
Figure 4.27 High-resolution spectra of complex **2p**.
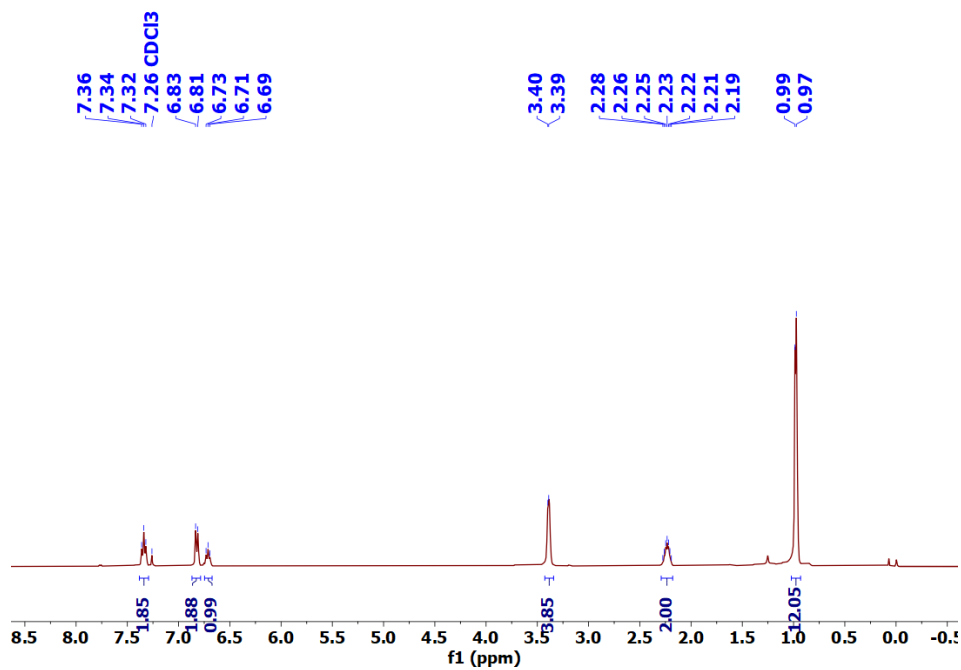
Figure 4.28 ^{1}H NMR of complex **2q**.
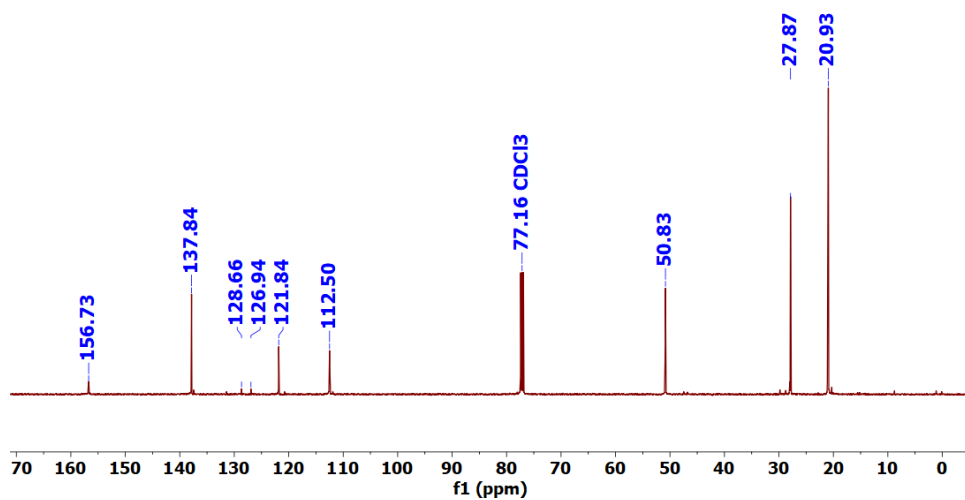
Figure 4.29 ^{13}C{^{1}H} NMR of complex **2q**.
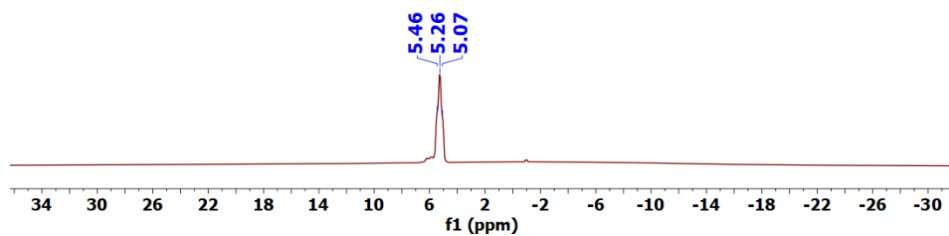
Figure 4.30 ^{11}B NMR of complex **2q**.
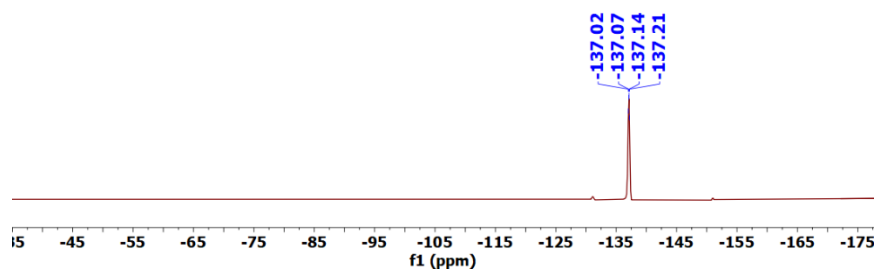
Figure 4.31 ^{19}F NMR of complex **2q**.

240
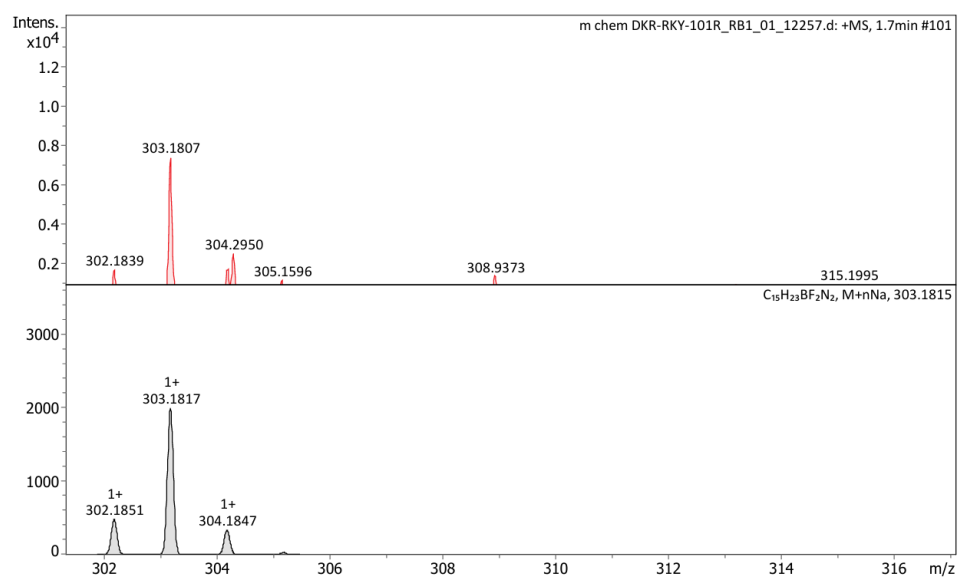
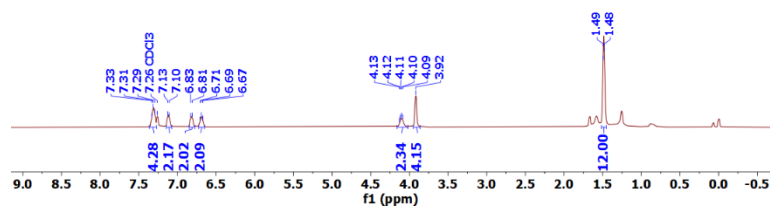**Figure 4.32 High-resolution mass spectra of complex 2q**.
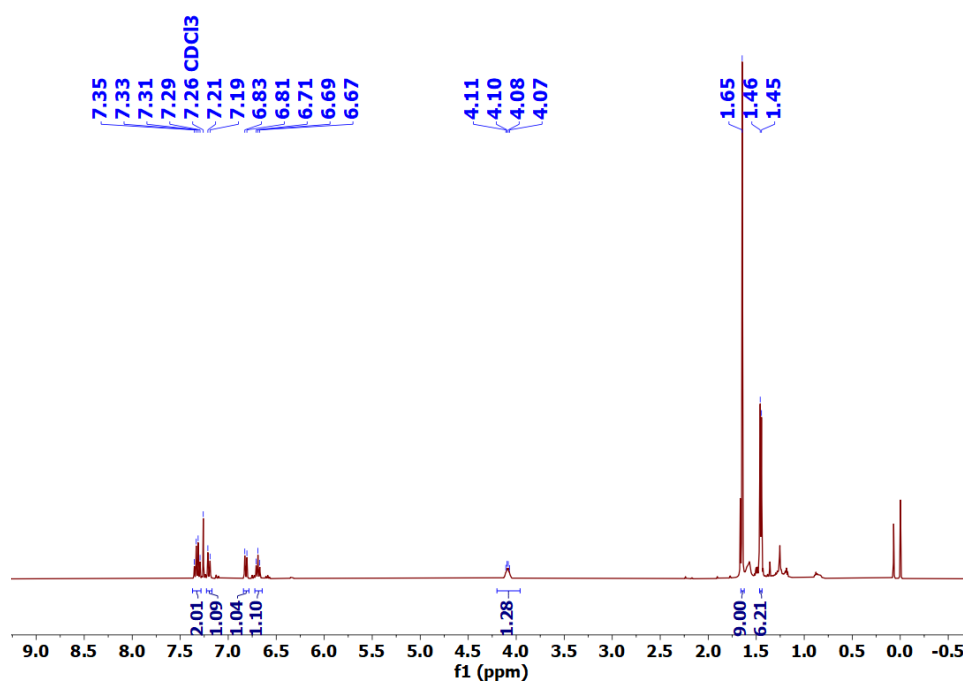
Figure 4.33 ^{1}H NMR of complex **2r**.
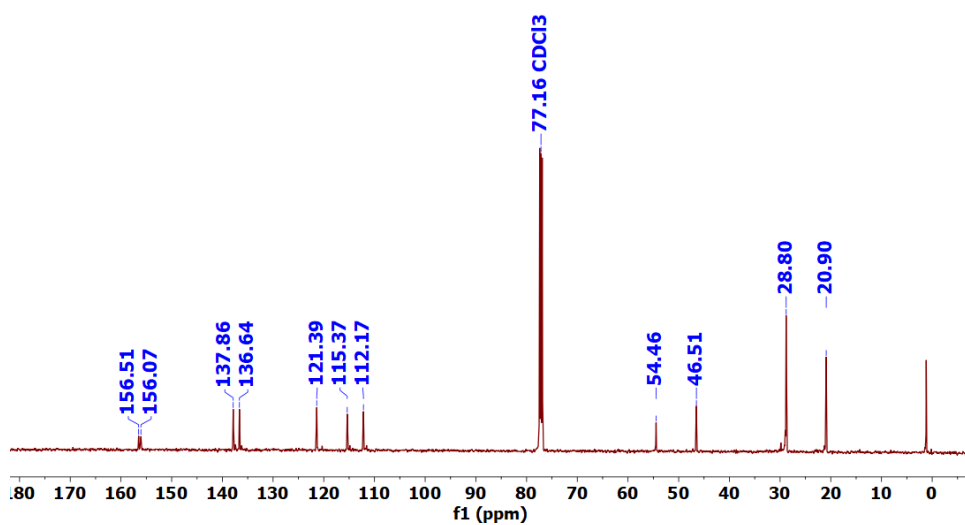
Figure 4.34 $^{13}C\{^1H\}$ NMR of complex **2r**.
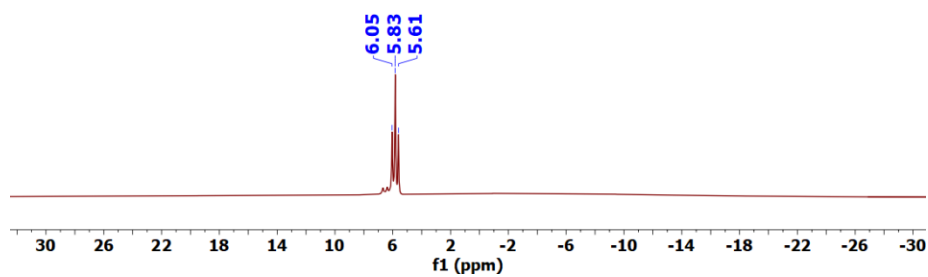
Figure 4.35 ^{11}B NMR of complex **2r**.

Figure 4.36 ^{19}F NMR of complex **2r**.

Figure 4.37 High-resolution mass spectra of complex **2r**.
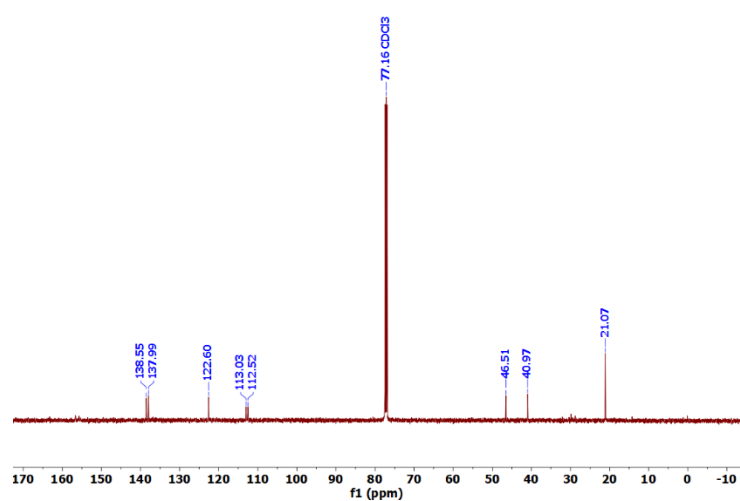

Figure 4.38 ^{1}H NMR of complex **2s**.
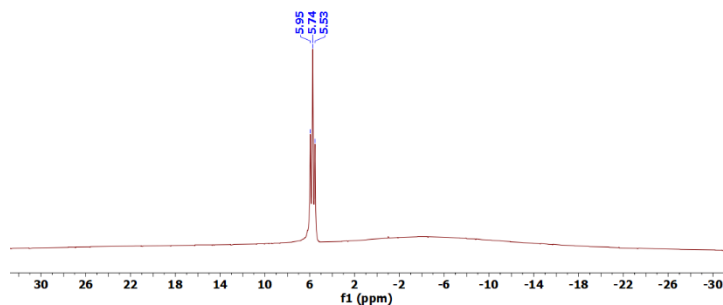

Figure 4.39 ^{13}C{^{1}H} NMR of complex **2s**.

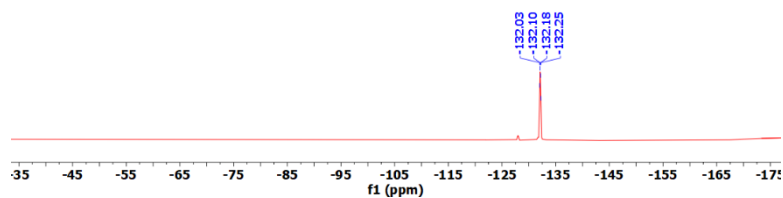**Figure 4.40** ^{11}B NMR of complex **2s**.
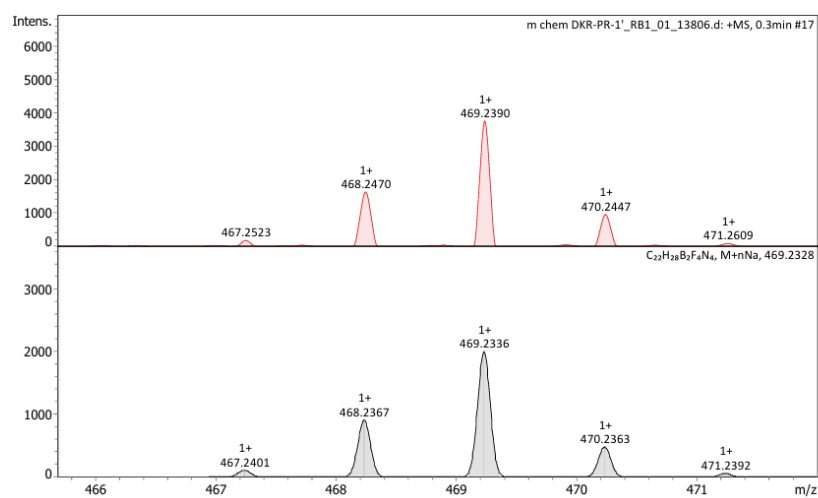

Figure 4.41 ^{19}F NMR of complex **2s**.
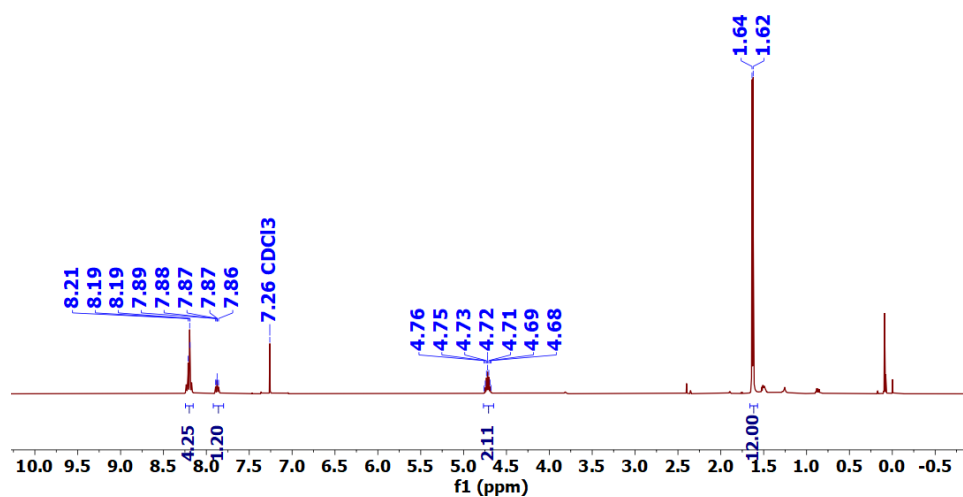

Figure 4.42 Mass spectrum of complex **2s**.

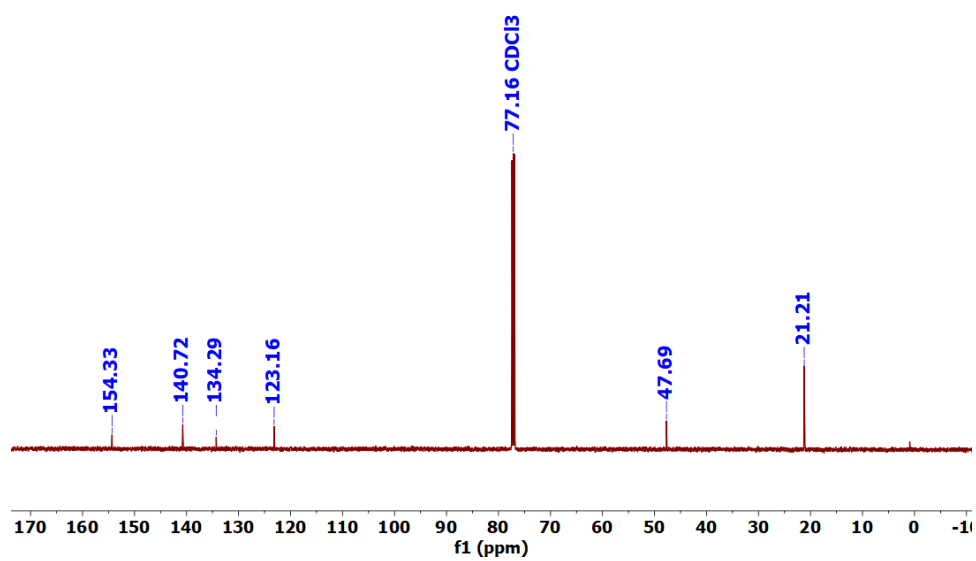**Figure 4.43** ^{1}H NMR of complex **3o**.

Figure 4.44 ^{13}C{^{1}H} NMR of complex **3o**.
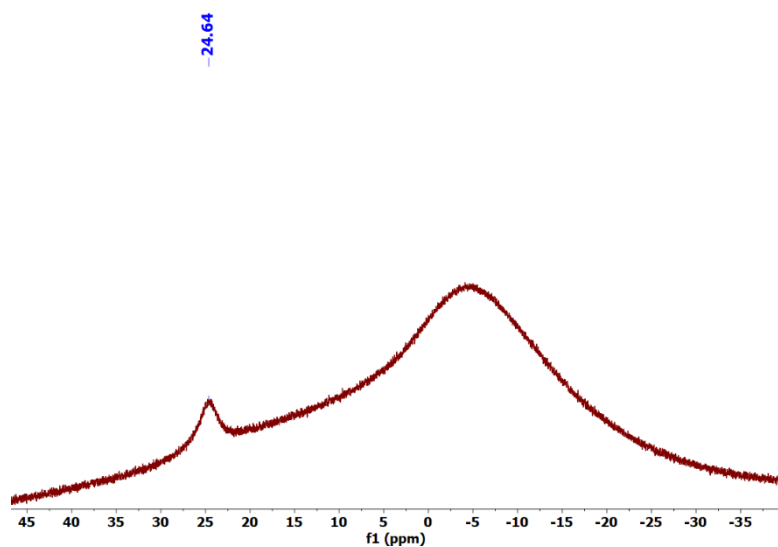
Figure 4.45 ^{11}B NMR of complex **3o**.
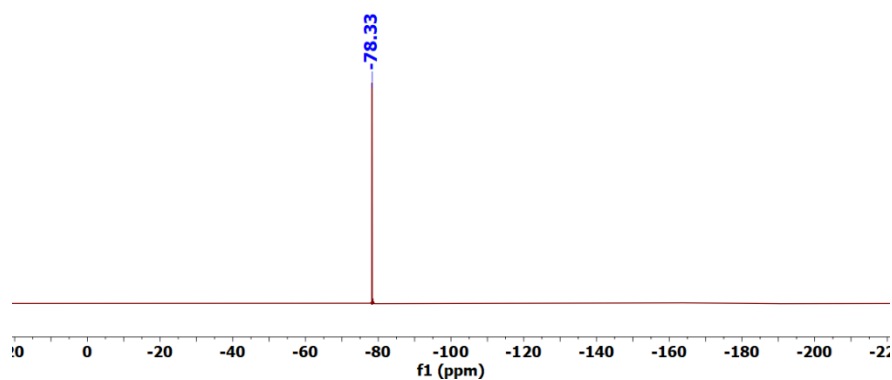
Figure 4.46 ^{19}F NMR of complex **3o**.
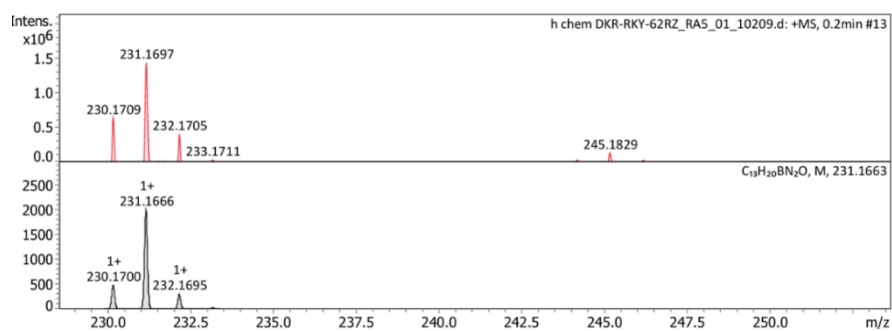
Figure 4.47 Mass spectrum of complex **3o**.
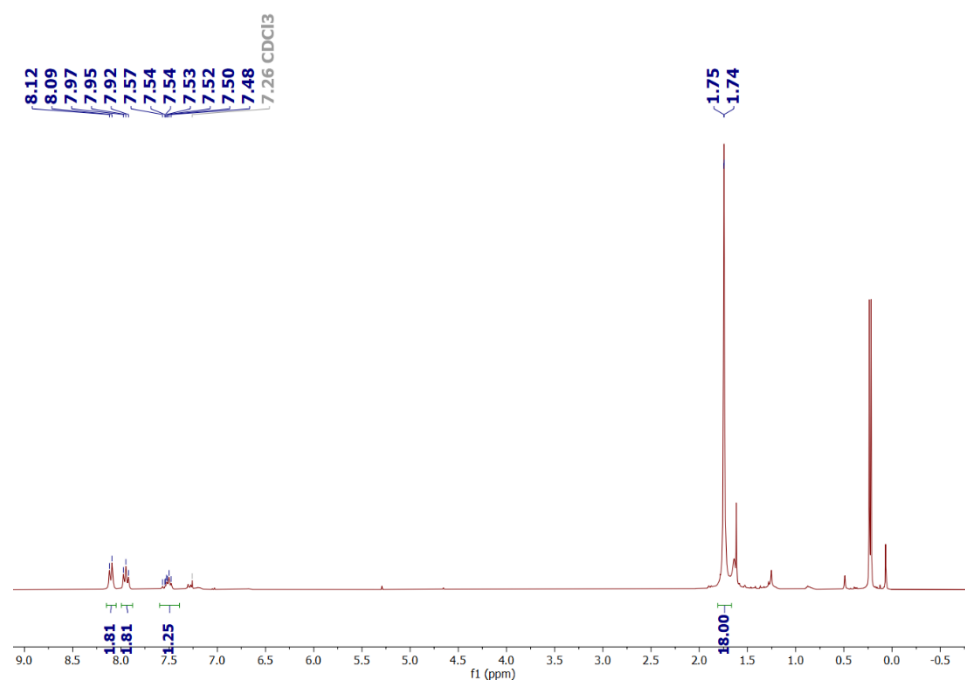
Figure 4.48 ^{1}H NMR of complex **3p**.
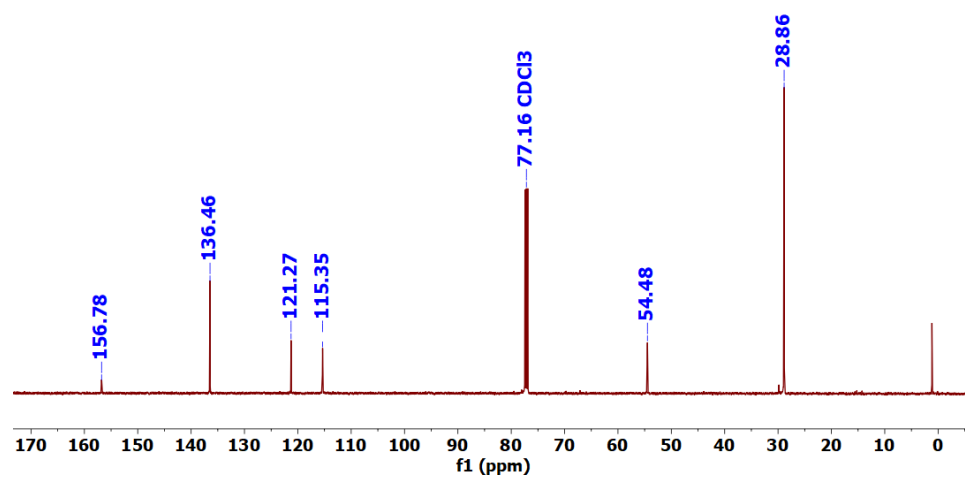
Figure 4.49 ^{13}C{^{1}H} NMR of complex **3p**.

Figure 4.50 ^{11}B NMR of complex **3p**.

Figure 4.51 ^{19}F NMR of complex **3p**.
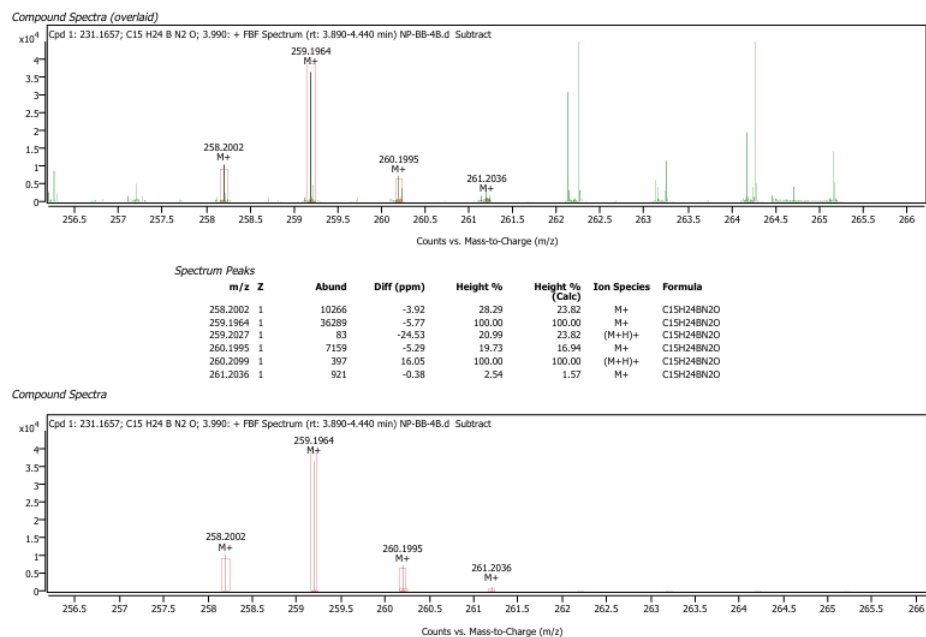
Figure 4.52 High-resolution mass spectra of complex **3p**.
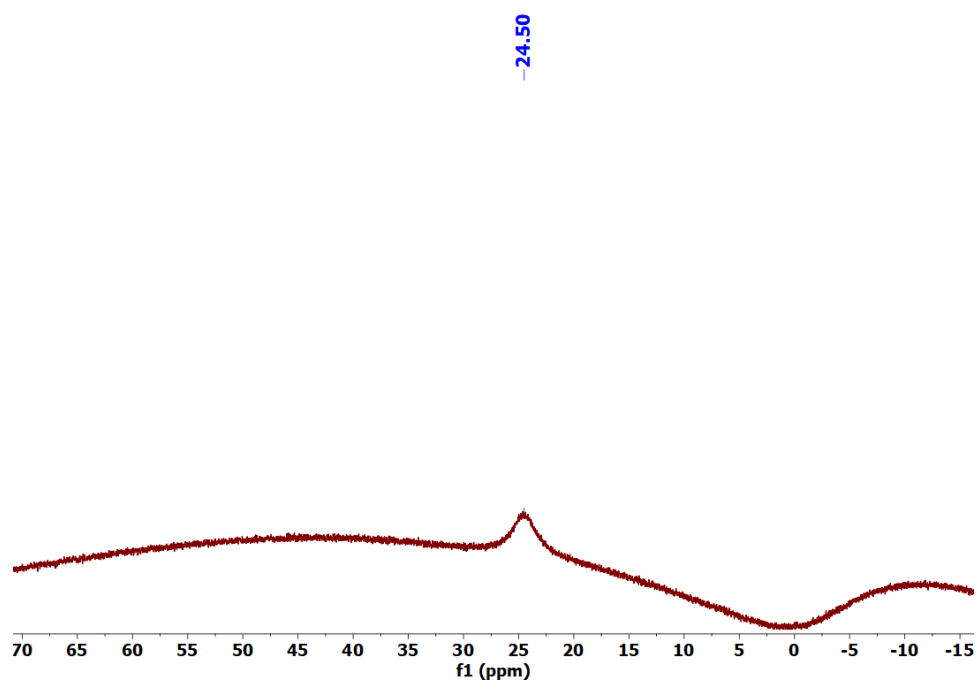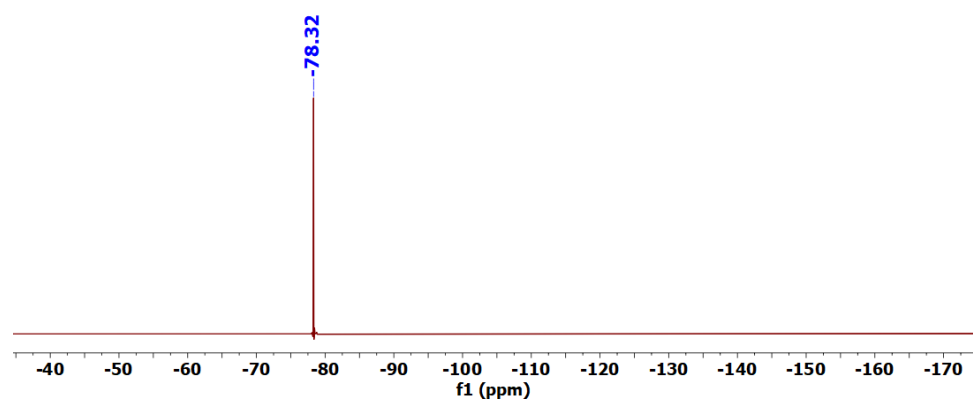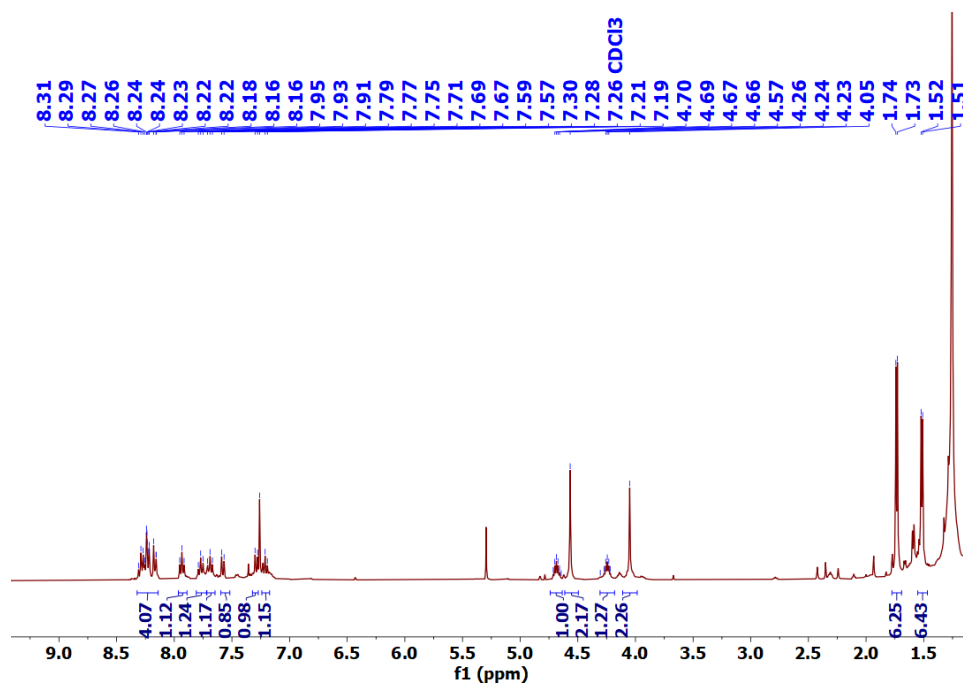

Figure 4.53 ^{1}H NMR of complex **3s**.
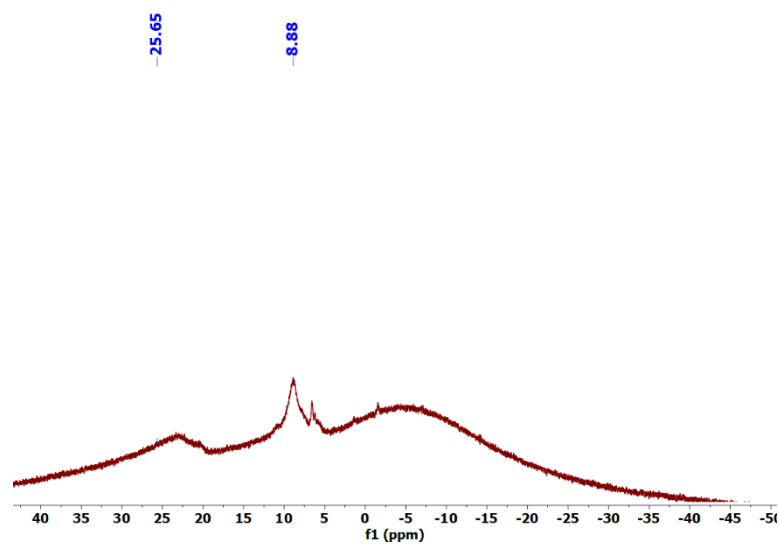
Figure 4.54 ^{11}B NMR of complex **3s**.
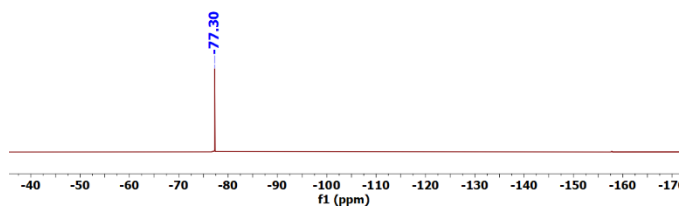
Figure 4.55 ^{19}F NMR of complex **3s**.

Cpd 1: 431.2418; C22 H30 B2 N4 O2; 4.921: + FBF Spectrum (rt: 4.854-5.104 min) NP-BB-4E.d Subtract

Spectrum Peaks

m/z	Z	Abund	Diff (ppm)	Height %	Height % (Calc)	Ion Species	Formula
425.2496	1	2793	-5.52	7.58	5.46	(M+Na)+	C22H30B2N4O2
426.2465	1	18877	-4.87	51.21	45.38	(M+Na)+	C22H30B2N4O2
427.2431	1	36860	-5.49	100.00	100.00	(M+Na)+	C22H30B2N4O2
428.2463	1	9377	-4.30	25.44	24.32	(M+Na)+	C22H30B2N4O2

Compound Spectra

Cpd 1: 431.2418; C22 H30 B2 N4 O2; 4.921: + FBF Spectrum (rt: 4.854-5.104 min) NP-BB-4E.d Subtract

Figure 4.56 High-resolution mass spectra of complex **3s**.

Figure 4.57 Variable temperature NMR of complex **3s**.

Crystallographic Details

The crystal data were collected on a SuperNova, Dual, Cu at home/near,

Eos diffractometer. The crystal was kept at 293(2) K during data

collection. Using Olex2 , the structure was solved with the SHELXT

structure solution program using Intrinsic Phasing and refined with the

251

SHELXL refinement package using Least Squares minimization. The structures were solved by direct methods and refined by full-matrix least squares, based on $F2$, using SHELXL Crystal structures were refined using Olex2-1.0 software. All non-hydrogen atoms were refined anisotropically. *[68-70]*

Table 4.4 Crystal data for Complex **2o, 2p, 2q, 2s, 3o, and 3s**.

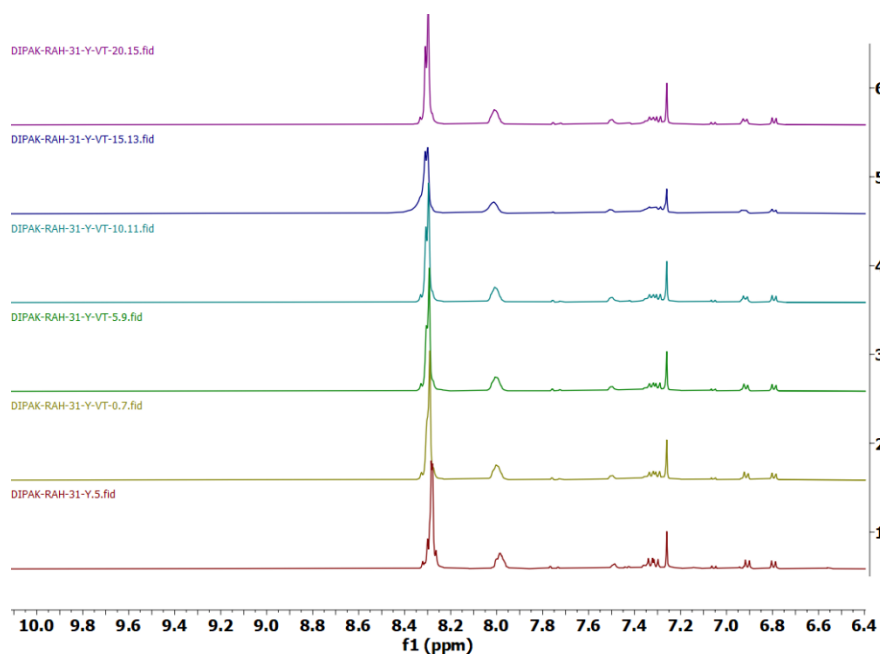| Chemical Compound	2o	2p	2q	2s	3o	3s
Empirical formula	$C_{13}H_{19}BF_2N_2$	$C_{15}H_{23}BF_2N_2$	$C_{14}H_{21}BF_2N_2$	$C_{22}H_{28}B_2F_4N_4$	$C_{14}H_{20}BF_3N_2O_4S$	$C_{24}H_{30}B_2F_6N_4O_8S_2$
Formula weight (g·mol^{-1})	252.11	280.16	266.14	446.1	380.19	702.26
Temperature (K)	293 (2)	100.0(3)	293 (2)	293 (2)	100	100
Radiation, λ (Å)	Mo-K_α, 0.71073	Mo-K_α, 0.71073	Mo-K_α, 0.7107	Mo-K_α, 0.71073	Mo-K_α, 0.7107	Mo-K_α, 0.7107
Crystal system	Monoclinic	Monoclinic	Monoclinic	Monoclinic	Monoclinic	Monoclinic
Space group	P2$_1$/n	P2$_1$/n	P2$_1$/c	C2/c	P2$_1$/c	P2$_1$/c
a (Å)	9.5921(4)	9.1264(3)	9.3405(5)	13.3386(5)	9.2942(2)	10.3086(4)
b (Å)	12.0880(4)	10.1090(3)	16.8314(11)	13.1647 (5)	9.5311 (3)	17.8125(6)
c (Å)	12.5853(5)	16.2580(5)	9.4240(5)	12.9062(5)	10.2050 (3)	16.8591(6)
α (°)	90	90	90	90	85.267(2)	90
β (°)	109.985(4)	96.589(3)	91.636(5)	92.361 (4)	84.014(2)	90.111(3)
γ (°)	90	90	90	90	78.471(2)	90
Volume (Å^3)	1371.38(10)	1490.04(8)	1480.98 (15)	2264.39(15)	879.16 (4)	3095.69(19)
Z	4	4	4	8	2	4
Calculated density (g·m^{-3})	1.221	1.249	1.194	1.309	1.436	1.507
***F*(000)**	536.0	600.0	636.0	936.0	396.0	1448.0
Reflections collected	15987	13212	23244	10429	23605	26904
Independent reflections	3335	3792	2898	2747	3090	6513
Refinement method	Full-matrix least-squares on F^2	Full-matrix least-squares on F^2	Full-matrix least-squares on F^2	Full-matrix least-squares on F^2	Full-matrix least-squares on F^2	Full-matrix least-squares on F^2
Goodness-of-fit on F^2	1.067	1.079	1.054	1.374	1.028	1.073
R$_{int}$	0.0372	0.0311	0.0567	0.0347	0.0309	0.0292

R indices (all data)	$R_1 = 0.0509$, $wR^2 = 0.1903$	$R_1 = 0.0380$, $wR^2 = 0.1004$	$R_1 = 0.0613$ $wR^2 = 0.2010$	$R_1 = 0.0721$ $wR^2 = 0.2030$	$R_1 = 0.0410$ $wR^2 = 0.1117$	$R_1 = 0.0497$ $wR^2 = 0.1377$
CCDC Number	2400926	2380077	2380076	2414316	2380341	2414328

Reference:

[1] Colling, M., Braunschweig, H. (2003) The Chemistry of Borylene Complexes. Eur. J. Inorg. Chem., 393-403. (DOI: 10.1002/ejic.200390054)

[2] Englert, U., Kollann, C., Braunschweig, H. (1998) Synthesis and Structure of the First Terminal Borylene Complexes. Angew. Chem. Int. Ed., 37, 3179-3180. (DOI: 10.1002/(SICI)1521-3773).

[3] Dahcheh, F., Martin, D., Stephan, D. W., Bertrand, G. (2014) Synthesis and Reactivity of a CAAC–Aminoborylene Adduct: A Hetero-Allene or an Organoboron Isoelectronic with Singlet Carbenes. Angew. Chem. Int. Ed., 53, 13159-13163. (DOI: 10.1002/anie.201408371)

[4] Ledet, A. D., Hudnall, T. W. (2016) Reduction of a diamidocarbene-supported borenium cation: isolation of a neutral boryl-substituted radical and a carbene-stabilized aminoborylene. Dalton Trans., 45, 9820-9826. (DOI: 10.1039/C6DT00300A)

[5] Légaré, M. N., Chabot, G. B., Dewhurst, R. D., Engels, B., Braunschweig, H. (2018) Nitrogen fixation and reduction at boron. Science, 359. 871. (DOI: 10.1126/science.aaq1684)

[6] Lin, Y. J., Liu, W. C., Liu, Y. H., Lee, G. H., Chien, S. Y., Chiu, C. W. (2022) A linear Di-coordinate boron radical cation. Nat. Commun., 13, 7051. (DOI: 10.1038/s41467-022-34900-7).

[7] Engesser, T. A., Lichtenthaler, M. R., Schleep, M., Krossing, I. (2016) Reactive p-block cations stabilized by weakly coordinating anions. Chem. Soc. Rev., 45, 789-899. (DOI: 10.1039/C5CS00672D)

[8] Sarazin, Y., Carpentier, J.-F. (2015) Discrete cationic complexes for ring-opening polymerization catalysis of cyclic esters and epoxides. Chem. Rev., 115, 3564-3614. (DOI: 10.1021/acs.chemrev.5b00033)

[9] Jung, H.-J., Cho, Y., Kim, D., Mehrkhodavandi, P. (2021) Cationic aluminum, gallium, and indium complexes in catalysis. Catal. Sci. Technol., 11, 62-91. (DOI: 10.1039/d0cy01741h)

[10] Braunschweig, H., Krummenacher, I., Légaré, M.-A., Matler, A., Radacki, K., Ye, Q. (2017) Main-group metallomimetics: Transition metal-like photolytic co substitution at boron. J. Am. Chem. Soc., 139, 1802-1805. (DOI: 10.1021/jacs.6b13047)

[11] Kölle, P., Nöth, H. (1985) The chemistry of borinium and borenium ions. Chem. Rev. 85, 399-418. (DOI: 10.1021/cr00069a004)

[12] Lambert, J. B., Zhang, S. (1999) Boron cation coordination chemistry: classification and stability. J. Am. Chem. Soc., 121, 10221–10229. (DOI: 10.1021/ja992064r)

[13] Holleman, A. F., Wiberg, E. (2001) Structural variants of boron cations and their unique chemistry. Inorg. Chem., 40, 601–605. (DOI: 10.1021/ic001234f)

[14] Erker, G., Stephan, D. W. (2010) Boron cation chemistry: insights into structure and reactivity. Chem. Soc. Rev., 39, 104–116. (DOI: 10.1039/B902325K)

[15] Lambert, J. B., Zhang, S. (1999) Three-coordinate boron cations: Structural and electronic characteristics. J. Am. Chem. Soc., 121, 10221–10229. (DOI: 10.1021/ja992064r)

[16] Reed, C. A., Crabtree, R. H. (2005) Boron cations and their reactivity: Insights into structural variations and hybridization states. Chem. Rev., 105, 1157–1194. (DOI: 10.1021/cr9801331)

[17] Tian, W.-J., Chen, W.-J., Yan. M., Li. R., Wei, Z.-H., Chen, T.-T., Chen, Q., Zhai, H.-J., Li, S.-D., Wang, L.-S. (2021) Transition-metal-like bonding behaviors of a boron atom in a boron-cluster boronyl complex $[(\eta^7\text{-}B_7)\text{-}B\text{-}BO]^-$. Chem. Sci., 12, 8157-8164. (DOI: 10.1039/D1SC00534K

[18] Braunschweig, H., Krummenacher, I., Légaré, M.-A., Matler, A., Radacki, K., Ye, Q. (2017) Main-group metallomimetics: Transition metal-like photolytic co substitution at boron. J. Am. Chem. Soc., 139, 1802-1805. (DOI: 10.1021/jacs.6b13047)

[19] Hayashi, Y., Rohde, J. J., Corey, E. J. (1996)A Novel Chiral Super-Lewis Acidic Catalyst for Enantioselective Synthesis. J. Am. Chem. Soc., 118, 5502-5503. (DOI:10.1021/ja960766s)

[20] Canales, E., Corey, E. J. (2007) Highly Enantioselective [2+2]-Cycloaddition Reactions Catalyzed by a Chiral Aluminum Bromide Complex. J. Am. Chem. Soc., 129, 12686-12687. (DOI: 10.1021/ja0765262)

[21] Bonnier, C., Piers, W. E., Parvez, M., Sorensen, T. S. (2008) Borenium cations derived from BODIPY dyes. Chem. Commun., 4593-4595. (DOI: 10.1039/B808739C)

[22] Chiu, C.-W., Gabbaï, F. (2008) Diarylborenium Cations: Synthesis, Structure, and Electrochemistry. Organometallics, 27, 1657–1659. (DOI: 10.1021/om701249n)

[23] Vedejs, E., Nguyen, T., Powell, D. R., Schrimpf, M. R. (1996) Generation of reactive borenium ions in the 2,3-benzazaborolidine series. Chem. Commun., 2721-2722. (10.1039/CC9960002721)

[24] Dureen, M. A., Lough, A., Gilbert, T. M., Stephan, D. W. (2008) B-H Activation by frustrated Lewis pairs: borenium or boryl phosphonium cation?. Chem. Commun., 4303-4305. (10.1039/B808348G)

[25] Wei, P., Atwood, D. A. (1998) Chelated Borates: Synthesis, Reactivity, and Cation Formation. Inorg. Chem., 37, 4934-4938. (DOI: 10.1021/ic971595a)

[26] Eisenberger, P., Crudden, C. M. (2017) Borocation catalysis. Dalton Trans., 46, 4874-4887 (DOI: 10.1039/C6DT04232E)

[27] Chen, C., Li, J., Daniliuc, C. G., Mück-Lichtenfeld, C., Kehr, G., Erker, G. (2020) The $[(NHC)B(H)C_6F_5]^+$ cations and their $[B](H)-CO$ borane carbonyls. Angew. Chem. Int. Ed., 59, 21460-21464 (DOI: 10.1002/anie.202009353)

[28] Tan, X., Wang, H. (2022) Recent advances in borenium catalysis. Chem. Soc. Rev., 51, 2583-2600. (DOI: 10.1039/D2CS00044J)

[29] Franz, D., Inoue, S. (2019) cationic complexes of boron and aluminum: An early 21st century viewpoint. Chem. Eur. J., 25, 2898-2926. (DOI: 10.1002/chem.201803370)

[30] Chen, C., Li, J., Daniliuc, C. G., Mück-Lichtenfeld, C., Kehr, G., Erker, G. (2020) The [(NHC)B(H)C$_6$F$_5$]$^+$ cations and their [B](H)−CO borane carbonyls. Angew. Chem. Int. Ed., 59, 21460-21464 (DOI: 10.1002/anie.202009353)

[31] Eisenberger, P., Crudden, C. M. (2017) Borocation catalysis. Dalton Trans., 46, 4874-4887 (DOI: 10.1039/C6DT04232E)

[32] Kundu, G., Ajithkumar, V. S., Raj, K. Vipin, Vanka, K., Tothadi, S., Sen, S. S. (2022) Substitution at sp^3 boron of a six-membered NHC·BH$_3$: Convenient access to a dihydroxyborenium cation. Chem. Commun., 58, 3783-3786. (DOI: 10.1039/D1CC06816D)

[33] Reed, C.A. (2010) H$^+$, CH$_3$$^+$, and R$_3Si^+$ carborane reagents: When triflates fail. Acc. Chem. Res., 43, 1, 121-128. (DOI: 10.1021/ar900159e)

[34] Swamy, V. S. V. S. N., Pal, S., Khan, S., Sen, S. S. (2015) Cations and dications of heavier group 14 elements in low oxidation states. Dalton Trans., 44, 12903-12923. (DOI: 10.1039/C5DT01912E)

[35] Großekappenberg, H., Reißmann, M., Schmidtmann, M., Müller, T. (2015) Quantitative assessment of the lewis acidity of silylium ions. Organometallics, 34, 20, 4952-4958. (DOI: 10.1021/acs.organomet.5b00556)

[36] Vidovic, D., Reeske, D., Findlater, M., Cowley, A. H. (2008) Synthesis and structures of boron dihalides supported by the C$_6$F$_5$-substituted β-diketiminate ligand [HC(CMe)$_2$(NC$_6$F$_5$)$_2$]$^-$. Dalton Trans., 17, 2293-2297. (DOI: 10.1039/B719722E)

[37] Bonnier, C., Parvez, M., Sorensen, T. S., Piers, W. E. (2008) Borenium cations derived from BODIPY dyes. Chem. Commun., 38, 4593-4595. (DOI: 10.1039/B808739C)

[38] Parveen, D. Yadav, R. K., Mondal, B., Dallon, M., Sarazin, Y., Roy, D. K. (2024) Bis (diiminate)-based boron difluoro complexes: effective synthon for bis (borenium) cations. Dalton Trans., 53, 14139-14143. (10.1039/D4DT02050B)

[39] Franz, D., Inoue, S. (2018) Cationic Complexes of Boron and Aluminum: An Early 21st Century Viewpoint. Chem. Eur. J., 25, 2898-2926 (DOI: 10.1002/chem.201803370)

[40] Narula, C. K.; Nöth, H. (1985)Competition between adduct and cation formation in reactions between diorganylborane derivatives and pyridine. Inorg. Chem., *24*, 2532-2539. (DOI: 10.1021/ic00210a014)

[41] Devillard, M., Mallet-Ladeira, S., Bouhadir, G., Bourissou, D. (2016) Diverse reactivity of borenium cations with >N–H compounds. Chem. Commun., 52, 8877-8880. (DOI: 10.1039/C6CC03183H)

[42] Chen, J., Lalancette, R. A., Jäkle, F. (2013) Synthesis and Lewis acid properties of a ferrocene-based planar-chiral borenium cation. Chem. Commun., *49*, 4893-4895. (10.1039/C3CC41556B)

[43] Cade, I. A, Ingleson, M. J. (2014) Syn-1,2-Carboboration of Alkynes with Borenium Cations. Chem. Eur. J., *20*, 12874 – 12880. (10.1002/chem.201403614)

[44] Hsu, C.-P., Liu, C.-A., Wen, C.-C., Liu,Y.-H., Chiu, C.-W. (2022) Chiral Bis(oxazoline) Ligand-Supported Alkyl Aluminum Cations. ChemCatChem., 14, e20210171. (DOI:10.1002/cctc.202101715)

[45] Lichtenberg, C. (2020) Main-Group Metal Complexes in Selective Bond Formations Through Radical Pathways. Chem. Eur. J., 26, 9674-9687. (DOI: 10.1002/chem.202000194)

[46] Hanft, A., Lichtenberg, C. (2018) New Perspectives for Aminotroponiminates: Coordination Chemistry, Redox Behavior, Cooperativity, and Catalysis. Eur. J. Inorg. Chem. 3361-3373 (DOI: 10.1002/ejic.201800465)

[47] Siwatch, R. K., Nagendran, S. (2014) Germylene cyanide complex: a reagent for the activation of aldehydes with catalytic significance.   Chem.   Eur.   J.,   20,   13551-13556.   (DOI: 10.1002/chem.201404204)

[48] Balachandra, C., Sharma, N. K. (2017) Novel fluorophores: Syntheses and photophysical studies of boron-aminotroponimines. Dyes and Pigm., 137, 532e538. (DOI: 10.1016/j.dyepig.2016.10.051)

[49] Osmialowski, B., Zakrzewska, A., Jedrzejewska, B., Grabarz, A., Zalesny, R., Bartkowiak, W., Kolehmainen, E. (2015) Influence of Substituent and Benzoannulation on Photophysical Properties of 1-

Benzoylmethyleneisoquinoline Difluoroborates. J. Org. Chem., *80,* 2072-2080. (DOI: 10.1021/jo502244j)

[50] Solovyev, A., Geib, S. J., Lacote, E., Curran, D. P. (2012) Reactions of boron-substituted N-heterocyclic carbene boranes with triflic acid. Isolation of a new dihydroxyborenium cation. Organometallics, 31, 54-56. (DOI: 10.1021/om201260b)

[51] Kundu, G., Balayan, K., Tothadi, S., Sen, S. S. (2022) Six-Membered Saturated NHC-Stabilized Borenium Cations: Isolation of a Cationic Analogue of Borinic Acid. Inorg. Chem., 61, 12991-12997. (10.1021/acs.inorgchem.2c00611)

[52] Koner, A., Sergeieva, T., Morgenstern, B., Andrada, D. M. (2021) A Cyclic Iminoborane-NHC Adduct: Synthesis, Reactivity, and Bonding Analysis. Inorg. Chem., 60, 14202-14211. (DOI: 10.1021/acs.inorgchem.1c01583)

[53] Wojnowski, T., Ordyszewska, A., Halenka, H., Anusiewicz, I., Chojnacki, J., Laskowska, K. K., Grubba, R. (2025) Activation of small molecules by ambiphilic NHC-stabilized phosphinoborenium cation: formation of boreniums with B–O–C, B–O–B, and B–O–P structural motifs. Dalton Trans., 54, 290-297. (DOI: 10.1039/D4DT02656J)

[54] Belcher, W. J., Hodgson, M. C., Sumida, K., Torvisco, A., Senge, K. R., Ware, D. C., Boyd, P. D. W., Brothers, P. J. (2008) Porphyrin complexes containing coordinated BOB groups: synthesis, chemical reactivity and the structure of [BOB (tpClpp)]$^{2+.}$ Dalton Trans.,12, 1602-1614. (DOI: 10.1039/B716189A)

[55] Frisch, M. J., Trucks, G. W., Schlegel, H. B., Scuseria, G. E., Robb, M. A., Cheeseman, J. R., Scalmani, G., Barone, V., Mennucci, B., Petersson, G. A., Nakatsuji, H. Caricato, M. Li, X., Hratchian, H. P., Izmaylov, A. F., Bloino, J., Zheng, G., Sonnenberg, J. L., Hada, M.; Ehara, M., Toyota, K., Fukuda, R., Hasegawa, J., Ishida, M., Nakajima, T., Honda, Y., Kitao, O., Nakai, H., Vreven, T., Montgomery Jr., J. A., Peralta, J. E., Ogliaro, F., Bearpark, M., Heyd, J. J., Brothers, E., Kudin, K. N., Staroverov, V. N., Kobayashi, R., Normand, J., Raghavachari, K., Rendell, A., Burant, J. C., Iyengar, S. S., Tomasi, J., Cossi, M., Rega, N.,

Millam, J. M., Klene, M., Knox, J. E., Cross, J. B., Bakken, V., Adamo, C., Jaramillo, J., Gomperts, R., Stratmann, R. E., Yazyev, O., Austin, A. J., Cammi, R., Pomelli, C., Ochterski, J. W., Martin, R. L., Morokuma, K., Zakrzewski, V. G., Voth, G. A., Salvador, P., Dannenberg, J. J., Dapprich, S., Daniels, A. D., Farkas, Ö., Foresman, J. B., Ortiz, J. V., Cioslowski, J., Fox, D. J. (2013) Gaussian 09, Revision E.01; Gaussian, Inc., Wallingford CT.

[56] Becke, A. D. (1993) Density-functional thermochemistry. III. The role of exact exchange. J. Chem. Phys., 98, 5648-5652. (DOI: 10.1063/1.464913)

[57] Lee, C., Yang, W. Parr, R. G. (1988) Development of the Colle-Salvetti correlation-energy formula into a functional of the electron density. Phys. Rev. B, 37, 785-789. (DOI: 10.1103/PhysRevB.37.785)

[58] Vosko, S. H., Wilk, L., Nusair, M. (1980) Accurate spin-dependent electron liquid correlation energies for local spin density calculations: a critical analysis. Can. J. Phys., 58, 1200-1211. (DOI: 10.1139/p80-159)

[59] Stephens, P. J., Devlin, F. J., Chabalowski, C. F., Frisch, M. J. (1994) Ab initio calculation of vibrational absorption and circular dichroism spectra using density functional force fields. J. Phys. Chem., 98, 11623-11627. (DOI: 10.1021/j100096a001)

[60] Dunning, T. H. Jr. (1989) Gaussian basis sets for use in correlated molecular calculations. I. The atoms boron through neon and hydrogen. J. Chem. Phys., 90, 1007-1023. (DOI: 10.1063/1.456153)

[61] Weinhold, F., Landis, C. R. (2005) Valency and bonding: A natural bond orbital donor-acceptor perspective, Cambridge University Press, Cambridge, U.K, (DOI: 10.1017/CBO9780511614569)

[62] Reed, A. E., Curtiss, L. A., Weinhold, F. (1988) Intermolecular interactions from a natural bond orbital, donor-acceptor viewpoint. Chem. Rev., 88, 899-926. (DOI: 10.1021/cr00088a005)

[63] Glendening, E. D., Badenhoop, J. K., Reed, A. E., Carpenter, J. E., Bohmann, J. A., Morales, C. M., Landis, C. R., Weinhold, F. (2013) NBO 6.0. (Theoretical Chemistry Institute, University of Wisconsin, Madison, WI).

[64] Yanai, T., Tew, D., Handy, N. (2004) A new hybrid exchange–correlation functional using the Coulomb-attenuating method (CAM-B3LYP). Chem. Phys. Lett., 393, 51-57. (DOI: 10.1016/j.cplett.2004.06.011)

[65] Chai, J.-D., Head-Gordon, M. (2008) Long-range corrected hybrid density functionals with damped atom–atom dispersion corrections. J. Chem. Phys., 128, 084106.

[66] Marenich, A. V., Cramer, C. J., Truhlar, D. G. (2009) Universal solvation model based on solute electron density and on a continuum model of the solvent defined by the bulk dielectric constant and atomic surface tensions. J. Phys. Chem. B, 113, 6378-6396. (DOI: 10.1021/jp810292n)

[67] London, F. (1937) Théorie quantique des courants interatomiques dans les combinaisons aromatiques. J. Phys. Radium. 8, 397-409. (DOI: 10.1051/jphysrad:01937008010039700)

[68] McWeeny, R. (1962) Perturbation theory for the fock-dirac density matrix. Phys. Rev., 126, 1028. (DOI: 10.1103/PhysRev.. 126.1028)

[68] Dolomanov, O. V., Bourhis, L. J., Gildea, R. J., Howard J. A. K., Puschmann, H. (2009) OLEX2: A complete structure solution, refinement and analysis program. J. Appl. Cryst., 42, 339-341. (DOI: 10.1107/S0021889808042726)

[69] Sheldrick, G. M. (2015) SHELXT– Integrated space-group and crystalstructure determination. Acta Cryst., A71, 3-8. (DOI: 10.1107/S2053273314026370)

[70] Sheldrick, G. M. (2015) Crystal structure refinement with SHELXL. Acta Cryst., C71, 3-8. (DOI: 10.1107/S2053229614024218)

Chapter 5

Synthesis of N-heterocyclic olefin borane adducts, and their reactivity with N-triflates and diacids
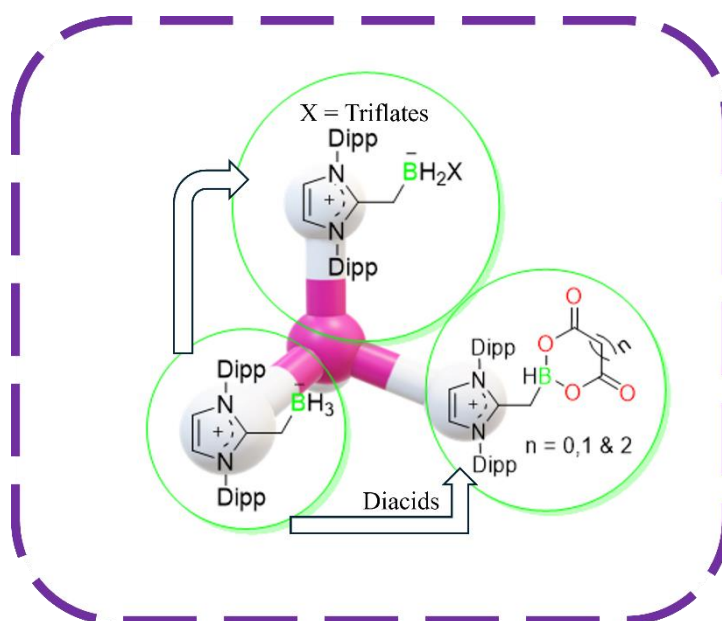
5.1 Introduction

N-heterocyclic carbenes (NHCs) a neutral carbon donor ligands and strong σ donors and weak π-acceptors. Later on, Ardungo and his co-workers reported another class of N-heterocyclic carbene, which is known as cyclic alkyl amino carbenes (CAACs). These carbenes have strong σ donor properties and better π-accepting ability than the classical carbenes. CAACs and NHCs chemistry is well explored in stabilization, low-valent, and as well as cationic complexes of (semi)metals across the periodic table. N-Heterocyclic olefins (NHOs), represent themself as comparatively young and emerging carbon-based donor ligand, and their characteristics and properties are similar to their well-known N-heterocyclic carbene counterparts.*[1-10]* N–N-Heterocyclic olefins (NHOs) can be defined as a class of simple molecules that possess an alkylidene moiety incorporated at the terminal position on a heterocyclic carbine scaffolding. *[11,12]* This architecture induced the polarization in the exocyclic C=C double bond and increased the nucleophilicity at the ylidic carbon atom. *[13,14]* The term NHO was coined in the chemical community in 2011, pioneering work started by Kunh and his co-workers since 1993, and they developed the general synthetic route for the carbon-based nucleophile ImMe$_4$=CH$_2$ (ImMe$_4$ = MeCNMe)$_2$C). *[15]* Beller and his co-workers synthesized sterically encumbered NHOs in situ and used those species for the isolation of cationic phosphine ligands such as [IPr-CH$_2$-PR$_2$ (I)] (IPr = (HCNDipp)$_2$C; Dipp = iPr$_2$C$_6$H$_3$; R = Cy, ^{t}Bu, and Ph); the resulting complexes were active and recoverable catalysts for C-N, C-C, and C-C bond formation reactions. *[16,17]*
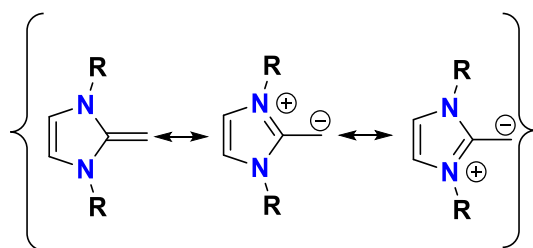

Figure 5.1 Resonating structure of N-heterocyclic olefin.

N-heterocyclic olefins exhibited similar coordination patterns such as phosphenes and their counterparts, N-heterocyclic carbenes. N-heterocyclic olefins are considered soft donor ligands compared to the NHCs because they have highly polarized exocyclic olefinic (C=C) double bonds, which receive the electron density from the nitrogen atoms present in the imidazole rings. NHO-based organo-catalysts are used in various catalytic transformations and effectively activate small molecules like CO_2, CO, O_2, N_2O, and CS_2. *[18-21]* Lu and co-workers have demonstrated a simple and practical procedure for synthesizing numerous NHO-CO_2 adducts from known structures of N-heterocyclic olefins in good yields up to 87 %. Due to this, NHOs might exhibit more affinity towards the metals that are present in low oxidation states, such as Ni(0), Pd(0), and group 14 elements present in the second oxidation state. *[22-23]* The electronic and steric properties are inherently tunable (procurable by either methylene carbon or in the ring) and might be utilized to advance both transition metal and main group element-based catalysis. Eric Reward and his co-workers reported the dihydride complex of group 14 elements in low oxidation states, GeH_2 and SnH_2 stabilized by the NHO ($IPrCH_2=[(HCNDipp)_2C=CH2]$; Dipp = 2,6-$iPr_2C_6H_3$). *[24]* They tried to isolate the EH_2 complexes (E = Ge and Sn) with widely utilized phosphine donors, but they failed to isolate the dihydride complexes of Ge and Sn. This signifies that NHOs are superior ligands to the traditional donors. E. Revard and others have been potentially preparing the NHOs and utilizing them in the isolation of electron-deficient main group species and their application in the activation of small molecules and various organic transformation reactions.*[25-27]*

In the recent couple of decades, electron-deficient species of main group elements, especially group 13 and 14, have been diligently considered as possible candidates for this role. The main issues hindering the practical use of the main group low valent species are not have more than one oxidation state, and they are unstable in low valent states. In this context, NHOs play a crucial role in the stabilization of low-valent

species across the periodic table. *[28-30]* Chiu and Ghadwal group explored the chemistry of boron dications supported by the NHOs [IPrCH$_2$.H$_2$B(miu-H)BH$_2$.IPrCH$_2$]+ and Cp*-substituted boron dications [IPrCH$_2$.BCp*]$^{2+}$. By following a similar protocol, Eric Revard and his co-workers reported the first base-free germylene supported by the NHO ligands. They treated NHO.GeCl$_2$ adduct with KC8 facilitates the sterically encumbered germylene. *[21]*
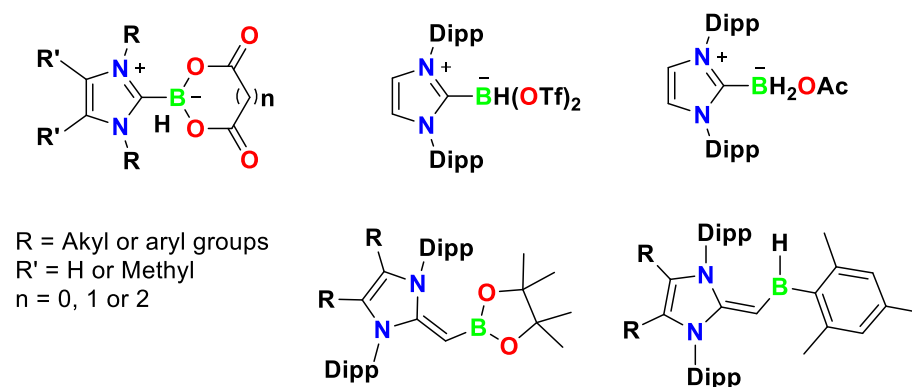

Figure 5.2 Previously reported boroxilates and NHO-boranes.

Although NHOs are strong donor ligands but their chemistry with boron derivatives is less explored in comparison to the NHC-borane counterparts. NHC-borane, an adduct of N-heterocyclic carbenes and boranes, is a versatile reagent and catalyst in organic synthesis, acting as a hydrogen donor source, in photopolymerization, radical reactions, as a reducing agent, and as a source of surface ligands in nanoparticle chemistry. *[32-34]* In recent years, N-heterocyclic olefins, strongly polarized, nucleophilic alkenes, have found a new role in small molecule activation, including CO$_2$ as organocatalysts, ligands for transition metals, as well as in main group elements. The most significant applications of NHOs are polymerization initiators or catalysts, either themselves or as frustrated Lewis pairs (FLPs), that are suited for the ring-opening polymerization (ROP) of worthwhile sourced lactones to yield biodegradable polyhydroxyalkanoates (PHAs).

Herein, we successfully synthesized the NHO-borane complex and treated it with the various diacids such as oxalic, malonic, phthalic, and glutaric acids, facilitating NHO-boryl oxalates. Further, all NHO-boryl

oxalates were characterized by various spectroscopic techniques, along with high-resolution mass spectrometry (HRMS). Moreover, we explore the reactivity of the NHO-borane complex with nitrogen-based triflate reagents. The formation of substituted NHO-boryl triflate complexes **6t** and **7t** highlights the versatility of the NHO-borane scaffolds provide diverse functionalization routes for the synthesis of NHO-stabilized boron-based reagents.

5.2 Results and Discussion

5.2.1 Synthesis and characterization NHO-boryl-oxalates

Boranes exhibit Lewis acidity, due to the electron deficiency of the B atom, which readily accepts electron pairs from the donors to form a Lewis acid−base adduct. Taking advantage of this inherent borane chemistry has been well exploited as a neutral Lewis acid and utilized in hydroboration reactions of alkenes and alkynes. In 2008, Curran and his co-workers reported the N-heterocyclic corbene (NHC)-borane adduct, a new class of radical hydrogen atom donor source for the synthesis of hydrocarbons from the xanthates. *[36]* Notably, the rate of radical hydrogen atom transfer observed in this study is significantly enhanced compared to the earlier findings reported by Robert and co-workers involving amine-boranes and phosphine-boranes. NHC-borane adducts based reagents have witnessed tremendous development and reduced the various functional groups, such as carbonyls and amine derivatives. NHC-boaranes are good precursors of boryl anion synthesis and are involved in various reactions leading to the formation of boracycles. Based on the previous reports, we conceptualized that NHOs are stronger σ donor ligands than the amines and phosphine ligands. Due to this, NHOs tend to transfer their electron density to the vacant orbital of the BH_3 unit and make more hydridic in nature of B-H bond which may provide an alternative source of hydrogen donor for various applications. Furthermore, this reactivity may enable the formation of various boron-containing oxalate derivatives upon treatment with diacids. To achieve our goal, we synthesized the N-heterocyclic olefin (NHO) by following the previously reported protocols. N-heterocyclic

carbene (NHC) is treated with the (chloromethyl)trimethyl silane to give N-heterocyclic olefin and it is characterized by various spectroscopic techniques. In ^{1}H NMR, a singlet signal appears at (2.5 ppm) for the 2H proton, which is attached to the exocyclic carbon, and also supported by the ^{13}C NMR, a peak appears at (30 ppm), which is consistent with the exocyclic carbon of the N-heterocyclic ring. Furthermore, NHO was treated with (BH$_3$·SMe$_2$) to facilitate the N-heterocyclic olefine borane conjugate. Further, it is characterized by the ^{1}H, ^{13}C NMR along with the heteronuclear NMR. In ^{1}H NMR, a quartet signal for exocyclic -CH$_2$- proton appeared at (2H, 2.09 ppm) due to the presence of B atom (I = 3/2). In ^{11}B NMR, a quartet signal is observed at (30.32 ppm), which indicates the tetra-coordinate nature of the boron center.
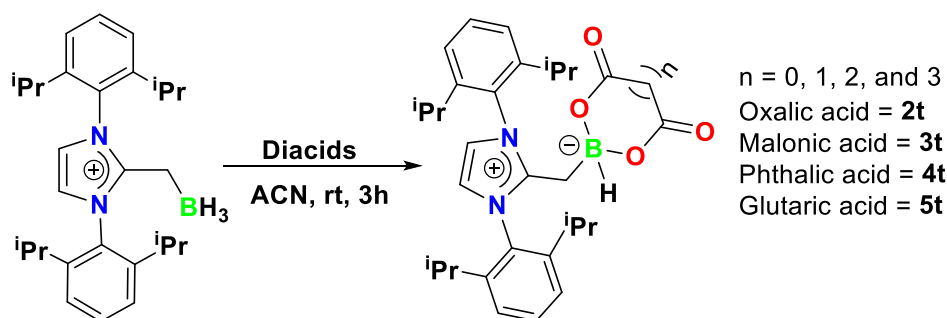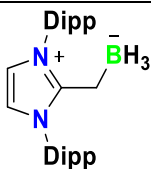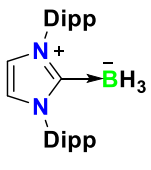

Scheme 5.1 General procedure of NHO-boryl oxalate synthesis.

For the synthesis of NHO boryl oxalate, we followed the well-stabilized NHCs-boryl oxalates procedures, diacids (oxalic, malonic, and phthalic acid) treated with NHO-borane adduct in acetonitrile and heated the reaction mixture at 80°C for 3h, but we were unable to isolate analytically pure products or obtain the mixture of products.

Further, we changed our synthetic approach after several unsuccessful attempts. Oxalic acid is treated with NHO-borane at room temperature overnight; surprisingly, the product is isolated with a good yield of 60%. NHO-boryl oxalate was characterized by ^{1}H, ^{13}C NMR, heteronuclear NMR, and high-resolution mass spectrometry. In ^{1}H NMR, a doublet signal appeared at (2.5 ppm), for the -CH2- unit olefin, which is comparatively downfield (0.30 ppm) than the NHO-borane. In ^{13}C

NMR, signals appeared slightly deshielded from the parent N-heterocyclic olefin borane complex.

Table 5.1 Reactivity comparison of NHO-Borane and NHC-borane with diacids.

S.N.	Diacids	Room Temp.	80°C
Dipp N+ BH3 N Dipp	Oxalic, malonic, glutaric	Good Yield	Not isolated
Dipp N+ →BH3 N Dipp	Oxalic, malonic, glutaric	Not isolated	Good Yield

 In the heteronuclear NMR ^{11}B spectrum of isolated oxalate showed a doublet was observed at 2.2 ppm, for the tentatively attributed to the NHO-boryl oxalate **2t**. In high-resolution mass spectrometry, the experimental value of the compound (mass) matches the calculated values of NHO-boryl oxalate of malonic acid. Curran and coworkers isolated several NHC-boryl ketones, and their ^{11}B NMR chemical shifts are close to our findings. Furthermore, his group also synthesized NHC-boryl oxalates of various acids (oxalic, malonic, glutaric, phthalic, and 2-hydroxybenzoic acid), We found that the ^{11}B chemical shift value of NHC-boryl is close to the Curran and coworkers' observations. This result is key to ensuring that we get our desired oxalate compound formations. We try to grow crystals for single-crystal structure analysis, but our several attempts are unsuccessful due to sensitivity issues.

The initial results of the modified synthetic protocol motivated us to test the reactivity of the NHO-borane adduct with various kinds of diacids having pKa values close to that of oxalic acid (malonic acid pKa = 2.83, phthalic acid pKa = 5.51). Treatment of complex **1t** with diacids in a ratio of 1:1 in acetonitrile afforded the respective NHO-boryl oxalates in good yields. The ^{11}B NMR of complexes (**3t** - **5t**) exhibits resonance at 1.5 and 1.3 ppm, and this reflects a tetracoordinate environment

around the boron center. In ^{11}B NMR of complex **3t-5t t** we observed that the signal appeared in a slightly shielded region in comparison to the five-membered NHO-boryl oxalate. This is due to the lower ring strain in the case of six-membered NHO-boryl oxalares.
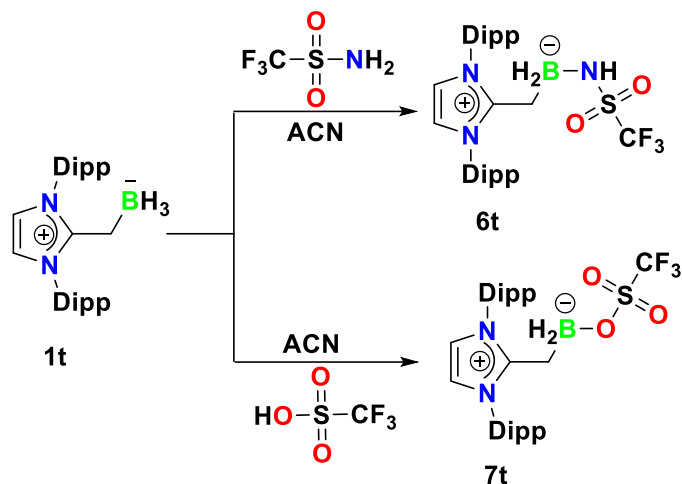
Scheme 5.2 General procedure for the synthesis of complexes **6t** and **7t**.

NHC-boranes are weak bases like traditional adducts with ammonia boranes and phosphine boranes so NHC-boranes do not react with weak acids like acetic acid at room temperature or elevated temperature, so they appear to be a weaker base than borohydrides. Later on, Solovyev and Lindsay NHC-boranes react with strong acids having pKa values ranging from 1-2 to give the substituted products. These kinds of reactions are very crucial for making less reactive NHC-borane to more active NHC-borane reagents. NHC-borane gave the three different types of substituted products on treatment with the trifluoromethanesufonic acid. It is known that NHC-borane treated with trifluoromethanesulfonic acid in a ratio of (1:1, 1:2.5, and 1:5) facilitates the monotrifluoformate NHC-BH$_2$(OTf), ditrifluoromethane-sulfonate NHC-BH(OTF)$_2$, and tritrifluoromethane-sulfonate NHC-B(OTf)$_3$, respectively. NHC-boranes reacted with various halogenating reagents such as (NIS) Niodosuccinimide, (NBS) N-bromosuccinimide, bromine, and iodine, resulting products were mono- and trisubstituted NHC-boranes that were isolated. Getting motivation from the previous acid-base type of reaction of NHC-boranes, we also tested the reactivity of NHO-borane

with strong acids, trifluoromethanesulfonamide, and triflic acid. We treated both acids with NHO-borane (**1t**) complex at room temperature in acetonitrile in the ratio of 1:1 afforded the NHO-borane complexes **6t** and **7t,** respectively. The reaction between NHO-borane, sulfonimide, and sulfonamide is very similar to its counterpart, NHC-borane acid-base type reactions in terms of fundamental mechanism. Complexes **6t** and **7t** are well characterized by ^{1}HNMR and ^{13}CNMR, along with heteronuclear NMR including ^{11}B and ^{19}FNMR. Respectively. In the ^{11}B NMR spectrum, the disappearance of the (30 ppm) quartet signal and the appearance of new signals at 29.57 and 29.87 ppm indicated the formation of triflate-substituted NHO-boryl complexes **6t** and **7t,** respectively. The [11]B chemical shift suggests the formation of a tricoordinated borane complex instead of a tetracoordinated boron complex. The tricoordinated environment around the boron atom is also supported by the ^{19}FNMR. ^{19}FNMR signals appear at 78.81 ppm and 78.67 ppm, respectively, which indicates that the triflate groups are present as a counter anion. Previous studies support our findings. Notably, D. Lindsay and co-workers reported NHC-stabilized borenium cations, wherein the cationic boron center *[37,38]* was paired with a triflate counteranion; they found a chemical shift in 19F NMR of 78.9 ppm, while in the case where triflate was bound covalently, it appeared at 76.68 ppm. Complexes **6t** and **7t** are highly air sensitive in comparison to the NHO-boryl oxalates. We attempted to obtain single crystals of all the synthesized NHO–borane complexes; however, repeated efforts were unsuccessful. Within three days, the solutions consistently transformed into a gel-like (jelly) material, preventing the nucleations.

5.3   Conclusion

In summary, we have successfully synthesized N-heterocyclic olefin borane adducts. Further, we treated the NHO-borane adduct with various diacids, leading to the formation of NHO-boryl oxalates with good yields at ambient temperature. All the boroxilates were characterized by the ^{1}HNMR, ^{13}CNMR, and heteronuclear NMR along with the high-

resolution mass spectroscopy. Moreover, we tested the reactivity of NHO-borane with N-based triflates. Interestingly, they facilitate the mono-substituted NHO-boryl triflate complexes, and further, they are characterized by various spectroscopy techniques. The B–H bond enthalpy in NHO–borane adducts is lower than that in the corresponding amine- and phosphine–borane complexes, owing to the strong σ-donating ability of NHOs. This enhanced σ-donation weakens the B–H bond, potentially making NHO–boryl oxalates promising candidates as hydrogen donor reagents

5.4 Experimental Section

General Methods

The reactions were performed either under an atmosphere of argon using standard Schlenk techniques or in the open air. Chemicals were purchased from Spectrochem, Sigma-Aldrich, and TCI and used as received. All the solvents were purified by distillation using the appropriate drying agents, deoxygenated using three freeze–pump–thaw cycles, and stored over molecular sieves under dry argon before use. The deuterated solvents used for NMR spectroscopy were deoxygenated by freeze–pump–thaw cycles and stored under an argon atmosphere over molecular sieves. NMR chemical shifts are reported in ppm and coupling constants in Hz. ^{1}H, ^{11}B, ^{13}C, and ^{19}F NMR spectroscopy data were obtained at ambient temperature using a Bruker 500 NMR spectrometer (operating at 500 MHz for ^{1}H, 126 MHz for ^{13}C, 160 MHz for ^{11}B and 471 MHz for ^{19}F). ^{1}H NMR spectra were referenced via residual proton resonances of CDCl$_3$ (^{1}H, 7.26 ppm) and ^{13}C NMR spectra were referenced to CDCl$_3$ (^{13}C, 77.16 ppm) and BF$_3$·OEt$_2$ used as an internal standard used for ^{11}B. HRMS spectrum was obtained by Bruker micrOTOF-Q II Daltonik.

Synthetic Details

General Synthesis of N-heterocyclic olefin

In a Schlenk tube, 1,3-bis(2,6-diisopropylphenyl)-1H-imidazol-3-ium-2-ide (2 g, 3.86 mmol, 1 eq.) dissolved in toluene was reacted with

trimethylsilyl methyl chloride (2.58 ml, 18.50 mmol, 4.79 eq.). After stirring for seven days, a minor residue formed, and the mixture was filtered through a Celite pad. The filtrate was then concentrated under a vacuum to afford the product.

¹H NMR (500 MHz, C_6D_6) δ 7.24 (dd, J = 8.5, 6.9 Hz, 2H), 7.17 (s, 4H), 5.86 (s, 2H), 3.37 (hept, J = 6.9 Hz, 4H), 2.44 (s, 2H), 1.38 (d, J = 6.9 Hz, 12H), 1.23 (d, J = 6.9 Hz, 12H). **¹³C NMR** (126 MHz, C_6D_6) δ 149.01, 134.99, 129.34, 124.60, 114.71, 28.78, 24.36, 23.91. **HRMS (ESI)** calculated for [$C_{28}H_{38}N_2$+H⁺] 524.4293 ($C_{28}H_{38}N_2$, found 524.4305. **Yield**: 66%

General procedure for synthesis of NHO-borane adducts (1T)

In a Schlenk tube, Borane dimethylsulfide (0.35ml, 3.6 mmol, 1.5 eq.) was added to a hexane solution of compound 2-methylene-2,3-dihydro-1H-imidazole (1 g, 2.4 mmol, 1 eq.). The mixture was allowed to stir at room temperature for three hours. Upon completion of the reaction, the mixture was filtered through a filter cannula, resulting in a white solid

¹H NMR (500 MHz, C6D6) δ 7.22 (t, J = 7.8 Hz, 2H), 7.08 (d, J = 7.8 Hz, 4H), 6.33 (s, 2H), 2.90 (hept, J = 6.8 Hz, 4H), 2.08 (q, J = 5.8 Hz, 2H), 1.32 (d, J = 6.8 Hz, 12H), 0.99 (d, J = 6.9 Hz, 12H). **¹³C NMR** δ 165.04, 146.05, 131.09, 124.69, 120.92, 29.03, 25.89, 22.82. **¹¹B NMR** (160 MHz, C_6D_6) δ 1.55, -30.50 (dd, J = 80.0, 54.6 Hz). **HRMS (ESI)** calculated for [$C_{28}H_{41}BN_2$-H⁺] 415.3289($C_{28}H_{41}BN_2$-H⁺) found 415.328. **Yield:** 76%

General procedure of NHO-boryl-oxalate synthesis

The NHO·BH₃ adduct (1 eq.) was dissolved in acetonitrile in a Schlenk tube, and diacids (1eq.) were introduced under a continuous flow of argon gas, and the mixture was stirred for three hours under an argon atmosphere. After the reaction time, the mixture was allowed to cool to room temperature. The solvent was removed under reduced pressure, and the residue was washed with hexane, yielding the white solid product

Complex 2t (Oxalic acid)

Complex **2t** was prepared by using **1t** (0.070 g, 0.16 mmol) and oxalic acid (0.015 g, 0.16 mmol)

^{1}H NMR (500 MHz, CDCl$_3$) δ 7.83 (s, 2H), 7.52 (t, J = 7.8 Hz, 2H), 7.29 (d, J = 7.8 Hz, 4H), 2.20 (hept, J = 7.7, 6.9 Hz, 4H), 2.01 (s, 3H), 1.16 (d, J = 6.8 Hz, 12H), 1.09 (d, J = 6.9 Hz, 12H). **^{13}C NMR** (126 MHz, CDCl$_3$) δ 162.08, 159.02, 145.39, 145.13, 132.75, 129.12, 125.76, 125.56, 29.30, 24.64, 23.50, 10.88. **^{11}B NMR** (160 MHz, CDCl3) δ 9.54, 7.57, 5.19, 4.79. **HRMS (ESI)** calculated for [C$_{30}$H$_{39}$N$_2$BO$_4$+H$^+$] 503.3081 [C$_{30}$H$_{39}$N$_2$BO$_4$+H$^+$] found: 503.3113. **Yield:** 60%

Complex 3t (malonic acid)

Complex **3t** was prepared by using **1t** (100 mg, 0.24 mmol) and malonic acid (0.025 g, 0.24 mmol)

^{1}H NMR (500 MHz, CDCl$_3$) δ 8.13 – 8.04 (m, 2H), 7.68 – 7.58 (m, 2H), 7.54 (q, J = 7.4, 6.9 Hz, 1H), 7.40 (d, J = 7.7 Hz, 4H), 2.30 (hept, J = 7.2 Hz, 4H), 2.10 (d, J = 2.3 Hz, 3H), 1.27 (d, J = 6.7 Hz, 13H), 1.19 (d, J = 6.9 Hz, 12H). **^{13}C{^{1}H} NMR** (126 MHz, CDCl3) δ 173.52, 144.82, 132.47, 128.90, 125.74, 125.28, 125.26, 124.71, 38.29, 29.05, 24.36, 23.21, 10.60. **^{11}B{^{1}H} NMR** (160 MHz, CDCl$_3$) δ 3.34 (d, J = 97.1 Hz).

Complex 4t (phthalic acid)

Complex **4t** was prepared by using **1t** (0.180 g, 0.43 mmol) and pathalic acid (0.070 g, 0.43 mmol)

^{1}H NMR (500 MHz, CDCl$_3$) δ 8.26 (dt, J = 7.8, 3.9 Hz, 1H), 8.06 (s, 1H), 7.78 (dd, J = 5.8, 3.4 Hz, 1H), 7.58 (t, J = 7.8 Hz, 1H), 7.50 (t, J = 7.8 Hz, 1H), 7.45 (dd, J = 6.0, 3.4 Hz, 1H), 7.42 – 7.38 (m, 1H), 7.36 (d, J = 7.8 Hz, 2H), 7.29 (d, J = 7.9 Hz, 2H), 7.12 (s, 1H), 2.64 (hept, J = 6.8 Hz, 2H), 2.28 (hept, J = 6.9 Hz, 2H), 1.98 (s, 2H), 1.23 (dd, J = 6.8, 3.5 Hz, 12H), 1.15 (dd, J = 10.1, 6.9 Hz, 12H). **^{13}C{^{1}H} NMR** (126 MHz, CDCl$_3$) δ 170.67, 170.61, 157.78, 145.83, 145.03, 133.84, 133.53, 133.10, 132.71, 131.73, 131.06, 131.00, 130.86, 130.82, 130.77, 129.10, 125.94, 125.49, 124.95, 122.45, 29.27, 28.92, 25.99, 24.56, 23.44, 22.77, 10.84. **^{11}B{^{1}H} NMR** (160 MHz, CDCl$_3$) δ 2.12 (d, J = 31.8 Hz).

Complex 5t (glutaric acid)

Complex **5t** was prepared by using **1t** (0.100 g, 0.24 mmol) and glutaric acid (0.032 g, 0.24 mmol)

^{1}H NMR (500 MHz, CDCl3) δ 7.97 (s, 2H), 7.60 (t, J = 7.8 Hz, 2H), 7.42 – 7.33 (m, 4H), 4.64 – 3.99 (m, 3H), 2.34 – 2.21 (m, 4H), 1.99 (s, 2H), 1.25 (d, J = 6.7 Hz, 12H), 1.16 (d, J = 6.9 Hz, 13H). **^{13}C{^{1}H} NMR** (126 MHz, CDCl$_3$) δ 177.99, 145.64, 145.10, 132.72, 129.22, 126.22, 125.53, 124.79, 35.57, 29.32, 25.83, 25.79, 25.69, 24.62, 23.51, 21.62. **^{11}B NMR** (160 MHz, CDCl$_3$) δ 1.31.

General procedure for NHO-boryl synthesis (6t and 7t)

The NHO–borane complex was subjected to evacuation under high vacuum for 30 minutes to ensure the removal of residual volatiles and moisture. Subsequently, anhydrous acetonitrile was added to the flask under an inert atmosphere, and the resulting solution was stirred briefly to ensure complete dissolution. Nitrogen-based triflate reagents were then introduced dropwise at room temperature, and the reaction mixture was stirred continuously for an additional 3 hours. Upon completion of the reaction, all volatiles were removed under reduced pressure. The resulting residue was washed with hexane to afford the desired substituted NHO–boryl complex as an off-white solid.

Complex 6t

^{1}H NMR (500 MHz, CDCl$_3$) δ 8.89 (s, 1H), 7.56 (dt, J = 26.8, 7.7 Hz, 2H), 7.34 (dd, J = 20.7, 7.9 Hz, 4H), 7.20 (s, 1H), 2.41 (p, J = 6.8 Hz, 3H), 2.21 (p, J = 6.8 Hz, 1H), 2.06 (s, 2H), 1.21 (t, J = 6.9 Hz, 12H), 1.13 (dd, J = 21.1, 6.9 Hz, 12H). **^{11}B NMR** (160 MHz, CDCl$_3$) δ 29.54.**^{19}F NMR** (471 MHz, CDCl$_3$) δ -78.67. **Yield:** 65%

Complex 7t

^{1}H NMR (500 MHz, CDCl$_3$) δ 7.59 (t, J = 7.8 Hz, 2H), 7.38 (d, J = 7.9 Hz, 4H), 7.23 (s, 2H), 2.50 – 2.39 (m, 4H), 2.15 (s, 2H), 1.27 (d, J = 6.7

Hz, 12H), 1.16 (d, J = 6.8 Hz, 12H). **^{11}B NMR** (160 MHz, CDCl$_3$) δ 29.16. **^{19}F NMR** (471 MHz, CDCl$_3$) δ -78.81.

Spectroscopic details of Ligands and Complexes
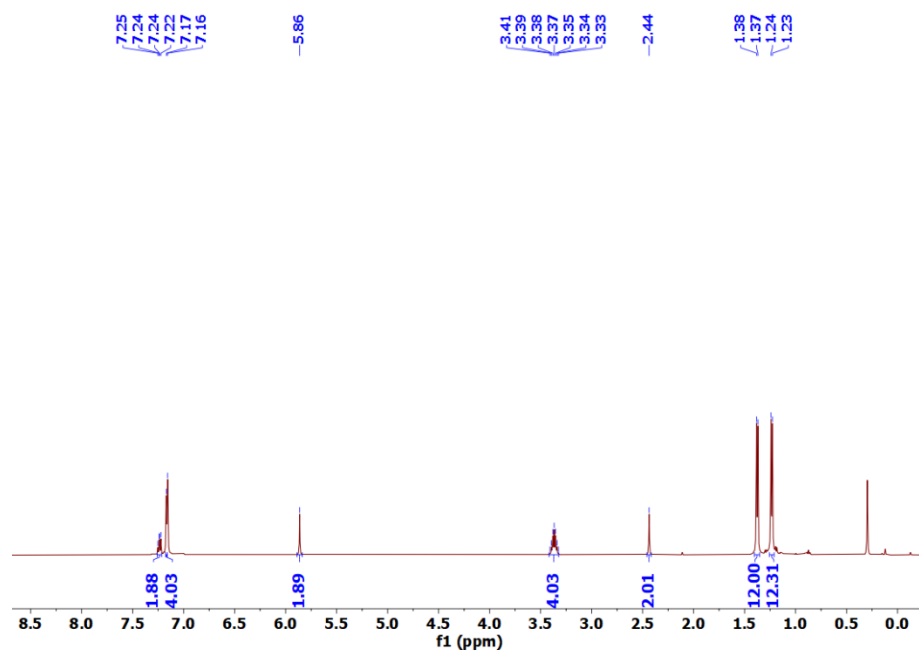
Figure 5.3 ^{1}HNMR of NHO.
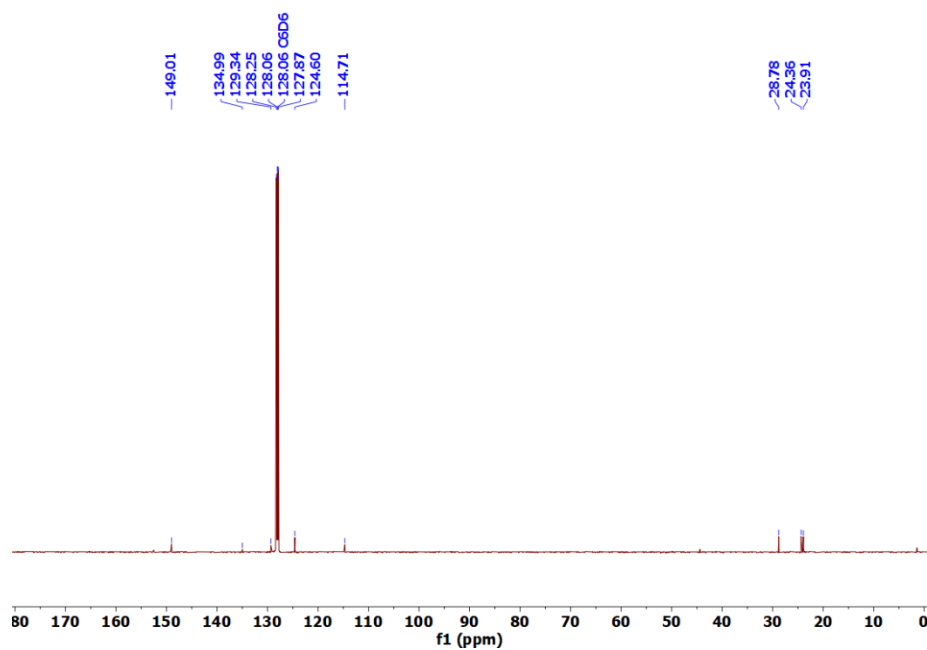
Figure 5.4 ^{13}C{^{1}H}NMR of NHO.
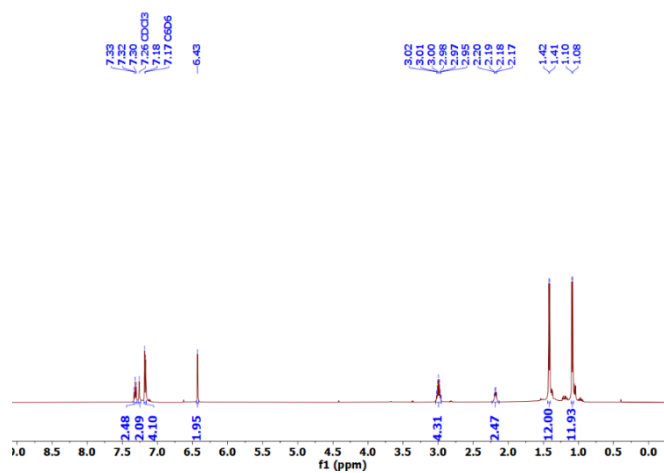
Figure 5.5 ^{1}HNMR of 1t.
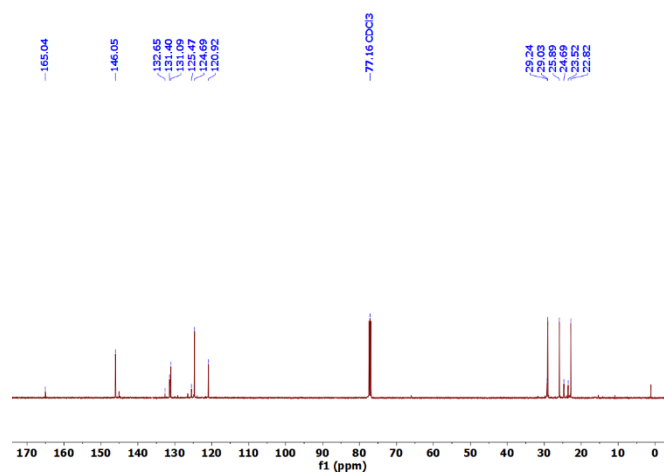
Figure 5.6 ^{13}C{^{1}H}NMR of 1t.
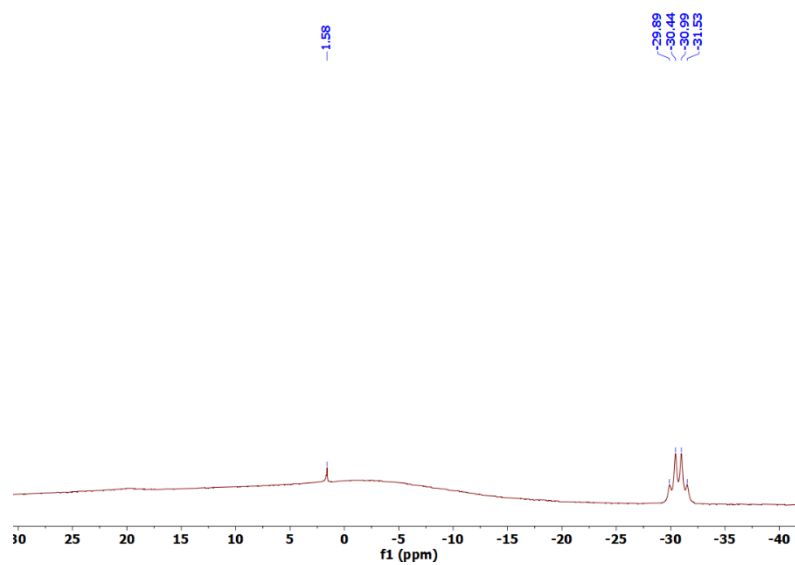
Figure 5.7 ^{11}BNMR of **1t**.
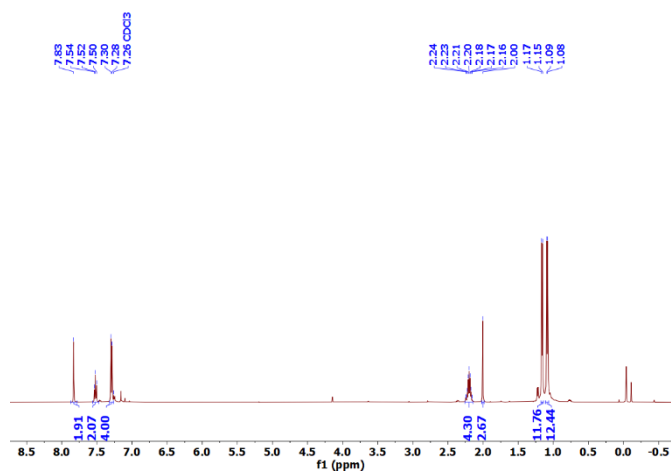
Figure 5.8 ^{1}HNMR of **2t**.
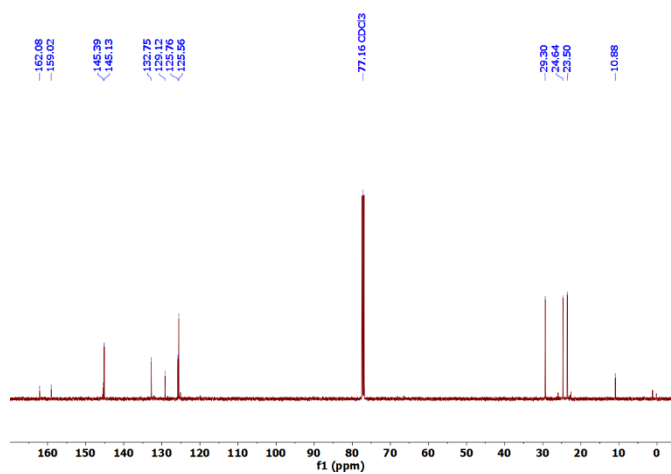
Figure 5.9 ^{13}C{^{1}H}NMR of **2t**.
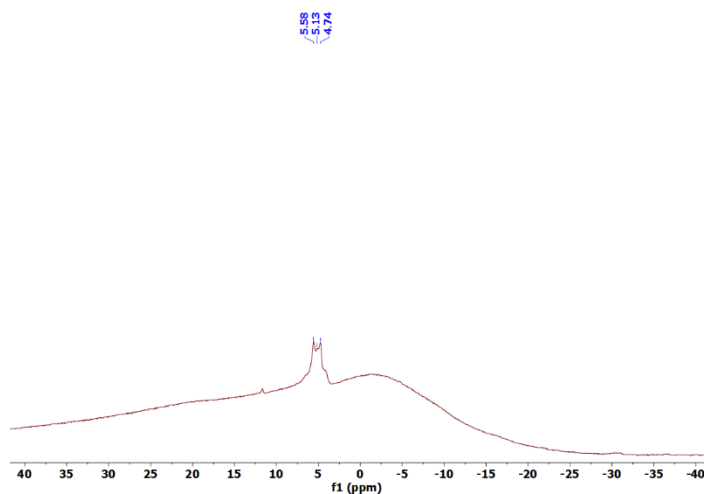
Figure 5.10 ^{11}BNMR of **2t**.

276
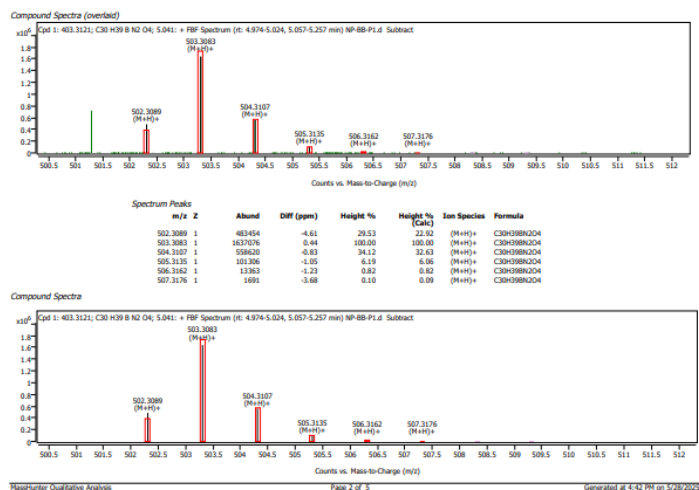
Figure 5.11 High-resolution spectra of **2t**.
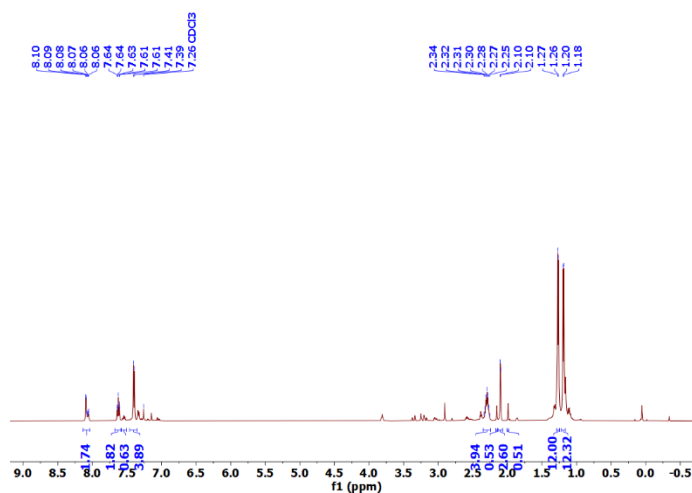
Figure 5.12 ^{1}HNMR of **3t**.
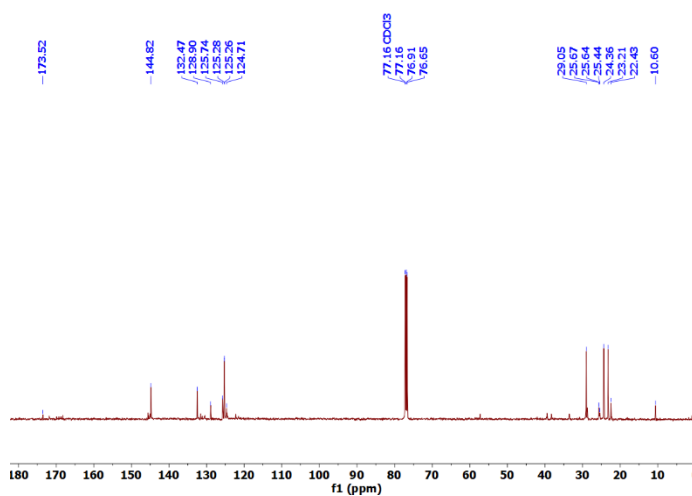
Figure 5.13 ^{13}C{^{1}H}NMR of **3t**.

277
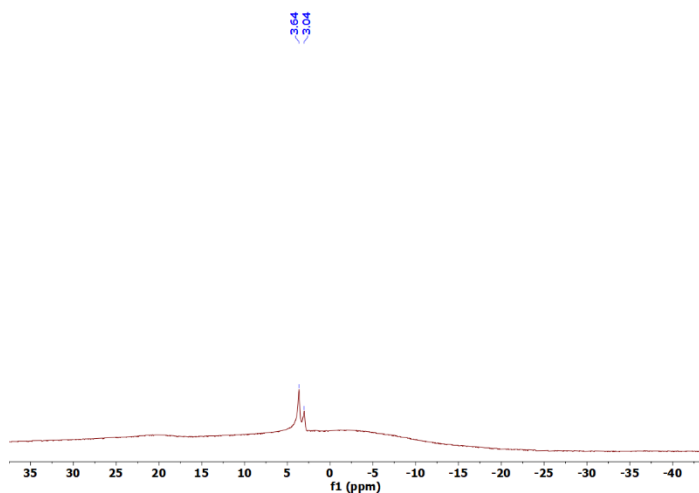
Figure 5.14 ^{11}BNMR of **3t**.
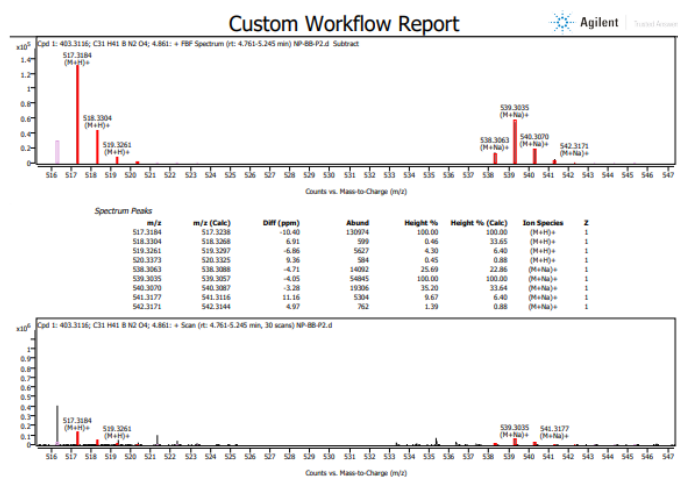
Figure 5.15 High-resolution mass spectra of **3t**.
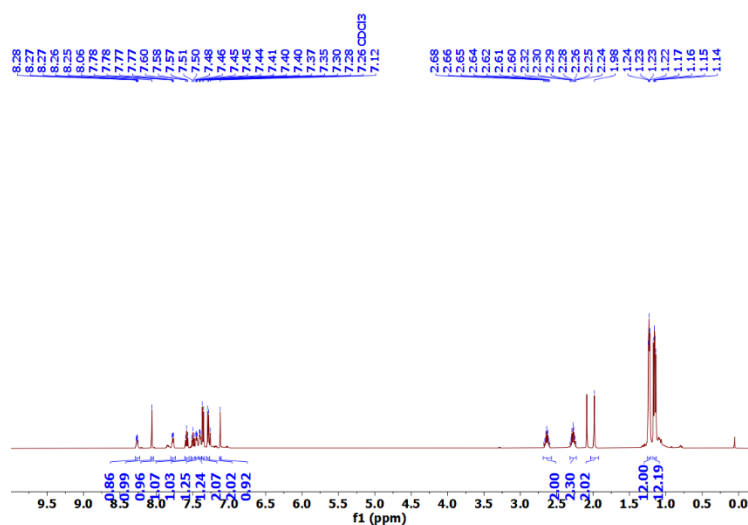
Figure 5.16 ^{1}HNMR spectra of **4t**.
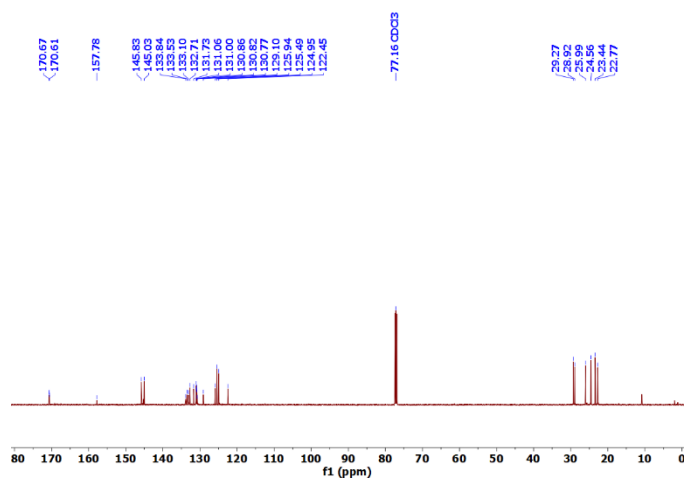
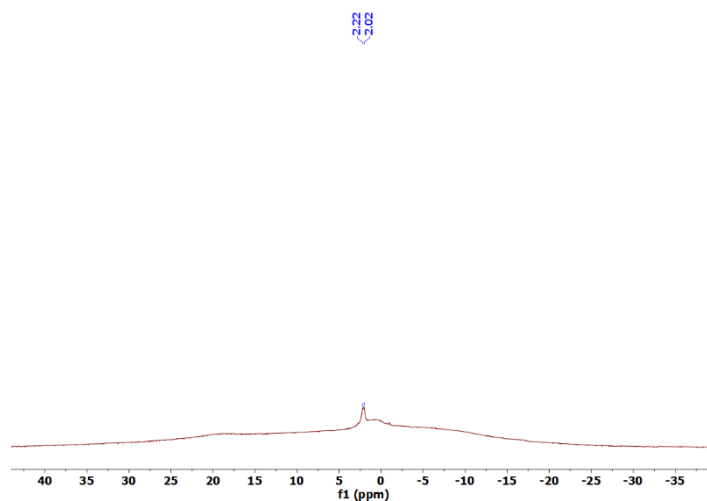**Figure 5.17** $^{13}\text{C}\{^1\text{H}\}$NMR of **4t**.
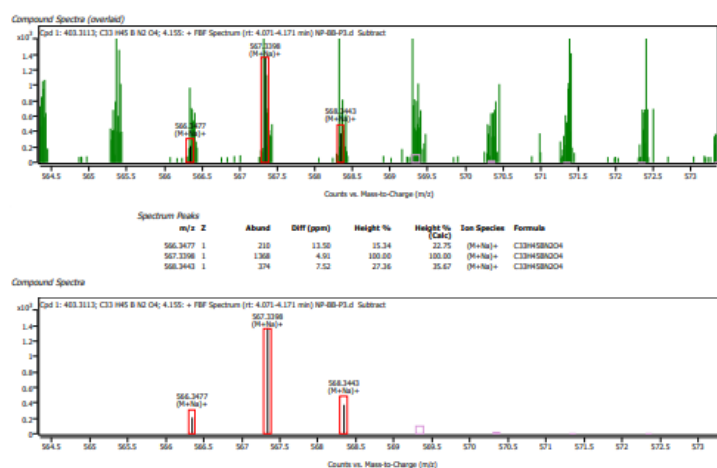

Figure 5.18 ^{11}BNMR of **4t**.

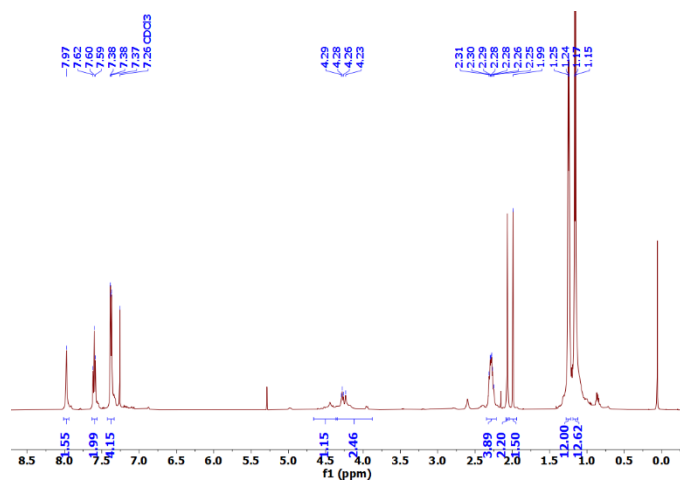**Figure 5.19** High-resolution mass spectra of **4t**.

Figure 5.20 ^{1}HNMR of **5t**.
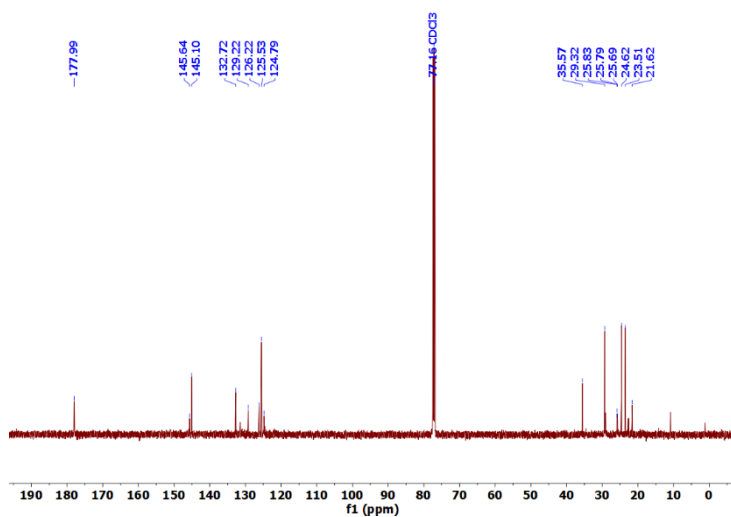
Figure 5.21 ^{13}C{^{1}H}NMR of **5t**.
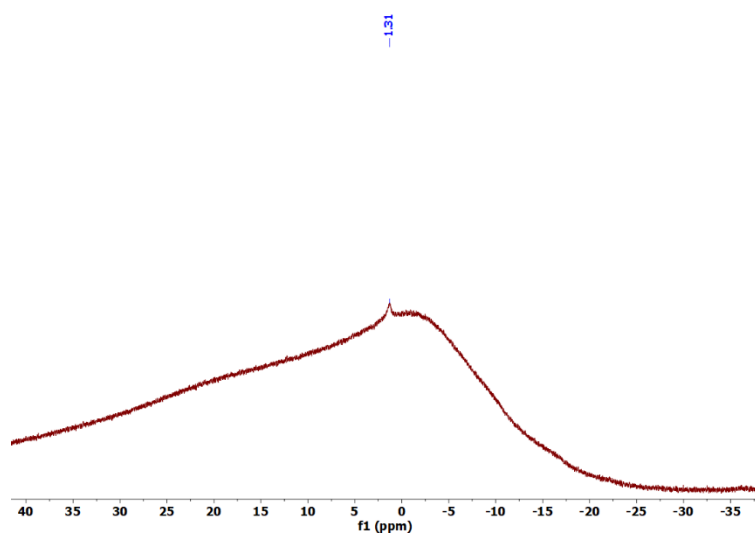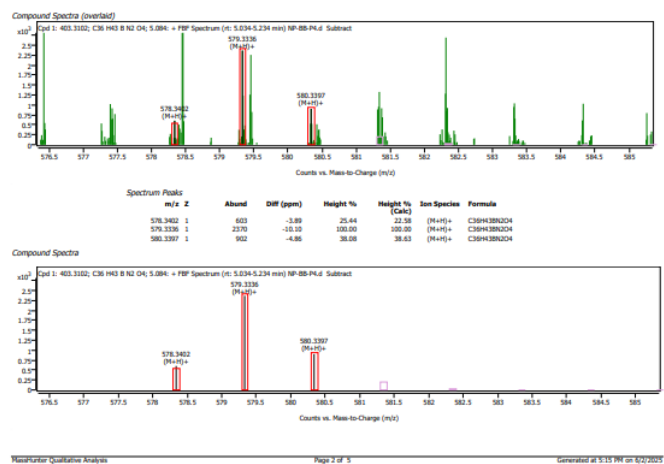

Figure 5.22 ^{11}BNMR of **5t**.

Figure 5.23 High-resolution mass spectra of **5t**.
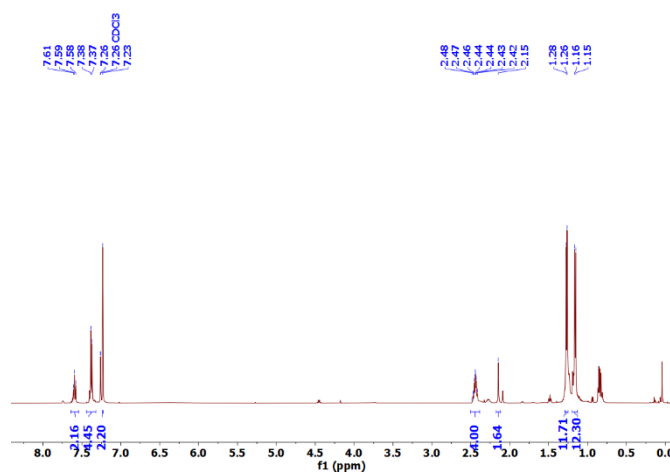
Figure 5.24 ^{1}HNMR of **6t**.
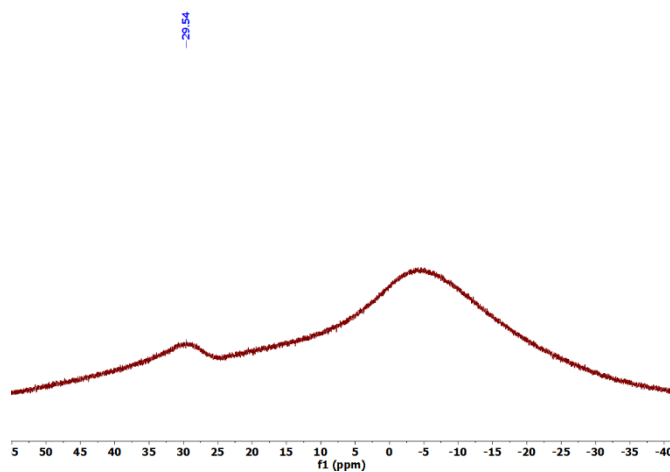
Figure 5.25 ^{11}BNMR of **6t**.

Figure 5.26 ^{19}FNMR of **6t**.
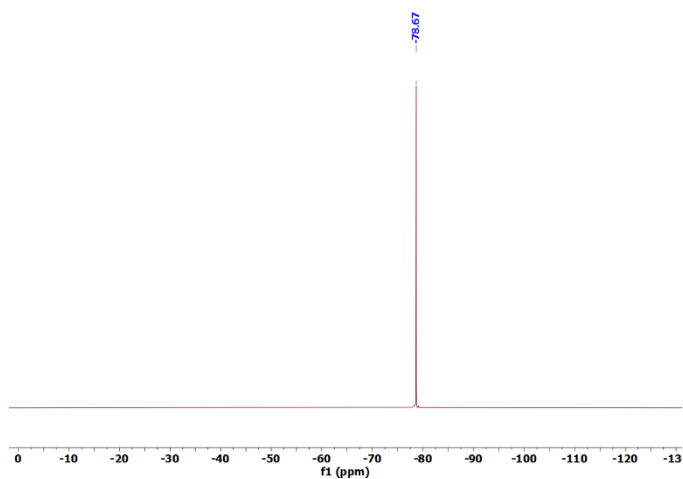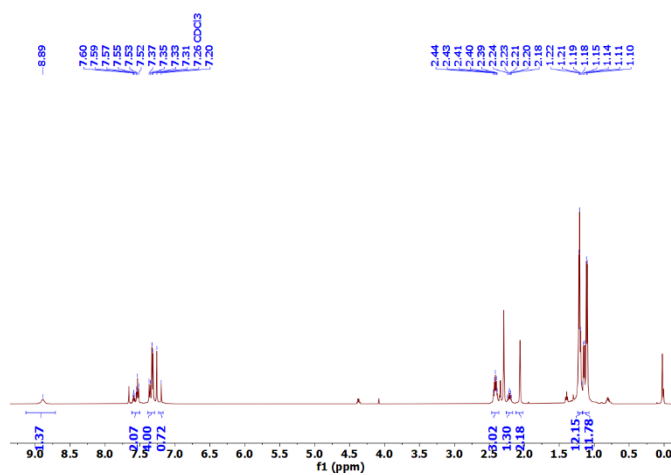

Figure 5.27 ^{1}HNMR of **7t**.

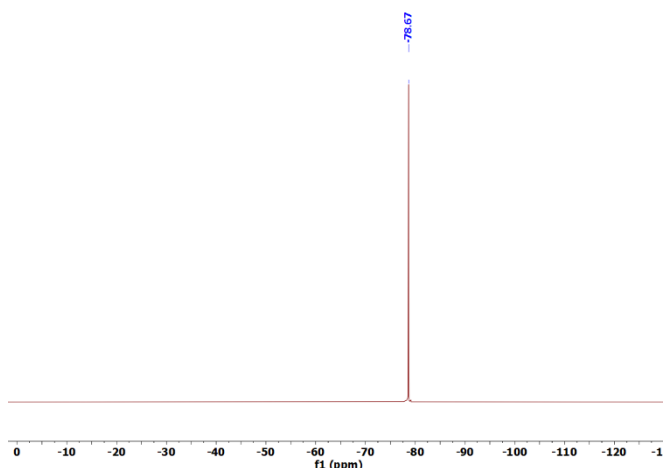

Figure 5.28 ^{11}BNMR of **7t**.

Figure 5.29 ^{19}FNMR of **7t**.

References:

[1] Gompper, R. Schaefer, H. (1967) Ketenderivate, XII. Beiträge zur Chemie der Dithiocarbonsäureester und Ketenmercaptale. Chem. Ber., 100, 591-604. (DOI: 10.1002/cber.19671000228)

[2] Crocker, R. D., Nguyen, T. V. (2016) The Resurgence of the Highly Ylidic N-Heterocyclic Olefins as a New Class of Organocatalysts. Chem. Eur. J., 22, 2208-2213. (DOI: 10.1002/chem.201503575)

[3] Roy, M. M. D., Reward, E(2017) Pushing Chemical Boundaries with N-Heterocyclic Olefins (NHOs): From Catalysis to Main Group Element Chemistry. Acc. Chem. Res., 50, 2017-2025. (DOI: 10.1021/acs.accounts.7b00264)

[4] Maji, B., Mayr, H.(2012) Structures and Reactivities of O-Methylated Breslow Intermediates. Angew. Chem. Int. Ed., 51, 10408-10412. (DOI: 10.1002/anie.201204524)

[5] Ghadwal, R. S. (2016) Carbon-based two-electron σ-donor ligands beyond classical N-heterocyclic carbenes. Dalton Trans., 45, 16081-16095. (DOI: 10.1039/C6DT02158A)

[6] Wang, Y. W., Abraham, M. Y., Gilliard, R. J. Jr., Sexton, D. R., Wei, P., Robinson, G. H. (2013) N-Heterocyclic Olefin Stabilized Borenium Cations. Organometallics, 32, 6639-6642. (10.1021/om400539z)

[7] Rivard, E. (2016) Group 14 inorganic hydrocarbon analogues. Chem. Soc. Rev., 45, 989-1003. (10.1039/C5CS00365B)

[8] Doddi, A., Peters, M., Tamm, M. (2019) N-Heterocyclic Carbene Adducts of Main Group Elements and Their Use as Ligands in Transition Metal Chemistry. Chem. Rev., 119, 6994–7112. (10.1021/acs.chemrev.8b00791)

[9] Arduengo, A. J., Harlow, R., Kline, M. A. (1991) Stable Crystalline Carbene. *J. Am. Chem. Soc.*, *113*, 361-363. (DOI: 10.1021/ja00001a054)

[10] Herrmann, W. A., Köcher, C. (1997) N-Heterocyclic Carbenes. Angew. Chem. Int. Ed., 36, 2162-2187. (DOI: 10.1002/anie.199721621)

[11] Mahantesh, G., Sharma, D., Dandela, R., Dhayalan, V. (2023) Synthetic Strategies of N-Heterocyclic Olefin (NHOs) and Their Recent Application of Organocatalytic Reactions and Beyond. Chem. Eur. J., 29, e202302106. (10.1002/chem.202302106)

[12] Enders, D., Niemeier, O., Henseler, A. (2007) Organocatalysis by N-Heterocyclic Carbenes. Chem. Rev., 107, 5606-5655. (DOI: 10.1016/j.ccr.2016.11.017)

[13] Jacobs, E., Nguyen, T. V., (2025) N-Heterocyclic Carbenes and N-Heterocycles as Synthetic Reagents and Building Blocks. Chem. Eur. J. 31, e202402339. (DOI: 10.1002/chem.202402339)

[14] Krachko, T., Slootweg, C. (2018) N-heterocyclic Carbene-Phosphinidene Adducts: Synthesis, Properties and Applications. Eur. J. Inorg. Chem., 20, 2734-2754. (DOI: 10.1002/ejic.201800459)

[15] Kuhn, N., Bohnen, H., Kreutzberg, J., Bläser, D., Boese, R. (1993) 1,3,4,5-Tetramethyl-2-methyleneimidazoline-an ylidic olefin. J. Chem. Soc. Chem. Commun., 1136-1137. (10.1039/C39930001136)

[16] Dumrath, , A., Wu, X.-F., Neumann, H., Spannenberg, A., Jackstell, R., Beller, M. (2010) Angew. Chem., Int. Ed., 49, 8988-8992. (DOI: 10.1002/anie.2010017873)

[17] Chong, C. C., Rao, B., Ganguly, R., Li, Y., Kinjo, R. (2017) Bis(N-heterocyclic olefin) Derivative: An Efficient Precursor for Isophosphindolylium Species.

[18] Wang, Y. B., Wang, Y. M., Zhang, W., Z., Lu, X. B. (2013) Fast CO_2 Sequestration, Activation, and Catalytic Transformation Using N-Heterocyclic Olefins. J. Am. Chem. Soc., 135, 11996-12003. (DOI: 10.1021/ja405114e)

[19] Huang, K., Sun, C. L., Jie Shi, Z. (2011) Transition-metal-catalyzed C–C bond formation through the fixation of carbon dioxide. Chem. Soc. Rev., 40, 2435-2452. (DOI: 10.1039/C0CS00129E)

[20] Powers, K., Hering-Junghans, C., McDonald, R., Ferguson, M. J., Rivard, E. (2016) Improved synthesis of N-heterocyclic olefins and evaluation of their donor strengths. Polyhedron, 108, 8-14. (DOI: 10.1016/j.poly.2015.07.070)

[21] Saptal, V. B., Bhanage, B. M. (2016) N-Heterocyclic Olefins as Robust Organocatalyst for the Chemical Conversion of Carbon Dioxide to Value-Added Chemicals. Chem.Sus. Chem., 9, 1980-1985. (DOI: 10.1002/cssc.201600467)

[22] Hering-Junghans, C., Andreiuk, P., Ferguson, M. J., McDonald, R., Rivard, E. (2017) Using N-Heterocyclic Vinyl Ligands to Access Stable Divinylgermylenes and a Germylium Cation. Angew. Chem. Int. Ed., 56, 6272– 6275. (DOI: 10.1002/anie.20160910032)

[23] Chong, C. C., Rao, B., Ganguly, R., Li, Y., Kinjo, R. (2017) Bis(N-heterocyclic olefin) Derivative: An Efficient Precursor for Isophosphindolylium Species. Inorg. Chem., 56, 8608-8614. (DOI: 10.1021/acs.inorgchem.6b02991)

[24] Thimer, K. C., Al-Rafia, S. M. I., Ferguson, M. J., McDonald, R., Rivard, E. (2009) Donor/acceptor stabilization of Ge(II) dihydride. Chem. Commun., 7119-7121. (DOI: 10.1039/b915950a)

[25] Al-Rafia, S. M. I., Ferguson, M. J., Rivard, E. (2011)

[26] Huang, K. Sun, C. L., Shi, Z. J. (2011) Transition-metal-catalyzed C–C bond formation through the fixation of carbon dioxide. Chem. Soc. Rev., 40, 2435-2452. (DOI: 10.1039/C0CS00129E)

[27] Antoni, P. W. Reitz, J., Hansmann, M. M. (2021) N2/CO Exchangeata Vinylidene Carbon Center: Stable Alkylidene KetenesandAlkylideneThioketenesfrom1,2,3-Triazole Derived Diazoalkenes. J.Am.Chem.Soc., 143, 12878−12885. (DOI: 10.1021/jacs.1c06906)

[28] Herz, K., Podewitz, M., Sen, S., Buchmeiser, M. R. (2019) Mechanism of Olefin Metathesis with Neutral and Cationic Molybdenum Imido Alkylidene N-Heterocyclic Carbene Complexes. J. Am. Chem. Soc., 141, 8264-8276. (DOI: 10.1021/jacs.9b02092)

[29] Arz, M. I., Geiß, D., Straßmann, M., Schnakenburg, G., Filippou, A. C. (2015) Silicon(I) chemistry: the NHC-stabilised silicon(I) halides Si2X2(Idipp)2 (X ¼ Br, I) and the disilicon(I)iodido cation [Si2(I)(Idipp)2]. Chem. Sci., 6, 6515. (DOI: 10.1039/c5sc02681d)

[30] Ghadwal, R. S., Schürmann, C. J., Andrada, D. M., Frenking, G. (2015) Mono- and di-cationic hydrido boron compounds. Dalton Trans., 44, 14359-14367. (DOI: 10.1039/C5DT02237A)

[31] Lee, W.-H., Lin, Y.-F., Lee, G.-H., Peng, S.-M., Chiu, C.-W. (2016) N-Heterocyclic olefin stabilized boron

dication. Dolton Trans., 45, 5937-5940. (DOI: 10.1039/C5DT03847B)

[32] Al-Rafia, S. M. I., Ferguson, M. J., Rivard, E. (2011) Interaction of Carbene and Olefin Donors with [Cl$_2$PN]$_3$: Exploration of a Reductive Pathway toward (PN)$_3$. Inorg. Chem., 50, 10543-10545. (DOI: DOI: 10.1021/ic201812a)

[33] Czysch, C. Dinh, T., Bixenmann, L., Komforth, P., Nuhn, L. (2022) Nontoxic N-Heterocyclic Olefin Catalyst Systems for Well-Defined Polymerization of Biocompatible Aliphatic Polycarbonates. ACS Polym., 2, 371-379. (DOI: 10.1021/acspolymersau.2c00017)

[34] Dove, A. P. (2012) Organic Catalysis for Ring-Opening Polymerization. ACS Macro Lett., 1, 1409-1412. (DOI: 10.1021/mz3005956)

[35] Naumann, S., Dove, A. P. (2016) N-Heterocyclic Carbenes for Metal-Free Polymerization Catalysis: An Update. Polym. Int., 65, 16-27. (10.1002/pi.5034)

[36] Ueng, S. H., Brahmi, M. M., Derat, E., Malacria, M., Curran, D. P. (2008) Complexes of Borane and N-Heterocyclic Carbenes: A New Class of Radical hydrogrn atom donor. J. Am. Chem. Soc., 130, 10083. (DOI: 10.1021/ja804150k)

[37] Bolt, D. A., Geib, S. J. Curran, D. P. (2018) Synthesis and characterization of N-heterocyclic carbene complexes of 1,3,2-dioxaborolane-4,5-dione (NHC-boryl oxalates). Tetrahedron, 74, 6961-6965. (DOI: 10.1016/j.tet.2018.10.031)

[38] McArthur, D., Butts, C., Lindsay, D. (2011) A Dialkylborenium Ion via Reaction of N-Heterocyclic Carbene-Organoboranes with Brønsted Acids - Synthesis and DOSY NMR Studies. Chem. Commun., 47, 6650-6652. (DOI: 10.1039/c1cc10767d)

Conclusions and Future Research Directions
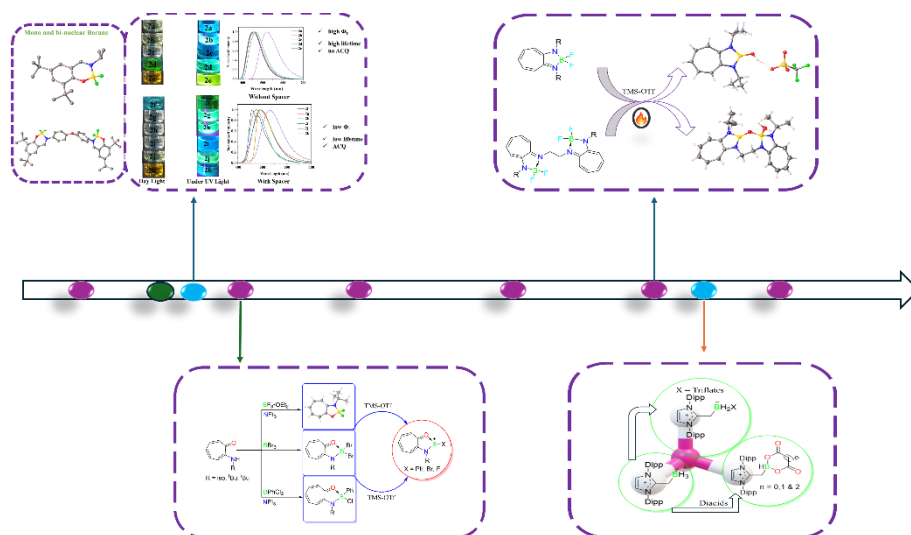
Conclusions

This work provides a comprehensive exploration of N, O, and N, N-based mono and bi-nuclear borane complexes, offering significant variation in their photophysical and stimuli-responsive behaviour. It presents innovative and highly efficient synthetic methodologies to prepare bi-nuclear Schiff bases and aminotroponiminate ligands in good to excellent yields, which serve as versatile scaffolds for the stabilization of reactive main-group metal centers. A series of mono and binuclear boron complexes derived from these ligands has been successfully synthesized and thoroughly characterized, showcasing their structural diversity and stability.

Further, we investigate the reactivity of mono and bi-nuclear boron complexes with fluoride-abstracting reagents. Interestingly, six-membered N, O chelated borane complexes were inactive towards fluoride abstracting reagents, while N, N chelated borane complexes facilitate the tricoordinated borenium cations. Notably, mono-nuclear aminotroponiminate-based BF_2 boranes facilitated the mono-nuclear borenium cations, bi-nuclear aminotroponiminate borane facilitates the novel oxy-bridged bore(boro)nium cation in a seven-membered ring scaffold. Moreover, 2-aminotropone was treated with boron trifluoride (BF_3) led to the formation of a neutral boron complex, whereas its reaction with boron tribromide (BBr_3) resulted in the generation of a boronium cation, highlighting the influence of the halide on the nature of the boron-containing species. In conclusion, N, N chelated boranes facilitate the tricoordinate boron cations, while N, O facilitates the boronium cations, highlighting the decisive role of ligand's steric aspect in the isolation of boron cations. In addition, we synthesised NHO-borane adducts and investigated their reactivity with diacids and triflates. Collectively, this work not only establishes a foundation for photoluminescent boron compounds and/or Lewis acidic boron cations, but it also provides a scope of their broad utility in catalysis and materials science.

Future research directions

BF$_2$-chelated dyes represent a promising class of functional materials owing to their remarkable photophysical properties, including high molar absorptivity, tunable fluorescence emission, large Stokes shifts, and notable thermal and chemical stability. The present documents reveal that the N, N and N, O donor ATIs ligands are versatile ligands and hold a broad range of chemistry with the boron. So our main focus is on modifying the ATIs ligands in terms of steric and electronic properties by changing the spacers and N-(alkyly) arylated substituents in bis and tris(aminotroponiminate) ligands, with their extended conjugation and tunable electronic properties (fluorescence quantum yields, shifting in emission blue to green with large Stokes shifts), are expected to influence by the geometry and electronic environment of boron complexes. By fine-tuning these ligand architectures, we aim to achieve greater control over metal–ligand interactions, ultimately leading to improved reactivity for the isolation of trinuclear boron cations.

Beyond photophysical properties, the synthesis of BF$_2$ complexes and the novel (borenium) cation highlights the promising potential of these ligand systems in main-group Lewis acid chemistry. A key area of future research will focus on expanding this by synthesizing (oxoborane) species from the (borenium) cation. These cationic species offer exciting opportunities for cooperative catalysis, where the metal center and boron fragments work in concert to activate small molecules such as CO_2 and H_2. Their unique electronic properties hold the potential to enable novel bond activation processes, providing a pathway for innovative and sustainable chemical transformations.

Overall, the continued development of tris(aminotroponiminate) and bis(aminotroponiminate) ligands, along with their corresponding metal complexes, will play a crucial role in advancing main-group catalysis. By systematically tuning ligand properties, we can unlock new reactivity

patterns and design highly efficient catalytic systems, further expanding the frontiers of main-group chemistry.